Exo-closo carborane complexes of rhodium and iridium. Synthesis and evaluation as hydrogenation catalysts

Rifat, Adem

Award date:
2003

Awarding institution:
University of Bath

EXO-CLOSO CARBORANE COMPLEXES OF RHODIUM AND IRIDIUM. SYNTHESIS AND EVALUATION AS HYDROGENATION CATALYSTS.

Submitted by Adem Rifat

for the degree of PhD of

the university of Bath

2003

COPYRIGHT

ProQuest LLC
789 East Eisenhower Parkway
P.O. Box 1346
Ann Arbor, MI 48106-1346

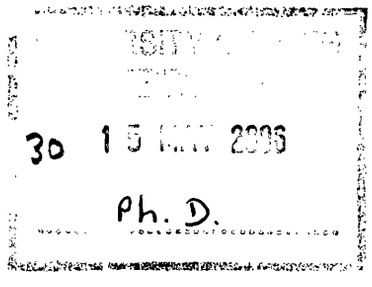
30 15 MAY 2006
Ph. D.

ACKNOWLEDGMENTS

Completion of this thesis would have been much more troublesome without the following people. My mum and brother who have helped me a great deal over the last month or two. Dr. Andy Weller, for constantly pushing forward and his endless enthusiasm for all things chemical. A big thanks to all the people in the lab, Jamie, Mike, Nathan, Nico, Susie, Gary Vicki and any one else over the three years I may have forgotten. Many good times and good conversation etc has been had with Fred, Koko and Didier. All of whom have been good friends. A big hug and a cheeky kiss to Lenka, thanks for being cheeky!

ABBREVIATIONS

Cp	Cyclopentadiene
NMR	Nuclear Magnetic Resonance
Hz	Hertz
Å	Angstrom
R	Alkyl group
δ	Chemical Shift
ppm	parts per million
$[BAr_f]^-$	$[B\{3,5\text{-}C_6H_3(CF_3)\}_4]^-$
COD	Cyclooctadiene
nbd	norbornadiene
Me	CH_3
Et	CH_2CH_3
Cy	Cyclohexyl
Dppe	diphenylphosphinoethane
Y	Anion
Ph	C_6H_5
M	Metal
L	Ligand
Δ	Difference

ABSTRACT

The treatment of $[L_2Rh(nbd)][Y]$ precursor complexes (where L = PPh_3, PCy_3, 1/2dppe or $P(OMe)_3$ and Y = [*closo*-$CB_{11}H_{12}]^-$ or [*closo*-$CB_{11}H_{11}Br]^-$) results in the formation of zwitterionic complexes of the type [L_2Rh(*closo*-$CB_{11}H_{12}$)]. These complexes have been fully characterised by elemental analysis, NMR spectroscopy and in some cases by X-ray diffraction techniques. When L = PPh_3 and Y = [*closo*-$CB_{11}H_6Br_6]^-$, $[BF_4]^-$, $[BAr_f]^-$ or [*closo*-$CB_{11}Me_{11}]^-$ complexes of the type $[(PPh_3)_2Rh]_2[Y]_2$ are formed in good yield which reflects the weaker coordinating power of these anions. The reactivity of [L_2Rh(*closo*-$CB_{11}H_{12}$)] and $[(PPh_3)_2Rh]_2[Y]_2$ complexes towards H_2 and olefins has been investigated. Both types of complex react with hydrogen in CH_2Cl_2 to ultimately give a chloride bridged diner. The zwitterionic complexes undergo BH activation in solution which results in hydroboration of the carborane in the presence of olefins. $[(PPh_3)_2Rh]_2[Y]_2$ reacts with cyclohexene to give dehydrogenation products that arise from CH activation. [L_2Rh(*closo*-$CB_{11}H_{12}$)] and $[(PPh_3)_2Rh]_2[Y]_2$ have been evaluated for their activity in the hydrogenation of some sterically hindered olefins. It is found that modulation of the anion has a significant effect on both rate of hydrogenation and the final yield of hydrogenated product. Iridium complexes of the type $[(PPh_3)_2Ir(COD)][Y]$ (Y = [*closo*-$CB_{11}H_{12}]^-$ and [*closo*-$CB_{11}H_6Br_6$] have also been prepared. Treatment of these complexes with H_2 in CH_2Cl_2 yields $[(PPh_3)_2Ir(H)_2$(*closo*-$CB_{11}H_{12}$)] and $[(PPh_3)_2Ir(H)_2$(*closo*-$CB_{11}H_6Br_6$)] respectively. $[(PPh_3)_2Ir(H)_2$(*closo*-$CB_{11}H_6Br_6$)] reacts cleanly with C_2H_4 to yield a stable *tris*-ethene complex. These compounds are proposed as model complexes for the hydrogenation of olefins mediated by rhodium metallocarboranes complexes.

1 INTRODUCTION

1.1 Carboranes

Carboranes are molecules containing the basic arrangement of carbon and boron atoms in a polyhedral structure. The majority of known carboranes contain two carbon atoms. This is due to the ease with which they can be formed by reaction of precursor boranes, such as *nido*-$B_{10}H_{14}$, with an appropriate alkyne.[1] However, carboranes that contain one, three or even four carbons are also well documented. Carborane analogues of boron clusters can be isolated because a $\{B\text{-}H\}^-$ fragments is isoelectronic and isolobal with a $\{C\text{-}H\}$ fragment (Figure 1.1).[2] This means the fragments have the same frontier orbitals and number of bonding electrons, and the molecular orbitals (MO's) have a similar symmetry and approximately the same energy meaning that, in theory, they are interchangeable.

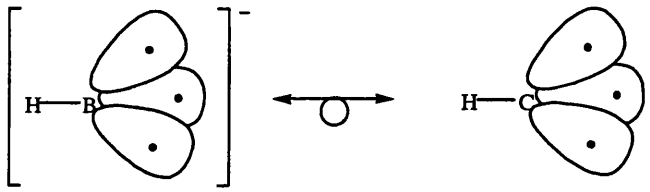

Figure 1.1: Frontier molecular orbitals of $\{B\text{-}H\}^-$ and $\{C\text{-}H\}$

The shape of a borane or carborane cluster can be predicted by the application of Wade's rules.[3] Counting the number of electron pairs donated to cluster bonding orbitals and relating this to the number of vertices gives the relevant polyhedral shape on which the

cluster is based. This polyhedron might be complete, or missing up to 2 vertices. Although clusters missing 3 vertices are also known. A *closo*-cluster has $n + 1$ electron pairs, where n is the number of cluster vertices. This cluster has the shape of a complete polyhedron (or deltahedron) containing n vertices. A *nido*-cluster has one missing vertex and $n + 2$ electron pairs donated to cluster bonding. It is based upon a parent deltahedron having $n + 1$ vertices, with the vertex of highest connectivity removed. An *arachno*-cluster ($n + 3$ electron pairs) has two missing vertices and is based upon a deltahedron containing $n + 2$ vertices (Figure 1.2).

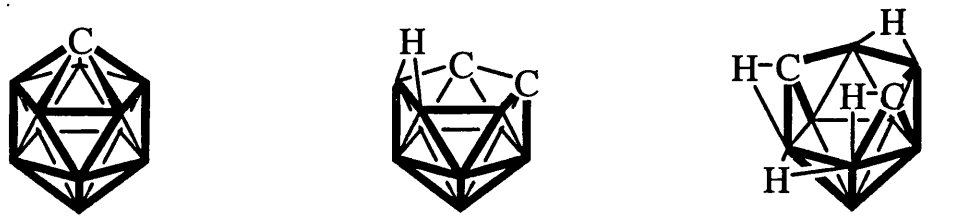

[*closo*-1-$CB_{11}H_{12}$]$^-$ [*nido*-7,8-$C_2B_9H_{12}$]$^-$ *arachno*-$C_2B_8H_{14}$

Terminal B-H hydrides omitted for clarity

Figure 1.2: *Closo, nido and arachno* clusters based on an icosohedral polyhedron

In general *nido*- and *arachno*- clusters are less thermally and chemically stable than their *closo*- counterparts. This is due to the presence of relatively more reactive hydrogens and the more open structure in *nido*- and *arachno*- clusters.

The properties and stability of anionic *closo*-monocarboranes, of general formula [*closo*-$CB_{n-1}H_n]^-$, have been studied extensively. Theoretical calculations performed on the [*closo*-$CB_{n-1}H_n]^-$ (n = 5-12) anions to determine their relative stabilities, show [*closo*-

$CB_{11}H_{12}]^-$ to be the most stable in this family of carboranes.[4-6] All the [*closo*-$CB_{n-1}H_n]^-$ (n = 5-12) compounds have been isolated and structurally characterised,[7-13] but only the chemistry of [*closo*-$CB_{11}H_{12}]^-$ and [*closo*-$CB_9H_{10}]^-$ and their derivatives has been studied extensively.

1.2 The [*closo*-$CB_{11}H_{12}]^-$ Anion

1.2.1 Synthesis

An effective route to [*closo*-$CB_{11}H_{12}]^-$ developed by Knoth[7] starts with the addition of sodium cyanide to decaborane (Equation 1.1 and 1.2).[14]

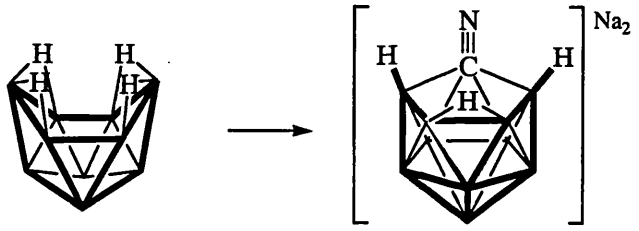

nido-$B_{10}H_{14}$ + 2NaCN ⟶ Na_2[*nido*$B_{10}H_{13}CN$] + HCN **1.1**

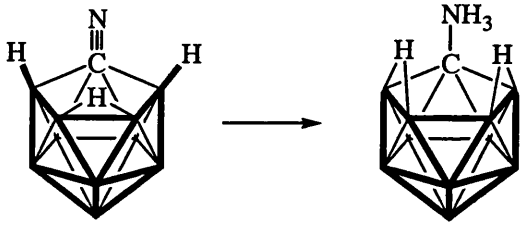

Na_2[*nido*$B_{10}H_{13}CN$] $\xrightarrow{H^+ \text{ ion exchange}}$ *nido*-$B_{10}H_{12}CNH_3$ **1.2**

The coordinated amine is then converted into trimethylamine by reaction with dimethyl sulfate (Equation 1.3).[15]

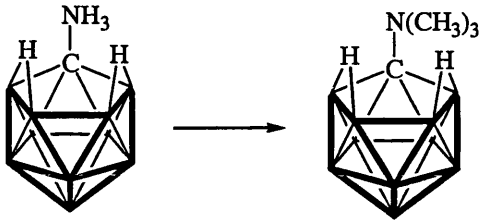

$$2\ nido\text{-}B_{10}H_{12}CNH_3 + (CH_3)_2SO_4 + 6NaOH \longrightarrow 2\ nido\text{-}B_{10}H_{12}CN(CH_3)_3 + 3Na_2SO_4 + 6H_2O \qquad \mathbf{1.3}$$

Removal of trimethylammonia by reductive deamination using sodium yields a tri-sodium salt of this carborane, which is converted into the caesium salt of a *nido* carborane (Equation 1.4-1.6).[16]

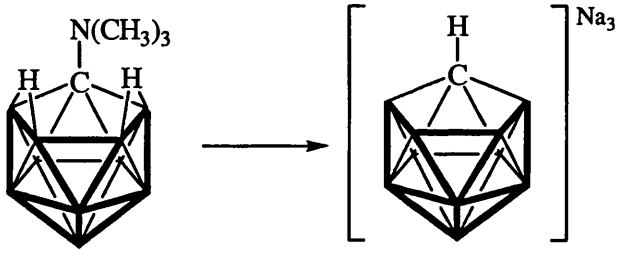

$$nido\text{-}B_{10}H_{12}CN(CH_3)_3 + 3Na \longrightarrow Na_3[nido\text{-}B_{10}H_{10}CH + Me_3N + 1/2H_2 \qquad \mathbf{1.4}$$

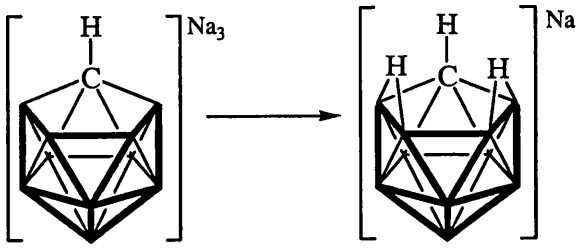

$$Na_3[nido\text{-}B_{10}H_{10}CH + 2H_2O \longrightarrow 2NaOH + Na[nido\text{-}B_{10}H_{12}CH] \quad \textbf{1.5}$$

$$Na[nido\text{-}B_{10}H_{12}CH] + CsCl \longrightarrow Cs[nido\text{-}B_{10}H_{12}CH] + NaCl \quad \textbf{1.6}$$

The final step is to add the extra B-H fragment to the cage, necessary to make the compound *closo* (Equation 1.7).[17]

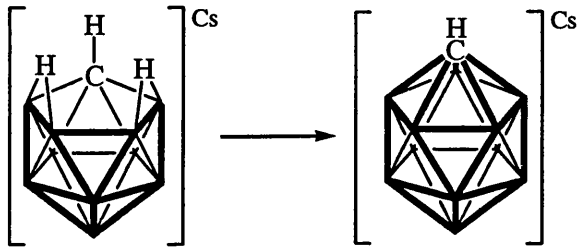

$$Cs[nido\text{-}B_{10}H_{12}CH] + H_3B.N(C_2H_5)_3 \longrightarrow Cs[closo\text{-}CB_{11}H_{12}] \quad \textbf{1.7}$$

1.3 Derivatisation of $[closo\text{-}CB_{11}H_{12}]^-$

An attractive property of the $[closo\text{-}CB_{11}H_{12}]^-$ anion is that the B-H vertices readily undergo electrophilic substitution which enables the preparation with relative ease of several halogen derivatives.[18-21] Of relevance here are $[12\text{-}Br\text{-}closo\text{-}CB_{11}H_{11}]^-$ and

[7,8,9,10,11,12-Br_6-*closo*-$CB_{11}H_6$]$^-$.[18, 19] The synthesis of these anions is shown in Figure 1.2.1.

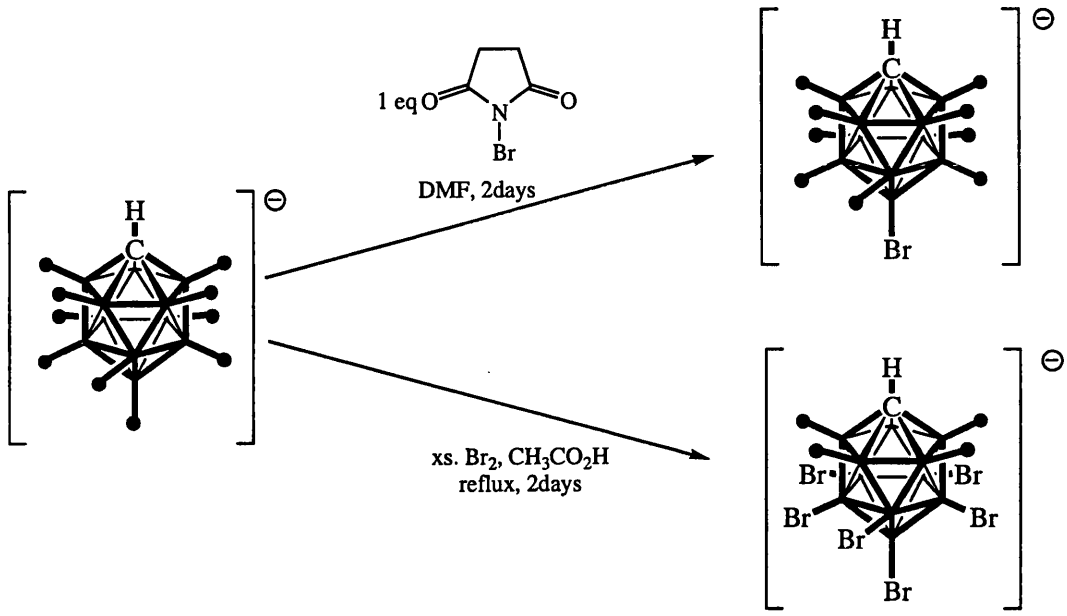

Figure 1.3.1: Synthesis of *mono-* and *hexa-* substituted *bromo* carboranes

These carboranes are readily accessible in multigram quantities. Whilst the bromo-derivatives have attracted much attention in the literature as discussed in section 1.2.4. the fluoro,[22] chloro[18] and iodo[23] derivatives of [*closo*-$CB_{11}H_{12}$]$^-$ are also well known.

Another useful functionalisation of the [*closo*-$CB_{11}H_{12}$]$^-$ anion is alkylation whereby all the {BH} vertices are substituted by alkyl groups. Although the synthesis is not as straightforward as for halogenation, [2,3,4,5,6,7,8,9,10,11,12-Me_{11}-*closo*-$CB_{11}H$]$^-$ can be conveniently prepared in good yield on a reasonably large scale (Figure 1.3.2).[24]

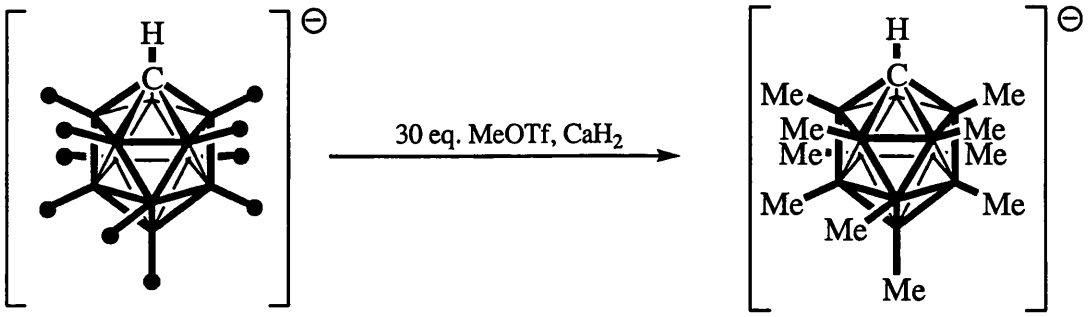

Figure 1.3.2: Preparation of [2,3,4,5,6,7,8,9,10,11,12-Me_{11}-*closo*-CHB_{11}]$^-$

Substitution of the {BH} vertices for either halo or alkyl substituents results in changes in stability, solubility and perhaps most importantly, the nucleophilicity of the [*closo*-CB_{11}]$^-$ anion. The effect on stability is demonstrated by comparing the silver(I) salts of [*closo*-$CB_{11}H_{12}$]$^-$ and [*closo*-$CB_{11}H_6Br_6$]$^-$. Ag[*closo*-$CB_{11}H_{12}$] is light sensitive and will decompose upon heating or standing in an aqueous solution.[17] This is due to the susceptibility of H(7)-H(11) and in particular H(12) to electrophilic attack. Ag[*closo*-$CB_{11}H_6Br_6$], on the other hand, is not overly light sensitive and can be prepared and handled in boiling water. The change in solubility properties is quite marked. For example the [*closo*-$HCB_{11}Me_{11}$]$^-$ anion is soluble in polar organic solvents such as Et_2O and CH_2Cl_2 and even shows a measurable solubility in hexane, depending on the cation.[25] Cs[*closo*-$CB_{11}H_{12}$] and it's derivatives are much less soluble. The low nucleophilicity of these anions is well documented and discussed in the following section.

1.4 Weakly coordinating nature of the [*closo*-$CB_{11}H_{12}$]$^-$ anion

The parent anion [*closo*-$CB_{11}H_{12}$]$^-$ is a relatively weakly coordinating anion by virtue of efficient delocalisation of its single charge over a relatively large cluster and thus the absence of any basic sites on the cage periphery. Several systems have been developed to rank the coordinating power of anions.[26, 27] However, the most reliable developed to date is based around [(^{i}Pr)$_3$Si(Y)] (Y = weakly coordinating anion) which has two accurate markers as to the degree of coordination of the anion to cation.[28] The first is in the C-Si-C bond angle. The expected angle for the sp^2-hybridised [(^{i}Pr)$_3$Si]$^+$ cation is 120°. Measurement of this bond angle of various cation/anion pairs gives a useful indication as to the degree of sp^2-hydridisation and thus coordinating power of the anion. The second marker is based upon the downfield ^{29}Si NMR chemical shift. The more positive ^{29}Si chemical shift indicates a more deshielded nucleus and thus the most cationic character. The measurement of the ^{29}Si NMR chemical shift in solution is sometimes complicated by competition from solvent molecules so it is often measured in the solid-state *via* CPMAS techniques. Some measured ^{29}Si NMR chemical shifts are shown in Table 1.4.1.

Compound	Solvent	$\delta(^{29}Si)$/ppm	Ref.
^{i}Pr$_3$SiH	toluene	12.1	29
^{i}Pr$_3$Si(OSO$_2$CF$_3$)	toluene	40	30
^{i}Pr$_3$Si[B(Ar$_f$)$_4$]	none	107.6	29
^{i}Pr$_3$Si(1-H-CB$_{11}$H$_5$Br$_6$)	none	110	31
^{i}Pr$_3$Si(1-H-CB$_{11}$F$_{11}$)	toluene	120	32

Table 1.4.1: ^{29}Si NMR chemical shifts for some selected anions

As can be seen the $[1\text{-H-}CB_{11}F_{11}]^-$ anion gives a very large ^{29}Si chemical shift indicating it is very weakly coordinating. The $[B(Ar_f)_4]^-$ and $[1\text{-H-}CB_{11}H_6Br_6]^-$ anions also give a large ^{29}Si chemical shift indicating that they are some of the most weakly coordinating anions known to date.[30]

The weakly coordinating nature of these anions allows the isolation of highly electrophilic species. For example the isolation of protonated benzene $[(HC_6H_6)^+]$ as a room temperature stable weighable solid can be achieved by employing $[closo\text{-}CB_{11}H_6Cl_6]^-$ as the anion.[33, 34] The synthesis of the protonated form of benzene is a two-step process. Firstly HCl is condensed onto solid $[R_3Si(closo\text{-}CB_{11}H_6Cl_6)]$ at low temperature to yield $H[closo\text{-}CB_{11}H_6Cl_6]$ in quantitative yield, which in turn, can be treated with bezene to yield the protonated form. Previous attempts to isolate these species with counterions such as $[SbF_6]^-$, $[HSO_4]^-$ or $[CF_3SO_3]^-$ failed because the anions are too nucleophilic[30] or promote cation decomposition.[35]

1.5 Weakly coordinating anions in catalysis

Weakly coordinating anions play a major role in catalysis mediated by Lewis acidic cationic centres. In a typical catalytic cycle a ligand (X) is displaced to leave a cationic metal centre and a vacant coordination site (Figure 1.5.3).

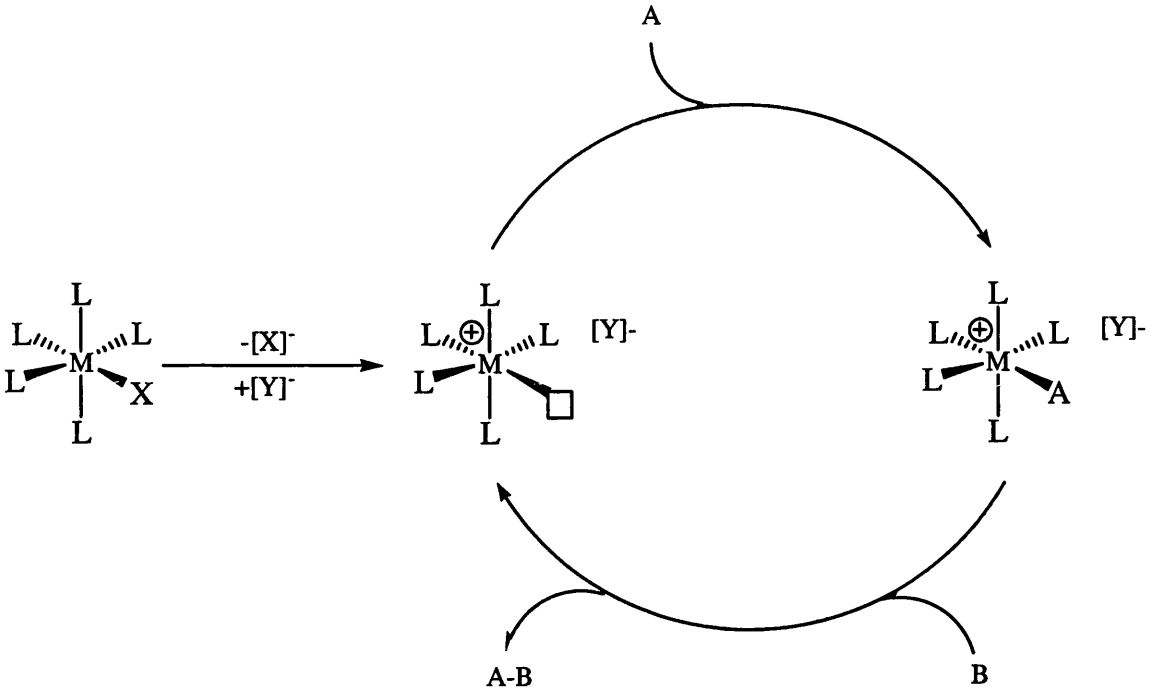

Figure 1.5.1: Generalised catalytic cycle for a Lewis acid catalyst

The substrate (A) is then free to coordinate to the metal centre and is activated towards reaction with (B) to give the product (A-B). In this generalized scheme, the more weakly coordinating the anion the greater the availability of the vacant coordination site and thus a more effective catalyst is generated.

This is borne out in several studies in which weakly coordinating anions have been compared against more traditional counterions such $[PF_6]^-$, $[ClO_4]^-$, $[BF_4]^-$ and $[SbF_6]^-$. For example, the reaction shown in Figure 1.5.2 is catalysed by the chiral cationic fragment $[CpRu(PP)L]^+$ (Cp = η^5-C_5H_5, PP = 1,2-bis[bis(pentafluorophenyl)phosphanyloxy]-1,2- diphenylethane) (L = acetone).[36]

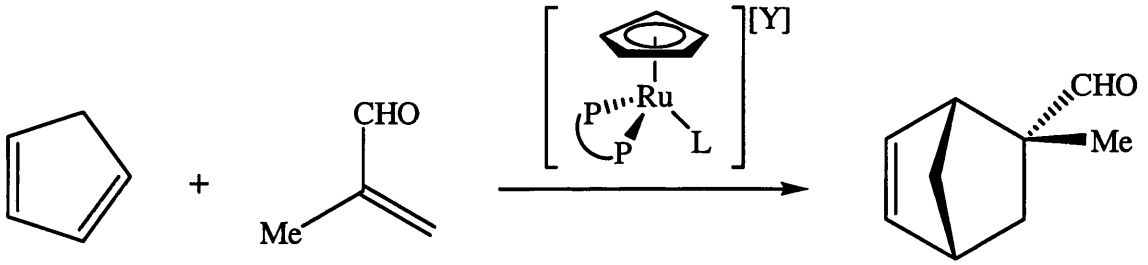

Figure 1.5.2: Chiral Lewis acidic Ru(II) fragment

A significant counterion effect is observed for this reaction. When the anion $[Y]^-$ is ^-OTf an 11% conversion after 70 hr is observed. An increase in performance is seen when the SbF_6^- anion is used which results in a 92% conversion after 19 hr. A further enhancement of the catalyst performance is made when the anion is modulated to $[BAr_f]^-$ (Figure 1.5.3) in which case 100% conversion is observed after only 5 hr.

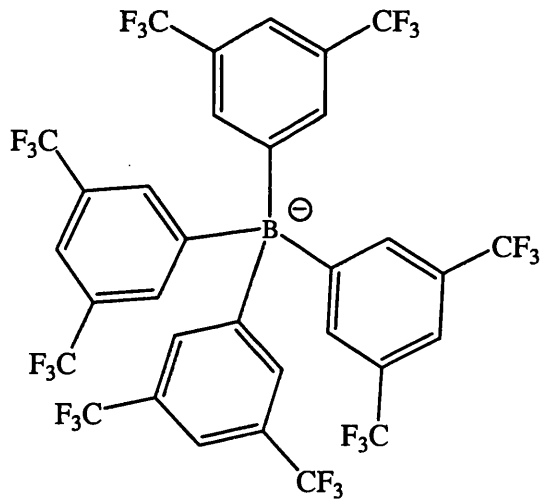

Figure 1.5.3: The $[BAr_f]^-$ anion

The origin of this counterion effect has been accounted for by invoking a hydrogen bonding model between the substrate and the anion. The solid-state structure of a

catalysts methacrolein adduct indicates that the anion forms hydrogen bonds between not only the ligands on the catalyst but also between the anion and the bound substrate. The hydrogen bonds, although weak, seem to be sensitive to the nature of the anion. Thus it is suggested that the smaller more coordinating anions form tighter hydrogen bonds to the catalyst/substrate adduct and thus inhibit the turnover of the catalyst.

In a related system[37] similar increases in rate of reaction of the Lewis acid catalysed reaction of acrylimide with cyclopentadiene can be achieved by modulating the anion part of the catalyst (Figure 1.5.4).

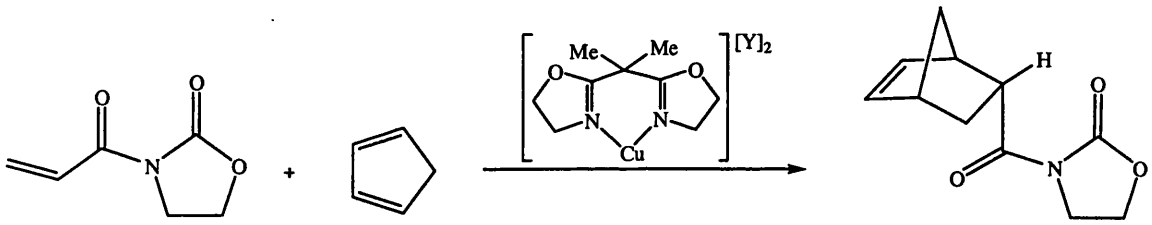

Figure 1.5.4: Lewis acid promoted reaction of acrylimide with cyclopentadiene

In this case the anions $[BF_4]^-$ and $[OTf]^-$ give 50% conversion after 7 hr. The $[PF_6]^-$ anion gives 65% conversion after 7 hr while the $[SbF_6]^-$ anion gives a 100% after 2 hr. Whilst no explanation was given for this anion effect it seems plausible to assume that the $[SbF_6]^-$ anion results in a catalyst which competes with the vacant coordination site least. i.e. there is less competition between substrate and anion thus resulting in a faster catalyst.

The silver(I) catalysed hetero-Diels-Alder reaction (Figure 1.2.5) has also been the subject of a thorough study on the effect of counterion.[38] In this case it was found that once again the anion had a marked effect on both the rate and conversion for the reaction shown in Figure 1.2.5.

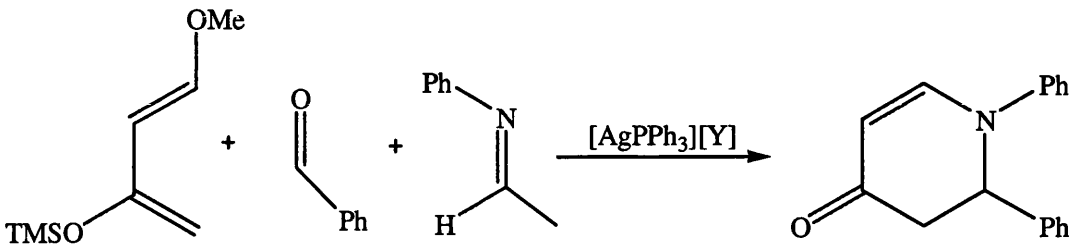

Figure 1.5.5: Hetero Diels-Alder reaction catalysed by $AgPPh_3^+$ fragments

As can be seen from Table 1.5.1 the isolated yield increases dramatically as the counterion is varied. In this case the weakly coordinating anions are those based around [*closo*-$CB_{11}H_{12}$]$^-$. As can be seen from Table 1.5.1 a large increase in isolated yield is achieved as the anion is changed.

Complex	Isolated Yield (%)
$[Ag(PPh_3)(BF_4)]$	35
$[Ag(PPh_3)(OTf)]$	70
$[Ag(PPh_3)(ClO_4)]$	90
$[Ag(PPh_3)(CB_{11}H_{12})]$	98
$[Ag(PPh_3)(CB_{11}H_6Br_6)]$	99

Table 1.5.1: Variation in yield for the silver(I) catalysed hetero-Diels-Alder reaction

The rate of this reaction is also improved significantly when using the [*closo*-$CB_{11}H_6Br_6$]$^-$ anion. For example the [*closo*-$CB_{11}H_{12}$]$^-$ anion gives 98% conversion after 40 mionutes. The [*closo*-$CB_{11}H_6Br_6$]$^-$ anion, however, gives 100% conversion after only

10 minutes. The effectiveness of these catalysts is suggested to arise from the weak coordinating ability of the anion, thus the substrate has less competition to the active metal centre than it would do when a more coordinating anion is employed.

Further anion effects have been noted in other catalytic systems. The most commericially important one being the polymerisation of ethene with Group IV based metal alkyl complexes (Figure 1.5.6).

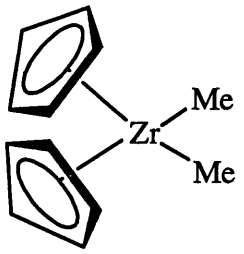

Figure 1.5.6: Zirconium(IV) based polymerization catalyst

These catalysts have received much attention due to their commercial importance.[39] It has been highlighted that the activator in this system can influence greatly not only the polymer produced but also the rate of the polymerization. For example when per-fluoro phenyl borates (such as $[B(Ar_f)_4]^-$ are employed as activators for the polymerization of ethene highly active catalysts are generated. Bochmann[40] has demonstrated that anions such as $[CN\{B(C_6F_5)_3\}_2]^-$ when used as initiators give a catalytic system that outperforms even $[B(C_6F_5)_4]^-$ in the polymerization of ethene. Whilst an in-depth discussion of this system is not warranted here the implication is that the anion (even a very weakly coordinating one) is important in stabilizing a highly Lewis acidic fragment

an intermediate in which the anion if then replaced by substrate to generate the active catalyst.

Other anion effects have been observed in homogeneous hydrogenation catalysts based upon Group IX metal complexes. These systems are dealt with in more detail in chapter 5.

1.6 Summary

Anions based around [*closo*-$CB_{11}H_{12}$]$^-$ are extremely robust by virtue of the high stability of the [CB_{11}]$^-$ core. Functionalisation of the periphery of the cluster is easily achieved *via* electrophilic substitution of one or more of the {BH} vertices. The monoanionic nature of these carboranes makes them suitable for partnering with cationic Lewis acidic fragments. This thesis will explore the synthesis of several novel metallocarboranes based upon Group IX metal phosphine fragments of which only a few examples are currently known. The use of weakly coordinating anions in catalysis has been highlighted in recent years and the effect of these weakly coordinating [*closo*-$CB_{11}H_{12}$]$^-$ anions in Lewis acidic promoted reactions will be explored.

1 W. L. Jolly, *Inorg. Synth.*, 1968, **11**, 19.
2 R. Hoffmann, *Angew. Chem. Int. Ed. Engl.*, 1982, **21**, 711.
3 K. Wade, *Adv. Inorg. Organomet. Chem.*, 1976, **18**, 1.
4 M. J. S. Dewar and M. L. McKee, *Inorg. Chem.*, 1980, **19**, 2662.
5 M. L. McKee, *J. Am. Chem. Soc.*, 1997, **119**, 4220.
6 P. Schleyer and K. Najafian, *Inorg. Chem.*, 1998, **37**, 3454.
7 W. H. Knoth, *J. Am. Chem. Soc.*, 1967, **89**.
8 D. E. Hyatt, F. R. Scholer, J. L. Todd, and J. L. Warner, *Inorg. Chem.*, 1967, **6**, 2229.
9 W. H. Knoth, *Inorg. Chem.*, 1971, **10**, 598.
10 J. Plesek, T. Jelinek, B. Stibr, and S. Hermanek, *J. Chem. Soc., Chem. Comm.*, 1988, 348.
11 T. Jelinek, S. Stibor, M. Holub, J. Bakardjiev, D. Hynk, D. L. Ormsby, C. A. Kilner, and M. Thornton-Pett, *J. Chem. Soc., Chem. Comm.*, 2001, 1756.
12 S. Stibor, O. L. Tok, W. Milius, J. Bakardjiev, M. Holub, D. Hynk, and B. Wrackmeyer, *Angew. Chem. Int. Ed. Engl.*, 2002, **41**, 2126.
13 S. R. Prince and R. Schaeffer, *J. Chem. Soc., Chem. Comm.*, 1968, 451.
14 W. L. Jolly, *Inorg. Synth.*, 1968, **11**, 33.
15 W. L. Jolly, *Inorg. Synth.*, 1968, **11**, 35.
16 W. L. Jolly, *Inorg. Synth.*, 1968, **11**, 39.
17 K. Shelly, D. C. Finster, Y. J. Lee, W. R. Scheidt, and C. A. Reed, *J. Am. Chem. Soc.*, 1985, **107**, 5955.
18 T. Jelinek, J. Plesek, S. Hermanek, and B. Stibr, *Collect. Czech. Chem. Commun.*, 1986, **51**, 819.
19 T. Jelinek, P. Baldwin, W. R. Scheidt, and C. A. Reed, *Inorg. Chem.*, 1993, **32**, 1982.
20 Z. Xie, C. W. Tsang, E. T. P. Sze, D. T. Yang, T. W. Chan, and C. W. Mak, *Inorg. Chem.*, 1998, **37**.
21 Z. Xie, C. W. Tsang, T. C. Xue, and C. W. Mak, *Inorg. Chem.*, 1997, **36**, 2246.
22 S. V. Ivanov, A. J. Lupinetti, J. S. Miller, O. P. Anderson, S. Solntsev, and H. Strauss, *Inorg. Chem.*, 1995, **34**, 6419.
23 Z. Xie, J. Manning, R. W. Reed, R. Mathur, A. Boyd, A. Benesi, and C. A. Reed, *J. Am. Chem. Soc.*, 1996, **118**, 2922.
24 A. Franken, B. T. King, P. Rao, B. C. Noll, and J. Michl, *Collect. Czech. Chem. Commun.*, 2001, **66**, 1238.
25 K. B., I. Zharov, and J. Michl, *Chemical Innovations*, 2001, 23.
26 K. Shelly and C. A. Reed, *J. Am. Chem. Soc.*, 1986, **108**, 3117.
27 Z. Xie, T. Jelinek, R. Bau, and C. A. Reed, *J. Am. Chem. Soc.*, 1994, **116**, 1907.
28 Z. Xie, R. Bau, A. Benesi, and C. A. Reed, *Organomet.*, 1995, **14**, 3933.
29 Z. Xie, D. J. Liston, T. Jelinek, V. Mitro, R. Bau, and C. A. Reed, *J. Chem. Soc., Chem. Comm.*, 1993, 384.
30 C. A. Reed, *Acc. Chem. Res.*, 1998, **31**, 133.
31 C. A. Reed, Z. Xie, R. Bau, and A. Benesi, *Science*, 1993, **262**, 402.
32 S. V. Ivanov, J. J. Rockwell, C. M. Polyakiv, O. P. Gaudinski, O. P. Anderson, S. Solntsev, and H. Strauss, *J. Am. Chem. Soc.*, 1998, **120**, 4224.
33 C. A. Reed, K. C. Kim, R. D. Bolskar, and L. J. Mueller, *Science*, 2000, **289**, 101.

[34] C. A. Reed, N. L. P. Fackler, K. C. Kim, D. Stasko, D. R. Evans, P. D. W. Boyd, and C. E. F. Rickard, *J. Am. Chem. Soc.*, 1999, **121**, 6314.
[35] J. W. Bausch, G. K. S. Prakash, G. A. Olah, D. S. Tse, D. C. Lorents, Y. K. Bae, and R. Malhorta, *J. Am. Chem. Soc.*, 1991, **113**, 3205.
[36] E. P. Kundig, C. M. Saudan, and G. Bernardinelli, *Angew. Chem. Int. Ed. Engl.*, 1999, **38**, 1220.
[37] D. A. Evans, T. Lectka, P. V. Matt, and S. J. Miller, *J. Am. Chem. Soc.*, 1999, **121**, 7559.
[38] N. J. Patmore, C. Hague, J. H. Cotgreave, M. F. Mahon, C. G. Frost, and A. S. Weller, *Chem. Eur. J.*, 2002, **9**, 2088.
[39] T. Marks and E. Chen, *Chem. Rev.*, 2000, **100**, 1391.
[40] J. Zhou, S. J. Lancaster, D. A. Walker, S. Beck, M. Thornton-Pett, and M. Bochmann, *J. Am. Chem. Soc.*, 2001, **123**, 223.

2 EXO-CLOSO CARBORANE COMPLEXES OF RHODIUM

2.1 Introduction

There are numerous examples of transition metal complexes incorporating polyhedral boranes and carboranes into their coordination sphere. [1, 2] While discussion of the structural diversity found across the periodic table for metallacarborane complexes is not warranted, the Reader should be aware that such diversity exists. The immediate discussion here will revolve around late transition metal complexes of carboranes, especially those of Rh(I) and Rh(III), and aims to give a feel for synthetic routes, bonding, typical solution state behaviour and some aspects of their reactivity.

Hawthorne[3-7] first developed the rhodium chemistry of the [*nido*-$C_2B_9H_{11}$]$^-$ carborane by synthesising complexes of the type [*exo*-$(Ph_3P)_2Rh$(*nido*-7,8-$C_2B_9H_{10}RR'$)] (**1**) [R=Me, R'=Ph], [R=R'=Me], [RR'=-$(CH_2C_6H_4CH_2)$-] and [RR'=-$(CH_2)_3$-] (Figure 2.1).

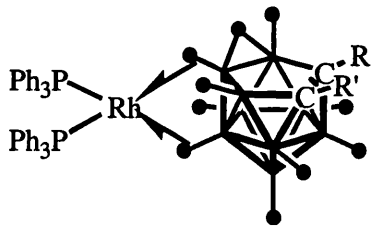

1

Figure 2.1: An *exo-nido* rhodacarborane.

The synthesis of **1** is achieved via a simple salt metathesis reaction of $[(Ph_3P)_3RhCl]$ and the Cs^+ salt of the carborane in a non-polar solvent, such as toluene (Equation 1.1).

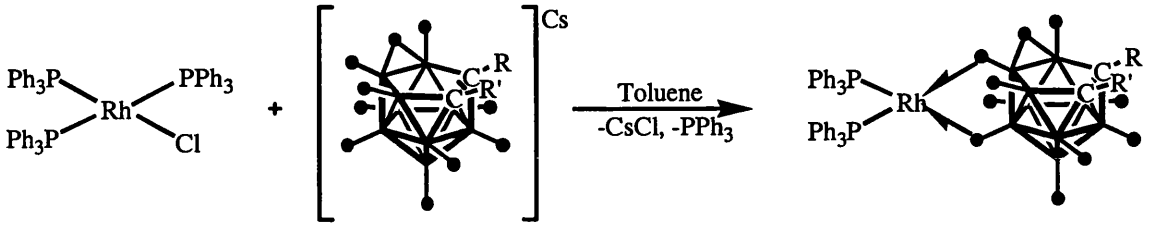

1

Equation 1.1: Synthesis of 1.

Precipitation of an insoluble metal halide (CsCl) provides the thermodynamic driving force for the reaction. The bonding between the cationic metal fragment and carborane anion is shown to be *via* two *exo* polyhedral 3 centre 2 electron interactions from terminal {B-H} vertexes.[3] These B-H-M bridges help to augment the electrostatic attraction between the anion/cation pair. Those {BH} units furthest from the {C-R} vertexes bind with the metal fragment preferentially. This is because they are the most nucleophilic, being richer in electron density than those nearer the more electronegative {C-R} vertexes.[8-11] In solution complexes of this type display an *exo-nido/closo* tautomerism whereby the $\{(Ph_3P)_2Rh\}^+$ fragment oxidatively adds to the B-H-B bridge of the carborane, resulting in a *closo* cluster complex, which contains a rhodium hydride. The equilibrium (Figure 2.2) is dependent on temperature, solvent and the nature of the R groups on the carborane.[5] Larger R groups tend to favour the *exo-nido* tautomer because the oxidative addition of the B-H-B bridge is inhibited due to steric interactions

between the bulky metal fragment and the carborane C-substituents. When the substituents are less bulky the *closo-* tautomer is favoured.

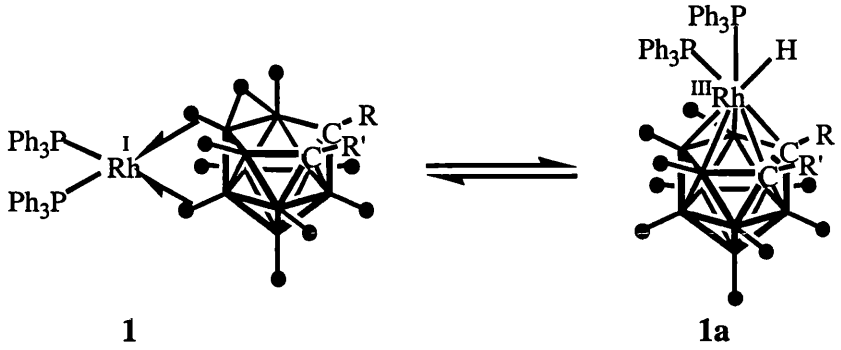

1 **1a**

Figure 2.2: *Exo-nido* to *closo* tautomerism exhibited by complex **1.**

Substitution with other groups such as thioether or phosphino groups at the cage carbon vertices alters the behaviour of *exo-nido* metallocarboranes significantly. Upon treatment of Cs[7-SPh-8-Ph-7,8-*nido*-$C_2B_9H_{10}$] or NR_4[7-PPh_2-8-Ph-7,8-*nido*-$C_2B_9H_{10}$] salts with $(Ph_3P)_3RhCl$ in toluene/ethanol, complexes of the type [*exo*-$(Ph_3P)_2$Rh-*nido*-7-SPh-8-Ph-7,8-$C_2B_9H_{10}$)] **(2)** and [*exo*-$(Ph_3P)_2$Rh-*nido*-7-PPh_2-8-Ph-7,8-$C_2B_9H_{10}$)] **(3)** can be obtained in good yield (Figure 2.3).[12] In these cases the carborane is bound to the rhodium through one 3c-2e B-H-Rh bond and by one Rh-P or Rh-S bond. The stronger interaction of the σ-donor atoms tethers the carborane to the metal inhibiting the ability of the metal centre to oxidatively add the B-H-B bond and convert to the *closo* tautomer. Thus the *exo* tautomers are generally favoured.

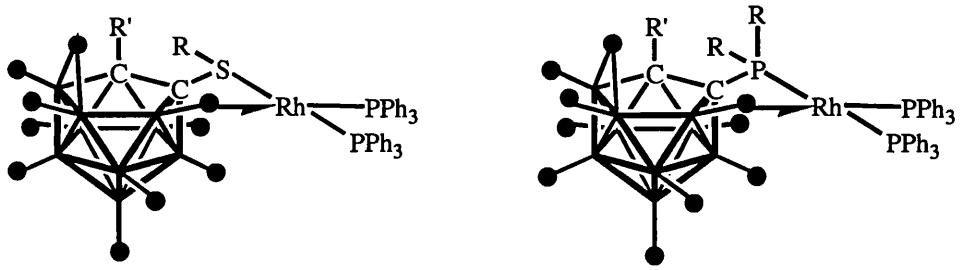

(2) (3)

Figure 2.3: Tethered *exo-nido* complexes.

Coordination of the anion [7-SR-8-R'-7,8- *nido*-$C_2B_9H_{10}$]$^-$ to a {Rh(cod)}$^+$ fragment has also been reported.[13] Thus the complex *exo-nido*[(cod)Rh(7-SPh-8-Me-7,8-$C_2B_9H_{10}$)] (**4**) (Figure 2.4) can be prepared in good yield *via* treatment of [Rh(acac)(cod)] with one equivalent of HBF_4 in THF followed by addition of the Cs^+ salt of the [7-SR-8-R'-7,8- *nido*-$C_2B_9H_{10}$]$^-$ anion.

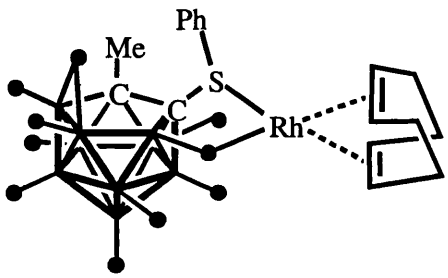

(4)

Figure 2.4: *exo*-[(cod)Rh(7-SPh-8-Me-7,8- *nido*-$C_2B_9H_{10}$)]

Isomerisation of (**4**) to a *closo* isomer (Figure 2.5), (**4a**), occurs in CH_2Cl_2 solution over a 24h period. This isomerisation is irreversible unlike the tautomerism exhibited by complex (**1**). Mechanistically it has been shown[13] that the isomerisation occurs *via*

oxidative addition of a B-H-Rh bond across the Rh(I) centre to give a coordinatively unsaturated Rh(III) hydrido fragment. Insertion of the hydride into a Rh-olefin bond results in the formation of a highly reactive 14e Rh(III) fragment. Migration of the bridging B-H-B proton into the B-Rh bond forces the rhodium fragment to take up a facial η^5 bonding mode on the top face of the *nido* cluster, accompanied by several 1,3-hydride shifts in the cod ligand to give an η^3 allyl capped rhodium.

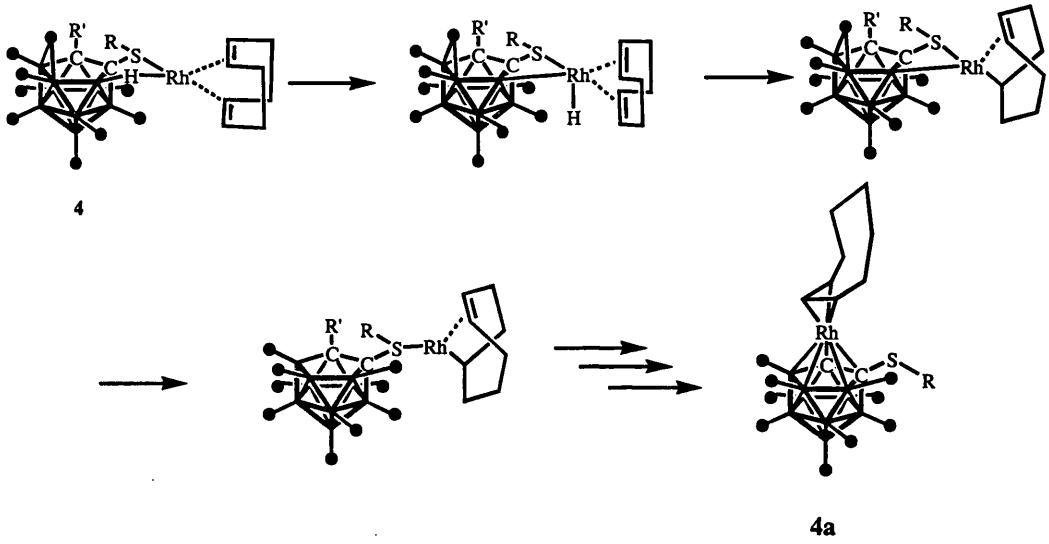

Figure 2.5: Isomerisation of *exo-nido*-[(cod)Rh(7-SPh-8-Ph-7,8-$C_2B_9H_{10}$)]

Complexes (**1**), (**2**) and (**4**) are all fluxional in solution. Complex (**3**) is static, however. The $^{31}P\{^1H\}$ NMR spectrum for complex (**2**) displays a broad peak at room temperature which becomes two doublet of doublets at low temperature. Two mechanisms, possibly operating in tandem (Figure 2.6) can be proposed for the fluxionality. The loss of ^{109}Rh-^{31}P coupling suggests rapid breaking and reforming of Rh-PPh_3 bonds is occurring (Path way A). In addition the B-H-Rh bond could break followed by rapid rotation around the remaining S-Rh bond (Pathway B).

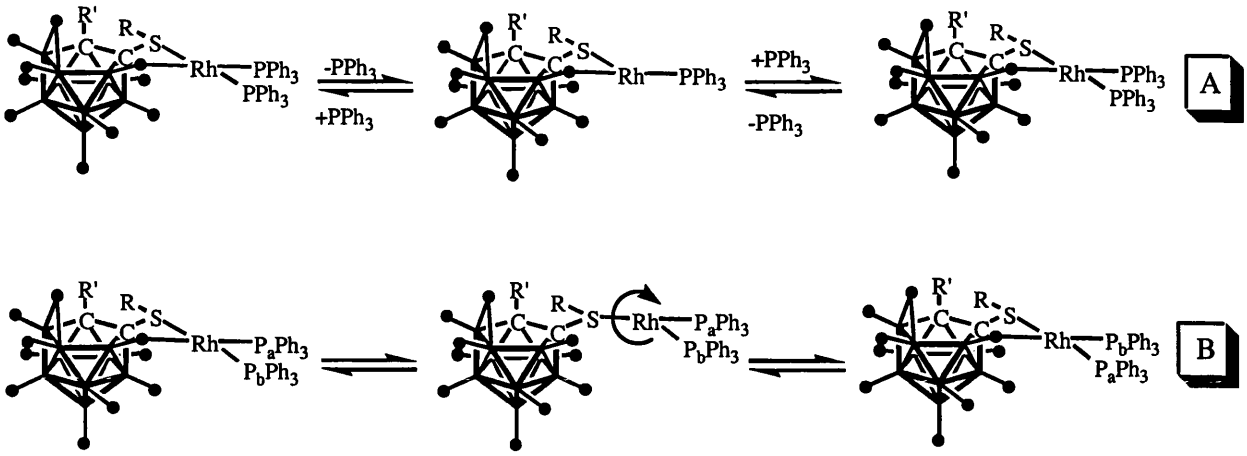

Figure 2.6: Fluxionality proposed for (**2**)

Complex (**4**) is fluxional as evidenced by two broad resonances in the ^{1}H NMR spectrum for the olefinic protons at room temperature. At low temperature four olefinic protons are resolved. The fluxionality occurs via breaking of the B-H-Rh bond followed by rotation around the S-Rh bond in a similar process as outlined for complex (**2**). For complex **1** only one well-resolved phosphorous environment is observed in the room temperature $^{31}P\{^{1}H\}$ NMR spectrum. In this case (Figure 2.7) the phosphines must remain bound to the metal center because no loss of ^{109}Rh-^{31}P coupling is seen. Rapid movement of the $\{(Ph_3P)_2Rh\}^+$ fragment over the polyhedral surface of the cage coupled with rotation around the Rh-H-B bond results in the phosphines becoming equivalent. Even at low temperatures this fluxional process persists, indicating that this it is of very low energy.

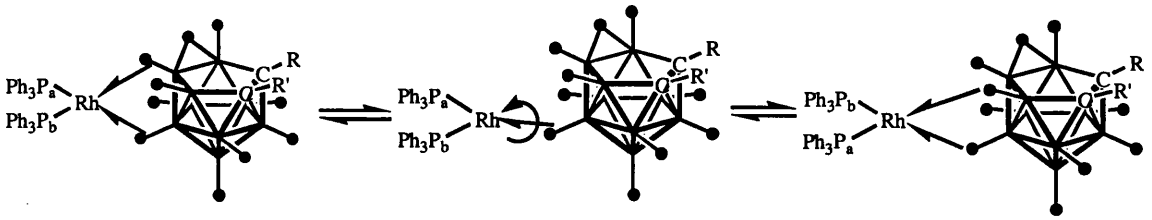

Figure 2.7: Proposed mode of fluxionality in (**1**).

Closo-metallacarboranes have been partnered with cationic metal fragments. Stone[14] has demonstrated that the anion $[Re(CO)_3(\eta^5\text{-}7,8\text{-}C_2B_9H_{11})]^-$ interacts with $\{(Ph_3P)_2Rh\}^+$ and $\{(Ph_3P)_2RuCl\}^+$ fragments *via* 3c-2e interactions (Figure 2.8) to give $[Re(CO)_3(\eta^5\text{-}2,3,10\text{-}(\mu\text{-}H)_3\text{-}exo\text{-}\{RuCl(PPh_3)_2\}\text{-}closo\text{-}7,8\text{-}C_2B_9H_8)]$ (**5**) and $[Re(CO)_3(\eta^5\text{-}2,10\text{-}(\mu\text{-}H)_2\text{-}exo\text{-}\{Rh(PPh_3)_2\}\text{-}closo\text{-}7,8\text{-}C_2B_9H_8)]$ **6** respectively.

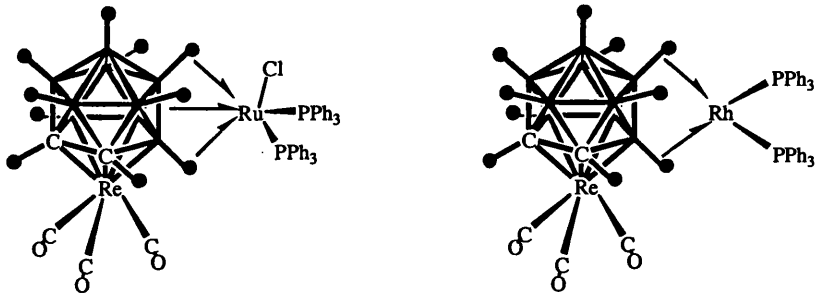

(**5**) (**6**)

Figure 2.8: *closo*-metallacarboranes with *exo*-$\{ML_n\}^+$ fragments.

The synthesis of **6** is achieved in a similar procedure as outlined in Equation 2.1 for complex **1**. The reaction between the $Cs[Re(CO)_3(\eta^5\text{-}7,8\text{-}C_2B_9H_{11})]$ and $(Ph_3P)_3RhCl$ in CH_2Cl_2 gives (**6**) in good yield along with the elimination of CsCl and PPh_3. Solution studies on these complexes indicate that they are fluxional with the mechanism for this

proposed to be similar to that of the *exo-nido* complexes discussed for (**1**). Other, monoanionic *closo*-carborane complexes are known. [*closo*-$CB_{11}H_{12}]^-$ has been coordinated to a $\{(cod)Rh\}^+$ fragment. Synthesis of [*closo*-$CB_{11}H_{12}Rh(cod)]$ (**7**), is achieved by reaction of Ag[*closo*-$CB_{11}H_{12}]$ with $[(COD)RhCl]_2$ in CH_2Cl_2 (Figure 2.9).[15]

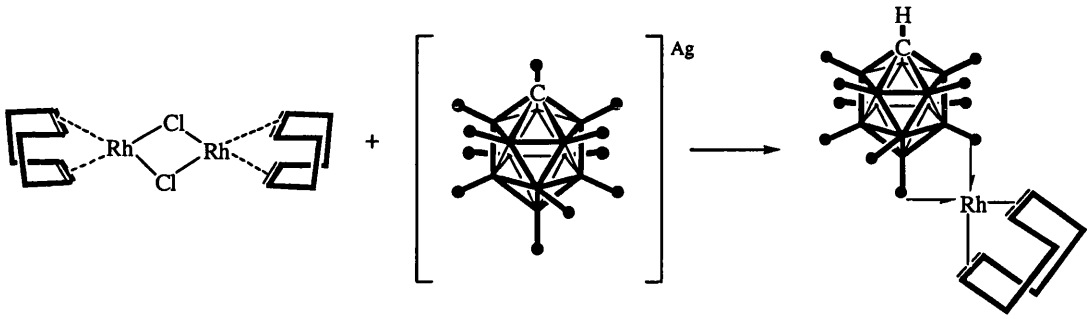

(7)

Figure 2.9: Synthesis of [*closo*-$CB_{11}H_{12}Rh(cod)]$

In the solid-state the cage is shown to be bound to the metal fragment through two 3c-2e B-H-M bonds *via* the antipodal (B12) B-H and one B-H vertex on the lower pentagonal belt. Like other *exo-closo* metallacarboranes the molecule is fluxional in solution, as determined by ^1H and ^{11}B NMR spectroscopy. Three peaks are observed for the carborane cage in a 5:5:1 ratio, two of which are shifted upfield due to coordination to the metal centre. Procession of the $\{(cod)Rh\}^+$ fragment over the lower pentagonal belt protons *via* an intermediate (Figure 2.10) where one B-H-M bond breaks, followed by rapid rotation around the remaining B(12)-H-M bond was proposed as a mechanism to account for the observed NMR spectra.

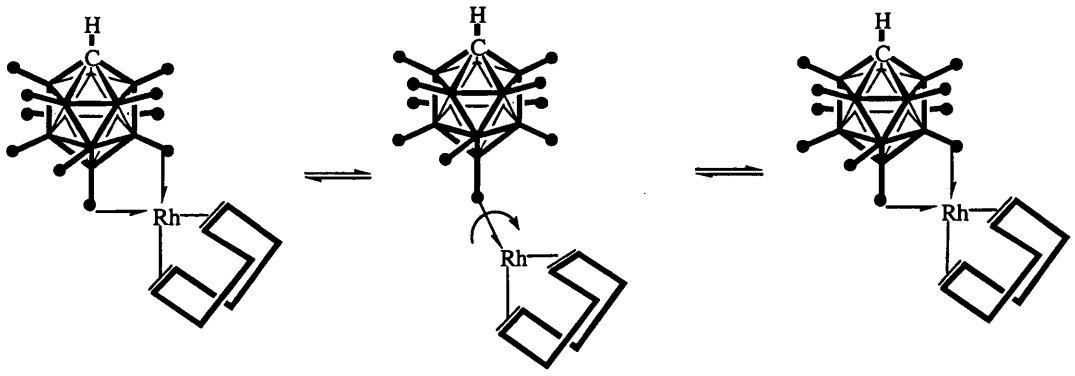

Figure 2.10: Proposed mechanism of fluxionality in [(COD)Rh(*closo*-$CB_{11}H_{12}$].

The labile nature of the B-H-Rh interactions is further demonstrated by the displacement of the carborane by donor solvent molecules such as THF to yield [(COD)Rh$(THF)_2$][*closo*-$CB_{11}H_{12}$]. $\{(Ph_3P)Ag\}^+$, $\{(Ph_3P)_2Ag\}^+$, $\{Cp(CO)_3Mo\}^+$, $\{Cp_2ZrMe\}^+$ fragments have also been shown to form complexes via 3c-2e.

Ortho-*closo*-carboranes of the type shown in Figure 2.11 have also been partnered with cationic rhodium fragments.

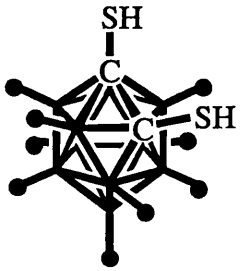

Figure 2.11: Substituted 1,2-dicarba-*closo*-dodecacarboranes.

In the case of the 1,2-dicarba-*closo*-dodecaborane-1,2-dithiolate ligand, half-sandwich complexes **(8)** (Figure 2.12) were prepared and were shown to undergo B-H bond

activation in the presence of acetylenes.[16, 17] Initial insertion of the acetylene into a Rh-S bond followed by direct oxidative addition of a B-H bond across the Rh(I) centre is responsible for the observed reaction. Such transition metal promoted B-H activations are not without precedent. Hawthorne has shown that *exo-nido* complexes will hydroborate butylacrylates[18] whilst Sneddon has shown that $Cp_2Ti(CO)_2$, H_2PtCl_4 and

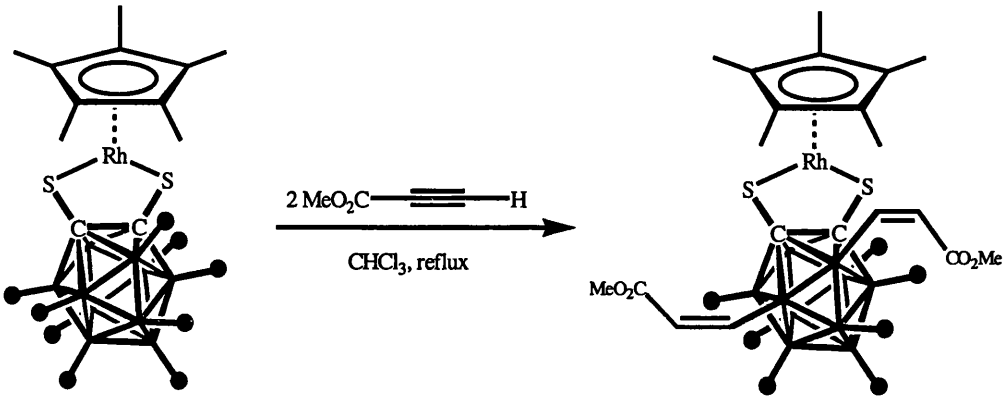

(8)

Figure 2.12: B-H activation of closo-carboranes

$PdBr_2$ catalyse the hydroboration of decaborane with various olefins.[19, 20] Interestingly, the proposed mechanism for hydroboration (Figure 2.13) with $Cp_2Ti(CO)_2$ is suggested to involve a transition state having a 3c-2e B-H-Ti bond with donation of electron density from a B-H bonding orbital to the metal centre. The activated B-H bond then undergoes facile insertion of an olefin.

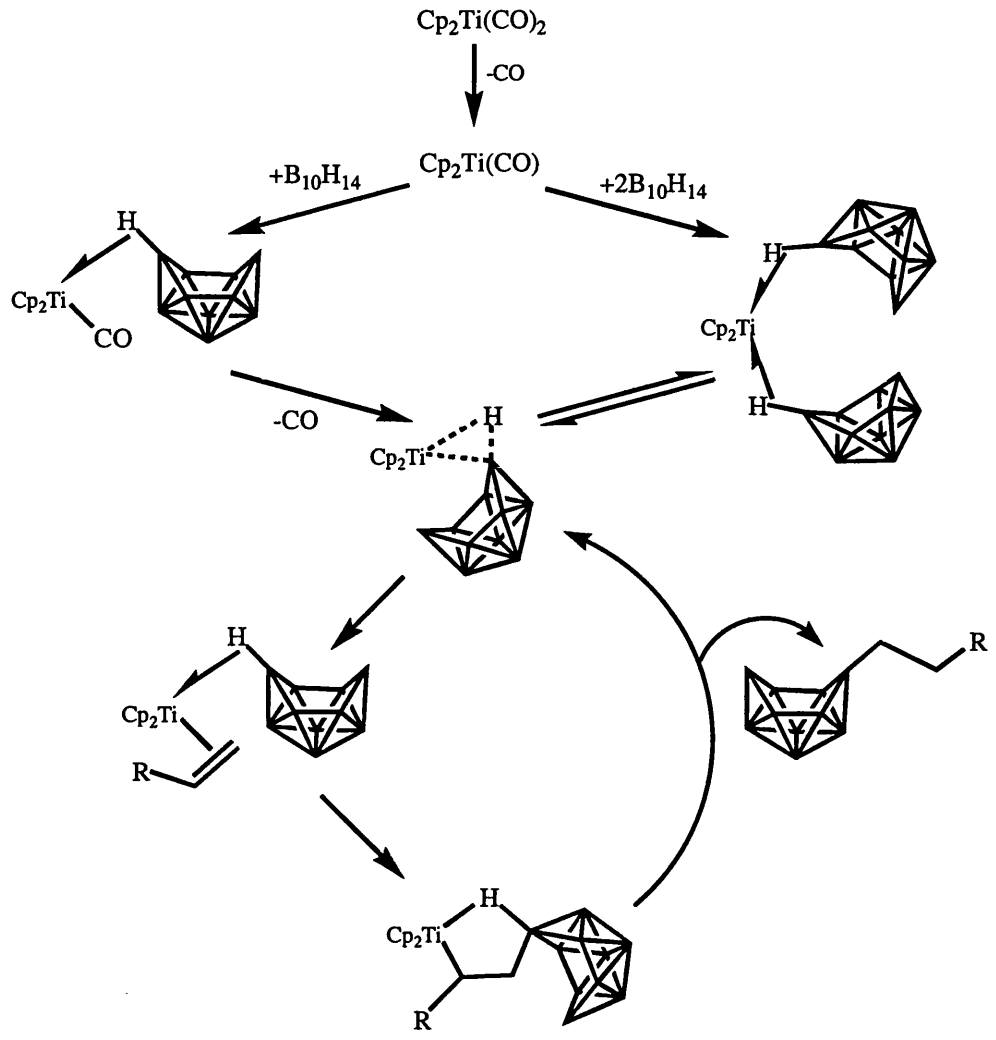

Figure 2.13: Hydroboration mediated by Cp_2TiCO_2

In the case of the Pt and Pd catalysts direct oxidative addition of a B-H bond occurs, presumably via an initial H-B-M 3c-2e bond.

Exo-nido complexes of the type described thus far have been tested for their utility in several catalytic reactions mediated by other rhodium-based catalysts. Hydrogenation of olefins has received much attention[21, 22] while hydrosilation,[22, 23] hydrogenation of ketones [23], alkene isomerisation[21] and cyclopropanation[24] have also been investigated.

The detailed mechanisms operating for olefin isomerisation and hydrogenation in complexes of the type [*closo*-3,3-$(PPh_3)_2$-3-H-3,1,2-$RhC_2B_9H_{11}$] were thoroughly elucidated by Hawthorne.[4, 21] It is now recognized that the precursor to the active catalytic species involved in hydrogenation is in fact an *exo-nido* tautomer formed in equilibrium from the *closo* precursor. Oxidative addition of a B-H bond across a Rh(I) centre generates, in low concentrations, complexes containing a B-M σ-bond. It is these species that are attributed to the catalytic activity (Figure 2.14).

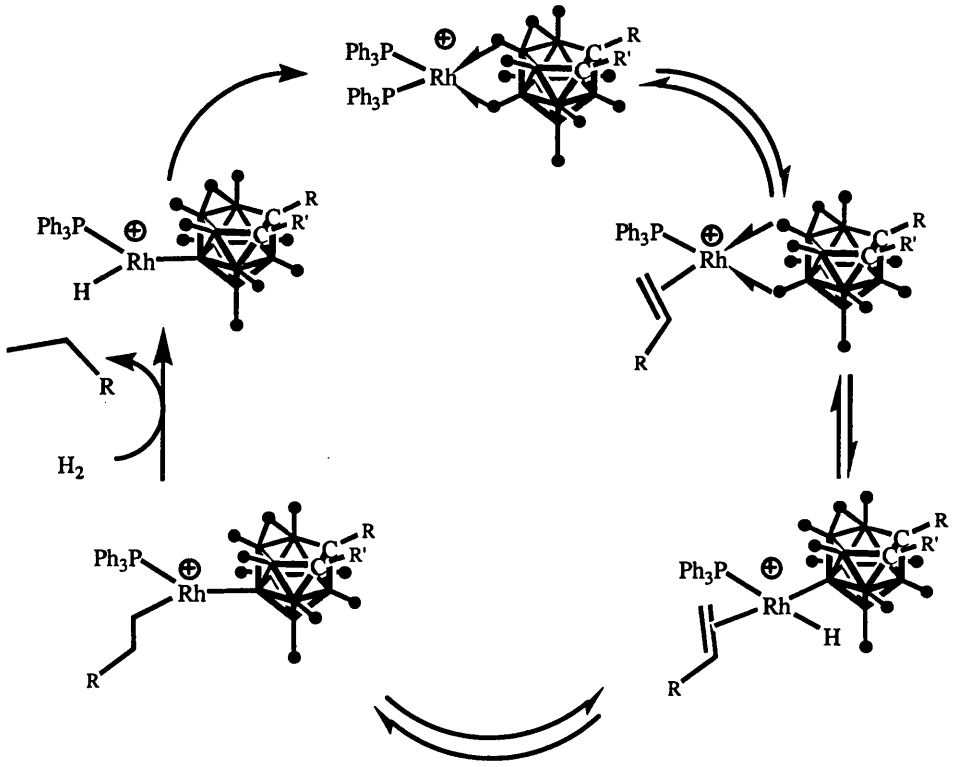

Figure 2.14: Simplified scheme for catalytic hydrogenation of olefins employing [*closo*-3,3-$(PPh_3)_2$-3-H-3,1,2-$RhC_2B_9H_{11}$] as precursors.

Teixidor has shown that complex **2** is an excellent catalyst for the hydrogenation of 1-alkenes.[12] Complex **2** was shown to be eight times more effective in hydrogenating 1-

hexene than the well-known Wilkinson's complex and also a more active hydrogenation catalyst than complex **1**. The increased activity of this catalyst is based upon two factors. Firstly, the thioether moiety tethers the metal fragment to the carborane, which inhibits *exo-nido* to *closo* tautomerism. As discussed the catalytic activity is attributed to B-Rh^{III}-H species generated by oxidative addition of a B-H vertex across the rhodium centre. Such oxidative addition would be less likely if *closo-* tautomers are present in solution. Secondly, the B-H-M bridge is formed through the top belt of the *nido-* cage which is thought to produce a more reactive complex than if the less active lower belt vertices are used in binding to the rhodium. The enhanced activity is further demonstrated by the activity complex **4** displays for the hydrogenation of the internal alkene cyclohexene. At 20 atm of H_2 and 25°C, complex **4** will give a 32% yield of cyclohexane. Complexes **1** and **2** will not reduce cyclohexene at all. It has also been demonstrated that the *closo-* isomer of complex **4a** (Figure 2.5) is an active catalyst for the hydrogenation of cyclohexene giving an 82% conversion under identical conditions. A different mechanism must be operating which has been proposed to involve a η^3 to η^1 rearrangement of the allyl ligand followed by oxidative addition of H_2 to the metal centre. Whatever the mechanism the striking difference in activities that can be achieved by simple modulation of the metallic fragment is interesting.

The partnering of *nido-* or *closo-* carboranes with electrophilic metal fragments is interesting from a fundamental point of view where investigations into bonding and reactivity can be made. Given that [*closo*-$CB_{11}H_{12}]^-$ and its derivatives have been identified as very weakly coordinating anions[25] we were interested in investigating the

chemistry of these anions with $\{L_2Rh\}^+$ fragments where L = phosphine. Combined with the fact that *exo-nido* and tethered *exo-nido* complexes discussed are catalytically active species in a range of organic transformations it seemed likely that *exo-closo* complexes would be catalytically active and might even exhibit superior activity than those described to date. This chapter deals with the synthesis of a series of novel *exo-closo* carborane complexes partnered with $\{L_nM\}^+$ fragments, while chapter 4 develops their reactivity and use in catalysis.

2.2 RESULTS AND DISCUSSION

2.2.1 Norbornadiene Precursor Complexes

Driven by a need to prepare metallocarborane complexes partnered with weakly coordinating anions it seemed desirable to have an air-stable feed-stock from which the metallacarboranes could be synthesized. An attractive aspect of the Schrock-Osborn cationic rhodium catalysts is that air-stable pre-catalysts such as $[(L)_2Rh(nbd)][Y]$ (L=phosphine, Y=anion) can readily be prepared.[26, 27] In such a system both phosphine and anion are easily modulated allowing the preparation of a large library of air-stable metallacarborane precursors. Complexes of the type $[(Ph_3P)_2Rh(nbd)][Y]$ are prepared in good yield via reaction of $(Ph_3P)_3RhCl$ with the appropriate Cs[Y] salt in the presence of 2,5-norbornadiene in a 3:1 mixture of CH_2Cl_2/acetone (Equation 2.2.1).

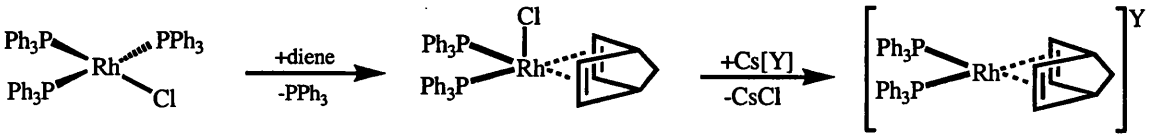

Equation 2.2.1: Synthesis of precursors

After filtration of the orange solution the complexes are crystallized in high purity by addition of ethanol and cooling to -30°C overnight. The compounds $[(Ph_3P)_2Rh(nbd)][Y]$, Y = [*closo*-$CB_{11}H_{12}]^-$ **(I)**, [*closo*-$CB_{11}H_{11}Br]^-$ **(II)**, [*closo*-$CB_{11}H_6Br_6]^-$ **(III)**, [*closo*-$HCB_{11}Me_{11}]^-$ **(IV)** and $[\{B[C_6H_3(CF_3)_2]_4\}]^-$ **(V)** were all prepared in this way. Complexes **(I)**-**(V)** all display a doublet in their $^{31}P\{^1H\}$-NMR

spectra centered at δ 30.5 ppm [J(RhP) 155 Hz]. The ^{11}B-NMR spectra are consistent with the uncoordinated anion for each respective complex. For **I** three doublet resonances in the ratio 1:5:5 are observed centered at δ -7.3, -13.6 and -16.4 ppm, assigned to B(12), B(7-11) and B(2-6) respectively. For **II** the antipodal B(12)-Br resonance is observed as a singlet at δ -3.2 ppm with the B(7-11) and B(2-6) as doublet resonances at δ -12.7 and -17.1 ppm respectively. These are also in a 1:5:5 ratio. For **III** both the B(12) and B(7-11) resonances are observed as singlets at δ 1.7 and -6.6 ppm respectively with the B(2-6) resonance observed as a doublet at δ -17.1 ppm. Complex **IV** displays three singlet resonances at δ 2.5 B(12), -5.5 B(7-11) and –8.9 B(2-6) ppm respectively. To confirm the structural metrics of these precursors, the molecular structure of **IV** was determined and is shown in Figure 2.2.1 with selected bond lengths and angles displayed in Table 2.2.1. The bond lengths and angles are unremarkable and are fully consistent with other structurally characterised $[(PPh_3)_2Rh(nbd)]^+$ fragments.[28]

Modulation of the phosphine L can be achieved in a number of ways. Treatment of $[(nbd)RhCl]_2$ with Ag^+ salts of the appropriate carborane in the presence of excess 2,5-norbornadiene results in the formation of $[(nbd)_2Rh]^+$ cations. Treatment of these complexes with 2 equivalents of tertiary or 1 equivalent of a chelating phosphine results in the formation of cationic $[(PR_3)_2Rh(nbd)]^+$ fragments (Equation 2.2.2).[29]

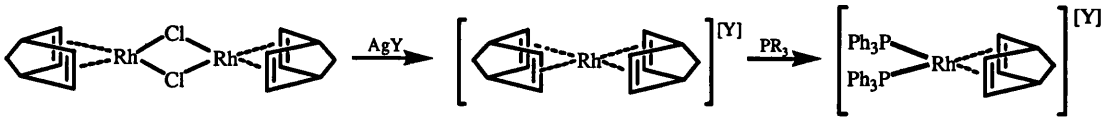

Equation 2.2.2: Variation of L in $[L_2Rh(diene)][Y]$ complexes.

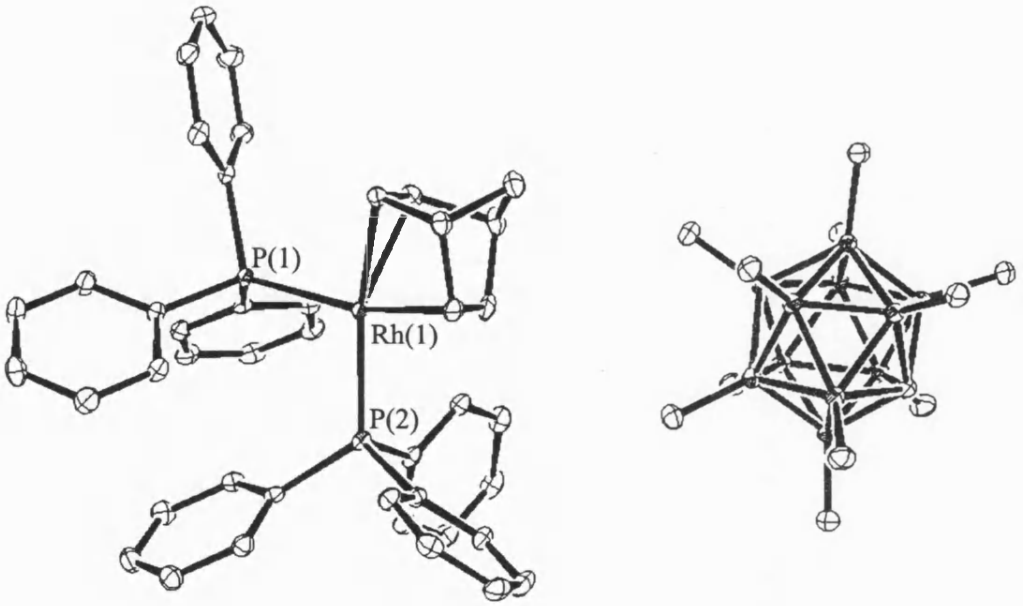

Rh(1)-P(1)	2.3300(5)
Rh(1)-P(2)	2.3621(5)
P(1)-Rh(1)-P(2)	98.513(18)

Table 2.2.1: Relevant bond lengths (Å) and angles(°) for complex **IV**

Figure 2.2.1: ORTEP drawing of complex **IV**. Ellipsoids are drawn at the 30% probability level. All hydrogens have been omitted for clarity.

A further, simpler method, involves treating $[(nbd)RhCl]_2$ with the relevant Ag^+ salt in THF and treating the resulting THF complex generated *in-situ* with the appropriate phosphine.[30] Another synthetic route utilizes the carborane adduct itself as a precursor. Addition of PR_3 to [(cod)Rh(*closo*-$CB_{11}H_{12}$)] in CH_2Cl_2 results in the clean formation of the salt $[(R_3P)_2Rh(cod)][Y]$. In these ways the new complexes $[(Cy_3P)_2Rh(nbd)][closo\text{-}CB_{11}H_{12}]$ **VI**, [(dppe)Rh(nbd)][*closo*-$CB_{11}H_{12}$] **VII** and $[\{(MeO)_3P\}_2Rh(cod)][closo\text{-}CB_{11}H_{12}]$ **VIII** have been prepared. Compounds **VI**, **VII** and **VIII** show ^{11}B spectra assigned to free [*closo*-$CB_{11}H_{12}]^-$ as found for **I-V**. In the ^1H-NMR spectra the cage C-H resonances are all observed at δ 2.21 ppm, as found for **I**. The $^{31}P\{^1H\}$ NMR spectra of all three complexes show a single phosphorous environment displaying ^{109}Rh-^{31}P coupling. Complexes **I** to **VIII** form a useful starting point for examining the formation of *exo-closo* metallacarboranes as discussed next.

2.2.2 $[(Ph_3P)_2Rh(closo\text{-}CB_{11}H_{12})]$, IX

Treatment of a stirred CH_2Cl_2 solution of **I** with H_2 results in the reduction of the diene, evidenced by ^1H NMR spectroscopy in CD_2Cl_2 by the formation of norbornane, and subsequent coordination of the [*closo*-$CB_{11}H_{12}]^-$ anion to the $\{(Ph_3P)_2Rh\}^+$ fragment generated *in situ*. The reaction was accompanied by a colour change from orange to deep red. Layering the reaction mixture with hexanes resulted in the formation of large red blocks of [$(Ph_3P)_2Rh$(*closo*-$CB_{11}H_{12}$)], **IX**, in good yield (Figure 2.2.2).

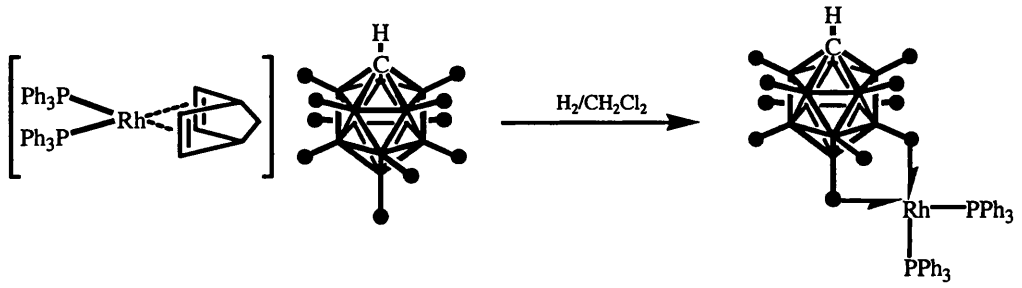

Figure 2.2.2: Synthesis of complex **IX**

Complex **IX** was fully characterized by X-ray crystallography, elemental analysis and multinuclear NMR spectroscopy. The solid-state structure of complex **IX** is shown in Figure 2.2.2 with relevant bond lengths and angles given in Table 2.2.2. The $\{(Ph_3P)_2Rh\}^+$ fragment in **IX** is coordinated with the cage via two three-centre-two-electron B-H-Rh bonds. It was possible to locate the {CH} vertex of the carborane by inspection of its thermal parameters and bond lengths to neighbouring atoms. The cage bonds, as expected, via the most basic [BH(12)] and one of the lower pentagonal belt vertices[8, 31] giving the molecule approximate C_S symmetry in the solid state. The rhodium(I) centre adopts a pseudo square planer geometry as reflected in the P(1)-P(2)-B(12)-B(7) dihedral angle of 7.35°. The two Rh-B distances are similar, [Rh(1)-B(7) 2.359(3) Å and Rh(1)-B(12) 2.407(3) Å]. These bond lengths are comparable to those observed in [(cod)Rh(*closo*-$CB_{11}H_{12}$)][15] [2.391(3) and 2.385(3) Å], and similar to those found in [*exo-nido*-6,10-{$(PPh_3)(PCy_3)Rh$}-6,10-μ-$(H)_2$-7,8-μ-(1',2'-$CH_2C_6H_4CH_2$)-7,8-$C_2B_9H_8$][32] [2.338(8) and 2.398(8) Å].

In solution the $\{Rh(PPh_3)_2\}^+$ fragment is fluxional over the surface of the cage as evidenced by local C_{5v} symmetry for the cage being observed in both the $^{11}B\{^1H\}$ and

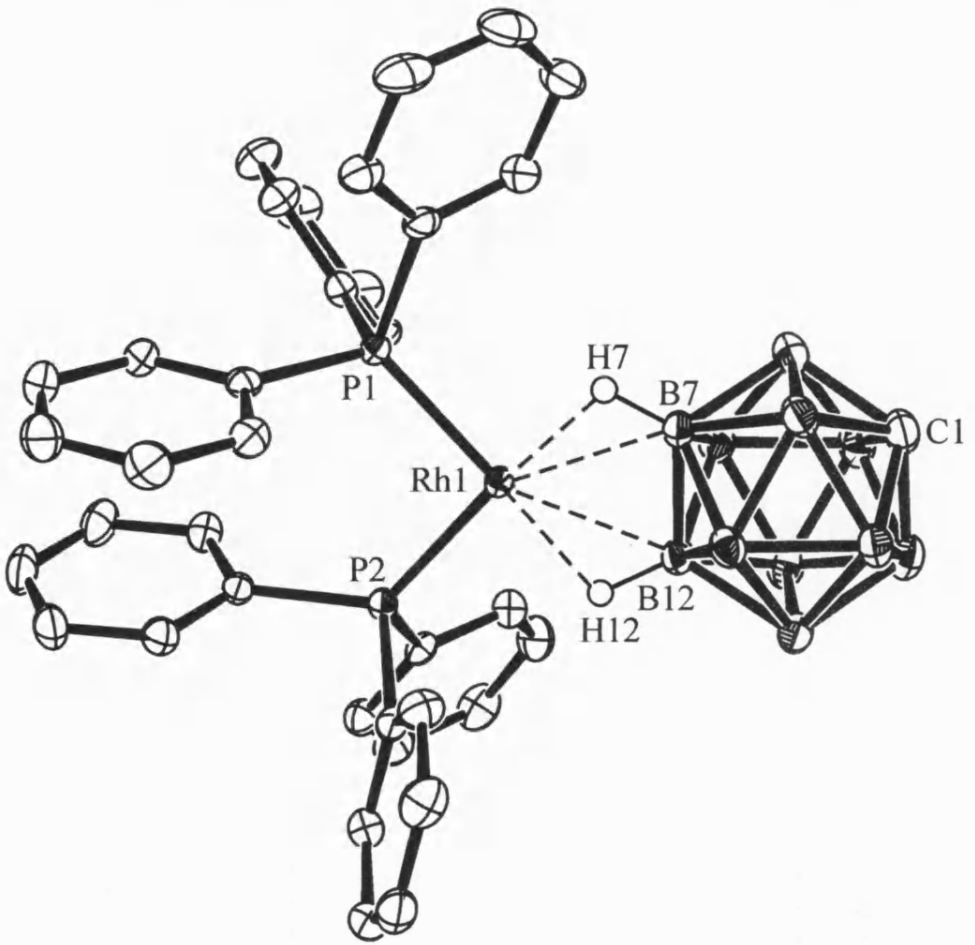

Rh1-P1	2.2192(6)
Rh1-P2	2.2391(6)
Rh1-B7	2.359(3)
Rh1-B12	2.407(3)
P1-Rh1-P2	95.73(2)
P2-Rh1-B7	150.39(7)
P2-Rh1-B12	107.98(6)
P1-Rh1-B7	113.88(7)
P1-Rh1-B12	155.46(6)
B7-Rh1-B12	42.57(9)

Table 2.2.2: Selected bond lengths (Å) and angles (°) for complex **IX.**

Figure 2.2.2: ORTEP drawing of $[(Ph_3P)_2Rh(CB_{11}H_{12})]$, **IX**, Ellipsoids are drawn at the 30% probability level. Hydrogen atoms apart from H(7) and (12) are omitted for clarity.

$^1H\{^{11}B\}$ NMR spectra which is different to the approximate C_s symmetry observed in the solid-state. Thus in the $^1H\{^{11}B\}$ NMR spectrum of **XI** at room temperature three signals for cage {B-H} vertexes are observed at δ 1.70, -0.02 and -1.97 ppm in a 5:5:1 ratio. The latter two are shifted to higher field compared with **I**, the upfield shift of those {B-H} vertexes involved in agostic bonding has been demonstrated previously[15] and is discussed in more detail in section 2.2.7. Thus the integral 5 peak at δ –0.02 ppm can be assigned as the {B(7-11)H} protons and the integral 1 peak at δ –1.97 ppm being assigned as the antipodal {B(12)H} vertex with the {B(2-6)H} protons relatively unchanged, indicating they are not interacting with the rhodium. The signal corresponding to the cage C-H is observed as a broad peak δ 2.60 ppm shifted by 0.40 ppm downfield compared with **I** upon coordination to the rhodium fragment. The ^1H and $^{11}B\{^1H\}$ NMR spectra of **IX** are displayed in Figure 2.2.3, below.

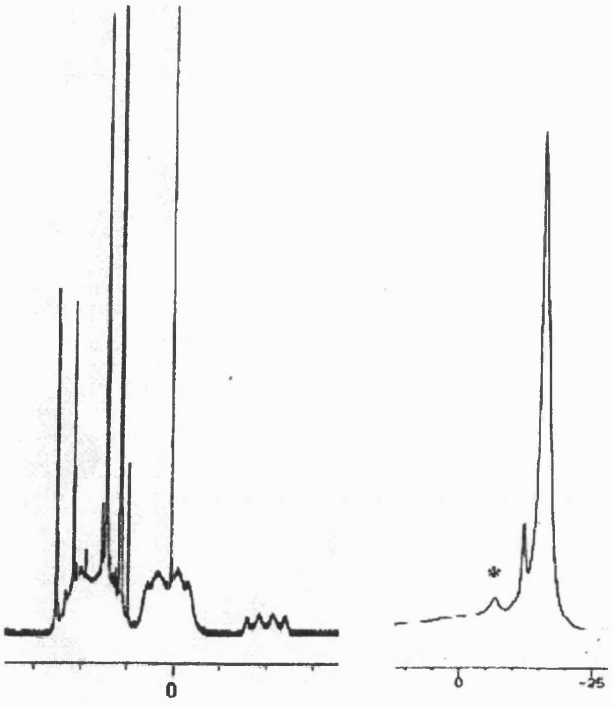

Figure 2.2.3: ^1H (left) and $^{11}B\{^1H\}$ (right) NMR spectra of **IX**.

In the ^{1}H NMR spectrum of **IX** the peaks assigned to the {B-H} vertexes appear as well-resolved broad quartets. The ^{11}B-^{1}H coupling constant for BH(12) is reduced from 143 Hz in complex **I** to 119Hz in **IX** which reflects the weakening of the B-H bond upon coordination to the metal. The [JBH(7-11)] coupling constant is also reduced from 136 Hz in **I** to 97 Hz in complex **IX**. The reduced coupling constant compared to that of a two-centre two-electron bond mirrors the reduction in ^{13}C-^{1}H coupling found for C-H-M agostic linkages *versus* C-H bonds,[33] and is consistent with the interactions observed in the solid state for **XI** persisting in solution. In the $^{11}B\{^{1}H\}$ NMR spectrum three environments are seen at δ -9.9, -13.5 and -14.1 ppm in the ratio 1:5:5 (Figure 2.2.3), showing local C_{5v} symmetry for the cage. The upfield shifts again reflecting the coordination of the metal to the carborane. The $^{31}P\{^{1}H\}$ NMR spectrum displays a single phosphorus environment at δ 49.0 ppm [J(RhP) = 149 Hz]. All these spectroscopic markers suggests the metal is fluxional over the surface of the cage in solution as observed for other $\{L_2M\}$ fragments coordinated to [*closo*-$CB_{11}H_{12}]^-$,[15] [*nido*-$C_2B_9H_{11}]^-$,[6] and the mechanism will be discussed in more detail in section 2.2.6.

2.2.3 [(dppe)Rh(closo-$CB_{11}H_{12}$)], X

Treatment of complex **VII** with H_2 in CH_2Cl_2 results in reduction of the diene to give [(dppe)Rh(*closo*-$CB_{11}H_{12}$)], **X**, in quantitative yield as evidenced by $^{1}H\{^{11}B\}$, ^{1}H, ^{11}B and $^{31}P\{^{1}H\}$ NMR spectroscopy (Figure 2.2.4). Despite repeated attempts crystals suitable for a single crystal X-ray diffraction study could not be grown, however the characterization is unambiguous based on the NMR data. The $^{31}P\{^{1}H\}$ NMR spectrum

of **X** displays one phosphorous environment at δ 80.3 ppm [J(RhP) = 189 Hz] indicating that the phosphines are equivalent in solution and that the metal fragment must be fluxional over the surface of the cage. In the $^{1}H\{^{11}B\}$ NMR spectrum three resonances are observed for the {B-H} protons in a 5:5:1 ratio at δ 1.80, 0.41 and -1.40 ppm, assigned as [BH(2-6)], [BH(7-11)] and [BH(12)] respectively. The B(12)-H coupling constant [J(BH) = 116 Hz] is some 20 Hz smaller than that of uncoordinated [*closo*-$CB_{11}H_{12}]^-$. These resonance all resolve to broad quartets in the ^{1}H NMR spectrum.

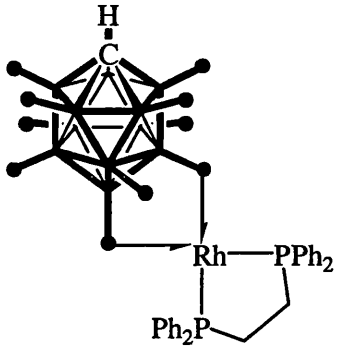

Figure 2.2.4: Schematic representation of complex **X**.

The ethylene backbone in the dppe ligand is observed as a doublet of doublets at δ 2.13 [J(PH) = 21 Hz, $^{3}J(PH)$ = 1.6 Hz]. The {C-H} vertex is observed as a broad singlet at δ 2.55 ppm, shifted by 0.35 ppm downfield compared to that of free [*closo*-$CB_{11}H_{12}]^-$. The $^{11}B\{^{1}H\}$ NMR spectrum displays one broad peak assigned as a 1:5:5 coincidence which becomes a doublet [J(BH) = 121Hz] in the ^{11}B NMR spectrum. This data is consistent with coordination of the $\{(dppe)Rh\}^+$ fragment to the carborane *via* 3c-2e bonds. In this case the {B(12)H} and {B(7-11)H} vertexes are shifted upfield in both the ^{11}B NMR and the ^{1}H NMR spectra indicating that these vertices are interacting with the metal

fragment. The high symmetry of the NMR spectra (C_{5v} symmetry for the cage) indicates that the complex is fluxional in solution. The mechanism of this fluxionality is discussed in more detail in section 2.2.6.

2.2.4 [{(MeO)$_3$P}$_2$Rh(closo-CB$_{11}$H$_{12}$)], XI

Treatment of a stirred solution of complex **VIII** with H_2 in CH_2Cl_2 results in the clean formation of [{(MeO)$_3$P}$_2$Rh(*closo*-CB$_{11}$H$_{12}$)], complex **XI.** The conversion is quantitative according to $^{31}P\{^1H\}$, ^1H and ^{11}B NMR spectroscopy. Despite repeated efforts crystals suitable for a structure determination could not be grown. The bright yellow complex (Figure 2.2.5) is highly air-sensitive and requires careful manipulation under anaerobic conditions.

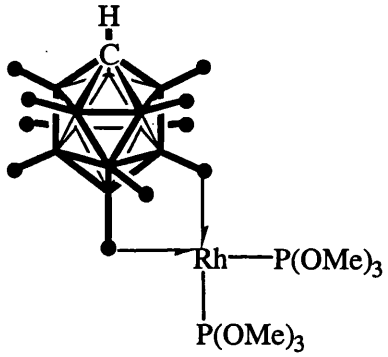

Figure 2.2.5: Schematic representation of complex **XI**

The ^1H NMR spectrum of **XI** reveals three {B-H} environments at δ 1.81, 0.22 and -2.45 ppm observed as quartets in a 5:5:1 ratio, assigned as [B*H*(2-6)], [B*H*(7-11)] and [B*H*(12)] respectively. The [BH(12)] coupling constant [J(BH) 120 Hz] is reduced by

some 15 Hz compared to that of uncoordinated [*closo*-$CB_{11}H_{12}]^-$. The {C-H} vertex is seen at δ 2.56 ppm, a downfield shift of 0.26 ppm compared to uncoordinated [*closo*-$CB_{11}H_{12}]^-$. The $^{11}B\{^1H\}$ NMR spectrum contains two, almost coincident resonances at δ -15.0 and -16.0 ppm. The {B(12)} and {B(7-11)} vertices being shifted upfield due to interaction with the rhodium. The $^{31}P\{^1H\}$ NMR spectrum displays one environment at δ 126 ppm [J(RhP) = 294 Hz]. The high symmetry and chemical shifts observed in the ^{11}B and ^1H NMR spectra for the cage in this complex suggests that the $\{P(OMe_3)_2Rh\}^+$ fragment is fluxional over the surface of the polyhedral carborane. The fluxionality is discussed in more detail in section 2.3.6.

2.2.5 [$(Cy_3P)_2$Rh(*closo*-$CB_{11}H_{12}$)], XII

Treatment of a stirred solution of **VI** with H_2 in CH_2Cl_2 results in the quantitative formation of [$(Cy_3P)_2$Rh(*closo*-$CB_{11}H_{12}$)], **XII,** as evidenced by ^1H, $^{31}P\{^1H\}$ and ^{11}B NMR spectroscopy. Deep red, single crystals of **XII** were grown by slow evaporation of a CH_2Cl_2 solution under a flow of argon. The molecular structure of **XII** is shown in Figure 2.2.6 and relevant bond lengths and angles are given in Table 2.2.3. The $\{(Cy_3P)_2Rh\}^+$ fragment is coordinated to the carborane via two 3c-2e bonds. The Rh-P bond lengths [2.2770(10) and 2.2630(11) Å] are slightly longer than those observed in [*cis*-$\{PCy_3\}_2$(acac)Rh] [2.252(1), 2.260(1) Å].[34] The Rh-B bond lengths [Rh(1)-B(7) 2.393(5) Å and Rh(1)-B(8) = 2.389(5) Å] are very similar to those found for complex **IX** [2.359(3) and 2.407(3) Å] and almost identical to those found for [(cod)Rh(*closo*-$CB_{11}H_{12}$)][15] [2.391(3) and 2.385(3) Å]. The rhodium adopts a pseudo square planer geometry as reflected in the P(1)-P(2)-B(12)-B(7) dihedral angle of 5.6°. Assignment of

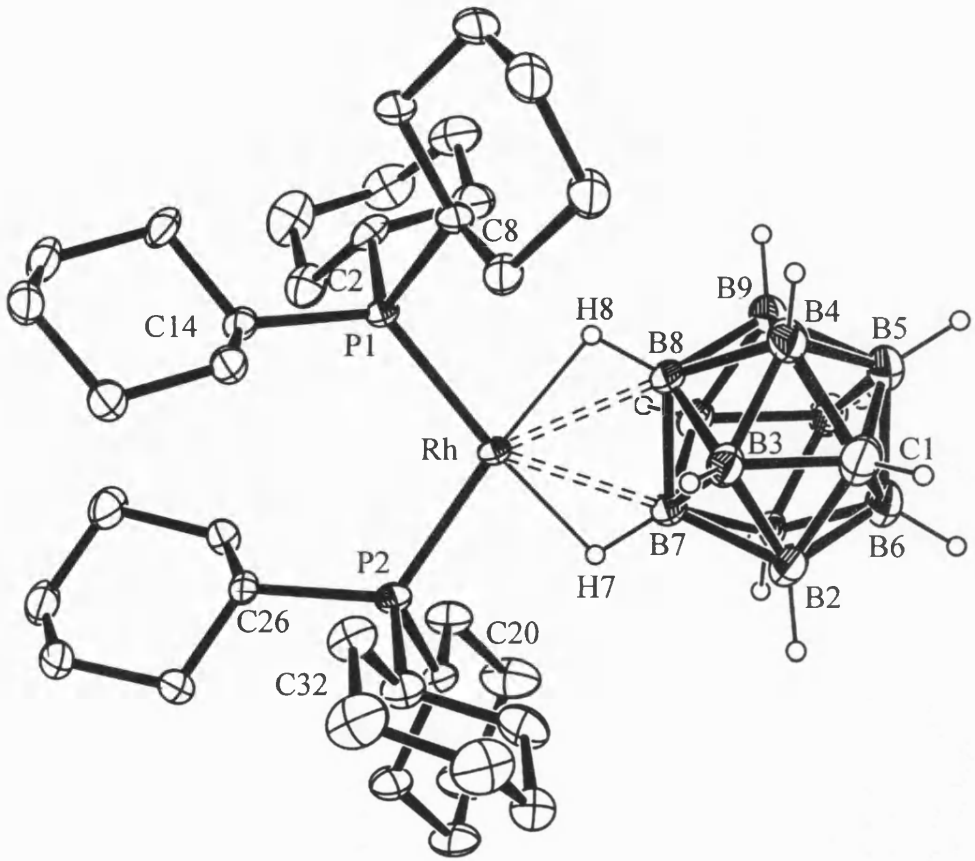

Rh1-P1	2.277(10)
Rh1-P2	2.263(11)
Rh1-B7	2.393(5)
Rh1-B8	2.389(5)
C1-B6	1.707(7)
C1-B2	1.738(7)
C1-B3	1.710(7)
C1-B4	1.742(8)
C1-B5	1.727(10)
P2-Rh1-B8	147.46(12)
P1-Rh1-B8	105.62(12)
P2-Rh1-B7	105.61(13)
P1-Rh1-B7	147.79(13)
P2-Rh1-P3	106.55(4)
B8-Rh1-B7	42.24(16)

Table 2.2.3: Selected Interatomic distances (Å) and Angles (°) for complex **XII**.

Figure 2.2.6: ORTEP drawing of complex **XII**. Cyclohexyl hydrogens have been omitted for clarity. Ellipsoids are drawn at the 30% probability level. Two cyclohexyl groups [C(26) and C(32)] are disordered, with the major (57%) component shown.

the {C-H} vertex was slightly more problematic than for **IX** due to a poorer quality data set. Analysis of several crystallographic markers were examined in order to locate the {C-H} vertex. Perhaps the most useful marker in determining the location of the {C-H} vertex is the bond length between the carbon atom and the upper pentagonal {BH} vertices. For example in complex **IX** the B-C bonds are all consistently about 0.08 Å shorter than the B-B bonds, as expected. In complex **XII** the bond distances to C(1) are consistently smaller than other bond distances in the cage only when the [BH(8)] and [BH(7)] vertices are assigned as those binding to the rhodium. The average {C(1)-B} length being 1.725 Å versus and average of 1.767 Å for other bond distances within the cage. Systematic assignment of cage heteroatoms as carbons and freely refining the site occupancy resulted in C(1) having the highest occupancy factor (0.93). The parameter αR_2 also reduces slightly but significantly only when this vertex is assigned as carbon. Coordination of the [*closo*-$CB_{11}H_{12}]^-$ anion to give the 7,8 isomer (Figure 2.2.7) is unusual because it is generally accepted that carboranes bind *via* the most electron rich {B-H} vertexes which are normally those furthest from the {C-H} vertex.[9, 10, 31] This assumption is supported by several crystallographically (including this work) characterized examples where the carborane is shown to bind via {B(12)-H} for monodendate complexes[9, 35] and through {B(12)-H} and {B(7)-H} for bidendate systems.[8, 15]

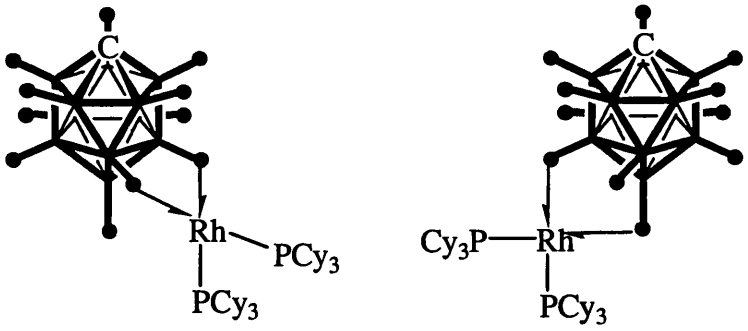

7,8 7,12

Figure 2.2.7: 7,8- and 7,12 isomers of complex **XII.**

DFT calculations on the model system $[(Me_3P)_2Rh(closo\text{-}CB_{11}H_{12})]$ at the B3LYP/DZVP level show that there is only a minimal energy difference between the expected 7,12 isomer and the 7,8 isomer with the 7,12 isomer being favored by just $1kcal^{-1}$. Additionally, the 2,7 and the 2,3 isomers are calculated to be about 6 $kcal^{-1}$ higher in energy. The fact that the 7,8 isomer is essentially as energetically favourable as the 7,12 isomer suggests that both could be present in solution and that assignment of the 7,8 isomer in **XII** is perfectly reasonable. Implications of this in the fluxional processes occurring in solution are discussed in the following section.

Spectroscopic markers indicate that the solid state structure, i.e. the 7,8 isomer, is not retained in solution. In the $^1H\{^{11}B\}$ NMR spectrum the {B(7-11)H} vertices are shifted upfield to δ -0.62 as well as the antipodal {B(12)H} vertex shifted upfield to δ -2.32 ppm. The {B(2-6)H} vertexes are obscured under the PCy_3 resonances. In the ^1H NMR spectrum the {B(12)H} resonance becomes a well-defined broad quartet with J(BH) = 130 Hz smaller by some 15Hz to that of uncoordinated $[closo\text{-}CB_{11}H_{12}]^-$. The {C-H} vertex resonates at δ 2.50 ppm, a downfield shift of 0.30 ppm compared to that of

uncoordinated [*closo*-$CB_{11}H_{12}]^-$. The $^{11}B\{^1H\}$ NMR spectrum displays two resonances in the ratio 1:10, at δ -11.2 ppm assigned as B(12), and δ -16.7 ppm assigned as coincident (B2-6) and B(7-11) vertices due to the upfield shift of the lower pentagonal belt {BH} vertexes upon coordination to the rhodium centre. The two resonances become well-defined doublets in the ^{11}B NMR spectrum with J(BH) 130 Hz for the resonance assigned as {B(12)}. The $^{31}P\{^1H\}$ NMR spectrum exhibits one phosphorous environment at δ 56.7 ppm with J(RhP) = 190Hz. Thus NMR data shows that on the NMR timescale the metal fragment interacts with all of the lower pentagonal belt protons as evidenced by the higher than expected symmetry observed in both the ^1H and ^{11}B NMR spectra. A mechanism where all the lower pentagonal belt protons may become equivalent, which is observed for complexes **IX, X, XI** and **XII**, is proposed in the following section.

2.2.6 Fluxional dynamics of [*closo*-$CB_{11}H_{12}]^-$ complexes

Complexes **IX, X, XI** and **XII** are all fluxional with respect to the movement of the $\{L_2Rh\}^+$ fragment over the polyhedral surface of the cage on the NMR timescale at room temperature. The ^{11}B and ^1H NMR spectra of these complexes display C_{5v} symmetry on the basis that only three {B-H} environments are observed, while X-ray studies show C_s symmetry. The $^{31}P\{^1H\}$ NMR spectra also show only one environment in all cases regardless of phosphine, and all retain ^{109}Rh-^{31}P coupling showing that any fluxional mechanism must retain a Rh-P bond, discounting a mechanism that involves rapid making and breaking of Rh-P bonds. The postulated mechanism for the fluxionality of

similar complexes e.g. [(cod)Rh(*closo*-$CB_{11}H_{12}$)][15] has been proposed to occur via a mechanism whereby the most basic [BH(12)] vertex remains bound to the metal centre and the {B(7)-H} vertex breaks allowing free rotation around the M-H-B bond (Figure 2.2.8).

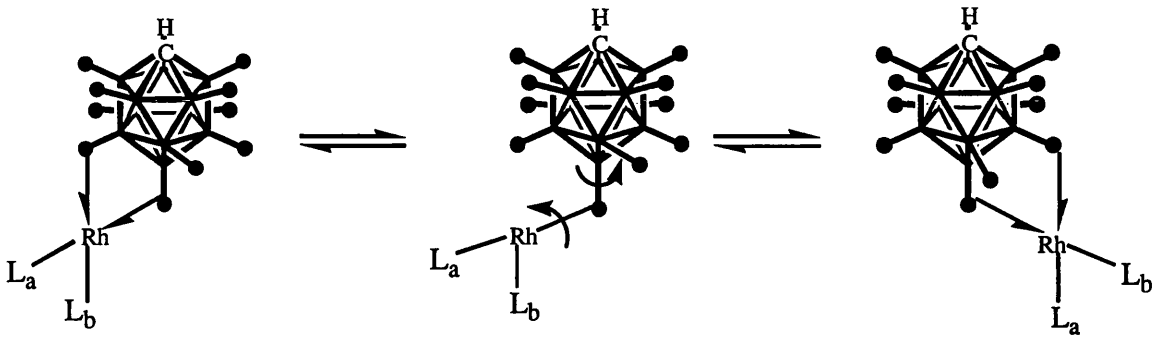

Figure 2.2.8: Fluxional mechanism proposed for [$(L)_2$Rh(closo-$CB_{11}H_{12}$)].

Rotation around the Rh-H vector has the effect of making the phosphines (L_a and L_b) equivalent whilst rotation around the B-H vector allows another {B-H} vertex to coordinate to the metal centre. This process is assumed to be very fast on the NMR timescale given that the NMR spectra are generally well resolved even at low temperature. The *exo-nido* systems **1** as discussed in section 2.1 and figure 2.6 are also fluxional via a similar mechanism, as are the *exo-closo* complexes **5** and **6**. Given the solid-state structural determination of a 7,8 isomer for an *exo-closo* metallacarborane and the supporting calculations, which suggest there is minimal difference in energy between the 7,12 and 7,8 isomers, there becomes the possibility of isomers of this type being involved in the fluxional process itself. The 7,8 isomer could then be proposed (Figure 2.2.9) as an intermediate in the conversion of 7,12 $\Leftrightarrow$ 8,12 $\Leftrightarrow$ 9,12 in solution.

The fluxional process is extremely facile indicating that any energy barriers to potential transition states would be very low.

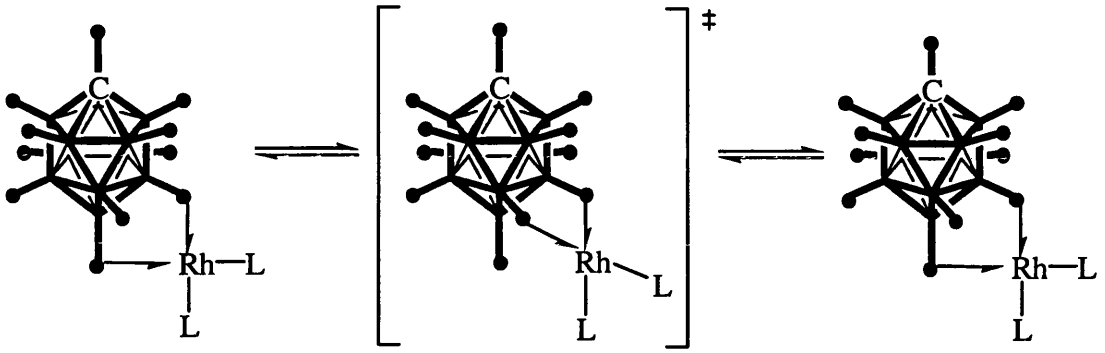

Figure 2.2.9: Potential mode of fluxionality for *exo-closo* metallacaroranes *via* a 7,8 intermediate

Although this intermediate state is not observed in solution it is perfectly reasonable to assume that it can be accessed in the fluxional process. This is especially so as this isomer is observed in the crystallographically characterized [$(Cy_3P)_2Rh$(*closo*-$CB_{11}H_{12}$] and on the basis of the DFT calculations. Thus there are two reasonable modes of fluxionality to account for the observed dynamic processes occurring in solution.

2.2.7 Chemical shift changes as markers for *closo*-carborane coordination

Large upfield shifts in both ^{11}B and ^{1}H NMR spectra are now well documented for *closo*- carboranes coordinating to transition metal centres[15, 36] and the results presented here are in full accord with this. These upfield shifts are consistent with the fact that the ^{11}B chemical shift is sensitive to both coordination environment and its orbital

characteristics, both of which are expected to change significantly on coordination to a metal centre.[11] Table 2.2.4 shows relevant ^{1}H and ^{11}B NMR data for several transition metal fragments coordinated to [*closo*-$CB_{11}H_{12}$]$^{-}$. The ^{11}B chemical shift change ($\Delta\delta$ ^{11}B) on coordination of the metal fragment always shows an upfield shift of the B(12) vertex with a smaller shift for B(7-11) and very little change for B(2-6). Although chemical shifts of these types of complexes can be calculated[37] there seems to be no correlation with J(HB) or with the ^{1}H or ^{11}B chemical shifts. For example [(Ph_3P)Ag(*closo*-$CB_{11}H_{12}$)] and [$Cp(CO)_3Mo$(*closo*-$CB_{11}H_{12}$] both show comparable changes in chemical shift of the ^{11}B vertices but [(Ph_3P)Ag(*closo*-$CB_{11}H_{12}$)] displays no highfield resonances for the bridging Ag-*H*-B proton.

	δ (^{1}H) (CH) ppm[a]	δ (^{1}H) BH (ppm)[b]	J(BH) Hz	$\Delta\delta$ (^{11}B)(ppm)[c]		
				B(12)	B(7-11)	B(2-6)
{(cod)Rh}$^{+}$	2.61	*-3.92*, 0.06, 1.66	109	-8.9	-1.9	-0.2
{(PPh_3)$_2$Rh}$^{+}$	2.58	*-1.97*, -0.02, 1.70	119	-9.9	-13.5	-14.1
{(Cy_3P)$_2$Rh}$^{+}$	2.50	*-2.32*, -0.62	135	-6.1	3.1	0.3
{(dppe)Rh}$^{+}$	2.55	*-1.40*, 0.41, 1.80	116	-8.4	-2.1	-0.7
{($(MeO)_3P_2$Rh}$^{+}$	2.55	*-2.45*, 0.22, 1.81	120	-7.7	-2.4	-0.4
{$Cp(CO)_3$Mo}$^{+}$	2.53	*-15.11*, 1.79, 1.66	87	-6.2	-1.2	0.6
{(PPh_3)Ag}$^{+}$	2.59	*2.34*, 1.94, 1.76	118	-6.1	-0.7	-1.3
{(PPh_3)$_2$Ag}$^{+}$	2.21	*2.21*, 1.85, 1.58	128	-0.9	0.1	0.7

[$Cp(CO)_3$Mo(*closo*-$CB_{11}H_{12}$)][35], [Ag(PPh_3)$_n$(*closo*-$CB_{11}H_{12}$)] (n=1, 2)[37], [(cod)Rh(*closo*-$CB_{11}H_{12}$)][15]. All measured in CD_2Cl_2 or $CDCl_3$ solutions.

[a] δ(^{1}H) CH for uncoordinated [*closo*-$CB_{11}H_{12}$] = 2.20 ppm.
[b] Antipodal vertex in italics.
[c] Chemical shift change from uncoordinated [*closo*-$CB_{11}H_{12}$]$^{-}$ [δ -7.3, -13.6, -16.4 ppm].

Table 2.2.4: Selected ^{1}H and ^{11}B NMR data for metallocarboranes

However, [$Cp(CO)_3Mo$(*closo*-$CB_{11}H_{12}$)], displays a highfield resonance at –15 ppm for the bridging Mo-*H*-B proton with a much reduced J(BH) coupling of 87Hz. Another useful spectroscopic marker for coordination of the carborane to a metal fragment is the small downfield shift in the ^{1}H NMR of the {C*H*} vertex by 0.3 - 0.4 ppm. These spectroscopic markers are useful indicators as to which vertices of the carborane are interacting with the metal fragment and can also give some information regarding the nature of the interaction. For example [(cod)Rh(*closo*-$CB_{11}H_{12}$)] displays a large upfield shift of the a [BH(12)] resonance in the ^{1}H NMR spectrum along with a significant reduction in J(BH) compared to that of uncoordinated [*closo*-$CB_{11}H_{12}]^-$, which suggests a relatively strong interaction between carborane and metal fragment. However, [$(PPh_3)_2Ag(CB_{11}H_{12})$] shows almost no change in the chemical shift of the [B(12)-*H*] vertex and only a very small reduction in the J(BH) coupling constant suggesting that the cation/anion interaction is much weaker in this case. Structural studies support this data. [(cod)Rh(*closo*-$CB_{11}H_{12}$)] is a closely associated ion pair while [$(PPh_3)_2Ag(CB_{11}H_{12})$] is a dimer with bridging carboranes.

2.2.8 [$(Ph_3P)_2$Rh(*closo*-$CB_{11}H_{11}Br$)], XIII

Treatment of a stirred CH_2Cl_2 solution of **II** with H_2 resulted in the reduction of the diene as evidenced by appearance of norbornane in ^{1}H NMR spectrum and subsequent coordination of the [*closo*-$CB_{11}H_{11}Br]^-$ anion to the rhodium to afford [$(Ph_3P)_2Rh(CB_{11}H_{11}Br)$], **XIII**. The reaction was accompanied by a colour change from orange to deep red. Despite repeated attempts, crystals suitable for an X-ray diffraction

study could not be grown. However NMR spectroscopy reveals the gross structural motifs in **XIII**. In the $^{1}H\{^{11}B\}$ NMR spectrum two resonances δ 1.72 and -0.46 ppm in a 5:5 ratio are observed and assigned as [B(2-6)*H*] and [B(7-11)*H*] respectively. The large upfield shift of the [B*H*(7-11)] protons compared to that of complex **II** is indicative of coordination of the metal fragment as discussed previously. A small downfield shift of the {C-H} vertex of 0.32 ppm is also observed consistent with coordination of the metal fragment. This shift is similar in magnitude to the downfield shift of the {C-H} vertex in complex **IX** [0.40 ppm]. In the ^{1}H NMR spectrum of **XIII** two broad quartets are observed for the {B-H} protons. The coupling constant for [BH(7-11)] is reduced from 141 Hz in complex **II** to 128 Hz in complex **XIII**. In the $^{11}B\{^{1}H\}$ NMR spectrum three resonances are observed at δ -1.6, -14.8 and -17.2 ppm assigned as B(12), B(7-11) and B(2-6) respectively. The antipodal {B-Br} vertex is apparently shifted downfield whilst the [BH(7-11)] vertexes are shifted by some 2.1ppm upfield when compared to the uncoordinated $[CB_{11}H_{11}Br]^{-}$ in complex **II**. The $^{31}P\{^{1}H\}$ NMR spectrum displays one phosphorous environment at δ 45.0 ppm and also shows coupling to rhodium [J(RhP) = 193 Hz]. For this complex it appears that the cage binds via the lower pentagonal belt protons and that the complex is fluxional in solution as evidenced by the high symmetry of the cage suggesting that some process operates whereby the $\{(Ph_3P)_2Rh\}^{+}$ fragment migrates around the lower pentagonal belt of the carborane cage. No evidence for interaction of the upper pentagonal belt vertexes is seen. A possible structure (Figure 2.2.10) for complex **XIII** is one whereby two 3c-2e bonds are formed from the lower pentagonal belt vertices.

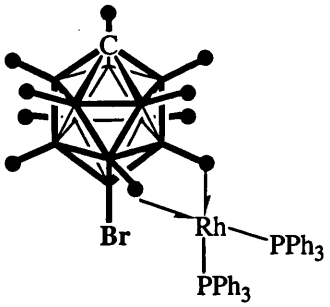

Figure 2.2.10: Suggested structure of **XIII.**

Two mechanisms to account for the fluxionality in complex **XIII** can be postulated. Breaking of one of the B-H-M bonds followed by rotation around the remaining B-H-M bond (Figure 2.2.11) would equivalence the phosphines and allows the carborane to recoordinate *via* a different {BH} vertex. An alternative mechanism whereby the B-Br vertex coordinates weakly to the metal center and remains bound whilst the lower pentagonal belt protons rapidly exchange is an attractive proposal. The small downfield shift of the B(12)-Br resonance suggests perhaps this vertex is bonding but the downfield shift could equally arise due to the coordination of the lower pentagonal belt vertices to the metal perturbing the B(12) resonance. Alternatively both mechanisms could be operating.

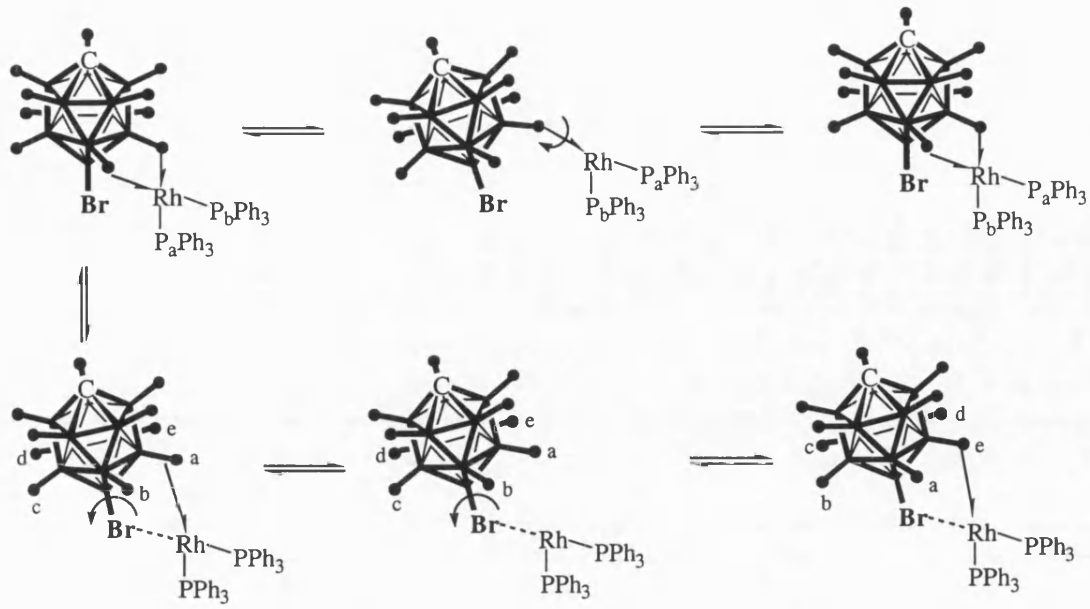

Figure 2.2.11: Possible mechanisms for the fluxionality in **XIII.**

It should be noted that the $[CB_{11}H_{11}Br]^-$ anion has been shown to coordinate to the $\{Cp(CO)_3Mo\}^+$ fragment via the {B-Br} vertex.[38] In solution it was shown that only 5% of the {B(7)H} isomer was present. Therefore the interaction of the {BBr} vertex with the $\{(Ph_3P)_2Rh\}^+$ fragment is perfectly feasible.

2.2.9 $[(Ph_3P)(PPh_2\text{-}\eta^6\text{-}C_6H_5)Rh]_2[closo\text{-}CB_{11}H_6Br_6]_2$, XIV

Treatment of complex **III** with H_2 in CH_2Cl_2 results in a colour change from orange to red and the formation of $[(Ph_3P)(PPh_2\text{-}\eta^6\text{-}C_6H_5)Rh]_2[closo\text{-}CB_{11}H_6Br_6]_2$, complex **XIV**, in essentially quantitative yield by $^{31}P\{^1H\}$ and ^1H NMR spectroscopy. The complex was crystallised by layering a CH_2Cl_2 solution of complex **XIV** with hexanes. The solid-state structure (Figure 2.2.12) of **XIV** shows a dimeric phenyl bridged motif. The

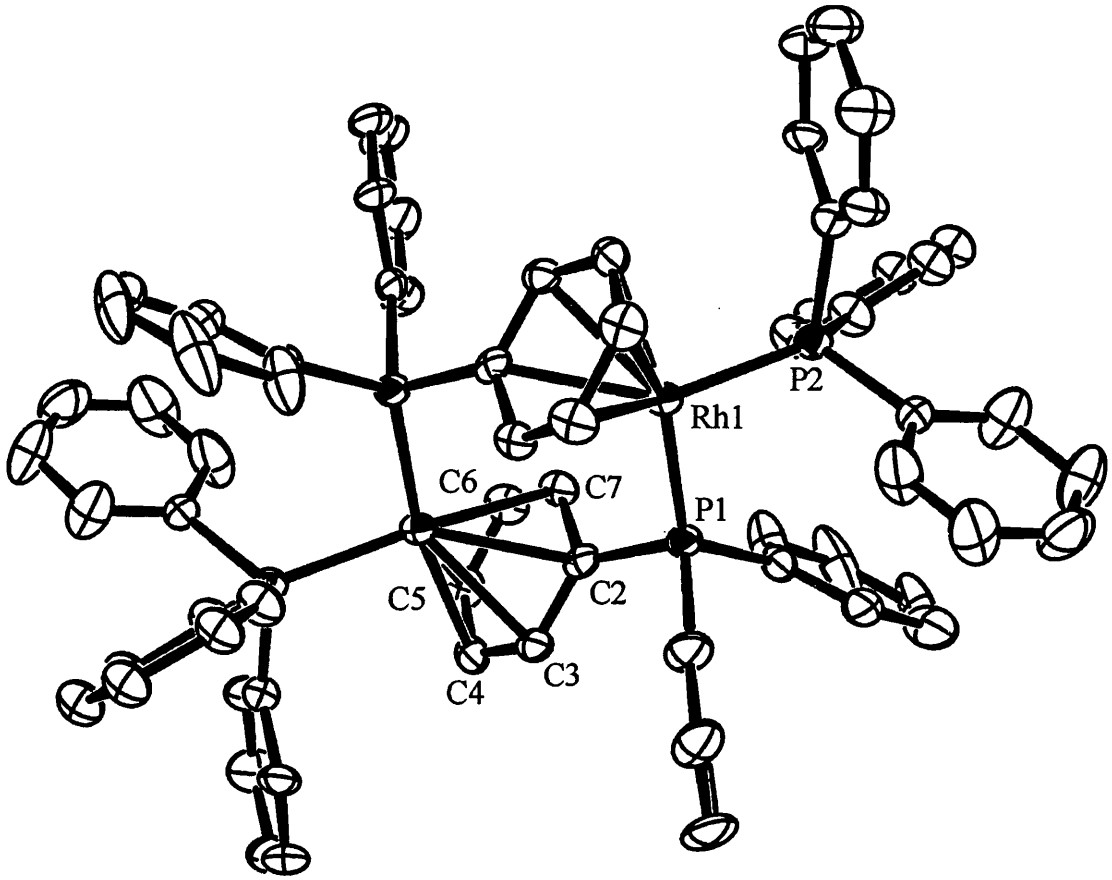

Rh1-P1	2.248(2)
Rh1-P2	2.262(3)
Rh1-C2	2.399(8)
Rh1-C3	2.365(8)
Rh1-C4	2.269(8)
Rh1-C5	2.333(9)
Rh1-C6	2.316(9)
Rh1-C7	2.254(8)
Rh1-Br7	5.848(1)
Rh1-P1-C2	108.9(3)
P1-Rh1-P2	95.96(8)

Table 2.2.5: Selected Interatomic distances (Å) and Angles (°) for complex **XIV**.

Figure 2.2.12: ORTEX drawing of the dicationic portion of complex **XIV**. Thermal ellipsoids are drawn at the 30% probability level. The disorder present in non-bridging phenyl ring and it's symmetry equivalent is not shown, with only the major component (65% occupancy) drawn.

molecule crystallizes with a crystallographically imposed inversion center. The two carborane anions do not interact with the metal centers, the shortest Rh-Br distance in the lattice being 5.85 Å. One of the non-bridging phenyl rings in the complex shows disorder, which was successfully modeled at 65:35 occupancy. The Rh-P bond lengths [2.248(2) and 2.262(3) Å] are very similar to those found in a comparable η^6-arene structure $[(Ph_2(^nBu)P)_2Rh(\eta^6\text{-}C_7H_8)]$ [2.244(3) and 2.258(4) Å].[39] The C-Rh bond lengths [average 2.399(8) Å] are also very similar to those found for $[(Ph_2(^nBu)P)_2Rh(\eta^6\text{-}C_7H_8)]$ 2.367(9) Å. The two $\{(Ph_3P)_2Rh\}^+$ fragments satisfy their electron count by forming η^6 π-arene to metal interactions. Such dimeric bridging structures are known with chelating phosphines,[29, 40, 41] for example $[(dppe)Rh]_2[BF_4]_2$[29]but to our knowledge this is the first example of such a structure with a monodendate phosphine. The $^{31}P\{^1H\}$ NMR spectrum of **XIII** displays two phosphorous environments at δ 44.6 and 47.5 ppm respectively. The two phosphorous environments show coupling to ^{31}P and ^{103}Rh which can be modeled as a second-order AA'BB'XX' spin system. This is in agreement with similar dimers formed with chelating phosphines such as $[(dppb)Rh]_2[ClO_4]_2$.[29, 41] The complex $^{31}P\{^1H\}$ NMR spectrum can be simulated (Figure 2.2.13) using the program gNMR.[42]

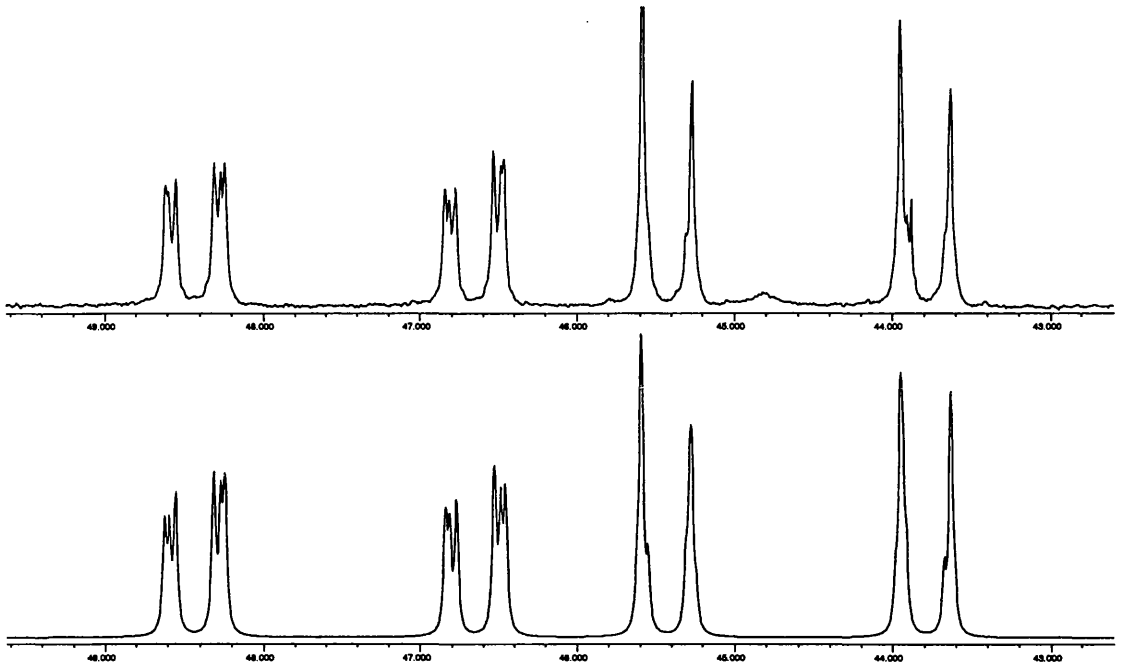

Figure 2.2.13: Experimental (top) and simulated (bottom) $^{31}P\{^{1}H\}$NMR spectrum of the cationic portion of **XIV.**

Resolved coupling constants can be found in appendix A. Comparison of ^{109}Rh-^{31}P coupling constants in complex **XIV** to those observed for similar complexes shows that they are broadly comparable. Typical values for one bond ^{109}Rh-^{31}P coupling constants in similar systems[29] are between 190 and 220 Hz and the coupling constants found here [J(RhP) = 217 Hz] are almost identical to those found in the literature. In complex **XIV** the phosphorous atoms bound to bridging phenyl rings are assigned as those resonating at δ 47.5 ppm, this assignment is based upon the extra smaller coupling to rhodium through bridging arene ring. Whilst with complexes such as $[(dppb)Rh]_2[ClO_4]$ diastereomers are observed due to the chirality induced at the phosphines bound to the

bridging phenyl rings, no such diastereomerism is observed for complex **XIV**, with it's monodendate phosphines and thus only one set of resonances is observed.

The ^{1}H NMR spectrum of complex **XIV** shows the presence of several triplet resonances between δ 7.5 and 5.32 ppm for the arene groups. Resonances at δ 6.97 [t, *J*(HH) 6.6], 6.58 [t, *J*(HH) 6.6], 5.32 [t, *J*(HH) 6.6] in the ratio 4:4:2 can be assigned as those on the bridging phenyl rings. The assignment is based on ^{1}H-^{1}H COSY NMR spectroscopy experiments. These show that these resonances couple to one another but not to the remaining aromatic protons indicating that they are on the same unique phenyl ring. The upfield shift confirms that they are the bridging phenyl protons due to increased shielding caused by coordination to the rhodium. However it appears that the solid-state structure is not retained in solution due to the fact that only three proton resonances are observed for the bridging phenyl groups. If the solid-state structure were retained in solution 5 resonances should be observed due to a lack of symmetry through the P-Rh-P plane. Therefore some mechanism must be operating whereby these protons become equivalent. A mechanism by which this could happen (Figure 2.2.14) involves libration around the arene-Rh bond to give a transition state where there is a mirror plane through the molecule. Continued rotation would result in an inversion of the original geometrical isomer. This process must be extremely facile as no change in the ^{1}H NMR spectrum is observed at 218K in CD_2Cl_2. We can discount other mechanisms such as phosphine dissociation or arene decoordination because well-defined second-order ^{109}Rh-^{31}P coupling is observed which would be lost if rapid Rh-P breaking was occurring.

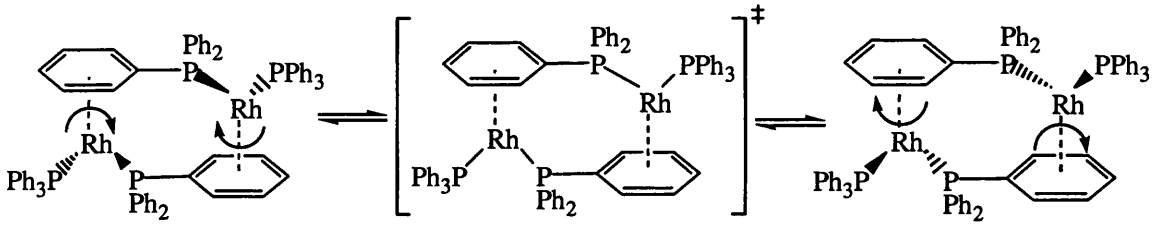

Figure 2.2.14: Fluxionality proposed for complex **XIV**.

The formation of complex **XIV** must be ascribed to the counterion. In all of the complexes discussed in the preceding sections the counterion possesses {B-H} vertexes available for donation into vacant orbitals on the rhodium center. In the case of the $[CB_{11}H_{11}Br]^-$ anion it is unclear whether the {B-Br} vertex interacts with the rhodium and cannot be ruled out. However, such an interaction is going to be significantly weaker than the already weakly coordinating 3c-2e B-H-M bond and may only occur due to the close proximity of the cage to the rhodium due to the 3c-2e bonds formed through the lower pentagonal belt. When the $[closo\text{-}CB_{11}H_6Br_6]^-$ anion is used in which the possibility of 3c-2e bonds formed through lower pentagonal belt vertexes are effectively 'switched off' by halogenation, the rhodium center must find an alternative method to gain coordinative and electronic saturation. The upper pentagonal belt vertexes are also unavailable for the formation of 3c-2e bonds due to the bulky nature of the $[CB_{11}H_6Br_6]^-$ anion. Similar ^1H and ^{31}P NMR spectra are observed when complexes **IV** [anion = *closo*-1-H-$CB_{11}Me_{11}$] and **V** [anion = $B(Ar)_f$] are treated with H_2 in the same way as for **III** indicating that these anions are all much weaker nucleophiles than either the $[CB_{11}H_{12}]^-$ or $[CB_{11}H_{11}Br]^-$ anions. The more traditional weakly coordinating anion $[BF_4]^-$ also results in an arene bridged dimer when the complex $[(Ph_3P)_2Rh(nbd)][BF_4]$ is

treated with H_2 in CH_2Cl_2. The implication of these observations in the hydrogenation of olefins is dealt with in some detail in chapter 4.

2.3 Summary

We have demonstrated that cationic rhodium diene complexes are air stable precursors to a variety of new metallocarboranes (Figure 2.2.15), which have been well characerised *via* multinuclear NMR spectroscopy and in some cases by X-ray diffraction studies. When the anion $[Y]^-$ is [*closo*-$CB_{11}H_{12}]^-$ or [*closo*-$CB_{11}H_{11}Br]^-$, zwitterions are formed in which the carborane moiety is relatively tightly bound to the metal centre *via* bridging 3 centre 2 electron B-H-M interactions. $^{11}B\{^1H\}$, ^{11}B, $^1H\{^{11}B\}$ and ^1H NMR spectroscopy is a useful diagnostic guide with large upfield shifts being observed for those vertices involved in bonding to rhodium centres in the ^{11}B and ^1H NMR spectra.

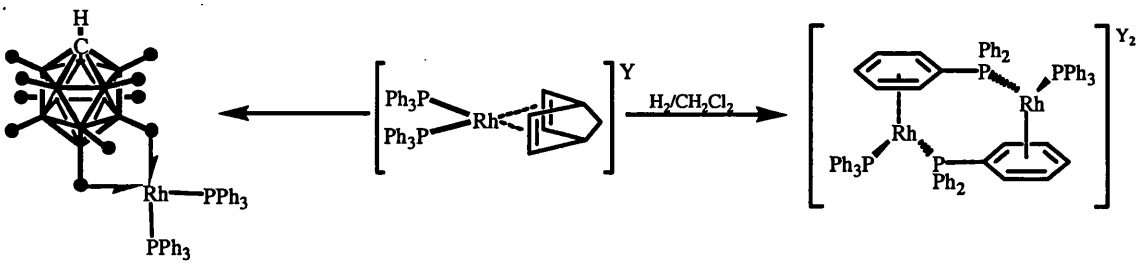

Figure 2.2.15: Formation of metallocarboranes

When employing the more coordinating [*closo*-$CB_{11}H_{12}]^-$ or [*closo*-$CB_{11}H_{11}Br]^-$ anions it has proven possible to be able to modulate the phosphine which results in further novel metallocarboranes. These metallocarboranes display similar properties to the PPh_3 anologue. When the anion $[Y]^-$ = [*closo*-$CB_{11}H_6Br_6]^-$, [*closo*-$CB_{11}Me_{11}]^-$, $[B(Ar_f)_4]^-$ or $[BF_4]^-$ arene bridged dimers are afforded as the sole product according to Figure 2.2.15.

The formation of these dimers reflects the low nucleophilicity of these anions compared to [*closo*-$CB_{11}H_{12}$]$^-$ or [*closo*-$CB_{11}H_{11}Br$]$^-$.

1 A. K. Saxena and N. S. Hosmane, *Chem. Rev.*, 1993, **93**, 1081.

2 D. E. Kadlecek, A. M. Shedlow, S. O. Kang, P. J. Carroll, and L. G. Sneddon, *J. Am. Chem. Soc.*, 2003, **125**, 212.

3 R. T. Baker, M. S. Delaney, R. E. King, C. B. Knobler, J. A. Long, T. B. Marder, T. E. Paxson, R. G. Teller, and M. F. Hawthorne, *J. Am. Chem. Soc.*, 1984, **106**, 2965.

4 P. E. Behnken, J. A. Belmont, D. C. Busby, D. M.S., R. E. King III, C. W. Kreimendahl, T. B. Marder, J. J. Wilczynski, and M. F. Hawthorne, *J. Am. Chem. Soc.*, 1984, **106**, 3011.

5 C. B. Knobler, T. B. Marder, E. A. Mizusawa, R. G. Teller, J. A. Long, P. E. Behnken, and M. F. Hawthorne, *J. Am. Chem. Soc.*, 1984, **106**, 2990.

6 J. A. Long, T. B. Marder, P. E. Behnken, and M. F. Hawthorne, *J. Am. Chem. Soc.*, 1984, **106**, 2979.

7 J. A. Long, T. B. Marder, and M. F. Hawthorne, *J. Am. Chem. Soc.*, 1984, **106**, 3004.

8 D. J. Crowther, S. L. Borkowsky, D. Swenson, T. Y. Meyer, and R. F. Jordan, *Organomet.*, 1993, **12**, 2897.

9 K. Shelly and C. A. Reed, *J. Am. Chem. Soc.*, 1986, **108**, 3117.

10 K. Shelly, D. C. Finster, Y. J. Lee, W. R. Scheidt, and C. A. Reed, *J . Am. Chem. Soc.*, 1985, **107**, 5955.

11 S. Hermanek, *Chem. Rev.*, 1992, **92**, 325.

12 C. Vinas, M. A. Flores, R. Nunez, F. Teixidor, R. Kivekas, and R. Sillanpaa, *Organomet.*, 1998, **17**, 2278.

13 C. Vinas, M. A. Flores, R. Nunez, F. Teixidor, R. Kivekas, and R. Sillanpaa, *J. Am. Chem. Soc.*, 2000, **122**, 1963.

14 D. D. Ellis, P. A. Jelliss, and G. F. A. Stone, *Organomet.*, 1999, **18**, 4982.

15 A. S. Weller, M. F. Mahon, and J. W. Steed, *J. Organomet. Chem.*, 2000, **614-615**, 113.

16 M. Herberhold, H. Yan, W. Milius, and B. Wrackmeyer, *J. Organomet. Chem.*, 2000, **604**, 170.

17 M. Herberhold, H. Yan, W. Milius, and B. Wrackmeyer, *Chem. Eur. J.*, 2000, **6**, 3026.

18 J. D. Hewes, C. W. Kreimendahl, T. B. Marder, and M. F. Hawthorne, *J. Am. Chem. Soc.*, 1984, **106**, 5757.

19 D. E. Kadlecek, P. J. Carroll, and L. G. Sneddon, *J. Am. Chem. Soc.*, 2000, **122**, 10868.

20 M. J. Pender, P. J. Carroll, and L. G. Sneddon, *J. Am. Chem. Soc.*, 2001, **123**, 12222.

21 J. A. Belmont, J. Soto, R. E. King III, J. A. Donaldson, J. D. Hewes, and M. F. Hawthorne, *J. Am. Chem. Soc.*, 1989, **111**, 7475.

22 F. Teixidor, R. Nunez, M. A. Flores, A. Demonceau, and C. Vinas, *J. Organomet. Chem.*, 2000, **614**, 48.

23 H. Brunner, A. Apfelbacher, and M. Zabel, *Eur. J. Inorg. Chem.*, 2001, 917.

24 C. Vinas, R. Nunez, F. Teixidor, A. Demonceau, F. Simal, and A. F. Noels, *Tet. Lett.*, 1997, **38**, 7879.

25 C. A. Reed, *Acc. Chem. Res.*, 1998, **31**, 133.

26 R. Shcrock and J. A. Osborn, *J. Am. Chem. Soc.*, 1971, **93**, 2397.

[27] R. Shcrock and J. A. Osborn, *J. Am. Chem. Soc.*, 1976, **98**, 2134.
[28] A. Miyashita, A. Yasuda, H. Takaya, K. Toriumi, T. Ito, T. Souchi, and R. Noyori, *J. Am. Chem. Soc.*, 1980, **102**, 7932.
[29] D. P. Fairlie and B. Bosnich, *Organomet.*, 1988, **7**.
[30] R. Schrock and J. A. Osborn, *J. Am. Chem. Soc.*, 1971, **93**, 3089.
[31] T. Jelinek, P. Baldwin, W. R. Scheidt, and C. A. Reed, *Inorg. Chem.*, 1993, **32**, 1982.
[32] C. B. Knobler, T. B. Marder, E. A. Mizusawa, R. G. Teller, J. A. Long, P. E. Behnken, and M. F. Hawthorne, *J. Am. Chem. Soc.*, 1984, **106**, 2990.
[33] M. Brookhart and M. L. H. Green, *J. Organomet. Chem.*, 1983, **250**, 395.
[34] M. A. Esteruelas, F. J. Lahoz, L. A. Oro, L. Rodriguez, P. Steinert, and H. Werner, *Organomet.*, 1996, **15**, 3436.
[35] N. J. Patmore, M. F. Mahon, J. W. Steed, and A. S. Weller, *J. Chem. Soc.-Dalton Trans.*, 2001, 277.
[36] N. J. Patmore, J. W. Steed, and A. S. Weller, *Chem. Comm.*, 2000, 1055.
[37] M. A. Fox, M. F. Mahon, N. J. Patmore, and A. S. Weller, *Inorg. Chem.*, 2002, **41**, 4567.
[38] N. J. Patmore, M. J. Ingleson, M. F. Mahon, and A. S. Weller, *J. Chem. Soc.-Dalton Trans.*, 2003, 2894.
[39] C. S. Slone, C. Stern, C. A. Mirkin, G. P. A. Yap, L. M. Liable-Sands, and A. L. Rheingold, *J. Am. Chem. Soc.*, 1997, **119**, 3048.
[40] J. Halpern, D. P. Riley, and A. S. C. Chan, *J. Am. Chem. Soc.*, 1977, **99**, 8055.
[41] D. G. Allen, S. B. Wild, and D. L. Wood, *Organomet.*, 1986, **5**, 1009.
[42] P. Budzelaar, Cherwell Scientific Publishing. Oxford, UK.

3 EXO-CLOSO CARBORANE COMPLEXES OF IRIDIUM

3.1 Introduction

Homogeneous catalysts based upon iridium have been developed for a range of important reactions that include hydrogenation,[1, 2,3] hydroboration,[4] olefin oligomerisation[5] and dehydrogenation.[6-10] Counterion effects in these systems are becoming increasingly recognized and significant increases in efficiency can be achieved by simply modulating the anion employed.[11] It was of interest then, to isolate Lewis acidic Iridium fragments bound to weakly coordinating [*closo*-$CB_{11}H_{12}]^-$ anions or derivatives thereof. Such complexes could not only display novel chemistry but could also potentially be used as models for intermediates in the catalytic cycle for the reactions mentioned above. The following discussion aims to highlight relevant chemical systems based upon Iridium complexes and to highlight those involving carboranes in their coordination sphere.

The chemistry of systems based around the $\{(L)_2Ir(H)_2(sol)_2\}^+$ (sol = solvent) fragment is remarkably diverse and was developed almost exclusively by Crabtree.[1, 2] The Iridium based complexes $[(L)(L')Ir(COD)][PF_6]$ remain the benchmark for homogeneous hydrogenation catalysts. The chemistry of these fragments is dominated by their highly electrophilic character. However, they are remarkably stable to oxidizing addenda such as halocarbons and O_2, which is partly the reason for their remarkable activity in

hydrogenation and dehydrogenation. The mechanism for hydrogenation/dehydrogenation with Crabtree's system and the reasons for its activity are discussed in more detail in section 4.1. Transition metal complexes of weakly coordinating halocarbons are still relatively rare.[5, 12, 13] Often low-valent late-transition metal complexes would be expected to oxidatively add R-X groups. The electrophilic nature of complex **8** allows the isolation of a chelated *o*-diiodobenzene complex (Figure 3.1) which is thermally stable in solution and in the solid state.[14] The synthesis of $[(Ph_3P)_2Ir(H)_2(o\text{-}C_6H_4I_2)][BF_4]$ **9** (Figure 3.1) is achieved simply by adding $o\text{-}C_6H_4I_2$ to complex **8** in CH_2Cl_2. The arylhalide in **9** is only weakly bound as evidenced by its reaction with σ-donors such as ethanol or bibiridyl. Complex **9** is also an active catalyst for the dehydrogenation of cyclopentene but not cyclopentane as discussed in section 4.1.

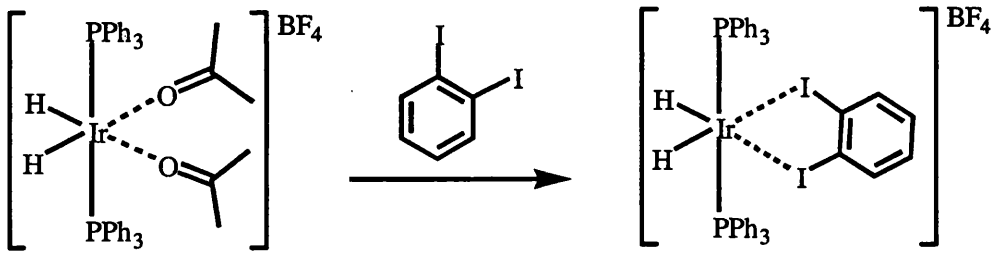

8 **9**

Figure 3.1: Synthesis of an iridium halocarbon complex

A variety of halocarbons can be coordinated to the $\{(Ph_3P)_2Ir(H)_2\}^+$ fragment such as $C_6H_4Br_2$, C_6H_4BrI, C_6H_5I and MeI.[14] Interestingly, these complexes are poor hydrogenation catalysts in CH_2Cl_2 solution indicating that the degree of interaction between these relatively weak donor molecules and highly electrophilic metal centre is

actually comparable to coordinating solvents such as acetone or THF. Eisenberg has prepared the electrophilic complex $[Ir(Me)(CO)(dppe)(o\text{-}C_6H_4I_2)][Bar_f]_2$ **10**.[5] The synthesis of the dicationic iridium(III) centre is achieved in two steps (Figure 3.2). Initially $Ir(CO)(Me)(dppe)I_2$ is treated with two equivalents of AgOTf in CH_2Cl_2 generating a *bis*-triflate adduct.

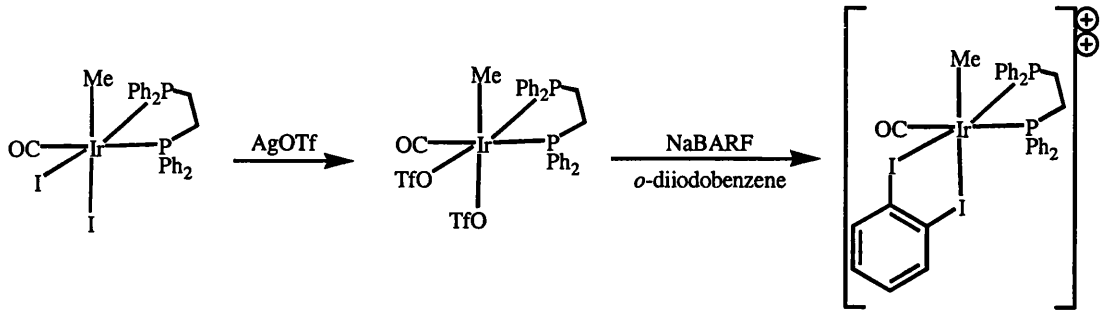

10

Figure 3.2: Synthesis of an electrophilic iridium catalyst

Subsequent salt metathesis with $NaBAr_f$ in CH_2Cl_2 in the presence of excess diiodobenzene results in the formation of complex **10** and precipitation of NaOTf from the solution. The diiodobenzene is quite labile in **10** and is readily displaced by CO and MeCN as well as ethylene and other olefins. The dicationic complex **10** is highly electrophilic as evidenced by its reaction chemistry. Addition of isobutylene, for example, to a CH_2Cl_2 solution of complex **10** results in an exothermic reaction where the momomers are rapidly consumed and the solvent begins to boil (Figure 3.3).

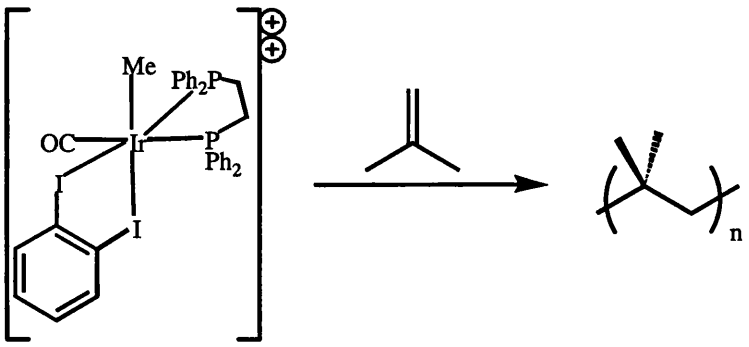

Figure 3.3: Reaction of **10** with isobutylene

The activity of these types of complex for polymerisation is highly unusual. The mechanism is thought to be cationic in nature, whereby the initial step of the reaction is the formation of a tertiary carbocation bonded directly to the iridium centre. This results directly from the electrophilic nature of complex **10**. Further studies on haloalkanes have been made.[12, 13] Indeed, crystallographically characterized CH_2Cl_2 complexes are now known.[19]

Hawthorne was the first to prepare a metallocarborane incorporating an Iridium centre.[15] Treatment of $[Ir(cod)(PR_3)_2][nido\text{-}7,8\text{-}C_2B_9H_{12}]$ (R = P(*p*-tolyl)$_3$) with H_2 in pentane at -22°C yields 3,9-[*cis*-$(H)_2$-*trans*-$(PR_3)_2$-Ir]-3,9-μ-$(H)_2$-*nido*-$C_2B_9H_{10}$, **11** in reasonable yield. The bonding is shown to be similar to those *exo-nido* complexes discussed in section 2.1 (Figure 3.4) where the $[nido\text{-}C_2B_9H_{12}]^-$ moiety is exopolyhedrally bound to the $\{(H)_2(PR_3)_2Ir\}^+$ fragment via two 3c-2e bonds.

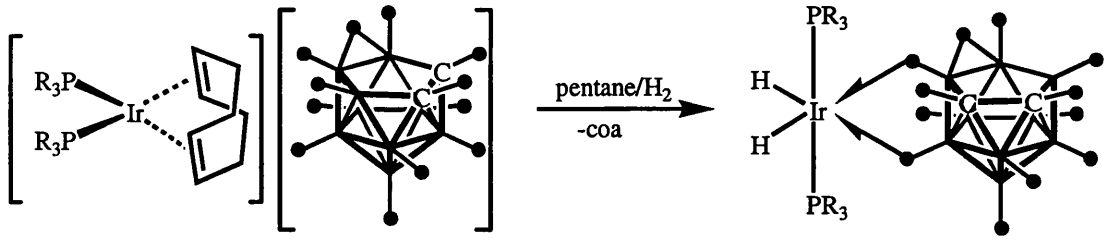

11

Figure 3.4: Synthesis of $[Ir(H)_2(P\{p\text{-tolyl})_3\}_2(nido\text{-}C_2B_9H_{12})]$

When complex **11** is refluxed in benzene (Figure 3.5) the thermodynamically favoured complex $[closo\text{-}3,3\text{-}(PPh_3)_2\text{-}3\text{-}H\text{-}3,1,2\text{-}Ir(C_2B_9H_{11})]$, **11a**, is formed in 90% yield. The formation of the *closo-* isomer is analogous to the *exo-nido-* to *closo-* tautomerism discussed in section 2.1 for complex **1**. However, the isomerisation is not reversible in this case.

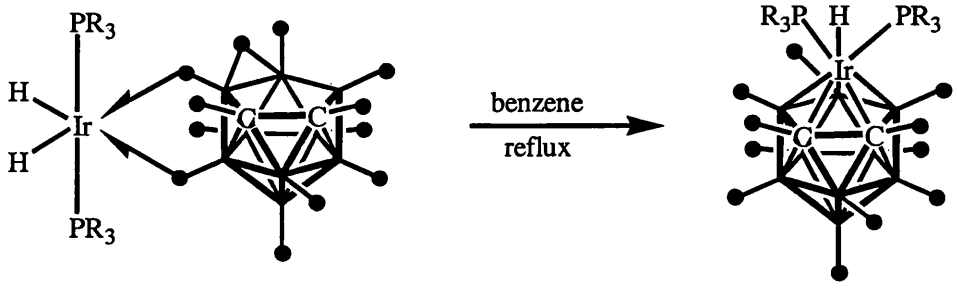

11a

Figure 3.5: Formation of $[closo\text{-}3,3\text{-}(PPh_3)_2\text{-}3\text{-}H\text{-}3,1,2\text{-}Ir(C_2B_9H_{11})]$

Iridium coordination to exo-dithio-7,8-dicarba-nido-undecaborate derivatives has been reported.[16, 17] The treatment of $[(Ph_3P)_2Ir(CO)Cl]$ with $AgNO_3$ in acetonitrile followed by reaction of the acetonitrile adduct generated in-situ with $[NMe_4][exo\text{-dithio-}7,8\text{-}$

dicarba-*nido*-undecaborate] in ethanol results in formation of complexes of the type $[LIr(PPh_3)_2]$ (L = exo-dithio-7,8-dicarba-nido-undecaborate) **12** (Figure 3.6) being formed in good yield.

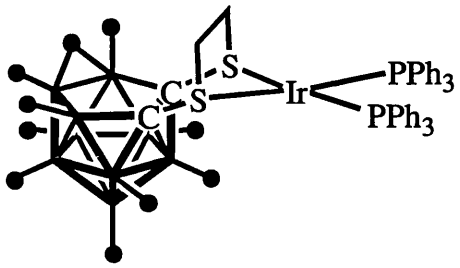

12

Figure 3.6: An *exo*-dithioether iridium complex

Contrary to those tethered *exo-nido* complexes discussed in section 2.1 no 3c-2e bonds are observed between the carborane and the metal fragment **12.** Stone has also prepared several iridium based metallocarboranes with B-H-M interactions.[18] $[ReIr(CO)_3(\eta^5\text{-}C_5Me_5)(\eta^5\text{-}7\text{-}CB_{10}H_{11})]$ **13** (Figure 3.7) can be synthesised *via* treatment of $[Re(CO)_3(\eta^5\text{-}7\text{-}CB_{10}H_{11})][N(PPh_3)_2]_2$ with $[Ir(NCMe)_3(\eta^5\text{-}C_5Me_5)][BF_4]_2$ in CH_2Cl_2 at 0°C or below.[19]

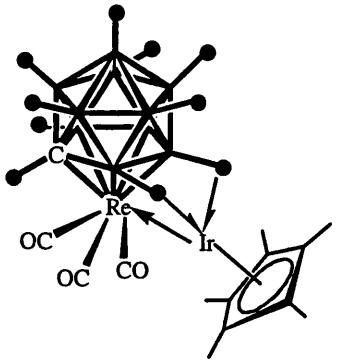

13

Figure 3.7: An *exo-closo* iridium metallocarborane

Complex **13** is thermally unstable above 0°C in CH_2Cl_2. However, **13** is a useful synthon in the preparation of more stable metallocarboranes. For example, treatment of **13** with PMe_3 at -78°C in CH_2Cl_2 leads to the formation of [ReIr-$(CO)_3(PMe_3)(\eta^5$-$C_5Me_5)(\eta^5$-7-$CB_{10}H_{11})$] **14** (Figure 3.8).[19]

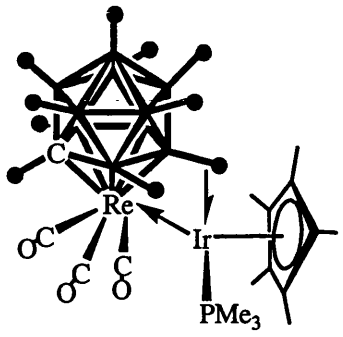

14

Figure 3.8: Schematic representation of complex **14**

The complex [NEt_4][10-endo-{$Au(PPh_3)$}-*nido*-7,8-$C_2B_9H_9Me_2$] **15** (Figure 3.9), has also been shown to be a useful reagent for preparing mixed metal metallocarboranes.[18, 20]

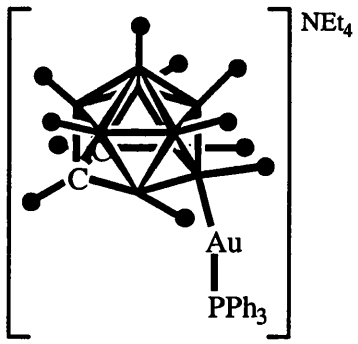

15

Figure 3.9: [NEt_4][10-endo-{$Au(PPh_3)$}-*nido*-7,8-$C_2B_9H_9Me_2$]

Treatment of $[IrCl(PPh_3)_2]$ with $TlBF_4$ in THF followed by removal of solvents *in vacuo*, dissolution in CH_2Cl_2 and treatment with a CH_2Cl_2 solution of **16** results in the formation of the mixed metal metallocarborane $[IrAuH(\mu\text{-}\sigma\text{:}\eta^3\text{-}7,8\text{-}C_2B_9H_8Me_2)(PPh_3)_3]$ **16** in good yield (Figure 3.10).

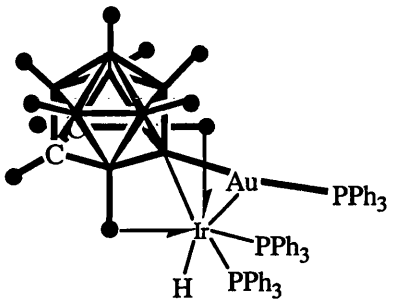

16

Figure 3.10: $[IrAuH(\mu\text{-}\sigma\text{:}\eta^3\text{-}7,8\text{-}C_2B_9H_8Me_2)(PPh_3)_3]$

Oxidative addition of one B-H group across the iridium(I) centre results in a direct B-M bond. The carborane also forms to 3c-2e bonds to the iridium centre as well as forming an Ir-Au bond. Oxidative addition of B-H bonds across iridium(I) centres has been observed before. Hawthorne prepared the complex $IrHCl(1\text{-}PMe_2\text{-}1,2\text{-}C_2B_{10}H_{11})_2[1\text{-}PMe_2\text{-}1,2\text{-}C_2B_{10}]$ **17** (Figure 3.11) as long ago as 1975.[21] In this case the precursor complex $[Ir(1\text{-}PMe_2\text{-}1,2\text{-}C_2B_{10}H_{11})_3Cl]$ is generated *in situ* by treatment of the carborane $1\text{-}PMe_2\text{-}1,2\text{-}C_2B_{10}H_{11}$ with $[Ir(C_8H_{14})_2Cl]$ in cyclohexane.

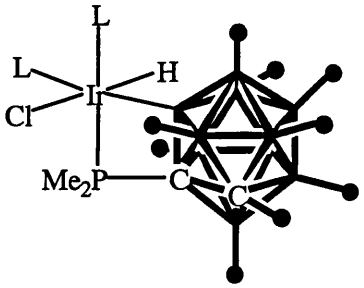

17

Figure 3.11: $Ir(L)_2[1\text{-}PMe_2\text{-}1,2\text{-}C_2B_{10}]HCl$ ($L=1\text{-}PMe_2\text{-}1,2\text{-}C_2B_{10}H_{11}$)

Full conversion to **17** is achieved by refluxing the solution. The intramolecular B-H activation is analogous in many ways to the familiar *ortho*-metallation reaction exhibited by many low-valent metal phosphines.

More recently a similar complex $[IrH_2(o\text{-}HCB_{10}H_9CCH_2PPh_2\text{-}B,P)(PPh_3)(L)]$ ($L=PPh_3$) **18** (Figure 3.12) was prepared.[22] Complex **18** itself is a useful precursor to novel η^2-C_{60} complexes.

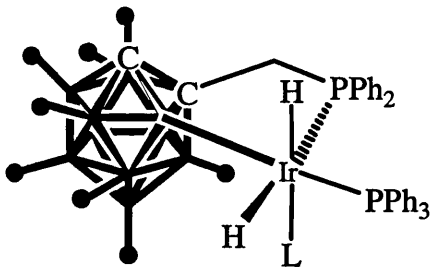

18

Figure 3.12: $[Ir(H)_2(o\text{-}HCB_{10}H_9CCH_2PPh_2\text{-}B,P)(PPh_3)(L)]$ ($L=PPh_3$)

The relative lack of metallocarborane complexes incorporating iridium compared to the large number of metallocarboranes known based upon rhodium is surprising. In the

course of our studies we hoped to isolate *exo-closo* metallocarboranes incorporating [*closo*-$CB_{11}H_{12}]^-$ and [*closo*-$CB_{11}H_6Br_6]^-$ into their coordination sphere. Such metallocarborane complexes of iridium are of course interesting in their own right. However, we hoped to be able to isolate iridium complexes that could be used as model complexes in the hydrogenation of olefins with iridium based catalysts. We were especially interested in determining the role of the anion in the hydrogenation cycle. Although Crabtree[2] has detected olefin complexes assigned as intermediates in the catalytic cycle in NMR studies no crystallographically characterized intermediates are known except $[(PPh_3)_2Ir(H)_2(OCMe_2)_2]^+$ in which solvent as opposed to olefin is bound to the $\{(Ph_3P)_2Ir(H)_2\}^+$ fragment. The use of robust weakly coordinating anions such as [*closo*-$CB_{11}H_6Br_6]^-$ could potentially allow us to isolate the $\{(Ph_3P)_2Ir(H)_2\}^+$ fragment and examine its reactivity with olefins and hydrogen. Results to this end are discussed in the following section.

3.2 RESULTS AND DISCUSSION

3.2.1 Cyclooctadiene Precursor Complexes

Given the success achieved by employing air-stable precursors to rhodacarborane complexes it seemed likely that such a strategy could be employed in the preparation of iridium based metallocarboranes. Complexes of the type $[(Ph_3P)_2Ir(cod)][Y]$ are readily prepared via addition of four equivalents of PPh_3 to $[Ir(cod)Cl]_2$ in ethanol followed by salt metathesis (Figure 3.2.1).

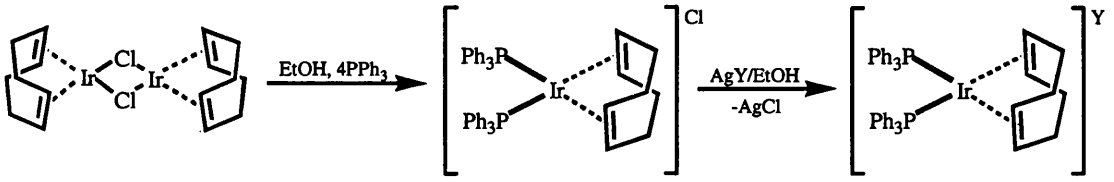

Figure 3.2.1: Synthesis of complexes of the type $[(Ph_3P)_2Ir(cod)][Y]$

After removal of volatiles the residue was redissolved in CH_2Cl_2, filtered and the red complexes were crystallized by addition of ethanol followed by cooling overnight at -30°C. The compounds $[(Ph_3P)_2Ir(cod)][Y]$, Y = [*closo*-$CB_{11}H_{12}]^-$ **XV**, [*closo*-$CB_{11}H_6Br_6]^-$ **XVI** were prepared in this manner. Complexes **XV**, and **XVI** display a singlet resonance in the $^{31}P\{^1H\}$ NMR spectra centred at δ 18.8 ppm. The ^{11}B NMR spectra are consistent with the uncoordinated anion for each respective complex. For **XV** three doublet resonances in the ratio 1:5:5 are observed centered at δ -7.3, -13.6 and -

16.4 ppm, assigned to B(12), B(7-11) and B(2-6) respectively. For **XVI** both the B(12) and B(7-11) resonances are observed as singlets at δ 1.7 and -6.6 ppm respectively with the B(2-6) resonance observed as a doublet at δ -17.1 ppm. In the ^{1}H-NMR spectra the cage {CH} resonances are observed at δ 2.21 and 2.55 ppm respectively for complexes **XV** and **XVI**. Three resonances due to olefin are observed at δ 4.16 (4H), 2.20 (4H) and 1.95 (4H) ppm for each compound. As for complex **I-VIII** discussed in the preceding chapter it was anticipated that complexes **XV** and **XVI** would be useful precursors to metallocarboranes based upon iridium. Results obtained to this end are discussed in the next section.

3.2.2 $[(Ph_3P)_2Ir(H)_2(closo\text{-}CB_{11}H_{12})]$, XVII

Treatment of a stirred CH_2Cl_2 solution of **XV** with H_2 results in the reduction of the diene, as evidenced by ^{1}H NMR spectroscopy in CD_2Cl_2 by the formation of cyclooctane (^{1}H NMR), and subsequent coordination of the $[closo\text{-}CB_{11}H_{12}]^-$ anion to the 14e$^-$ $\{(Ph_3P)_2Ir(H)_2\}^+$ fragment generated *in situ*. The reaction (Figure 3.2.2) was accompanied by a colour change from red to colourless. Layering the reaction mixture with hexanes resulted in the formation of colourless crystalline blocks of $[(Ph_3P)_2Ir(closo\text{-}CB_{11}H_{12})]$, **XVII**, in good yield.

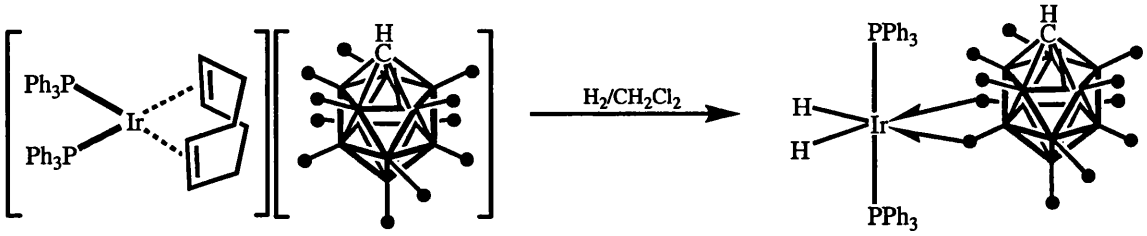

Figure 3.2.2: Formation of complex **XVII**

Complex **XVII** was fully characterized by X-ray crystallography, elemental analysis and multinuclear NMR spectroscopy. Initial crystallographic studies with [*closo*-$CB_{11}H_{12}$]$^-$ were in part unsuccessful due to disorder in the cage, which made assignment of the carbon vertex impossible. Unambiguous location of the carbon vertex was achieved by employing the [1-Me-*closo*-$CB_{11}H_{11}$]$^-$ anion to form [$(Ph_3P)_2Ir(H)_2$(1-Me-*closo*-$CB_{11}H_{11}$] **XVIIa** which showed NMR spectra identical to **XVII** apart from the replacement of {CH} for {CMe}. The solid-state structure of complex **XVIIa** is shown in Figure 3.2.3 with relevant bond lengths and angles in Table 3.2.1. The $\{(Ph_3P)_2Ir(H)_2\}^+$ fragment in **XVIIa** is coordinated with the cage *via* two three-centre-two-electron B-H-Ir bonds. The cage binds through the [BH(7)] and [BH(8)] vertices. The hydrogens were located in the difference map but were not freely refined. The two Ir-B distances are similar [Ir-B(7) 2.478(4) Å and Ir-B(8) 2.510(4) Å]. These distances compare with those found for 3,9-[{P(*p*-tolyl)$_3$}$_2$Ir(H)$_2$]-3,9-μ-(H)$_2$-7,8-$C_2B_9H_{10}$ [2.480(11) Å and 2.452(11)Å respectively.[15] The two iridium-phosphine distances [Ir-P(1) 2.3193(9) Å and Ir-P(2) 2.3194(8) Å] are almost identical to those found for 3,9-[{P(*p*-tolyl)$_3$}$_2$Ir(H)$_2$]-3,9-μ-(H)$_2$-7,8-$C_2B_9H_{10}$ [2.312(3) Å and 2.301(3) Å].[15] The hydride ligands were located but were not freely refined. The angle [P(1)-Ir-P(2)

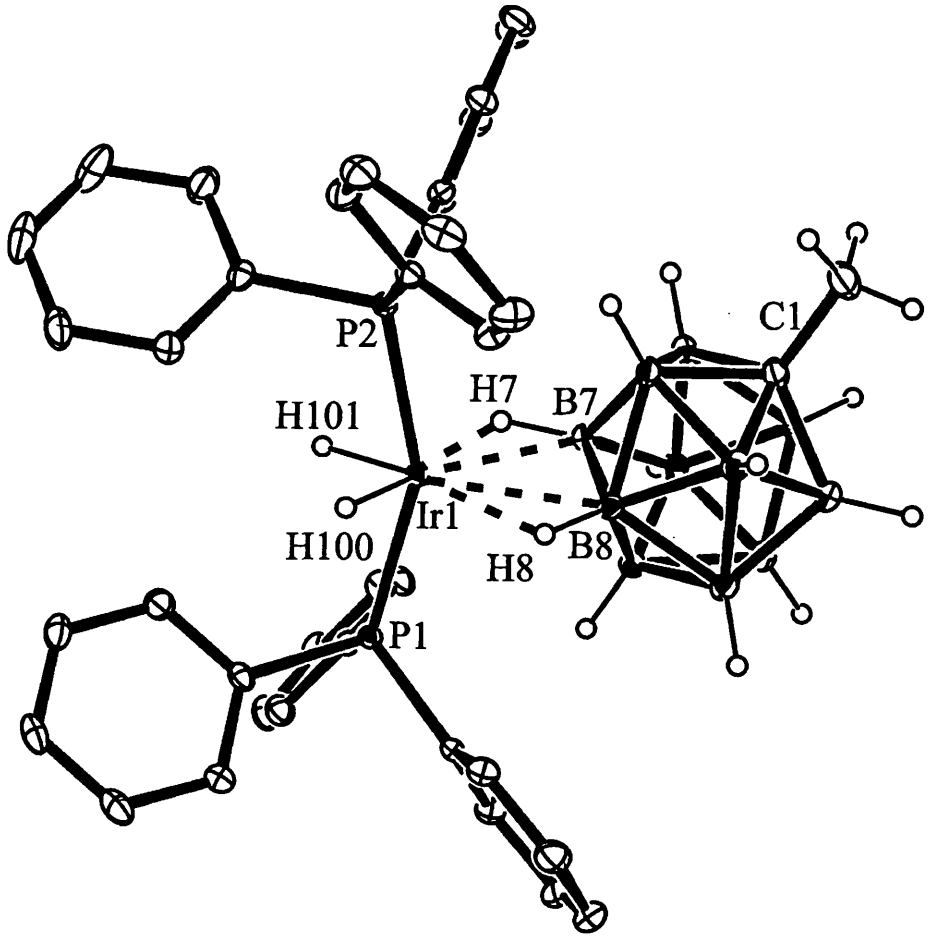

Ir1-P1	2.3195(8)
Ir1-P2	2.3196(8)
Ir1-B8	2.511(4)
Ir1-B7	2.479(3)
P1-Ir1-B8	99.02(9)
P1-Ir1-P2	154.52(3)
B7-Ir1-B8	40.56(13)

Table 3.2.1: Selected bond lengths (Å) and angles (°) for complex **XVIIa.**

Figure 3.2.3: ORTEP drawing of complex **XVIIa**. Ellipsoids are drawn at the 30% probability level. Phenyl hydrogens have been omitted for clarity.

154.52(3)°] is slightly smaller than that found for 3,9-[$(H)_2\{P(p\text{-tolyl})_3\}_2$Ir]-3,9-μ-$(H)_2$-7,8-$C_2B_9H_{10}$ [158.9(1)°].[15] The two phosphines are slightly distorted from the ideal *trans-* configuration being pushed together slightly as a result of the large steric demand of the bulky carborane ligand.

The ^{1}H NMR spectrum of **XVII** displays a broad quartet at δ -5.2 ppm [J(BH) 106 Hz] integrating as two protons which is assigned as [B*H*(7)] and [B*H*(8)]. The coupling constant is reduced by 30 Hz compared to that of uncoordinated [*closo*-$CB_{11}H_{12}$]$^-$ indicating coordination of the cage to the metal fragment *via* these vertices. A broad peak at δ -20.9 ppm also integrating as two protons is assigned as the two hydride ligands. The expected *cis*-^{31}P-^{1}H coupling is not observed due to broadening of the hydride signals as a result of being *trans-* to the quadrupolar ^{11}B nuclei. The ^{1}H and ^{11}B NMR spectra suggest that the cage is static in solution. The ^{11}B NMR spectrum displays resonances at δ 0.1, -9.8, -16.5 and -25.1 ppm. The intensities of these signals are in a 1:1:7:2 ratio. For the solid-state structure of complex **XVII** seven resonances would be expected in a 1:1:1:2:2:2:2 ratio. We can assume that in complex **XVII** some resonances are coincident i.e. the resonance with intensity 7 at δ -16.5 ppm is due to a 2+2+2+1 coincident. The ^{1}H NMR spectrum shows that only two [B*H*] vertices are interacting with the metal fragment in solution. This contrasts with complex **XII**, for example, where all five lower pentagonal belt [BH] vertices interact with the metal fragment on the NMR timescale. The ^{31}P{^{1}H} NMR spectrum displays a single broad resonance centred at δ 18.8 ppm suggesting that the molecule does not retain the solid-state structure and is fluxional as the phosphorous atoms are equivalent on the NMR

timescale at room temperature. Upon cooling a CD_2Cl_2 solution of complex **XVII** to -70°C the $^{31}P\{^1H\}$ for **XVII** resolves into two doublet resonances at δ 25.0 and 22.7 ppm respectively [J(PP) 350Hz] as expected for an AB spin system. This is fully consistent with the solid-state structure. The resonance at δ -20.9 ppm in the ^1H NMR does not sharpen upon cooling indicating that it is broad due to quadrupolar coupling to ^{11}B rather than being broad as a result of any fluxional process. At low temperature (203K) an additional singlet resonance at δ 25.0 ppm (ca. 25%) is also seen in the $^{31}P\{^1H\}$ NMR spectrum which is accompanied by the appearance of two broad resonances in the ^1H NMR spectrum at δ -21.3 and -20.5 ppm respectively. These resonances are assigned as the 7,12 isomer of complex **XVII**. The small ^1H-^1H coupling of the now inequivalent protons is not seen due to the presence of the ^{11}B nuclei in the *trans-* position, which results in broadening of the resonance. This temperature dependent equilibrium is shown in Figure 3.2.4. In the 7,12 isomer the phosphine ligands are equivalent and are thus observed as a singlet.

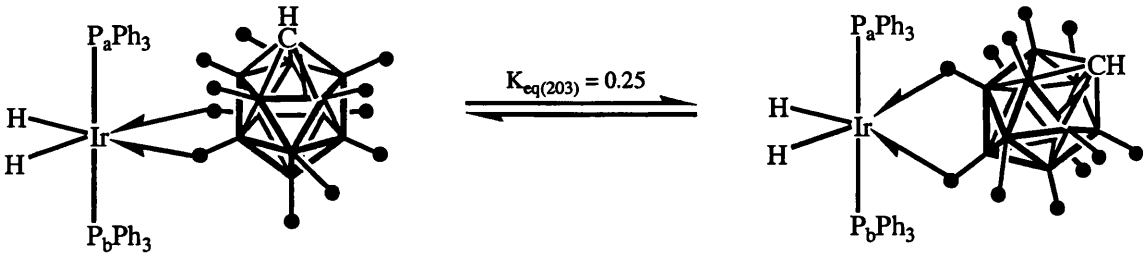

7,8- 7,12-

Figure 3.2.4: Equilibrium between 7,8- and 7,12- isomers for complex **XVII**

Given that no ^{31}P-^{31}P coupling is observed in the room temperature $^{31}P\{^1H\}$ NMR spectrum the phosphines must be becoming equivalent in solution at room temperature.

A mechanism of fluxionality (Figure 3.2.5) can be proposed that involves phosphine dissociation.

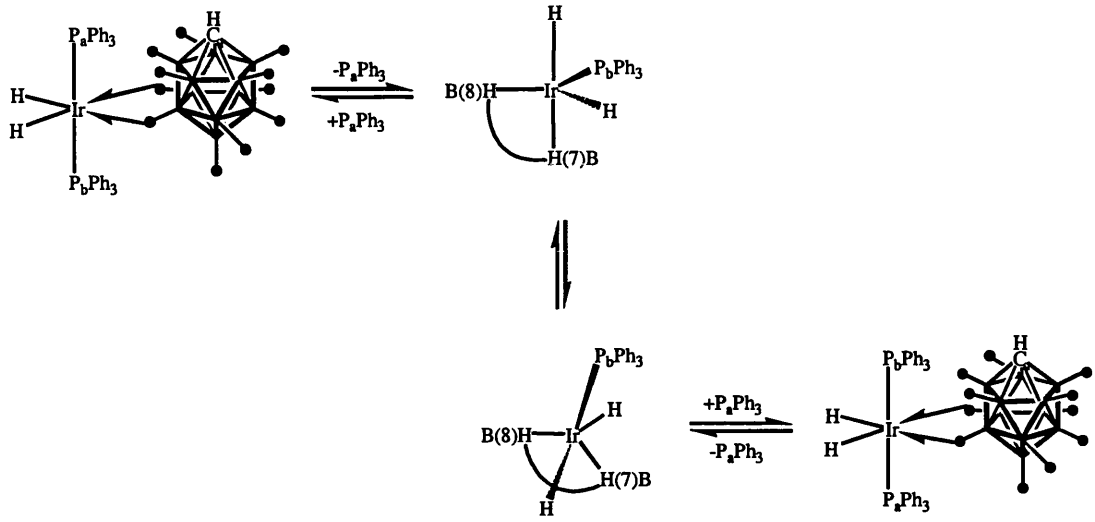

Figure 3.2.5: Fluxionality proposed for complex **XVII**

The resulting five coordinate intermediate could undergo a Berry pseudo rotation. Recoordination of the phosphine would give a complex where P_aPh_3 and P_bPh_3 switch places thus becoming equivalent. Anion dissociation can be ruled out because the observed symmetry is lower than the expected C_{5v}. If complex **XVII** were fluxional in the same way as complex **IX**, for example, C_{5v} symmetry would be observed for the cage. What is not clear, however, is whether the two isomers detected in solution at low temperature are interconverting. Given that two isomers are seen at low temperature suggests that both isomers are present in solution and that they both undergo the same fluxional process but do not interconvert. The resonance for the 7,12- isomer could perhaps be too broad to detect at room temperature given that it is present in low concentration relative to the 7,8- isomer. Alternatively the resonance for the 7,12-

isomer could be overlapping with the broad resonance for the 7,8- isomer at room temperature, thus obscuring it. Certainly no evidence is observed for the 7,12- isomer at room temperature. It remains possible, however, that for some reason the equilibrium shown in Figure 3.2.4 favours the 7,8- isomer at room temperature while at lower temperatures the 7,12- isomer is more favoured.

3.2.3 $[(Ph_3P)_2Ir(H)_2(closo\text{-}CB_{11}H_6Br_6)]$, XVIII

Treatment of a stirred CH_2Cl_2 solution of **XVI** with H_2 results in the reduction of the diene, as evidenced by ^1H NMR spectroscopy in CD_2Cl_2 by the formation of cyclooctane, and subsequent coordination of the $[closo\text{-}CB_{11}H_6Br_6]^-$ anion to the $\{(Ph_3P)_2Ir(H)_2\}^+$ fragment generated *in situ* (Figure 3.2.6).

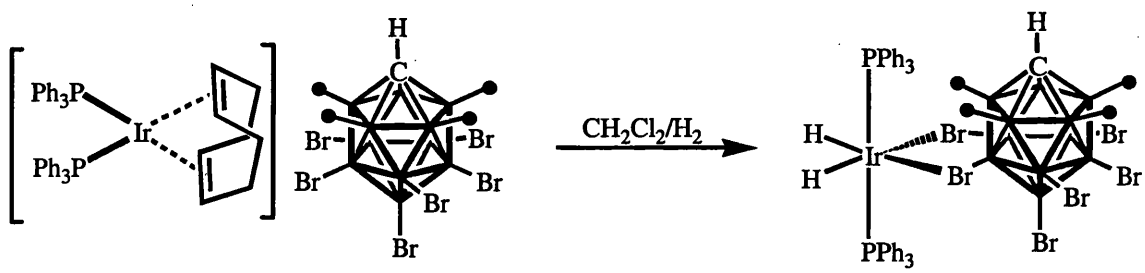

Figure 3.2.6: Synthesis of complex **XVIII**

The reaction was accompanied by a colour change from red to pale yellow. Layering a C_6H_5F solution of **XIX** with hexanes resulted in the formation of colourless crystalline blocks of $[(Ph_3P)_2Ir(H)_2(closo\text{-}CB_{11}H_6Br_6)]\bullet C_6H_5F$, **XVIII**, in good yield. Complex

XVIII was fully characterized by X-ray crystallography, elemental analysis and multinuclear NMR spectroscopy. The solid-state structure of **XVIII** is shown in Figure 3.2.7 with relevant bond lengths and angles shown in Table 3.2.2. The $\{(Ph_3P)_2Ir(H)_2\}^+$ fragment in **XVIII** is coordinated with the cage *via* two B-Br vertices. The cage binds through [B(7)-Br] and [B(8)-Br] vertices. The B-Br distances [B(7)-Br(7) 1.974(9) and B(8)-Br(8) 1.984(11) Å] which are consistent with $[Fe(TPP)(CB_{11}H_6Br_6)]$ (TPP = tetraphenylporphryin) [B(7)-Br(7) 1.93(2)Å], the only other known transition metal complex coordinated to the $[CB_{11}H_6Br_6]^-$ anion.[23] The B-Br distances of those vertexes bound to the metal centre are not much different to those not bound to the metal centre e.g. [B(11)-Br(11) 1.956(11)Å]. This is consistent with $[Fe(TPP)(CB_{11}H_6Br_6)]$ in which all the 'free' B-Br distances are very similar. Also in $[Ag(closo\text{-}CB_{11}H_6Br_6)]$[24] the average B-Br bond distance [1.97(2)Å] is comparable to those distances found in complex **XVIII**. The fact that the B-Br bond lengths remain little changed upon coordination to the metal centre suggests that the cage is only weakly bound. The Ir-Br bond lengths [Ir-Br(7) 2.6799(10) Å and Ir-Br(8) 2.6554(9) Å] are considerably longer than that found in *trans*-$[IrBr(CO)\{P(C_6F_5)_3\}_2]$ [Ir-Br 2.461 Å] reflecting the weak nature of the coordination of the carborane anion. The Ir-P bond lengths [Ir-P(1) 2.322(2) Å and Ir-P(2) 2.335(2) Å] are similar to those found for 3,9-$[(H)_2\{P(p\text{-}tolyl)_3\}_2Ir]$-3,9-$\mu$-$(H)_2$-7,8-$C_2B_9H_{10}$] [2.312(3) Å and 2.301(3) Å].[15] As for complex **XVII** the two phosphorous atoms are not perfectly *trans*- orientated [P(1)-Ir-P(2) 155.33°] as a result of the large steric demand of the bulky anion. The hydride ligands were not located in the difference map but must lie *cis*- to one another and mutually *trans*- to the bromine atoms.

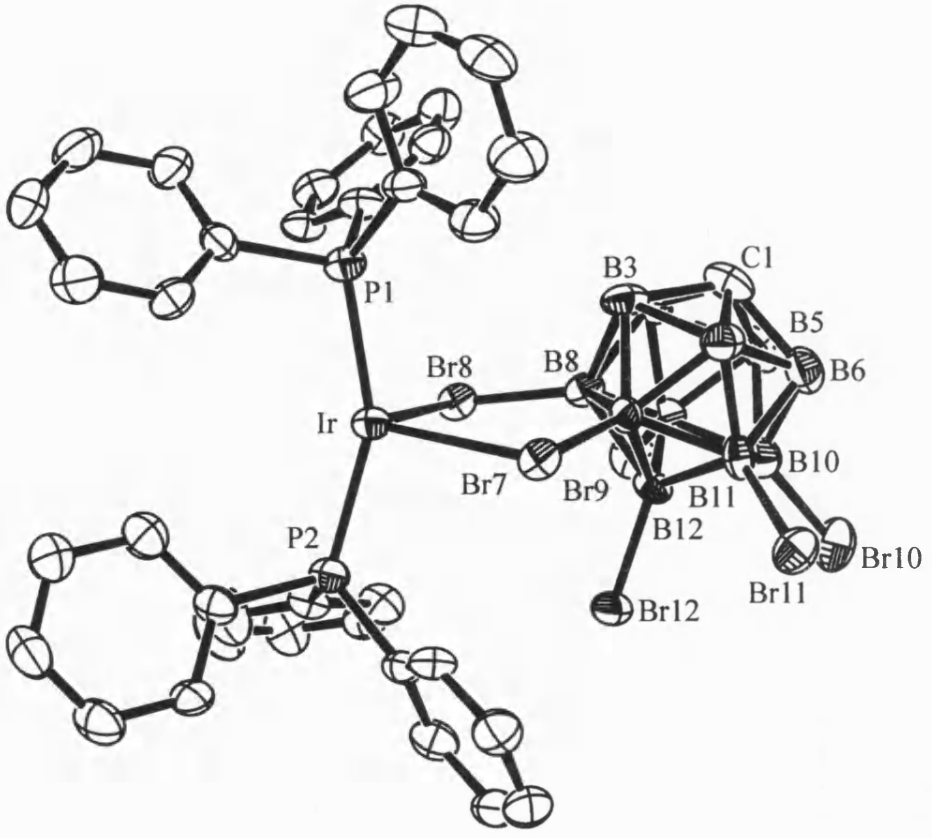

Ir-P1	2.322(2)
Ir-P2	2.335(2)
Ir-Br8	2.6554(9)
Ir-Br7	2.6799(10)
B7-Br7	1.974(9)
B8-Br8	1.984(11)
B9-Br9	1.956(11)
B10-Br10	1.943(12)
B11-Br11	1.956(11)
P2-Ir-P1	155.33(9)
P1-Ir-Br7	96.23(7)
P1-Ir-Br8	94.69(6)
Br8-Ir-Br7	87.20(3)
B8-Br8-Ir	105.4(3)
B7-Br7-Ir	105.2(3)

Table 3.2.2: Selected bond lengths (Å) and angles (°) for complex **XVIII**.

Figure 3.2.7: ORTEP drawing of $[(Ph_3P)_2Ir(H)_2(CB_{11}H_6Br_6)]$, **XVIII**. Ellipsoids drawn at the 50% probability level. All hydrogens have been omitted for clarity

The ^{11}B NMR spectrum of **XVIII** displays three resonances observed at δ -0.78, -9.8 and -21.9 ppm in a 1:5:5 ratio assigned as B(12), B(7-11) and B(2-6) respectively (Figure 3.2.8). Coordination of the anion has the effect of reducing the observed J(BH) coupling so that the B(2-6)-H resonance is now observed as a broad singlet rather than a doublet as observed for uncoordinated [*closo*-$CB_{11}H_6Br_6]^-$ (Figure 3.2.8).

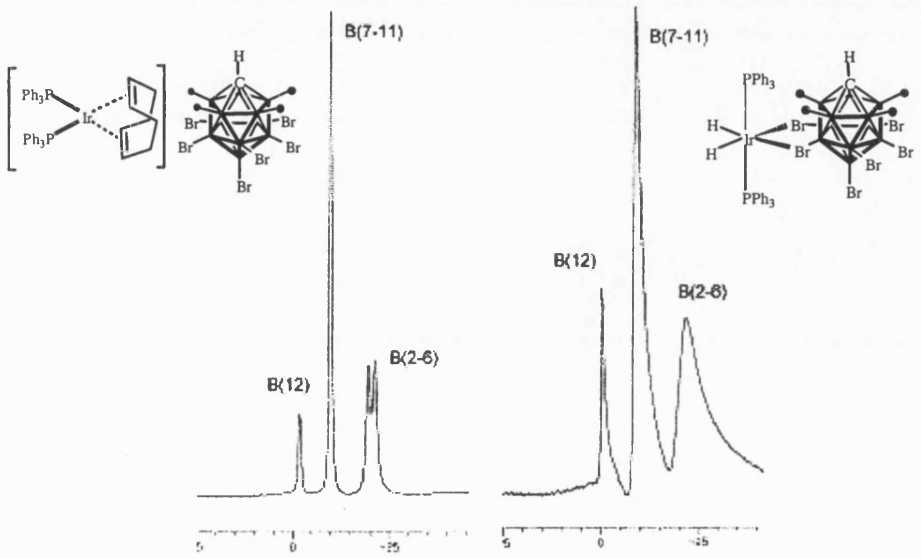

Figure 3.2.8: ^{11}B NMR of **XVI** and **XVIII** respectively

A triplet at δ -25.7 ppm [J(PH) 18 Hz] in the ^1H NMR spectrum, integrating to 2H, is assigned to the hydride ligands. As for **XVII** the solid-state structure is not retained in solution as evidenced by a single broad resonance observed at δ 16.4 ppm in the $^{31}P\{^1H\}$ NMR spectrum at room temperature, although the two phosphines are inequivalent in the solid state due to the orientation of the carborane. A fluxional process must be occurring to equivalence the PPh_3 ligands. Well-resolved ^{31}P coupling to the hydride

ligands indicates that the fluxionality does not involve initial dissociation of a PPh_3 group, which contrasts to complex **XVII** where it was proposed that initial phosphine dissociation was responsible for the observed fluxionality at room temperature. A variable temperature study of complex **XVIII** in CH_2Cl_2 results in the 'freezing out' of the fluxionality at ca. -50°C as evidenced by the $^{31}P\{^1H\}$ NMR spectrum. Two resonances [δ 21.1 and 17.1 ppm, J(PP) 338 Hz] are now observed as expected for inequivalent *trans* phosphines in an AB system. A further resonance at δ 26.0 ppm also appears at low temperature along with new triplet hydride resonance in the ^1H NMR spectrum. This complex is assigned as a dichloromethane complex $[(Ph_3P)_2Ir(H)_2(CH_2Cl_2)][closo\text{-}CB_{11}H_6Br_6]$, **XVIIIa** (Figure 3.2.9). The relative intensity of **XVIIIa** at -80°C is ca. 20%.

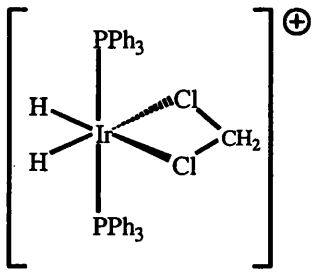

Figure 3.2.9: Suggested structure of **XVIIIa**

NMR data supports the assignment of **XVIIIa**. Only one resonance is observed in the $^{31}P\{^1H\}$ NMR indicating the phosphines are equivalent. A well resolved triplet resonance at δ -23.2 [J(PH) 14Hz] ppm is observed in the ^1H NMR confirming that the hydrides are also equivalent in agreement with the proposed structure for **XVIIIa**. Furthermore, a sample of **XVIII** dissolved in d_8-toluene cooled to -80°C shows only

resonances assigned as **XVIII** and no resonances due to **XVIIIa** as would be expected in the absence of CH_2Cl_2. The fluxionality in complex **XVIII** most likely involves the dissociation of the carborane to perhaps generate a solvento complex (e.g. **XVIIIa**). Recoordination of the carborane in the opposite orientation would result in the phosphines becoming equivalent (Figure 3.2.10).

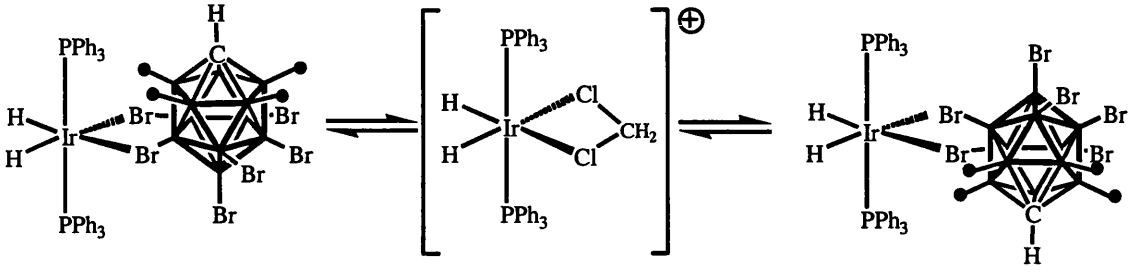

Figure 3.2.10: Fluxionality proposed for **XVIII**

3.2.4 $[(Ph_3P)_2Ir(C_2H_4)_3][closo\text{-}CB_{11}H_6Br_6]$, XIX

Treatment of complex **XVIII** with C_2H_4 in CH_2Cl_2 results in the formation of $[(Ph_3P)_2Ir(C_2H_4)_3][closo\text{-}CB_{11}H_6Br_6]$, **XIX** in virtually quantitative yield as evidenced by ^1H, $^{31}\{^1H\}$ and ^{11}B NMR spectroscopy (Figure 3.2.11).

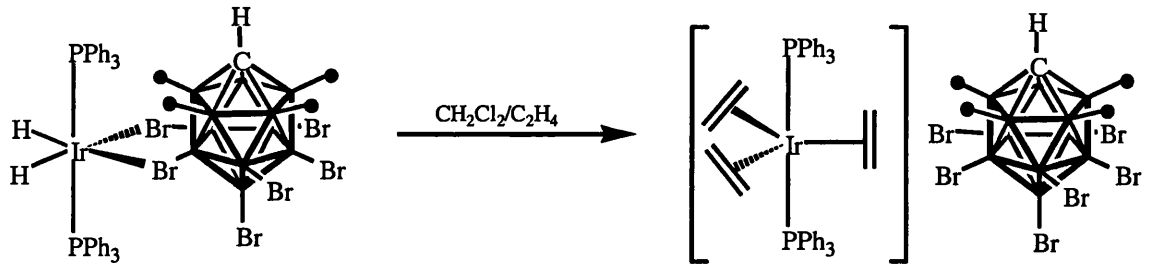

Figure 3.2.11: Synthesis of complex **XIX**

Complex **XIX** crystallizes from $CDCl_3$ upon standing at 25°C, as large colourless prisms. The solid-state structure of **XX** is displayed in Figure 3.2.12 with relevant bond lengths and angles shown in Table 3.2.3. The two phosphine groups are *trans-* orientated [P(1)- Ir-P(2) 177.74(8)°]. The Ir-P bond distances [Ir-P(1) 2.379(2) Å and 2.370(2) Å] are slightly longer than those found for complex **XVII** [Ir-P(1) 2.3195(8) Å and 2.3196(8) Å] and complex **XVIII** [Ir-P(1) 2.322(2) Å and 2.335(2) Å]. They are also longer than those found for $[(Ph_3P)_2Ir(H)_2(OCCH_3)_2]$ [Ir-P(1) 2.337(4) Å and 2.339(4) Å].[14] The three C_2H_4 ligands circle the Ir(I) centre, lying perpendicular to the Ir-P axis. The Ir-C bond lengths e.g. [Ir-C5 2.254(8) Å and 2.256(8) Å] are all similar within the molecule but are slightly longer than those found for $[IrCl(\eta^2\text{-}C_2H_4)(PN)]$ (PN = (4S)-2-[2-(diphenylphosphanyl)phenyl]-4-isopropyl-1,3-oxazoline) [Ir-C(19) 2.123(6)Å and 2.137(5) Å].[25] The anion is not interacting with the metal centre (closest Ir-Br distance 5.250 Å). The room temperature ^1H NMR spectrum of complex **XIX** displays two broad peaks at δ 5.50 and 3.21 ppm assigned as free and coordinated ethene respectively. The broadness of these peaks is due to slow exchange between free and uncoordinated ethylene. In the room temperature $^{31}P\{^1H\}$ NMR spectrum a broad resonance at δ 0.0 ppm is observed. The low temperature $^{31}P\{^1H\}$ NMR spectrum displays a now sharp signal at δ 0.0 ppm. The stability of **XIX** in chlorinated solvents is somewhat surprising considering that $[(PPh_3)_2Ir(\eta^2\text{-}C_2H_4)_3][BF_4]$ is unstable above -30°C.[26] The enhanced stability of this complex must arise as a result of the $[closo\text{-}CB_{11}H_6Br_6]^-$ anion.

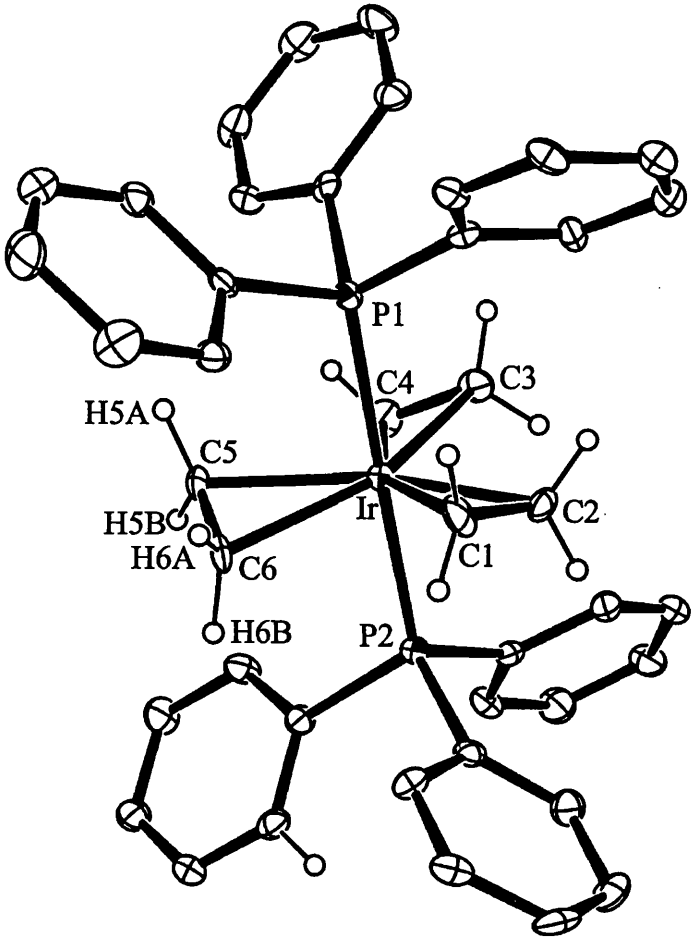

Ir-P1	2.379(2)
Ir-P2	2.370(2)
Ir-C1	2.221(8)
Ir-C2	2.220(8)
Ir-C3	2.273(9)
Ir-C4	2.268(9)
Ir-C5	2.254(8)
Ir-C6	2.256(8)
P1-Ir-P2	177.74(8)
C4-Ir-P1	95.4(3)
C3-Ir-P1	84.8(3)

Table 3.2.3: Selected bond lengths (Å) and angles (°) for complex **XIX**

Figure 3.2.12: ORTEP drawing of the cationic portion of complex **XIX**. Ellipsoids are drawn at the 30% probability level. All phenyl hydrogens have been omitted for clarity

The ^{11}B NMR spectrum displays three resonances according to uncoordinated carborane with a well resolved doublet [J(HB) 166 Hz] assigned as BH(2-6). Upon cooling a sample of **XIX** to -30°C in CH_2Cl_2 sharp signals are observed for bound ethene at δ 3.09 ppm integrating as 12 protons and for free ethene at δ 5.39 ppm respectively.

3.2.5 $[(Ph_3P)_2Ir(C_2H_4)_3][closo\text{-}CB_{11}H_6Br_6]$, XX

Under vacuum a CH_2Cl_2 solution of complex **XIX** will readily dissociate one molecule of ethene to give $[(PPh_3)_2Ir(C_2H_4)_2][closo\text{-}CB_{11}H_6Br_6]$, **XX**, in virtually quantitative yield as evidenced by ^1H and $^{31}P\{^1H\}$ NMR spectroscopy (Figure 3.2.13)

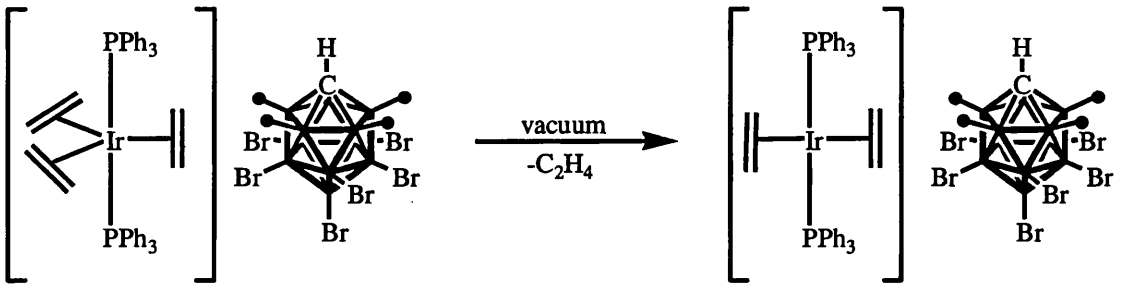

Figure 3.2.13: Formation of complex **XX**

Complex **XX** could not be isolated as a crystalline solid but was characterised *in situ* after formation from complex **XIX**. The ^1H NMR spectrum of **XX** displays one peak at δ 3.20 ppm integrating as 8 protons assigned as two molecules of metal bound ethene. The $^{31}P\{^1H\}$ NMR spectrum displays one broad singlet at δ 16.1 ppm. Crabtree has spectroscopically characterised the complex $[(PPh_3)_2Ir(C_2H_4)_2][PF_6]$, previously.[2] In this case the two molecules of ethene were assigned as being *trans-* to one another on the

basis that no ^{31}P coupling is observed in the ^{13}C NMR spectrum. A large *trans*-phosphorous coupling would be expected if the ethene were *trans*- to a PPh_3 ligand. On the basis of Crabtree's report we assign the same configuration for complex **XX**.

3.3.6 Reactivity of XIX and XX with H_2

A CH_2Cl_2 solution of complex **XIX** reacts with H_2 to regenerate complex **XVIII** in quantitative yield according to ^1H, $^{31}P\{^1H\}$ and ^{11}B NMR spectroscopy. In effect complex **XVIII** and **XIX** represent structurally characterised intermediates on the catalytic cycle for the hydrogenation of olefins. Complex **XIX** represents the resting state for the catalyst in which the anion is displaced in the presence of excess olefin. Complex **XVIII** appears to be re-usable in ethene reduction. This attractive property is attributed to the anion [*closo*-$CB_{11}H_6Br_6]^-$ which returns to stabilise the metal fragment after hydrogenation is complete but is sufficiently weakly coordinating to move aside to allow the olefin to bind to the metal centre. This 'catch and release' mechanism is outlined in Figure 3.2.14.

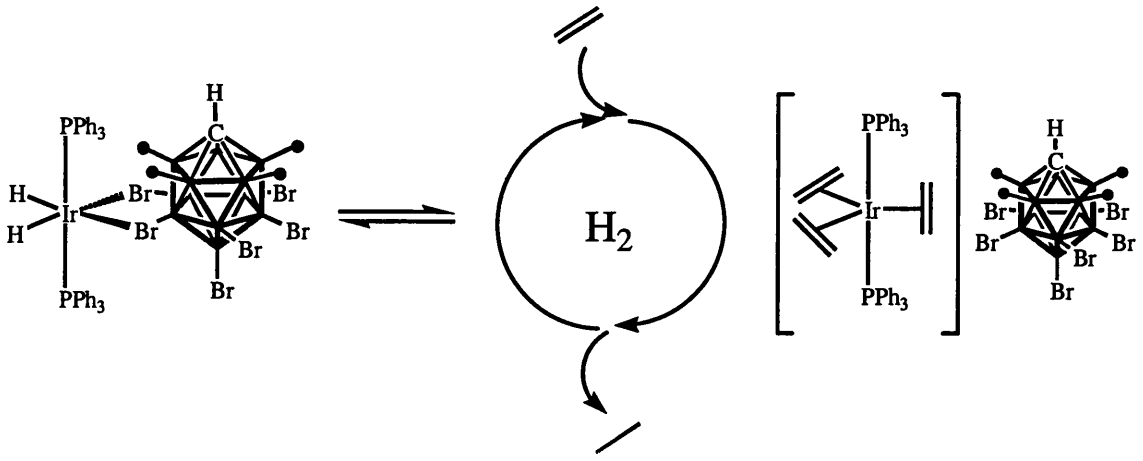

Figure 3.2.14: Catch and release in the hydrogenation of olefins with complex XVIII

The coordinating power of the anion seems to be of paramount importance in the stabilisation of the reactive $\{(Ph_3P)_2Ir(H)_2\}^+$ cation. Although the situation is a finely balanced one as it needs to be weakly coordinating enough to move aside to allow for substrate coordination. For example, when $[(Ph_3P)_2Ir(cod)][Y]$ (Y= $B(Ar)_f$, PF_6) are treated with H_2 in CH_2Cl_2 the major organometallic product is the iridium dimer $[Ir_2(\mu\text{-}H)_3H_2L_4][BAr_f]$ (Figure 3.2.15).

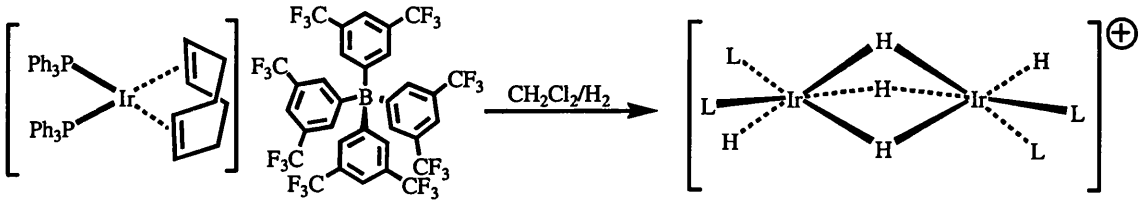

Figure 3.2.15: Reaction of $[(Ph_3P)_2Ir(cod)][BAr_f]$ with H_2

The inability of the $[B(Ar)_f]^-$ and $[BF_4]^-$ anions to stabilise the $14e^-$ fragment generated results in the decomposition of formation of a catalytically inactive hydride bridged dimer. In contrast $[closo\text{-}CB_{11}H_6Br_6]^-$ provides just enough stabilisation to the metal centre to prevent the formation of this dimer. The ability of the anion to stabilise a highly electrophilic metal centre is a useful property and it will be seen in the subsequent chapter that modulation of the counterion can result in not only a marked increase in observed catalytic rate but also in the catalyst stability.

3.2.3 Summary

We have demonstrated that cationic iridium(I) cyclooctadiene complexes are air-stable precursors to [*closo*-$CB_{11}H_{12}$]$^-$ and [*closo*-$CB_{11}H_6Br_6$]$^-$ carborane complexes of iriduium(III). In each case the $\{(PPh_3)_2Ir(H)_2\}^+$ fragment is stabilised by a carborane. In the case of the [*closo*-$CB_{11}H_{12}$]$^-$ anion the cage is bound to the metal fragment *via* two 3 centre 2 electron B-H-Ir bonds which are static at room temperature. However the complex is fluxional in CD_2Cl_2 and this fluxionality is proposed to proceed *via* initial phosphine dissociation. In the case of the [*closo*-$CB_{11}H_6Br_6$]$^-$ anion the cage is bound through two {BBr} vertices by much weaker B-Br-M interactions. The molecule is fluxional in CD_2Cl_2 but this fluxionality appears not to involve dissociation of phosphine proceeding instead via anion dissociation *via* a CH_2Cl_2 intermediate. The complex [$(PPh_3)_2Ir(H)_2$(*closo*-$CB_{11}H_6Br_6$)] is a useful precursor to hghly stable *bis*- and *tris*-complexes of iridium. These complexes have previously been characterised *via* NMR spectroscopy only. The stability of [$(PPh_3)_2Ir(\eta^2\text{-}C_2H_4)_3$][*closo*-$CB_{11}H_6Br_6$] over [$(PPh_3)_2Ir(\eta^2\text{-}C_2H_4)_3$][$BF_4$] is noteworthy and must be due to the inherently more stable carborane monoanion.

1 R. H. Crabtree, *Acc. Chem. Res.*, 1979, **12**, 331.

2 R. H. Crabtree, P. C. Demou, D. Eden, J. M. Mihelcic, C. A. Parnell, J. M. Quirk, and G. E. Morris, *J. Am. Chem. Soc.*, 1982, **104**, 6994.

3 A. Pfaltz, J. Blankenstein, R. Hilgraf, E. Hormann, S. McIntyre, F. Menges, M. Schonleber, S. P. Smidt, B. W. Wustenberg, and N. Zimmermann, *Adv. Synth. Cat.*, 2002, 345.

4 J. F. Hartwig, T. Ishiyama, J. Takagi, K. Ishida, N. Miyaura, and N. Anastasi, *J. Am. Chem. Soc.*, 2001, **124**, 390.

5 P. Albietz, B. Cleary, W. Paw, and R. Eisenberg, *Inorg. Chem.*, 2002, **41**, 2095.

6 R. H. Crabtree, C. P. Parnell, and R. J. Uriarte, *Organomet.*, 1987, **6**, 696.

7 C. M. Jensen, *Chem. Comm.*, 1999, 2443.

8 S. Niu and M. B. Hall, *Chem. Rev.*, 2000, **100**, 353.

9 M. Torrent, M. Sola, and G. Frenking, *Chem. Rev.*, 2000, **100**, 439.

10 R. H. Crabtree and M. J. Burk, *J. Am. Chem. Soc.*, 1987, **109**, 8025.

11 A. Lightfoot, P. Schnider, and Pfaltz A., *Angew. Chem. Int. Ed.*, 1998, **37**, 2897.

12 M. Butts, B. Scott, and G. Kubas, *J. Am. Chem. Soc.*, 1996, **119**, 11831.

13 D. M. Tellers and R. G. Bergman, *J. Am. Chem. Soc.*, 2001, **123**, 11508.

14 R. H. Crabtree, J. W. Faller, F. Mellea, and J. M. Quirk, *Organomet.*, 1982, 1361.

15 J. A. Doi, R. G. Teller, and M. F. Hawthorne, *Chem. Comm.*, 1980, 80.

16 C. Vinas, M. R. Cirera, F. Teixidor, R. Kivekas, R. Sillanpaa, and J. Llibre, *J. Organomet. Chem.*, 1998, **568**, 149.

17 F. Teixidor, J. A. Ayllon, C. Vinas, R. Sillanpaa, R. Kivekas, and J. Casabo, *Inorg. Chem.*, 1994, **33**, 4815.

18 J. C. Jeffery, P. A. Jelliss, and F. G. A. Stone, *J. Chem. Soc. Dalton Trans.*, 1993, 1083.

19 J. C. Jeffery, P. A. Jelliss, L. H. Rees, and F. G. A. Stone, *Organomet.*, 1998, **17**, 2258.

20 J. A. K. Howard, J. C. Jeffery, P. A. Jelliss, T. Sommerfeld, and F. G. A. Stone, *J. Chem. Soc. Chem. Comm.*, 1991, 1664.

21 M. F. Hawthorne and E. L. Hoel, *J. Am. Chem. Soc.*, 1975, 6388.

22 A. V. Usatov, E. V. Martynova, F. M. Dolgushin, A. S. Peregudov, M. Y. Antipin, and Y. N. Novikov, *Eur. J. Inorg. Chem.*, 2002, 2565.

23 D. R. Evans and C. A. Reed, *J. Am. Chem. Soc.*, 2000, **122**, 4660.

24 Z. Xie, B. M. Wu, C. W. Mak, J. Manning, and C. A. Reed, *J. Chem. Soc. Dalton Trans.*, 1997, 1213.

25 D. Carmona, D. Ferrer, E. Lalaguna, M. Lorenzo, F. Lahoz, S. Elipe, and L. Oro, *Eur. J. Inorg. Chem.*, 2002, 259.

26 J. M. Brown, R. A. John, and A. R. Lucy, *J. Organomet. Chem.*, 1985, **279**, 245.

4 COUNTERION EFFECTS IN HYDROGENATION

4.1 Introduction

Chapters 2 and 3 sought to outline the synthesis and reactivity of novel metallocarboranes incorporating both rhodium and iridium centres partnered with weakly coordinating anions based around [*closo*-$CB_{11}H_{12}]^-$ and derivatives thereof. Given the success achieved in synthesizing several new *exo-closo* metallocarboranes the logical next step seemed to be the evaluation of these new compounds in the hydrogenation of olefins. Given the increasing appreciation of counterion effects in the literature we were interested in investigating the possible enhancement of rhodium based hydrogenation catalysts, specifically those based around the Schrock-Osborn system. The following section seeks to highlight counterion effects that are known in the literature as well as discussing the mechanism of hydrogenation for Schrock-Osborn type catalysts. Hydrogenation with iridium based complexes will also be outlined along with decomposition pathways.

The discovery of an efficient homogeneous catalyst for the hydrogenation of olefins was first reported in 1965 by Wilkinson.[1, 2] The complex [$(PPh_3)_3RhCl$] (**1**) (Figure 4.1) is now ubiquitous in inorganic chemistry and is a paradigm in the understanding of inorganic mechanisms.

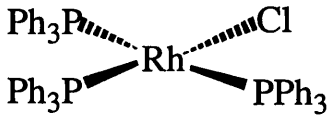

(1)

Figure 4.1: Wilkinson's complex

Since its discovery numerous studies have been carried out to determine the mechanism of hydrogenation operating for complex (1).[3-8] The generally accepted mechanism is that outlined in Figure 4.2

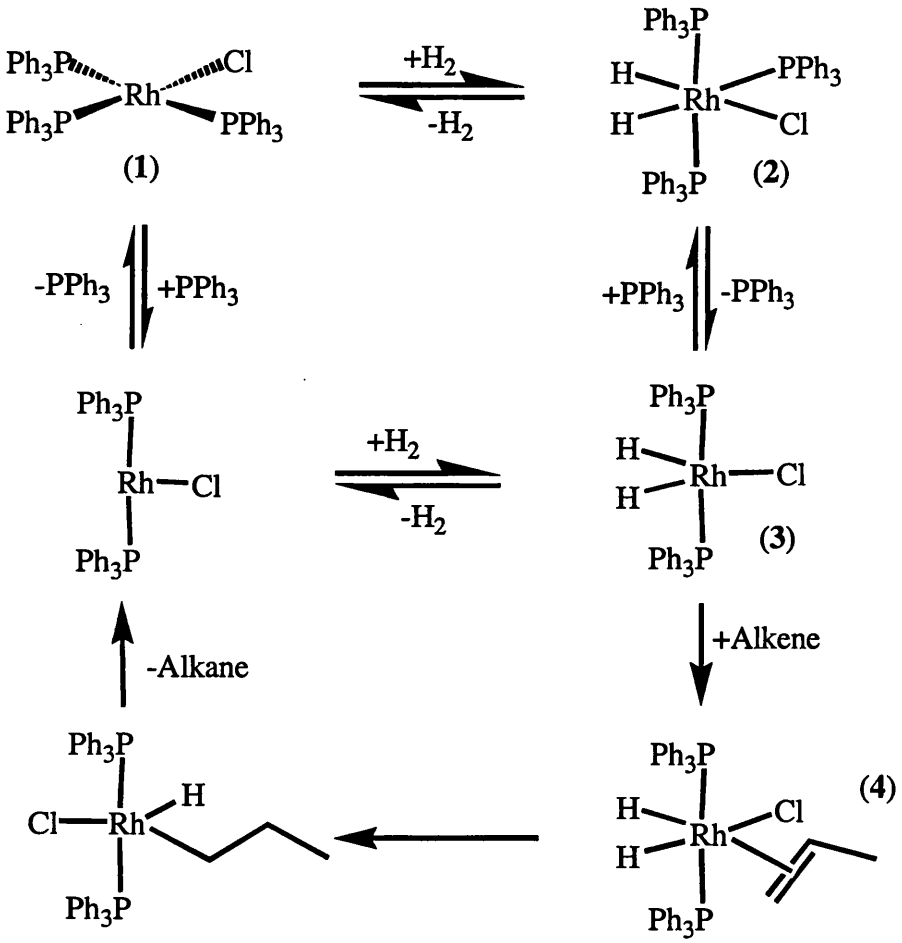

Figure 4.2: Hydrogenation of olefin with Wilkinson's complex

Two initial pathways are possible according to Figure 4.2. Initial dissociation of phosphine from complex (**1**) would generate a coordinatively unsaturated 14e$^-$ bis(phosphine)rhodium species which adds H_2 in a *cis-* manner to generate complex (**3**). Alternatively, oxidative addition of H_2 across complex (**1**) results in the formation of complex (**2**) which readily dissociates phosphine to again form (**3**). Dissociation of phosphine is the key step of the catalytic cycle. Complex (**2**) has been shown to dissociate the PPh_3 group *trans-* to the hydride ligand with $k_{diss} = 400\ s^{-1}$.[9] Subsequent coordination of olefin generates complex (**4**). The insertion of the olefin into the metal-hydride bond is proposed to be the rate-determining step in the cycle.[7] Subsequent reductive elimination of the alkane completes the cycle. Investigations into the mechanism of hydrogenation still throw new light on this system. Duckett and co-workers have recently detected several new hydrides in the hydrogenation cycle using Wilkinson's complex by employing parahydrogen induced polarization (PHIP).[10] The most important new species detected was an intermediate formulated as $[Rh(H)_2Cl(PPh_3)_2(olefin)]$ (**5**) (Figure 4.3).

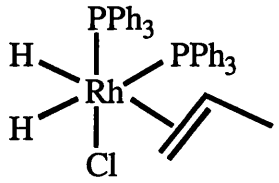

(**5**)

Figure 4.3: Intermediate in olefin hydrogenation using Wilkinson's complex

Complex (**5**) is essentially an isomer of complex (**4**) and is the first time a kinetically significant complex has been detected for $[(PPh_3)_3RhCl]$ under catalytic conditions. It

was proposed that complex (**5**) is observed as opposed to any other possible isomers because it is kinetically more stable.

Schrock and Osborn[11] made an important contribution to the chemistry of homogeneous hydrogenation catalysts based around rhodium by preparing a series of complexes of the type $[(L)_2Rh(nbd)][BF_4]$ (L = tertiary phosphine, nbd = 2,5-norbornadiene) (**6**) (Figure 4.4).

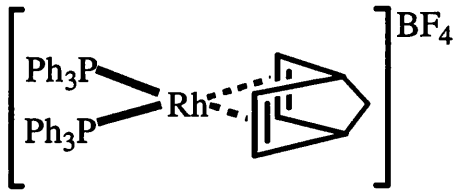

(**6**)

Figure 4.4: Schrock-Osborn type catalyst

The synthesis of these catalyst precursors has been discussed in section 2.2. The Schrock-Osborn catalytic precursors differ in two main ways from Wilkinson's complex. Firstly one of the phosphine ligands has been removed from the coordination sphere and the $\{(Ph_3P)_2Rh\}^+$ fragment is 'capped' by a diene ligand. Secondly the anion has been modulated from Cl^- to $[BF_4]^-$. The modulation of the anion in this way prevents the formation of halide bridged dimers which can inhibit catalytic activity.[11] The mechanism for the hydrogenation of olefins is outlined in Figure 4.5. The initial hydrogenation of the catalyst precursor results in the reduction of the diene precursor to form $[(Ph_3P)_2(H)_2Rh(Sol)_2]^+$ (Sol = Solvent) (**7**). Typically the solvent would be acetone,

THF or methanol. The two hydride ligands are mutually *cis-* to one another and both *trans-* to the solvent molecules. The labile nature of the solvent molecules is the key to the activity of this system. For example, when the strongly coordinating solvent acetonitrile is used, a catalytically inactive system is formed. The olefin complex (7) then undergoes insertion into the M-H bond resulting in the formation of a metal alkyl which rapidly eliminates alkane. Addition of H_2 across the resulting rhodium(I) centre regenerates the active catalyst.

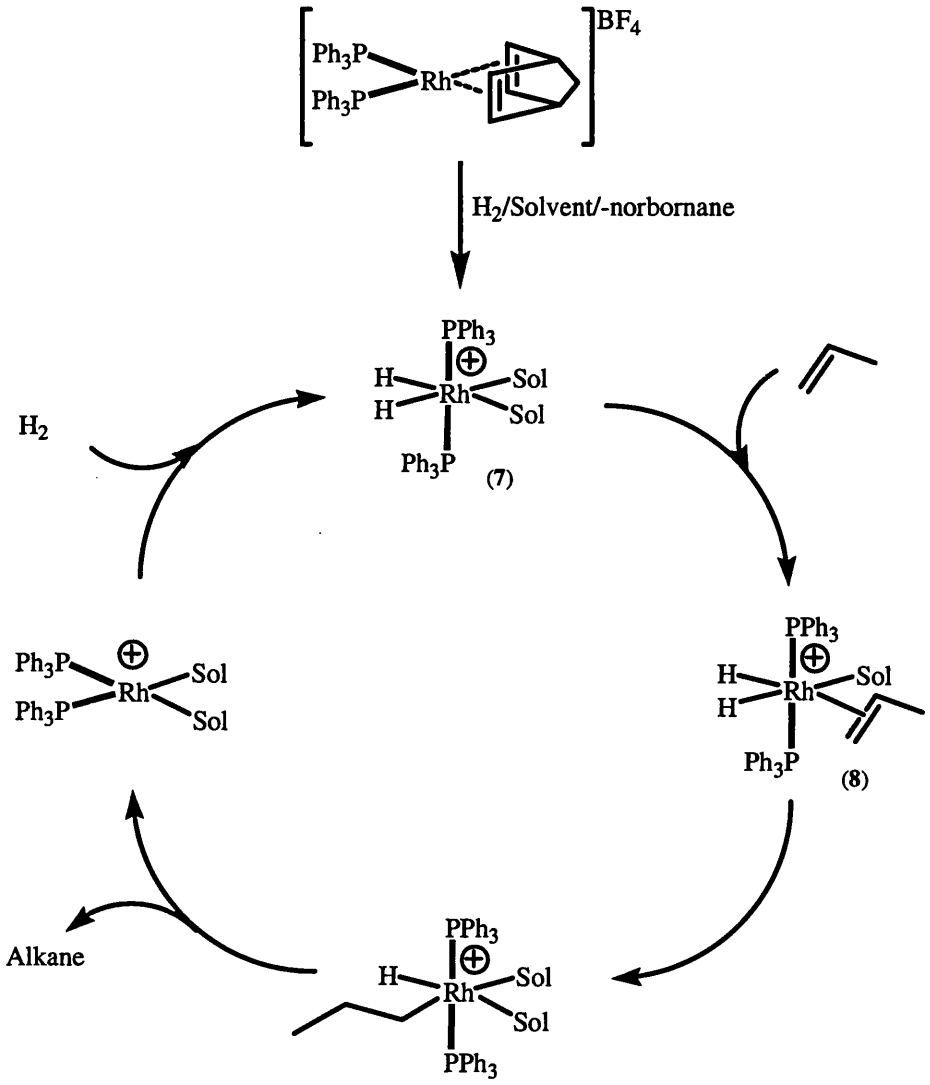

Figure 4.5: Mechanism of Hydrogenation using the Schrock-Osborn system

One disadvantage of this system is that complex **7** is also a good olefin isomerisation catalyst. This arises as a result of the acidity of complex **7** according to Equation 4.6.

$$[(Ph_3P)_2Rh(H)_2(Sol)_2]^+ \rightarrow [(Ph_3P)_2RhH(Sol)_2]^+ + H^+$$

Equation 4.6: Acidity of complex (7)

The monohydride is a highly efficient isomerisation catalyst. This can be problematic as isomerisation, for example, of 1-hexene, results in the formation of the internal alkene 2-hexene which is not hydrogenated by the Schrock-Osborn system. Isomerisation in this system can be suppressed by carrying out the hydrogenation under acidic conditions. One of the main drawbacks of both the Schrock-Osborn type catalysts and Wilkinson's complex is that while both are efficient for hydrogenating terminal alkenes, such as 1-hexene, neither is particularly efficient at hydrogenating internal alkenes such as cyclohexene or 2-hexene (see Table 4.1).

In a series of papers Crabtree systematically developed the chemistry of iridium based hydrogenation catalysts of the type $[Ir(cod)L_2][PF_6]$ (7), where L = tertiary phosphine or amine. Synthesis of these complexes is achieved by addition of four equivalents of L to $[(cod)IrCl]_2$ in non-polar solvents followed by salt metathesis (Figure 4.7).[12]

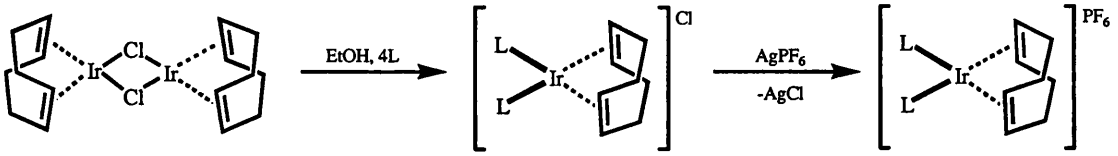

(8)

Figure 4.7: Synthesis of (**8**).

Mixed ligand complexes are prepared simply mixing the appropriate $[L_2Ir(cod)]^+$ and $[L'_2Ir(cod)]^+$ cations in acetone which results in formation of complexes of the type $[Ir(cod)LL'][PF_6]$ (L = PR_3, L' = PR'_3). Alternatively, where L = pyridine (py) addition of PCy_3 results in the isolation of the so-called Crabtree's catalyst (**9**) (Figure 4.8) in good yield.

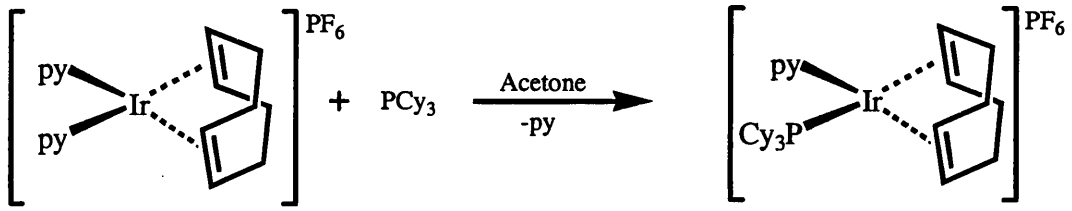

(9)

Figure 4.8: Synthesis of Crabtree's catalyst

It was shown that complexes of the type **8** and **9** are excellent catalysts for the hydrogenation of di-, tri- and tetra- substituted olefins.[13] Table 3.1 shows catalyst precursors based upon Iridium and Rhodium and their performance in the hydrogenation of various substituted olefins.[14]

Catalyst Precursor	Solvent	Substrate			
		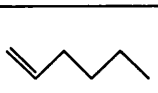		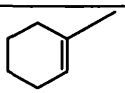	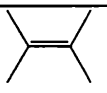
$[Ir(cod)PCy_3(py)]^+$	CH_2Cl_2	6400	4500	3800	4000
$[Ir(cod)(PMePh_2)_2]^+$	CH_2Cl_2	5100	3800	1900	50
	Me_2CO	10	0	0	0
$[Rh(cod)(PPh_3)_2]^+$	CH_2Cl_2	4000	10	-	0
$[RuHCl(PPh_3)_3]$	C_6H_6	9000	7	-	0

Table 4.1: Rates[a] of hydrogenation of substituted olefins with various precursors.[14]

[a] In mol of substrate reduced (mol of catalyst)$^{-1}$ h^{-1}.

In coordinating solvents the ability of the iridium-based catalysts to hydrogenate unhindered substrates such as 1-hexene is seriously reduced. However, using CH_2Cl_2 as solvent the catalysts are highly active even for the reduction of highly substituted olefins. The catalytic cycle (Figure 4.9) for the hydrogenation with this system was elucidated by Crabtree in an elegant work.[15] The initial step is hydrogenation of the precursor cyclooctadiene complex *via* a dihydride adduct **10**. Formation of $[trans\text{-}L_2Ir(ol)_2]^+$ **11** follows via coordination of olefin to the iridium(I) centre. Complex **11** rapidly reacts with H_2 to give **12**. Insertion of the olefin into the Ir-H bond **13** followed by rapid reductive elimination of alkane and coordination of substrate completes the cycle. The activity of these catalysts is attributed to several factors. The catalyst is extremely stable. Reactivity[14] of cationic $[L_2Ir(cod)]^+$ fragments suggest that the complex behaves as a Lewis acid rather than, as expected for a low valent late-transition metal, a Lewis base. Thus, the cationic fragment oxidatively adds H_2 or HCl much more rapidly than O_2 or RX. Therefore any Ir(I) species generated is short lived.

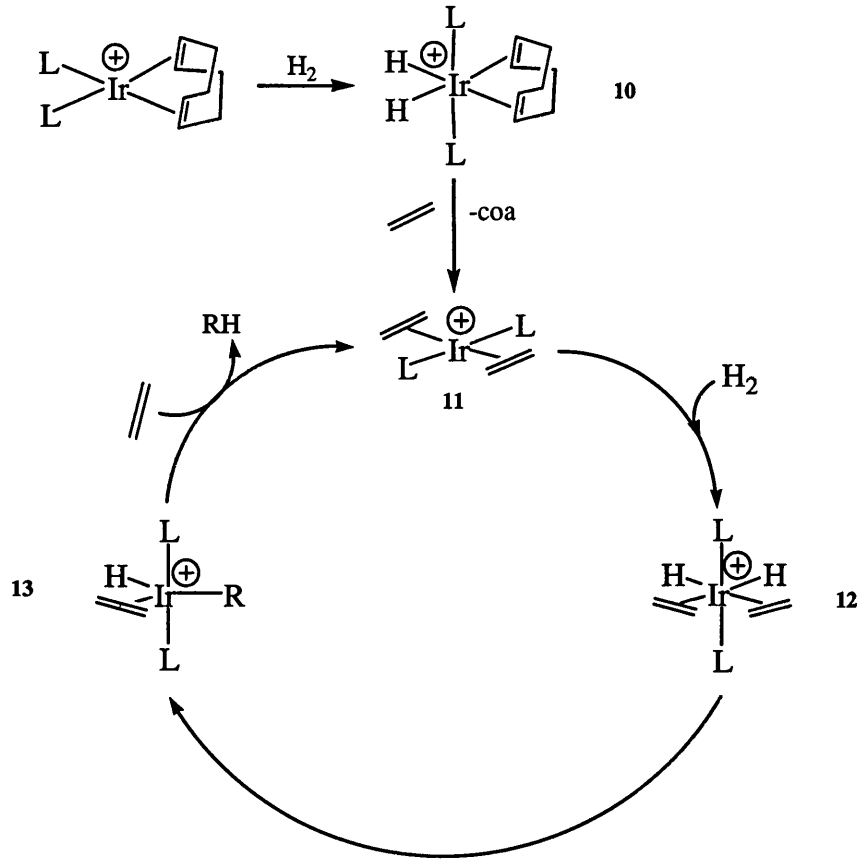

Figure 4.9: Hydrogenation cycle using Crabtree's Iridium based system.

Because the insertion of olefin into the M-H bond **12** → **13** is slow, the predominant species in solution is complex **12**. Given that **12** is an Ir(III) complex which cannot readily undergo oxidative addition itself gives the system more stability to oxidizing functions such as RX or O_2. The rapid rate of hydrogenation is attributed to the conformation that the substrate takes when bound to the iridium centre. So as to avoid unfavourable orbital interactions the olefin tends to adopt a coplanar orientation with respect to the M-H bonds[15] which has been shown to lead to the most rapid hydrogenation.[16] The fact that the olefin remains bound to the metal centre throughout the cycle (bulky olefins are hydrogenated at comparable rates to less bulky olefins) also

helps to increase the rate of hydrogenation as there is no competition from solvent. In fact hindered olefins are reduced at a lower temperature suggesting that relief of steric interactions promotes the insertion of the olefin into the M-H bond resulting in faster catalyst.

Catalyst deactivation is a major problem with these iridium based systems. Complexes of the type $[L_2Ir(cod)]^+$ ($L = PR_3$) tend to deactivate via formation of the hydride bridged dimer $[HL_2Ir(\mu\text{-}H)_3IrL_2H]^+$ (**14**) (Figure 4.10).

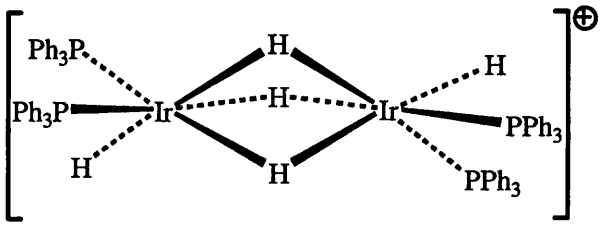

14

Figure 4.10: Deactivation product of $[L_2Ir(cod)]^+$ under hydrogenation conditions

For less hindered olefins the deactivation tends to occur when the substrate has been consumed but for more hindered olefins deactivation occurs before complete consumption of the substrate. For complex **9** deactivation remains a problem. In this case the deactivation product is $[(H_2LL'Ir)_3(\mu_3\text{-}H)]^{2+}$ **15** (Figure 4.11). Deactivation is thought to occur via two or more $\{L_2(H)_2Ir\}^+$ fragments coming together with nuclephilic attack of a metal hydride on the Lewis acidic metal fragment.[15]

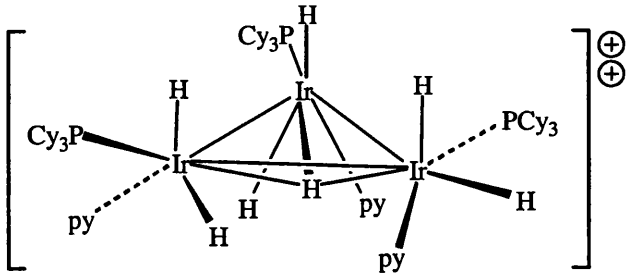

15

Figure 4.11: Deactivation product from Crabtree's catalyst

The dehydrogenation of alkenes with Iridium phosphine fragments has also been investigated by Crabtree[15, 17-19] and others.[20] The solvent complex $[(PPh_3)_2Ir(H)_2(Me_2CO)_2]$ **16** (Figure 4.12) is active as a dehydrogenation catalyst.

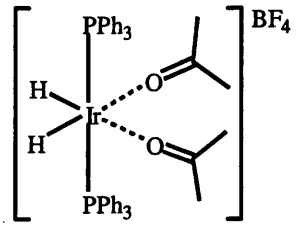

16

Figure 4.12: An Iridium based dehydrogenation catalyst

Complex **16** is capable of dehydrogenating a variety of alkanes and alkenes under relatively mild conditions. For example, in refluxing 1,2-dichloroethane, complex **16** will dehydrogenate cyclopentane to give $[IrCpH(PPh_3)_2][BF_4]$ in 32% yield (Figure 4.13).[19]

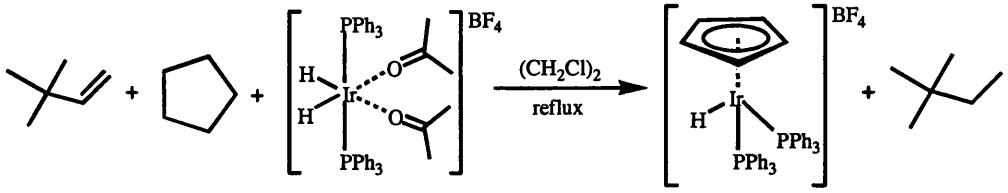

Figure 4.13: Dehydrogenation of cyclopentane by **16**

The presence of *tert*-butylethylene (tbe) is needed to act as a hydrogen acceptor and acts initially to strip H_2 from complex **16** to generate complex **17** (Figure 4.14). The exact structure of this intermediate is unclear. Various structures have been postulated. A Y-

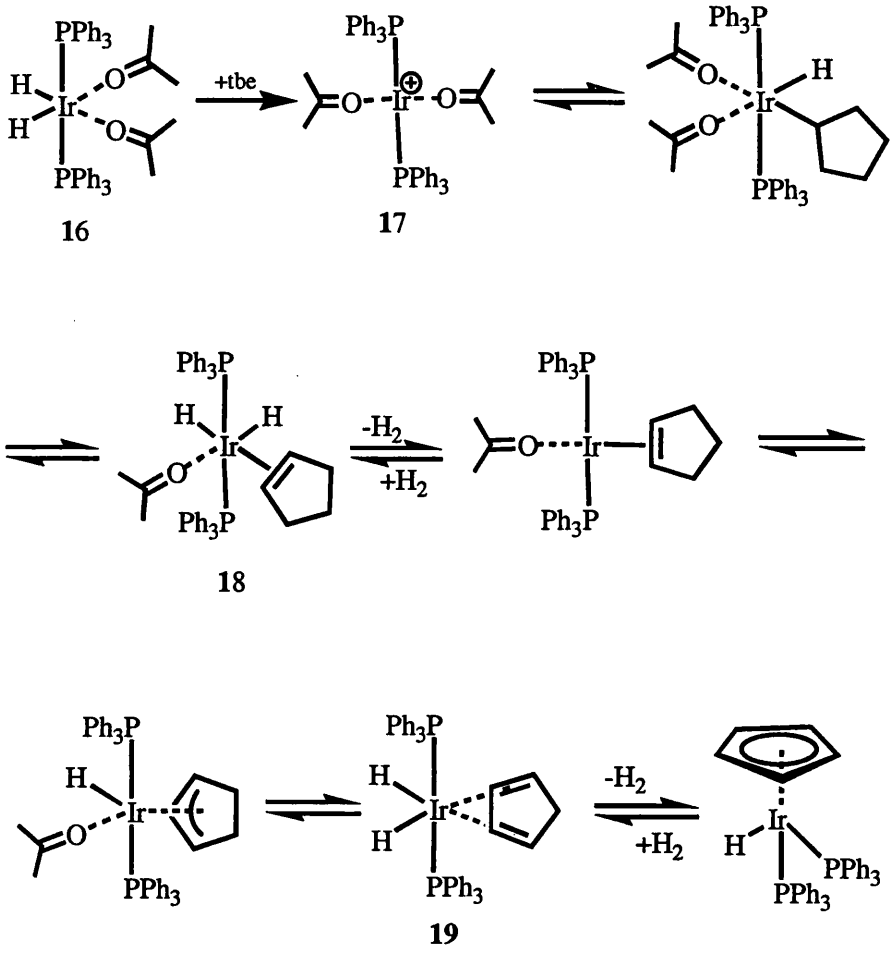

Figure 4.14: Dehydrogenation of cyclopentane

shaped 3-coordinate d^8 species,[21, 22] which would be generated *via* reversible loss of a solvent molecule is plausible. While another another postulated structure[15] is that of an unidentified hydride of formula $[Ir(H)_xL_2]_y$. Whatever the exact structure of complex **17** it is clearly highly reactive and capable of activating C-H bonds. The dihydride **18** has been isolated. The probable next step in the reaction is the dissociation of hydrogen from the metal centre, which regenerates complex **16** from **17** and is then reduced by a classical hydrogenation with tbe. It remains possible, however, that the tbe displaces solvent directly from **18** and is reduced on the same iridium centre before the dehydrogenation continues. This is perhaps unlikely given the steric demand of tbe. The next step involves allylic activation to give a π-allyl hydride followed by formation of complex **19** by similar allyl activation. Loss of H_2 from complex **19** results in oxidative addition of one of the remaining C-H bonds on the pentane and generates the observed product.

The scope of homogeneous hydrogenation catalysts based upon Iridium has been expanded by Pfaltz.[23-25] Iridium catalysts based upon phosphinooxazoline and phosphinite-oxazoline ligands (Figure 4.15) are capable of hydrogenating unfunctionalised olefins with high enantioselectivity.[24]

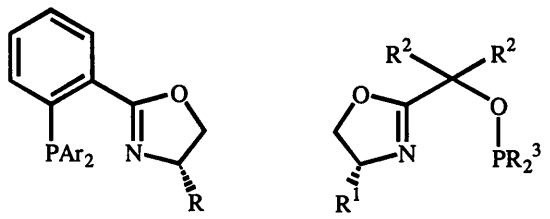

Figure 4.15: Chiral phosphinooxazoline and phosphinite-oxazoline ligand

Complexation of the ligands shown in Figure 4.15 is readily achieved via refluxing the desired ligand with $[Ir(cod)Cl]_2$ in CH_2Cl_2 followed by counterion exchange in a two-phase H_2O/CH_2Cl_2 system. Variation of R and of the Aryl group has a dramatic effect on the enantiomeric excess afforded by the catalyst in the hydrogenation reaction shown in Figure 4.16.

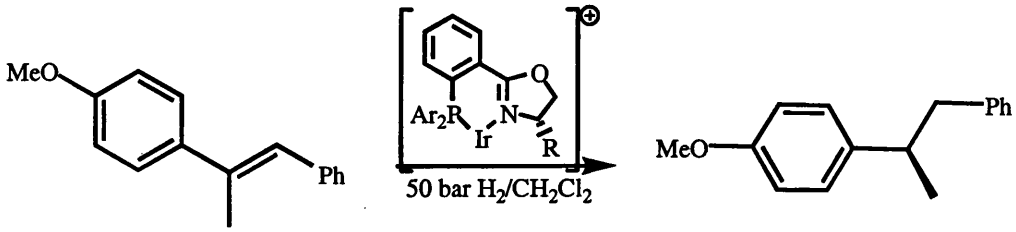

Figure 4.16: Hydrogenation of (E)-1-phenyl-2-(4-methoxyphenyl)-1-propene

A discussion of the reasons underlying the differences in observed enantioselectivities is not warranted here. More relevant is the effect of counterion on the reaction. When hexafluorophosphate $[PF_6]^-$ is employed as counterion, high catalyst loadings (ca. 4 mol%) must be used to achieve complete conversion of olefins. This is because at lower loadings (ca. 1 mol%) complete deactivation of the catalyst is observed before 50% of the substrate is hydrogenated. It is possible to improve the efficiency of the system by

vigorously excluding both air and moisture from the system. This enabled the catalyst loading to be lowered to 0.5mol% to give greater conversion but still with considerable deactivation. When the anion is modulated to $[B(Ar_f)_4]^-$ a surprising increase in stability and activity of the catalyst was observed. With this anion the catalyst loading can be lowered to 0.02mol% giving full conversion of olefin. The origin of this counterion effect is stil not fully understood but can be put down to two possible reasons. Firstly, in the case of the PF_6^- anion it is possible that traces of water react with the anion under catalytic conditions degrading it to oxyfluorophosphates and thus poisoning the catalyst. The $[B(Ar_f)_4]^-$ anion however is much more robust towards moisture and therefore no anhydrous conditions are needed. The second reason is more complex but seems to involve the interaction of the counterion with the catalyst. Studies have shown that the chiral iridium catalysts under discussion also deactivate in the same way as found for Crabtree's catalyst.[26] Interestingly, when the counterion employed is $[B(Ar_f)_4]^-$ less of this deactivation product is observed than when the PF_6^- anion is used. This suggests that the more bulky, weakly coordinating anion is actually more effective in stabilizing the active catalyst than the more traditional PF_6^- anion. Pulsed Gradient Spin Echo (PGSE) NMR spectroscopy was used on a model complex **20** to determine the amount of ion-pairing of various cation/anion pairs in solution.[27]

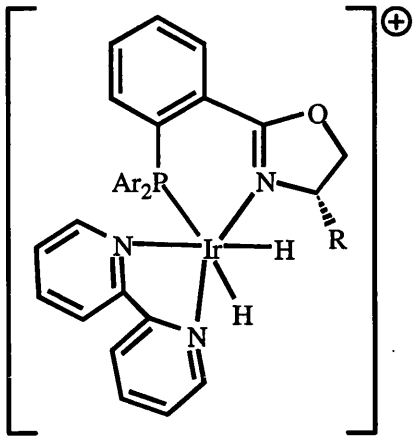

Figure 4.17: Model complex **20** used in PGSE studies

When the anion paired with complex **20** is PF_6^- the diffusion data shows that the anion moves faster than the cation in solution. This suggests that the anion moves independently and consequently at some distance from the cation. Conversely, when the anion is $[B(Ar_f)_4]^-$ the diffusion data shows that the cation and anion move at the same speed indicating that they are associated in solution. It may be that this association is enough to slow the intermolecular attack of another Ir-H bond and thus the catalyst deactivates more slowly with this anion. However, it should be noted that the data was obtained on a complex that *resembles* an intermediate in the catalytic cycle and not on an actual intermediate.

Osborn has demonstrated that counterion plays an important role in the hydrogenation of unsubstituted olefins such as 2-phenyl-1-butene mediated by rhodium catalysts (Figure 4.18).[28] The impressive ee%'s obtained for chiral iridium complexes are difficult to reproduce with rhodium catalysts and generally a coordinating function on the olefin is needed to obtain high ee's with chiral rhodium complexes.[28, 29]

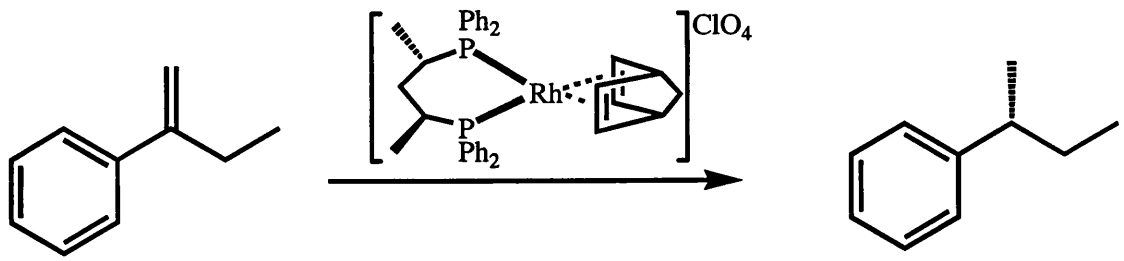

Figure 4.18: Hydrogenation of 2-phenyl-1-butene

In C_6H_6, 2-phenyl-1-butene can be hydrogenated with an ee of 29% at 70 atm H_2 (Figure 4.18). The ee% of the reaction can be improved to 66% if the reaction is run in the presence of a 0.1M equivalent of $[RSO_3]^-$ (R = alkyl). The sulphonate binds to the metal preferentially over the $[ClO_4]^-$ anion and results in a more enantioselective catalyst. In separate experiments further increases in ee% were achieved by adding up to 2 equivalents of NBu_4I to the reaction mixture. In this case the ee% is improved to 70% while the rate of hydrogenation increases from 380 turnovers per hour in the presence of sulphonate to 1200 turnovers per hour in the presence of iodide. Hydrogen pressure also affects the performance of the catalyst. In the case of the sulphonate increased hydrogen pressure results in a higher ee% and an overall increase in rate of hydrogenation whilst in the iodide case hydrogen pressure seems only to affect the overall rate of hydrogenation having very little effect on enantioselectivity. The mechanism for both catalysts is proposed to be via a dihydride mechanism in which H_2 oxidatively adds to the metal prior to olefin binding. An alternative unsaturated route is suggested to operate only for the sulphonate catalyst at lower pressures in which olefin is proposed to bind prior to hydrogen. The overall effect of the anion in this case is clear, but less so is the underlying reason as to why the anion has such an influence. In terms of the

enantioselectivity the anion must alter the chiral environment of the rhodium centre in such a way as to favour only a certain stereospecific addition of H_2 across the olefin.

More recently van Koten[30] and co-workers have determined that there is a strong anion effect in the activity catalyst precursors based upon cationic $[(dppb)Rh(COD)]^+$ fragments (Figure 4.19).

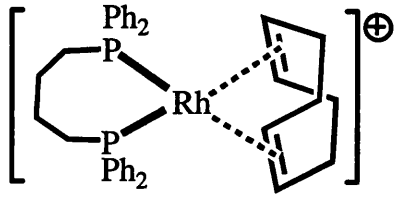

Figure 4.19: Cationic catalyst precursor for hydrogenation of 1-octene

The study demonstrated that for the hydrogenation of 1-octene significant variations of TOF hr^{-1} are observed upon variation of the anion. For example the $[BF_4]^-$ anion gives a TOF of 67 h^{-1} whilst the $[B\{C_6H_3(CF_3)_2\text{-}3,5\}_4]^-$ anion gives a superior TOF of 80 h^{-1}. Surprisingly a further increase in rate is observed when the anion is modulated to $[B\{C_6H_3(C_6F_{13})_2\text{-}3,5\}_4]^-$ when the TOF is doubled compared to $[BF_4]^-$ to 140 h^{-1}. The enhancement of catalytic activity is attributed to the degree of ion-pairing between the cation or anion, in other words, the ability of the anion/cation to associate in solution with a strong association resulting in a lower TOF. Thus the factors that determine the degree of ion pairing are both steric and electronic. For example, the $[BPh_4]^-$ anion results in significantly poorer catalyst than when the $[B\{C_6H_3(CF_3)_2\text{-}3,5\}_4]^-$ anion is used. This is a result of the electron withdrawing nature of the CF_3 substituents. This

effectively inhibits the formation of π-arene interactions, which decreases the amount of cation/anion association in solution. Increasing the bulk of the anion further reduces the coordinating power of the anion (i.e. through greater charge separation) resulting in a more active catalyst.

Given the precedent for variation in rates for Group 9 hydrogenation catalysts we wondered if we could observe an increase in efficiency for the Schrock-Osborn type catalyst outlined above. We hoped that by systematically varying the anion we could observe a trend in the reactivity of our systems with respect to hydrogenation. Ultimately by reactivity studies and by use of model compounds we hoped to be able to provide a plausible mechanism for the hydrogenation of olefins using *exo-closo*-metallocarboranes. Results to this end are detailed in the next chapter. Firstly, the reactivity of the metallocarboranes synthesised in section 2.1 towards hydrogen and olefins is investigated. Catalytic activity and kinetic data are evaluated for a range of catalysts based upon [*closo*-$CB_{11}H_{12}]^-$ are then presented and finally we comment on the role of counterion in this system and possible deactivation pathways.

4.2 RESULTS AND DISCUSSION

4.2.1 Reactivity of $[(Ph_3P)_2Rh(closo\text{-}CB_{11}H_{12})]$ with H_2

Treatment of a CD_2Cl_2 solution of $[(Ph_3P)_2Rh(closo\text{-}CB_{11}H_{12})]$, **IX** with H_2 (4 atm) results in the formation of a new hydride containing complex in approximately 50% yield as evidenced by ^1H and ^{31}P NMR spectroscopy. The $^{31}P\{^1H\}$ NMR spectrum of the reaction mixture displays two well-defined doublets at δ 48.9 [d, J(RhP) 193Hz], 39.3 [d, J(RhP) 114Hz] respectively. The first resonance is assigned to complex **IX** with the second resonance assigned as $[(Ph_3P)_2Rh(H)_2(closo\text{-}CB_{11}H_{12})]$ **XXI** (Figure 4.2.1).

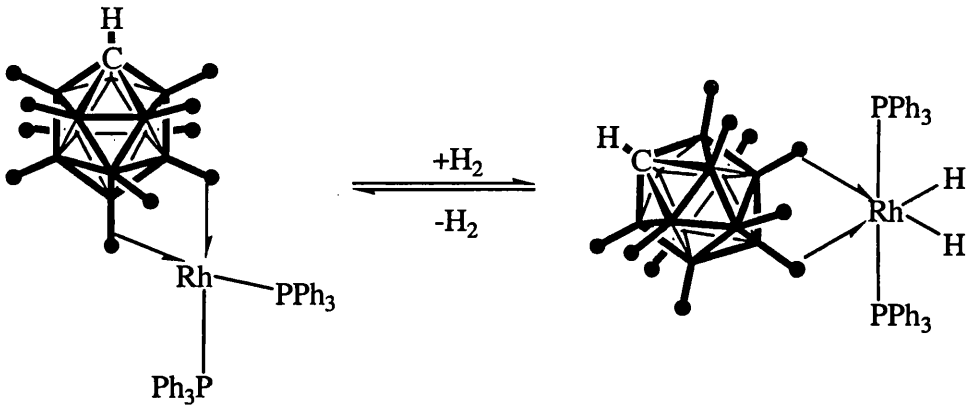

IX **XXI**

Figure 4.2.1: Reaction of complex **IX** with H_2

The ^{11}B NMR shows very little change compared to that of complex **IX**. The ^1H NMR spectrum displays two cage {CH} environments at δ 2.60 and 2.25 ppm respectively. The latter resonance is assigned to complex **XXI**. This shift is very similar to that of

uncoordinated [*closo*-$CB_{11}H_{12}]^-$ suggesting that the anion is only weakly bound in **XXI**. An apparent quartet at δ -17.5 ppm is assigned as the hydride ligands. The appearance of only one resonance suggests that the anion is fluxional in solution. The fluxionality is presumably similar to that found in complex **IX** whereby one of the B-H-M of the anion bonds breaks followed by rotation around the remaining B-H-M bond (Figure 4.2.2).

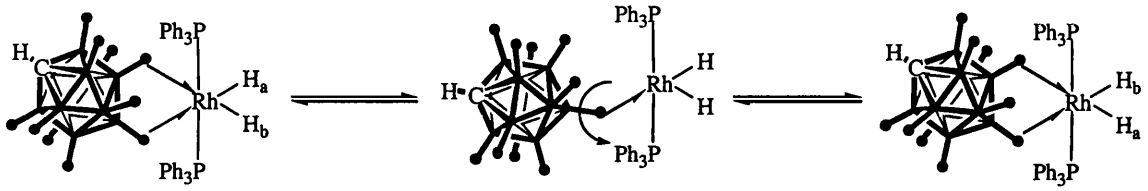

Figure 4.2.2: Potential mode of fluxionality in complex **XXI**

A similar complex to **XXI** [$(i\text{-}Pr_3P)_2Rh(H)_2(RSO_3)$] has been reported by Werner.[31] As for **XXI** the phosphines are assigned as being *trans-* to one another with mutually *cis-* hydrides. The room temperature ^1H NMR displays one doublet of triplets and only one resonance is seen in the $^{31}P\{^1H\}$ which suggests that the sulphonate ligand is also fluxional in solution.

Prolonged exposure of complex **IX** to H_2 (4 atm) in CH_2Cl_2 results in the irreversible formation of a new organometallic species as evidenced by ^1H and $^{31}P\{^1H\}$ NMR spectroscopy. Single crystal X-ray crystallography showed that this complex is a halide-bridged dimer of formula $[(Ph_3P)_2HRh(\mu\text{-}Cl)_2(\mu\text{-}H)RhH(PPh_3)_2][CB_{11}H_{12}]$ **XXII** (Figure 4.2.3).

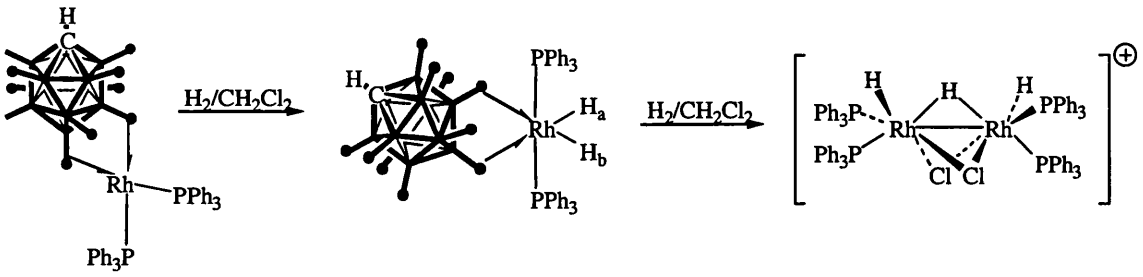

Figure 4.2.3: Formation of halide-bridged dimer **XXII**

The solid-state structure of **XXII** is shown in Figure 4.2.4 with relevant bond lengths and angles in Table 4.4.2. One carborane is located in the unit cell giving the metal complex an overall positive charge making each metal centre formally Rh^{3+}. The Rh-Rh distance is suggests a significant metal-metal interaction. The distance [Rh(1)-Rh(2) 2.776(1) Å] is similar to that found for *trans*-[{$Rh(C_5Me_5)Me$}$_2$(μ-CH_2)$_2$] [Rh(1)-Rh(2) 2.620(1) Å].[32] The Rh-Cl-Rh bond lengths are not the same within the molecule. For example Rh(1)-Cl(1) 2.538(3) Å and Rh(2)-Cl(1) 2.416(3) Å. The elongated bond length for Rh(1)-Cl(1) is due to the approximate *trans*- orientation of the terminal hydride ligands [H(2)-Rh(2)-Cl(1) 168° and H(1)-Rh(1)-Cl(2) 163°] meaning that each bridging chloride is approximately *trans*- to both a phosphine and a hydride. Similarly the Rh-P distance for the phosphines *trans*- to the bridging hydride has a slightly elongated bond length than the phosphine *cis*- to the bridging hydride Rh(1)-P(1) 2.257(3) Å and Rh(1)-P(2) 2.313(3) Å. The $^{31}P\{^1H\}$ NMR spectrum for **XXII** displays two strongly second order coupled resonances at δ 36.0 and 51.5 ppm respectively. In the ^1H NMR spectrum two resonances are observed in a 1:2 ratio at δ -11.0 and -16.5 ppm respectively. The latter resonance is observed as an apparent quartet [ddd] showing coupling to one ^{109}Rh centre and two ^{31}P nuclei. In the $^1H\{^{31}P\}$ NMR spectrum this peak collapses to a doublet

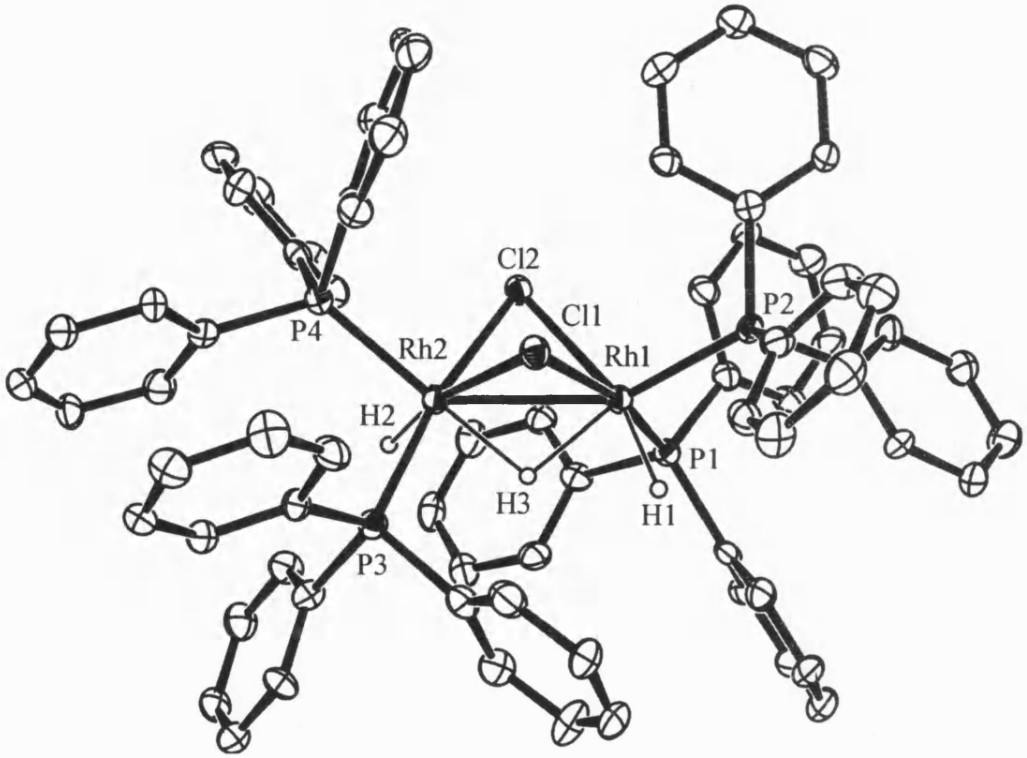

Rh(1)-Rh(2)	2.776(1)
Rh(1)-H(1)	1.59(7)
Rh(2)-H(2)	1.60(9)
Rh(1)-H(3)	1.82(6)
Rh(2)-H(3)	1.82(6)
Rh(1)-P(1)	2.257(3)
Rh(1)-P(2)	2.313(3)
Rh(2)-P(3)	2.257(3)
Rh(2)-P(4)	2.301(3)
Rh(1)-Cl(1)	2.416(3)
Rh(1)-Cl(2)	2.553(2)
Rh(2)-Cl(1)	2.538(3)
Rh(2)-Cl(2)	2.394(2)

Table 4.4.2: Selected Interatomic distances (Å) and Angles (°) for complex **XXII**.

Figure 4.2.4: ORTEP representation of the cationic portion of complex **XXII.** Ellipsoids are drawn at the 30% probability level. Phenyl hydrogens are omitted for clarity

resonance and is assigned as the terminal hydride ligand. The bridging hydride at δ -11.0 ppm is observed as a complex multiplet which resembles a triplet of septets which simplifies to a triplet in the $^{1}H\{^{31}P\}$ NMR spectrum. The large triplet coupling [J(PH) 75 Hz] arises from *trans-* coupling to the two chemically equivalent phosphorous atoms P(2) and P(4). Similar large coupling constants in binuclear rhodium phosphines with bridging hydrides have been observed previously.[28, 33, 34] The complex bridging hydride signal has been successfully simulated as an AA'BB'MXX' spin system. The simulated and experimental spectrum is shown in Figure 4.2.5.

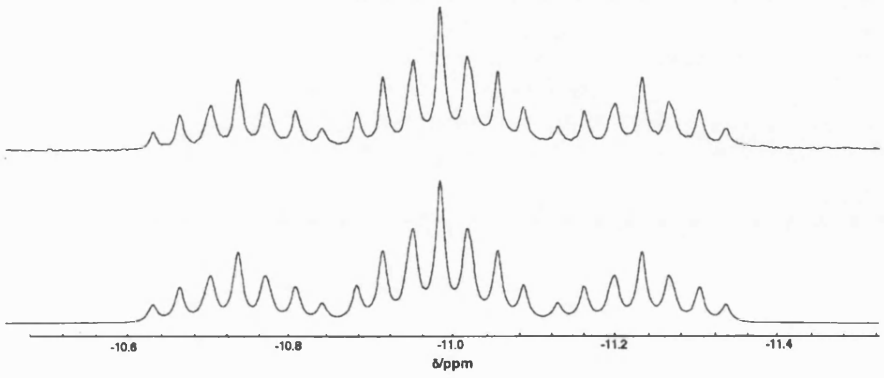

Figure 4.2.5: Simulated (top) and experimental (bottom) for bridging hydride region for complex **XXII**

Full details of the resolved coupling constants can be found in appendix A. Similar binuclear hydride bridged dimers have been reported previously. Crabtree[14] has reported $[Ir_2H_5(PPh_3)_4]^+$ and also the iridium congener of **XXII** $[Ir_2H_3Cl_2(PPh_3)_4]^+$ which can be formed via treatment of $[Ir_2H_5(PPh_3)_4]^+$ with HCl. The mechanism of formation for **XXII** must be quite complex and clearly involves the activation of the CH_2Cl_2 solvent. We

return to **XXII** as a decomposition product in the hydrogenation reactions, discussed in section 4.2.3.

4.2.2 B-H activation

Hawthorne has reported that several complexes are active catalysts in the B-H/D exchange for polyhedral boranes.[35] We were interested to see if **IX** would undergo B-H/D exchange. When complex **IX** is treated with D_2 for 3 hr the $^{11}B\{^1H\}$ NMR spectrum displays three signals at δ -7.4, -13.7 and -16.4 ppm respectively. Only the third peak at δ -16.4 shows ^1H coupling in the ^{11}B NMR indicating that the antipodal and lower pentagonal belt protons have been completely deuterated. To further confirm that this B-H/D exchange was operating Cs[-7,8,9,10,11,12-D_6-*closo*-$CB_{11}H_6$] was synthesized[36] and the complex [$(Ph_3P)_2$Rh(nbd)][7,8,9,10,11,12-D_6-*closo*-$CB_{11}H_6$] **I-d_6** was prepared in the same manner as for **I**. The NMR spectra of **I-d_6** are identical to complex **I** except that the ^{11}B NMR displays two singlet resonances at δ -7.4 and -13.7 ppm respectively with one doublet resonance at δ -16.4 ppm with J(BH) 152 Hz. When complex **I-d_6** was treated with an excess of H_2 in CD_2Cl_2 two complexes were detected in the ^1H NMR spectrum. One of the complexes was **XXI** and the other was **IX** indicating that complete D/H exchange has occurred. This suggests that hydrogen must have exchanged for deuterium on the carborane via some metal mediated process. A mechanism to account for this exchange process is shown in Figure 4.2.6.

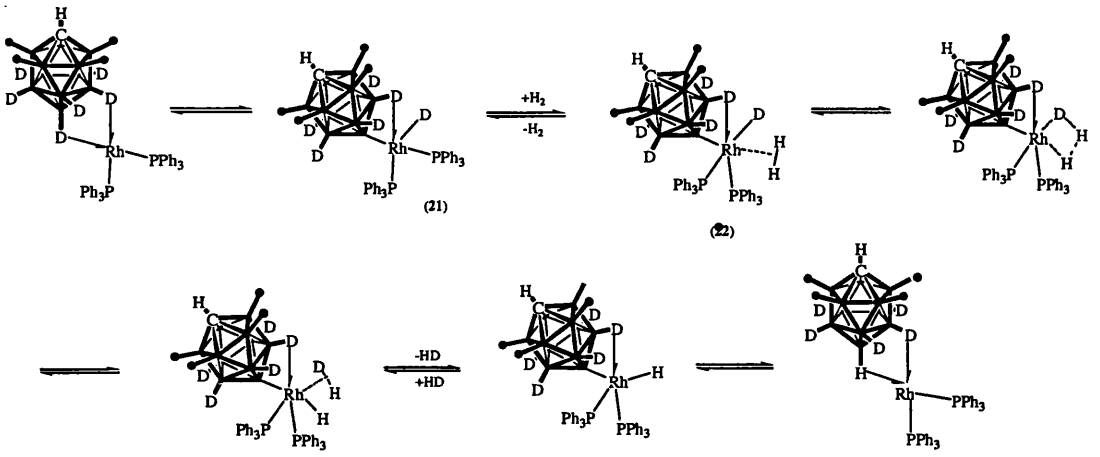

Figure 4.2.6: Proposed mechanism for H/D exchange on carborane

Initial oxidative addition of a B-D vertex across the rhodium centre would generate a coordinatively unsaturatesd Rh(III) complex **21**. Such complexes of [*closo*-$CB_{11}H_{12}$]$^-$ have recently been put forward as catalytically active hydrogenation catalysts in ionic liquids.[37] Also B-H activation in this way has been noted before by Hawthorne and others.[38, 39] Subsequent coordination of H_2 to the rhodium centre generates complex **22,** which can undergo H/D exchange. Dissociation of a D-H molecule followed by reductive elimination of a B-H from the rhodium centre generates a carborane which now has the antipodal vertex with a hydrogen atom rather than a deuterium.

Further proof that the D/H exchange mechanism was proceeding through an oxidative addition mechanism was obtained by treating complex **IX** with ethene in THF. We hoped that instead of coordination of hydrogen as in the above example that coordination of ethene could potentially allow us to functionalise the carborane in a catalytic process similar to that outlined in section 2.1 after Sneddon.[40] Initially complex **IX** was dissolved in THF in a Young's ampoule and freeze pump degassed. A small

amount of ethene (ca. 20 cm^3) was frozen in at liquid N_2 temperatures. The solution was allowed to warm to room temperature when it was stirred vigourously for 48 h. During this time the solution changes colour from deep red to orange. The $^{11}B\{^1H\}$ NMR spectrum of the reaction mixture displays two low intensity resonances at δ 1.6 and -3.5 respectively while a single resonance at δ 17.1 ppm is assigned as overlapping resonances from coordinated {BH} vertices indicating that the carborane is still bound to the metal centre. This resonance at δ 17.1 ppm broadens in the ^{11}B NMR spectrum indicating that these are {BH} vertices. The two resonances at δ 1.6 and -3.5 ppm do not split into doublets in the ^{11}B NMR spectrum indicating that ^1H coupling to those vertices has been lost. The ^1H NMR of the reaction mixture shows three resonances in a 1:1:1 ratio indicative of a $CH=CH_2$ group at δ 4.78 [br d J(HH) 15Hz], 4.08 [br d, J(HH) 12Hz] and 2.41 (dd). Identical resonances with roughly half the intensity in a 1:1:1 ratio are also observed at δ 4.89, 4.13 and 2.56 ppm respectively. Two cage {CH} vertices are observed at δ 2.31 and 2.18 ppm respectively in an approximate 1:2 ratio. The $^1H\{^{11}B\}$ NMR displays four resonances at 1.52, 1.38, 0.48 and 0.35 ppm respectively for the BH protons. The highfield shift of these latter two resonances is indicative of coordination of the carborane to the metal centre as discussed in section 2.2.7. The $^{31}P\{^1H\}$ NMR spectrum consists of a broad signal at δ 40.0 ppm. Upon cooling a CD_2Cl_2 solution of the reaction mixture to -70°C this resolves into two resonances at δ 60.2 [dd J(RhP) 192.5 Hz, J(PP) 33Hz] and δ 23.9 [dd, J(RhP) 158Hz, J(PP) 33Hz]. A similar set of resonances in lower intensity are observed almost coincident to these peaks at δ 60.5 and 23.4 ppm. The $[FAB]^-$ mass spectrum of the reaction mixture displays prominent peaks 169.2 m/z (see appendix B) with an isotope pattern as expected for boron containing compounds. This peak can be assigned to the $[12\text{-}CH=CH_2\text{-}closo\text{-}CB_{11}H_{11}]^-$ anion or the

[7,-CH=CH_2-*closo*-$CB_{11}H_{10}$]$^-$ anion respectively. Figure 4.2.4 outlines the reaction of **IX** with C_2H_4.

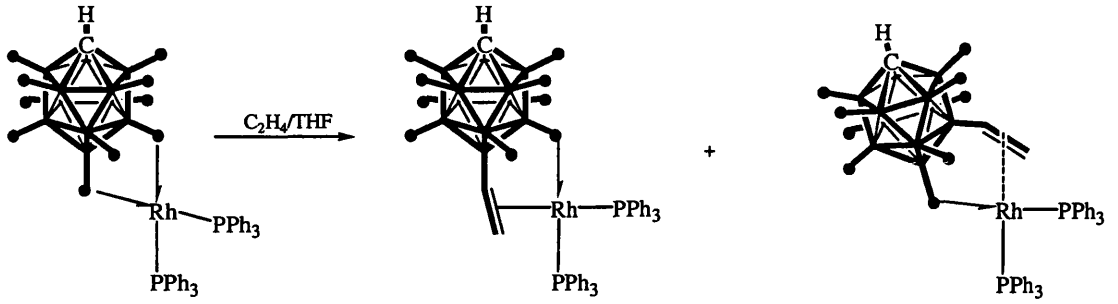

Figure 4.2.7: Reaction of **IX** with ethene

Sneddon has reported similar transition metal catalysed hydroboration of *arachno*-$C_2B_7H_{13}$ with C_2H_4 using $PdBr_2$ or H_2PtCl_4 as catalysts.[40] Although the ^1H resonances for the CH=CH_2 moiety appear at δ 6.46, 5.76 and 5.59 ppm which are somewhat different to those observed for **XXIII** and **XXIV**. This difference can be traced to two possible reasons. Firstly it appears that after hydroboration of one or more vertexes the carborane remains bound to the metal centre as evidenced by the $^1H\{^{11}B\}$ NMR and ^{11}B NMR spectra. If the carborane was bound as shown in Figure 4.2.7 then the chemical shifts of those olefinic hydrogens would be shifted to higher field. A similar shift to higher field is observed in the coordination of C_2H_4 to the $\{(PPh_3P)_2Ir\}^+$ fragment in complex **XX**. Free ethene resonates at δ 5.39 ppm in the ^1H NMR spectrum while coordinated C_2H_4 appears at δ 3.09 ppm, a shift of some δ 2.3 ppm upfield. Secondly the fluxional nature of the complexes in solution could have an effect on the chemical shifts of the CH=CH_2 protons and also the coupling constants/patterns. There are a number of

potential fluxional processes that could be occurring in solution solution for complexes **XXIII** and these are outlined in Figure 4.2.8.

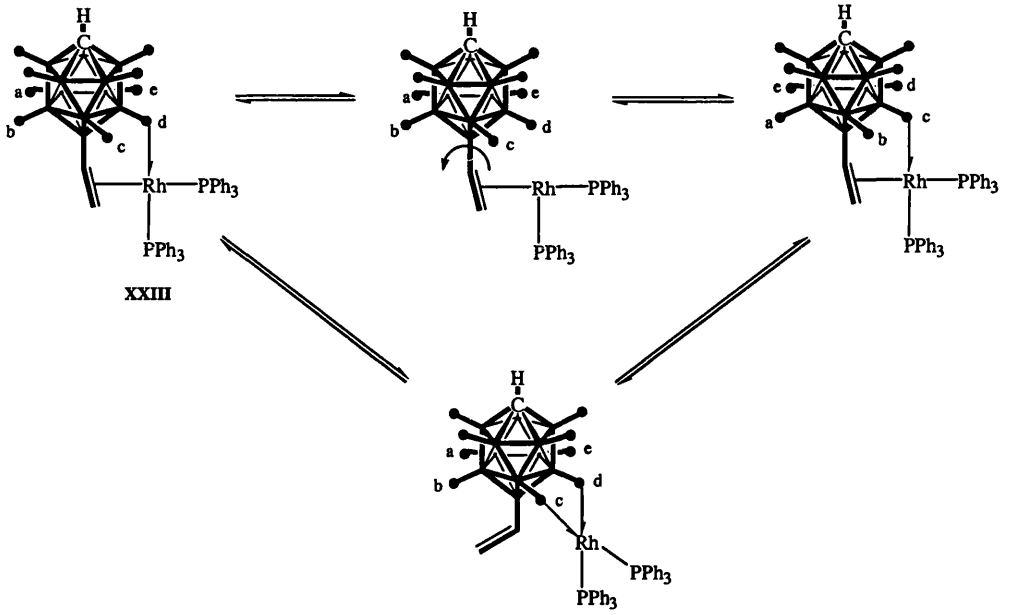

Figure 4.2.8: Fluxional processes proposed for a mixture of **XXIII** in CD_2Cl_2

When complexes **XXIII** and **XXIV** are treated with H_2 in CH_2Cl_2 a colour change from orange to red is observed. The resonances assigned as $CH{=}CH_2$ in the ^1H NMR spectrum disappear and are replaced by complex multiplets between δ 0.5 and 2.0 ppm. Two cage {C-H} vertexes are observed at δ 2.48 and 2.40ppm. A very broad quartet is observed at –1.02 ppm which is indicative of B-H-M interactions as discussed. The ^{11}B NMR now displays broad singlets at δ 7.6 ppm and δ 4.3 ppm. A further broad resonance is observed at δ -15.2 ppm assigned as overlapping resonances from metal coordinated {BH} vertices as observed for complex **IX**. The $^{11}B\{^1H\}$ NMR spectrum displays four singlet resonances at δ 7.6, 4.3 and –15.1 and -17.9 ppm respectively. The $^{31}P\{^1H\}$ NMR spectrum displays two doublets at δ 47.1 [J(RhP) 194 Hz] and 46 [J(RhP)

194] ppm respectively which are very similar to that observed for complex **IX**. A peak of smaller intensity is observed at δ 48.5 ppm with a similar coupling constant. [FAB]$^-$ mass spectrometry of this sample indicates an m/z peak at 171.1. The data obtained for this reaction suggest that the $\{(PPh_3)_2Rh\}^+$ fragment hydrogenates the $CH{=}CH_2$ moiety as proposed for **XXIII** and **XXIV** resulting in an alkylated carborane **XXV** according to Figure 4.2.9. The alkylated carborane, [12-Et-*closo*-$CB_{11}H_{11}$] has been prepared by an independent route and the [B(12)-H] vertex appears at δ 7.3 ppm in the ^{11}B NMR which is in close agreement with that observed for complex **25**.

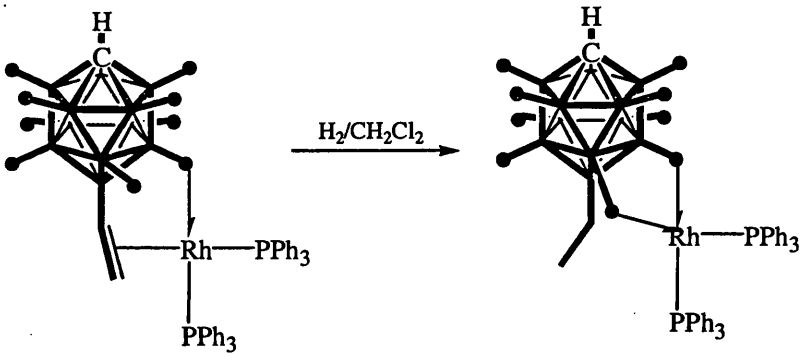

(XXIII) (XXIV)

Figure 4.2.9: Reaction of **XXIII** with H_2

Complex **XXV** can be repeatedly reacted with C_2H_4 in THF or CH_2Cl_2 to give greater substitution. Although total substitution of all 11 vertices was not achieved mass spectrometry indicates multiple substitution are possible *via* alternating reactions of **IX** with C_2H_4 and H_2 in THF in a cyclic fashion (Figure 4.2.10) (see appendix B).

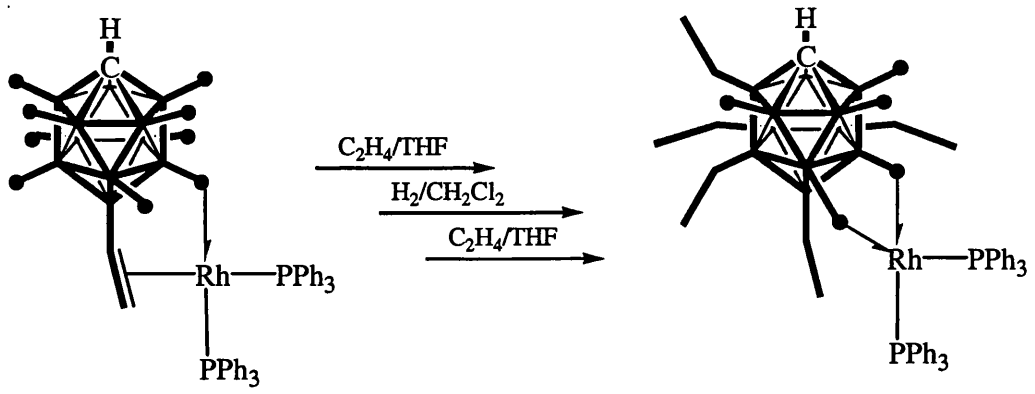

XXIII

Figure 4.2.10: Multiple substitution of BH vertices mediated by rhodium

Substitution is not limited to ethene. For example, when 1-hexene was heated in THF with complex **IX** for several days mass spectrometry (appendix B) and NMR data indicate that multiple substitutions are effected resulting in incorporation of hexyl-chains into the carborane. It remains unclear as to why the reaction with ethene does not proceed catalytically with this system, while hexane seems to. It may be that the alkenyl group has an electron-withdrawing effect on the remaining {BH} vertices inhibiting oxidative addition across the rhodium centre. Alternatively it may be that the coordination of the alkenyl moiety is sufficient to prohibit the oxidative addition on topological grounds. However, upon hydrogenation of the alkenyl substituents the carborane is 'activated' and undergoes oxidative addition and subsequent reaction with ethene. Although this does not provide any evidence for why the reaction stops after one substitution it indicates that either of the above reasons are plausible. The alkyl group would be expected to donate electron density into the carborane thus promoting the oxidative addition of a B-H bond. Alternatively any restraints upon the geometry of the

oxidative addition product are now removed, as the alkyl presumably does not interact significantly with the metal centre.

Treatment of complex **XVIII** with olefin was initially attempted in an effort to isolate the Iridium-boryl species (Figure 4.2.11) which would act as a model for the hydroboration process mediated by complex **IX**. When complex **XVIII** was treated with ca. 10 equivalents of tbe (*tert*-butylethylene) in CD_2Cl_2 and heated at 55°C complex **XVIII** is slowly consumed as evidenced by ^1H NMR and $^{31}P\{^1H\}$ spectroscopy. However, no new hydride peaks are observed in the ^1H NMR spectrum.

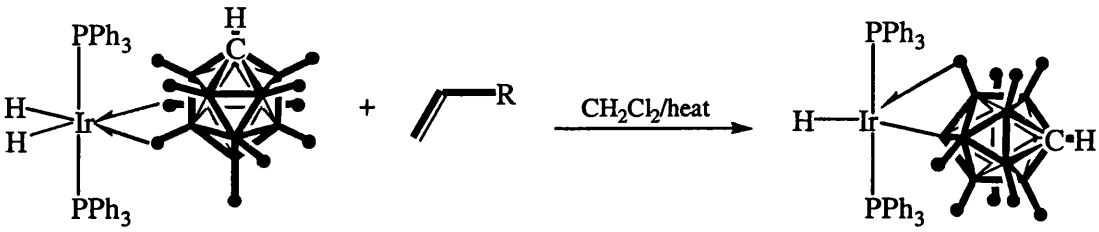

Figure 4.2.11: Attempted activation of **XVIII** with olefin

A new peak assigned as hydrogenated tbe was observed at δ 0.8 ppm as a sharp singlet. No new peaks are observed in the $^{31}P\{^1H\}$ NMR. Evidence for activation of the carborane is given by the ^{11}B NMR spectrum in which several new broad peaks are observed after 24 hr in the range δ + 10 to -8 ppm. After 24h no peaks assigned as **XVIII** are seen in the ^{11}B NMR spectrum. Two doublet resonances are observed at δ -13.6 and -16.4 ppm which appear as singlets in the $^{11}B\{^1H\}$ NMR. These resonances broaden and become less well resolved as the reaction proceeds. After 72 h the ^{11}B NMR consists of 7 or more unresolved resonances, some of which display ^1H coupling.

The mass spectrum of this sample indicates m/z peaks corresponding to multiple substitutions of {BH} vertices with ($CH=CH-C(CH_3)_3$) groups. In fact, up to 5 substitutions are observed (Figure 4.2.12).

Figure 4.2.12: Proposed carborane mediated by complex **XVIII**

Similar reactivity of complex **XVIII** is observed with C_2H_4. In this case C_2H_4 was frozen onto a CH_2Cl_2 solution of **XVIII** and the mixture warmed to room temperature. The homogeneous solution was stirred for 24 h. The $^{11}B\{^1H\}$ NMR of the reaction mixture after 24 h displays resonances at δ 6.9, 1.4, -2.89 and -6.58 ppm. A broad resonance at δ -16.8 ppm is assigned as the lower and upper pentagonal belt vertices. The resonances between δ 6.9 and -6.58 ppm, however, do not collapse to doublets in the ^{11}B NMR spectrum indicating that they have been substituted. Upon treatment of this solution with H_2 the ^1H NMR becomes very similar to that of complex **XVIII**. Although complete substitution of the carborane could not be achieved under these conditions several cycles could be performed. The mass spectrum of this sample shows m/z peaks assigned as carborane with up to 5 $\{B\text{-}C_2H_5\}$ vertices.

The mechanism for hydroboration using transition metal complexes has been discussed by Sneddon[40] and is similar to that of hydrosilation (Figure 4.2.13).

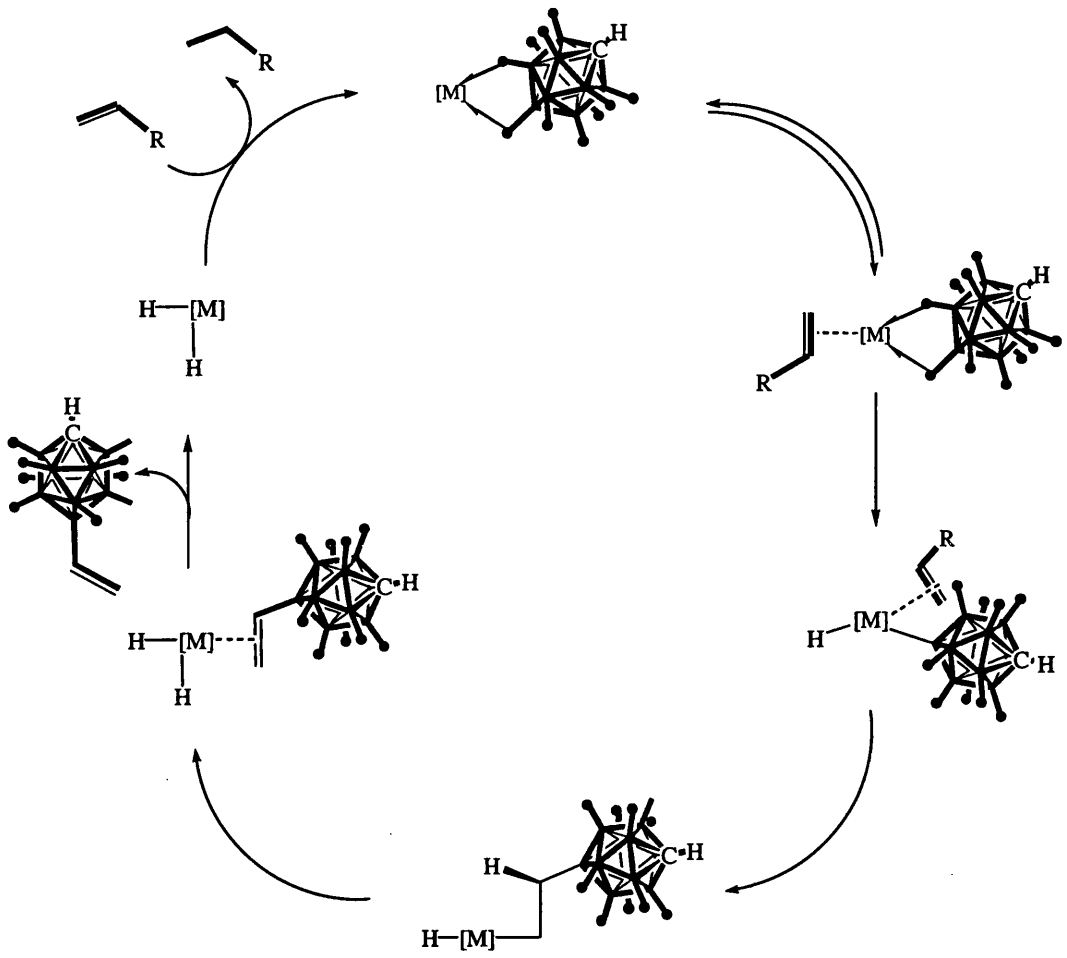

Figure 4.2.13: Mechanistic pathway for hydroboration of [*closo*-$CB_{11}H_{12}$]$^-$

The initial step is coordination of the olefin substrate to the metal centre. In the case of complex **XVIII** one mole of olefin is reduced *via* a classical hydrogenation mechanism to to generate an Ir(I) centre. Oxidative addition of the carborane across the metal centre results in a M^{III} boryl hydride. Olefin insertion into the M-B bond results in an alkyl hydride species. This is followed by β-hydride elimination, which results in an alkenyl

carborane. Dissociation of the carborane generates the product. The metal hydride generated is reduced by a mole of substrate to re-generate the M(I) centre. Coordination of a carborane, substituted or otherwise, regenerates the resting state of the catalyst. The β-hydride elimination pathway has been proposed by Sneddon as the predominant pathway for reactions of this type.[40]

4.2.2 Reactivity of $[(Ph_3P)_2Rh]_2[(closo\text{-}CB_{11}H_6Br_6)]_2$

The reaction of complex **XIV** with H_2 yields several products. The major species is the hydride bridged dimer characterised in section 4.2.1 *via* reaction of complex **IX** with H_2 in CH_2Cl_2. A benzene capped $\{(PPh_3)_2Rh\}^+$ fragment is also observed in the reaction mixture. This complex shows an integral 6 resonance at δ 5.9 ppm in the ^1H NMR spectrum along with a well-resolved doublet at δ 44 [JRhP 206 Hz] ppm in the $^{31}P\{^1H\}$ NMR spectrum. (Figure 4.2.14). This complex presumabley arises as a result of P-C bond cleavage. This type of decomposition pathway has been noted before.[18, 41]

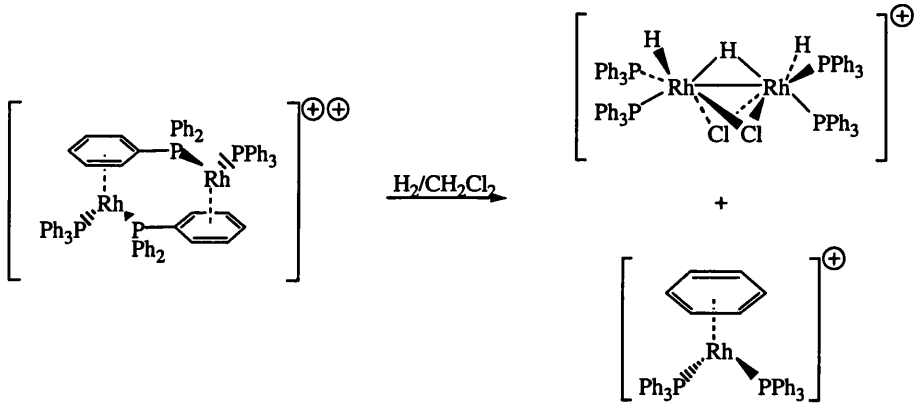

Figure 4.2.14: Reaction of **XVI** with H_2 in CH_2Cl_2

4.4.3 Reactivity of XIV with olefins

When complex **XIV** is treated with eight equivalents of cyclohexne in CD_2Cl_2 a colour change from orange to red is observed. The formation of the new complex $[(PPh_3)_2Rh(\eta^4\text{-}C_6H_8)][\textit{closo}\text{-}CB_{11}H_6Br_6]$, **XXVI** (Figure 4.1.15) is evidenced by ^1H, $^{31}P\{^1H\}$ NMR spectroscopy and by a single crystal X-ray crystallography study.

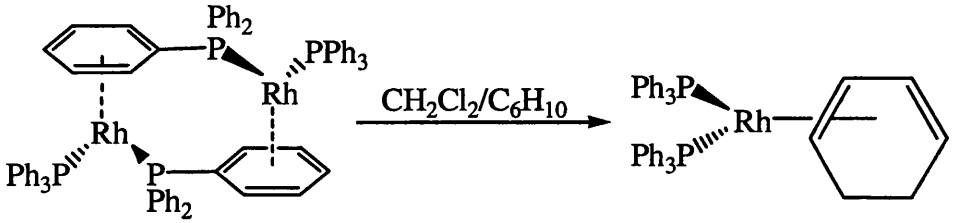

XIV **XXVI**

Figure 4.2.15: Reaction of **XIV** with cyclohexene

The solid-state structure of **XXVI** is shown in Figure 4.2.16 along with relevant bond lengths and angles in Table 4.2.2. The diene is η^4 coordinated to the $\{(PPh_3)_2Rh\}^+$ metal fragment with no close contacts between the metal centre and the anion. The distances [Rh(1)-C(4) 2.157(3) Å and Rh(1)-C(5) 2.200(3) Å] are comparable to those found for $[L_XRh(\eta^4\text{-}C_6H_8)]$[42] ($L_x$ = (2,6-$C_6H_3Me_2$)NC(Me)CHC(Me)N(2,6-$C_6H_3Me_2$) [Rh(1)-C(4) 2.100(5) Å and Rh(1)-C(5) 2.152(5) Å]. The distance [C(2)-C(3) 1.384(5) Å] is also in good agreement with that found for $[L_XRh(\eta^4\text{-}C_6H_8)]$ [(C(2)-C(3) 1.366(10) Å].[42] All

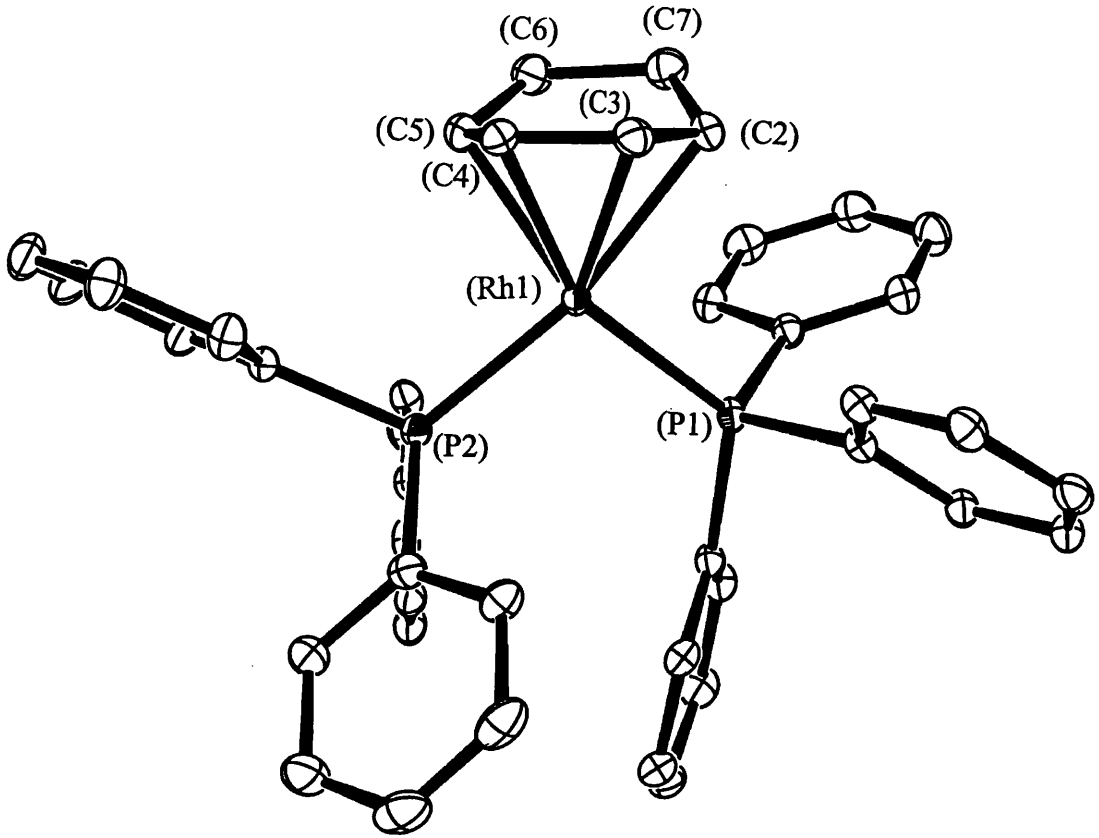

Rh(1)-C(2)	2.291(3)
Rh(1)-C(3)	2.186(3)
Rh(1)-C(4)	2.157(3)
Rh(1)-C(5)	2.200(3)
C(2)-C(3)	1.384(5)
C(3)-C(4)	1.437(5)
C(4)-C(5)	1.389(5)
C(5)-C(6)	1.488(5)
C(2)-C(7)	1.490(5)
P(1)-Rh(1)-P(2)	100.59

Table 4.2.2: Selected bond lengths (Å) and angles for complex (**XX**).

Figure 4.2.16: Cationic portion of complex **XXIV**. Ellipsoids are drawn at the 30% probability level. All phenyl hydrogens have been omitted for clarity.

other bond lengths and angles are unremarkable and are fully consistent with the structure. The ^{1}H NMR spectrum of **XXVI** displays resonances at δ 5.5 and 4.0 ppm integrating with relative intensity of 2:2. These broad singlets are assigned as the olefinic hydrogens. Two doublet resonances at δ 1.2 and 1.0 ppm with relative intensity 2:2 are assigned as the saturated part of the C_6H_8 ligand. The ^{1}H-^{1}H COSY NMR spectrum indicates coupling between the resonance at δ 4.0 ppm and those at δ 1.2 and 1.0 ppm which allows us to assign this resonance as the hydrogens bound to C(2) and C(5) respectively. The ^{31}P{^{1}H} NMR spectrum displays one resonance [δ 29.5 ppm, J(RhP) 177 Hz] in accordance with the two phosphorous atoms being equivalent. The observed reaction involves the dehydrogenation and the hydrogenation of one molecule of cyclohexene. Formation of a molecule of cyclohexane is observed in the ^{1}H NMR and is confirmed by GC analysis of the reaction mixture. The proposed mechanism of the reaction is shown in Figure 4.2.17.

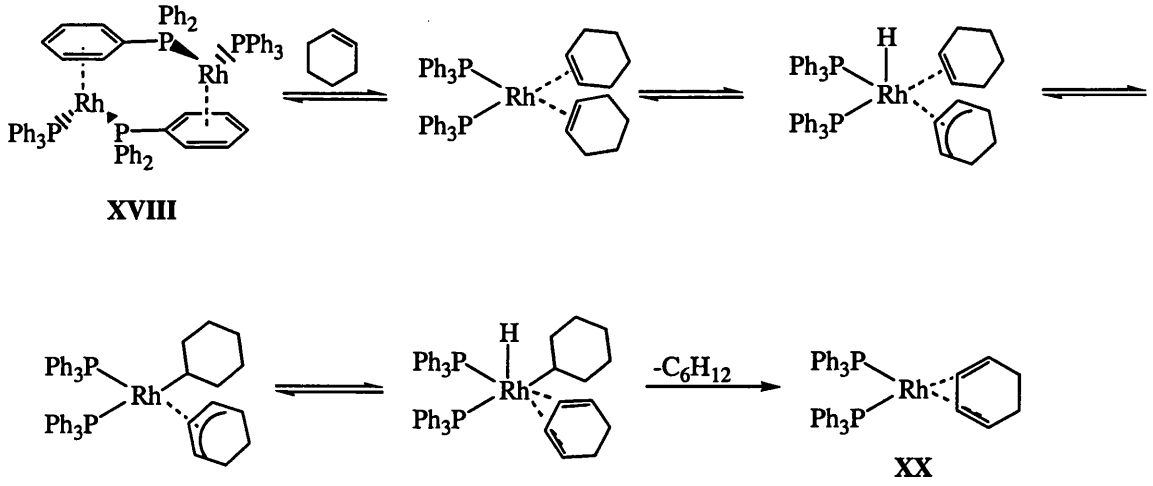

Figure 4.2.17: Mechanism of dehydrogenation by $\{(PPh_3)_2Rh\}^+$

The first step of the reaction is the coordination of cyclohexene resulting in the break-up of complex **XVIII**. The resulting *bis*-olefin complex rapidly C-H activates one of the cyclohexene molecules resulting in a π-allyl hydride complex. The remaining cyclohexene molecule inserts into the Rh-H bond followed by further C-H activation of the π-allyl ligand and followed finally by reductive elimination of one molecule of cyclohexane. A small amount (ca. 10%) of $[(PPh_3)_2Rh(\eta^6\text{-}C_6H_6)][closo\text{-}CB_{11}H_6Br_6]$ is observed in the ^1H and $^{31}P\{^1H\}$ NMR spectra. The ^1H NMR spectrum of this benzene capped species displays a single resonance at δ 5.9 ppm. The $^{31}P\{^1H\}$ NMR displays a doublet [δ 44 ppm, J(RhP) 206 Hz]. It is likely that this complex arises from a combination of further dehydrogenation of the diene and by $P\text{-}C_{aryl}$ bond cleavage. P-C bond cleavage has been observed in related iridium systems.[18]

Treatment of complex **XIV** with methylcyclohexene results in dehydrogenation of the olefin to give $[(PPh_3)_2Rh(\eta^4\text{-}C_7H_{10})][closo\text{-}CB_{11}H_6Br_6]$, **XXVII** (Figure 4.2.18) in good yield. The reaction with eight equivalents proceeds very slowly so 30 equivalents of the olefin were used resulting in the disappearance of **XXVII** in about 48 h after the start of the reaction.

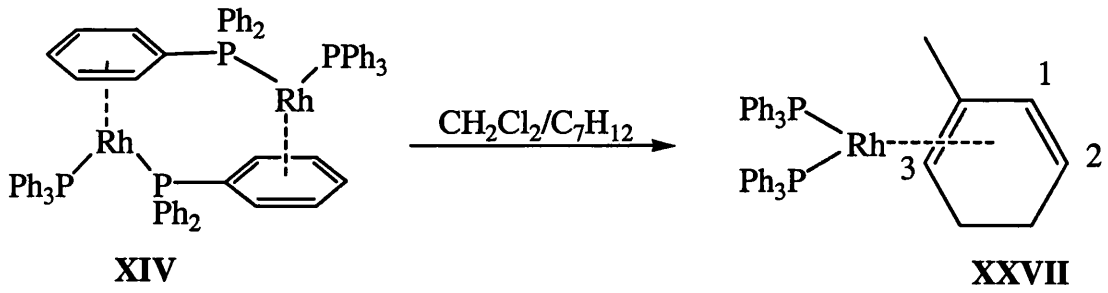

XIV **XXVII**

Figure 4.2.18: Dehydrogenation of methylcyclohexene with **XIV**

In accordance with the transfer dehydrogenation discussed one mole of methylcyclohexane is produced in the reaction as observed by ^1H NMR and G.C. analysis. The ^1H NMR spectrum displays four resonances at δ 1.79, 1.40, 1.10 and 0.90 ppm all with intensity 1, and all as multiplets. These four resonances all display coupling in the ^1H-^1H COSY NMR spectrum and are thus assigned as the saturated part of the diene ligand. An integral 3 resonance at δ 1.80 ppm is assigned as the methyl group. Three resonances at δ 4.5, 4.0 and 3.7 ppm all integrating as 1H are assigned as the olefinic hydrogens. On the basis of ^1H-^1H COSY NMR spectra the resonance at δ 4.5 ppm is assigned as H(1) in figure 4.2.18 as it displays coupling to another olefinic resonance but not to any aliphatic hydrogens. The resonance at δ 4.0 ppm is assigned as the H(2) on the basis that it displays coupling to H(1) and to one set of aliphatic hydroens. Thus the resonance at δ 3.7 ppm is assigned as H(3) and is confirmed in the ^1H-^1H COSY as it displays no coupling to either H(1) or H(2) but only to aliphatic hydrogens. The $^{31}P\{^1H\}$ NMR spectrum displays two resonances at δ 30.8 [dd, J(RhP) 170 Hz, J(PP) 33Hz] and 27.7 [dd, J(RhP) 181 Hz, J(PP) 33Hz] ppm respectively in accordance with two inequivalent phosphorous environments.

4.2.3 Anion effects in Group IX hydrogenation catalysts

With the synthesis and reactivity of several novel metallocarboranes in hand we decided to examine the effect of counterion on the hydrogenation properties of the Schrock-Osborn catalyst system. The catalyst precursors were all prepared in a highly crystalline

state according to the procedures outlined in the preceding sections. The catalyst precursors employed in this investigation are shown in Table 4.2.3. Reference to catalytic precursors from now on is based upon this table. i.e. precursor **2** refers to $[(PPh_3)_2Rh(nbd)][closo\text{-}CB_{11}H_{11}Br]$. The use of $[NBu_4][closo\text{-}CB_{11}H_6Br_6]$ as an additive was employed to investigate the effect of excess anion in the system. Three substrates were used in the study. Cyclohexene, 1-methyl-1cyclohexene and 2,3-dimethylbut-2-ene. The hydrogenation of these sterically demanding olefins is known to be less efficient with the Schrock-Osborn system and we were interested to determine if an improvement of calalyst performance could be gained by modulating the anion in a systematic fashion. The use of Crabtree's catalyst as a bench-mark is also included for comparison, where appropriate. Initial investigation into the hydrogenation of olefins was conducted at 1 mol % loading of catalysts in a small glass vial. The catalyst precursor was loaded into the vial and a suba seal was fitted.

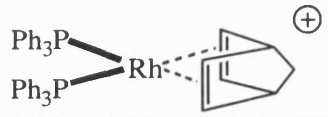	*Anion*
1	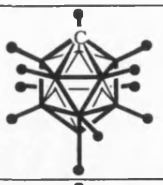
2	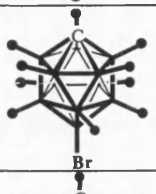
3	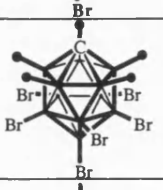
4	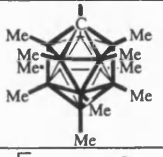
5	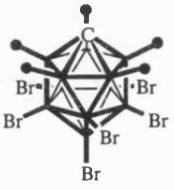 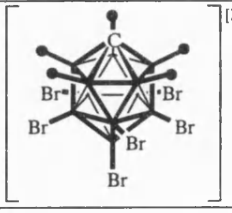 5 fold excess
6	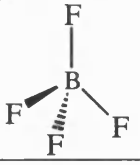
7	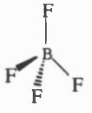 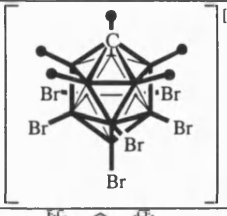 5 fold excess
8	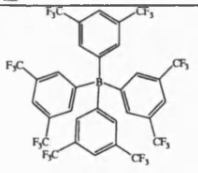

Table 4.2.3: Catalyst precursors used in the investigation of anion effects

CH_2Cl_2 was added via syringe along with the appropriate quantity of olefin. The solution was then purged with H_2 and pressurised to 10 psi directly from the H_2 cylinder. Conversion to the hydrogenated products was determined *via* G.C. analysis after the specified time. The results for precursors **1,2,3,4** and **6** in the hydrogenation of cyclohexene are given in Table 4.2.4.

Entry	Precursor	Substrate	Time (h)	Yield (%)	TOF (h^{-1})
1	**1**	cyclohexene	2	43	21.5
2	**2**	cyclohexene	0.5	45	90
3	**3**	cyclohexene	0.5	100	200
4	**4**	cyclohexene	0.5	100	200
5	**6**	cyclohexene	2	29	14.5

Table 4.2.4: Hydrogenation of cyclohexene with various precursors

As can be seen from the table there is a marked effect on both conversion and rate of reaction upon changing the counterion in this system. Precursor **1** is a moderately efficient catalyst for the hydrogenation of cyclohexene and compares more or less directly with precursor **6**. Precursor **2** displays a 4-fold improvement in TOF compared to **1** and a 6-fold improvement in TOF compared to **6**. Precursors **3** and **4** both show marked increases in performance with TOF of 200 h^{-1} which is some 10 times more efficient that **1** and over 13 times more efficient that precursor **6**.

Encouraged by these results we tested the same precursors with the more sterically hindered olefin, 1-methyl-1cyclohexene. The results are presented in Table 4.2.5. A similar increase in performance is gained in going from **1** to **3** with a 20-fold increase in

TOF. Precursor **4** gave even better results with a TOF some 40 times greater that that of precursor **1**. However, none of the precursors tested could match up to the performance of Crabtree's catalyst which is approximately 4 times more active than precursor **4**.

Entry	Precursor	Substrate	Time (h)	Yield (%)	TOF (h^{-1})
1	**1**	1-methyl-1-cyclohexene	6	4	<1
2	**3**	1-methyl-1-cyclohexene	5	95	19
3	**4**	1-methyl-1-cyclohexene	2	92	46
4	[(py)(PCy_3)Ir(cod)][PF_6]	1-methyl-1-cyclohexene	0.5	100	200

Table 4.2.5: Hydrogenation of 1-methyl-1-cyclohexene with various precursors

Finally precursor **3** was compared to Crabtree's catalyst in the hydrogenation of the highly hindered olefin 2,3-dimethylbut-2-ene (Table 4.2.6). We find that although a reasonable yield is obtained after 24 h with precursor **3** the TOF is quite low compared to Crabtree's catalyst.

Entry	Precursor	Substrate	Time (h)	Yield (%)	TOF (h^{-1})
1	**3**	2,3-dimethylbut-2-ene	24	68	2.8
2	[(py)(PCy_3)Ir(cod)][PF_6	2,3-dimethylbut-2-ene	0.5	95	190

Table 4.2.5: Hydrogenation of 2,3-dimethylbut-2-ene with various precursors.

These qualitative experiments give us some interesting results. It is obvious, for example, that precursor **3** gives an active catalyst that is much more efficient than that of precursor **1**. However, precursor **1** gives a catalyst that is better than precursor **6** which is

perhaps surprising given that $[BF_4]^-$ is supposed to be more weakly coordinating than [*closo*-$CB_{11}H_{12}]^-$. For example, $CpMo(CO)_3FBF_3$ is highly reactive and only stable at low temperatures while $CpMo(CO)_3$(*closo*-$CB_{11}H_{12}$) is stable to addition of H_2O.[43] What is clear however, is that while a vast improvement in catalytic activity is observed upon employing these new counterions they are still somewhat out-performed by Crabtree's complex. In view of the qualitative nature of the results obtained on the bench it was desirable to obtain some quantitative data for these precursors regarding the absolute rate at which they hydrogenate olefins. To this end first order rate constants were determined for catalyst precursors **1-8**. This was achieved by measuring the rate of uptake of hydrogen from a constant pressure vessel. Kinetic data for **1-8** are shown in full in the experimental section. Chart 4.2.1 gives an annotated form of this data. As can be seen the rates of hydrogenation vary markedly depending upon counterion. In general the data obtained from kinetic measurements correlates well to the data obtained on the bench. For example precursor **1** and **6** both give approximately 30% conversion which is in line with the data obtained in Table 4.2.4. The striking difference with these precursors is the rate constant. The rate of hydrogenation for **1** being 8.5 x 10^{-5} s^{-1} compared with 6 x 10^{-3} s^{-1} for precursor **6**. Precursor **6** results in a catalyst some 70 times faster than that of the catalyst generated by precursor **1**. In fact, without additives precursor **6** results in the fastest rate of hydrogenation. However, given the low conversion it must be concluded that this active catalyst is not long-lived. More promisingly precursor **2** shows a marked rate increase over precursor **1** as a result of a single halogenation of the carborane. The conversion is also significantly greater than for either precursor **1** or **6**. A further improvement in both rate and conversion is found

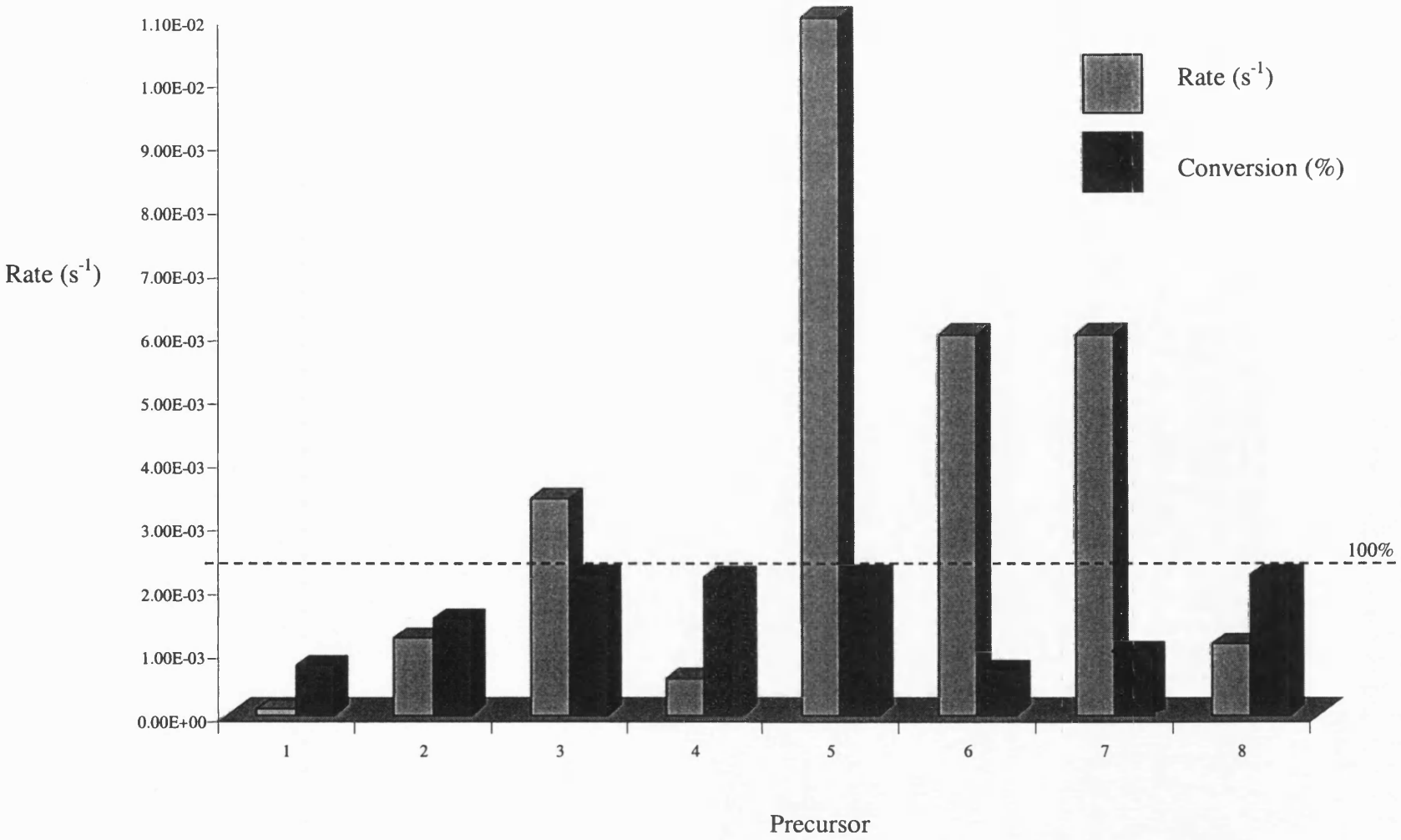

Chart 4.2.1: Chart indicating maximum rate and conversion for precursors **1-8** in the hydrogenation of cyclohexene

for precursor **3** which again is in good agreement with the data in Table 4.2.4. Precursors **4** and **8** are perhaps surprising given that **4** gave comparable results to **3** on the bench but shows a significantly slower rate constant than for **3**, although precursor **8** has a slightly faster rate constant than **4**. The overall conversions with **4** and **8**, however, are all good. Perhaps the most surprising result is the 4-fold increase in rate that is observed for precursor **5**. In this case 5 equivalents of $[NBu_4][closo\text{-}CB_{11}H_6Br_6]$ are added along with the catalyst precursor. Initially it was thought that this excess of anion would inhibit the activity of the catalyst. In fact the reverse is true the catalytic performance is enhanced. When 5 equivalents of $[NBu_4][closo\text{-}CB_{11}H_6Br_6]$ are added to give precursor **7** an enhancement of the conversion is observed. Although no overall increase in rate is detected a significant improvement of the catalytic system in terms of yield ensues. A significant decrease in conversion is observed when a 100-fold excess of $[NBu_4][closo\text{-}CB_{11}H_6Br_6]$ is added to the catalytic system, as determined *via* G.C.

For the hydrogenation of cyclohexene with precursors **1-8** we can write the following order in terms of rate of hydrogenation for the anions.

$$[closo\text{-}CB_{11}H_{12}]^- < [closo\text{-}CB_{11}H_{11}Br]^- \approx [BAr_f]^- \approx [closo\text{-}HCBMe_{11}]^- < [closo\text{-}CB_{11}H_6Br_6]^- < [BF_4]^- << [closo\text{-}CB_{11}H_6Br_6]^- + [NBu_4][closo\text{-}CB_{11}H_6Br_6]$$

Precursors **1** and **2** both give complexes, which contain B-H-M bridges as evidenced by NMR spectroscopy. The coordinating nature of these 3c-2e bonds is relatively strong. For example they are not displaced by THF or acetone. The reaction chemistry of **IX** as discussed in the preceding section involves a readily reversible oxidative addition of the

bound B-H vertices across the metal centre. Hawthorne has proposed that these metal boryl hydride species are the catalytically active species in hydrogenation reactions where an *exo-nido* species is employed as catalyst precursor. We can assume that similar species are being generated in CH_2Cl_2 solution from precursor **1** and are thus in part responsible for the activity of precursor **1**. Another mechanism operating in parallel, which has been proposed for other bidendate anions for rhodium diphosphine systems could potentially be operating in parallel in this system.[28] This process involves association of the olefin prior to the oxidative addition of hydrogen. It seems likely that both these mechanisms (Figure 4.2.20) are operating with this anion.

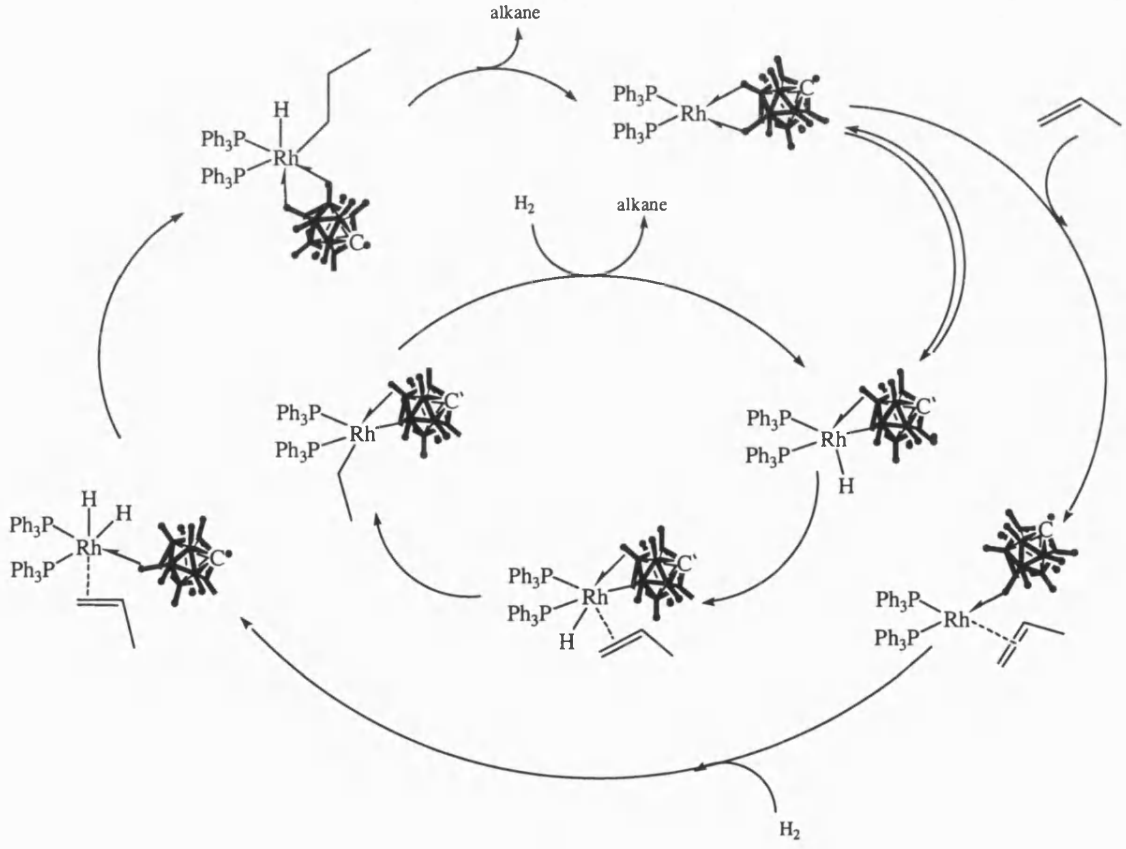

Figure 4.2.20: Proposed mechanisms for the reduction of cyclohexene with precursor **1**

The nature of these mechanisms whereby the anion is closely associated to the metal fragment results in a catalytic system, which is relatively slow. A slight increase in performance is achieved by modulating the anion to the [*closo*-$CB_{11}H_{11}Br]^-$. This is consistent with the removal of the most strongly coordinating {BH} vertex.

Several assumptions about the kinetic data must be made. One is that the absolute rate of the catalyst is probably never observed. This is based upon the fact that as soon as the hydrogenation experiment begins, (i.e. the active catalyst is generated) it begins to deactivate. Therefore the first order rate measured is reflective of the amount of active catalyst at any time. Secondly we must assume that at some point early on in the hydrogenation that the arene bridged dimer dissociates into two mononuclear metal complexes. This could be *via* addition of H_2 across the metal centre generating a fragment of the type $\{(PPh_3)_2Rh(H)_2\}^+$. The stabilization of this fragment could in principle be achieved in one of two ways. Solvent could coordinate to the metal centre resulting in a complex of the type $[(PPh_3P)_2Rh(H)_2(sol)_2]$ where sol = CH_2Cl_2 or the metal centre could be stabilized by coordination of the anion. In fact the nature of the stabilization of this metal fragment could be dependent on the counterion itself with a more coordinating counterion favouring a closely associated ion pair in solution. A more weakly coordinating anion would perhaps favour the formation of a solvent complex Figure 4.2.21.

Figure 4.2.21: Possible equilibrium between solvent complex and anion coordination

Both the complexes depicted in Figure 4.2.21 could potentially be active hydrogenation catalysts. We can use the complexes obtained in chapter 3 as models for the complexes proposed in this equilibrium. In fact complexes **IX, XXI, XVII** and **XVIII** are spectroscopically, and in the case of **IX, XVII** and **XVIII** crystallographically characterized, complexes that can be postulated as intermediates in the hydrogenation of olefins. Indeed we even observe an equilibrium between complex **XVIII** and CH_2Cl_2. How does this hypothesis fit with the kinetic data? Let us consider the case of the precursor **6** first. This gives the fastest rate, however, the conversion is very low. We can use the conversion as a guide to catalyst stability. In this case the catalyst must decompose very rapidly. A possible deactivation pathway is outlined in Figure 4.2.22. Here we are assuming that the $[BF_4]^-$ is weakly coordinating thus favouring the formation of the solvento complex. Treatemnt of $[(PPh_3)_2Rh(nbd)][BF_4]$ with H_2 CH_2Cl_2 in the absence of olefin also results in the formation of this hydride bridged dimer.

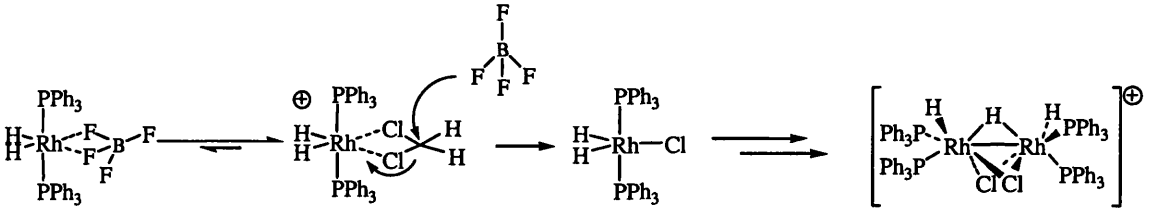

Figure 4.2.22: Possible deactivation pathway for precursor **6**

The catalyst is rapidly deactivated forming a chloro- complex which itself rapidly forms catalytically inactive dimers. Such reaction pathways have been observed previously by Kubas.[44] The rapid formation of catalytically inactive dimers would result in a low conversion.

With the [*closo*-$CB_{11}H_6Br_6$]$^-$ anion (precursor **3**) a slower rate is measured for the hydrogenation of cyclohexene than that for $[BF_4]^-$ (precursor **6**) but a conversion of 100% is observed. As implied by the total conversion of olefin any decomposition pathway is either inhibited by the anion or is much slower than the rate of hydrogenation for this anion. If we assume that the same equilibrium is operating it must lie more to the side favouring anion coordination which results in a less active catalyst but one that is long-lived.

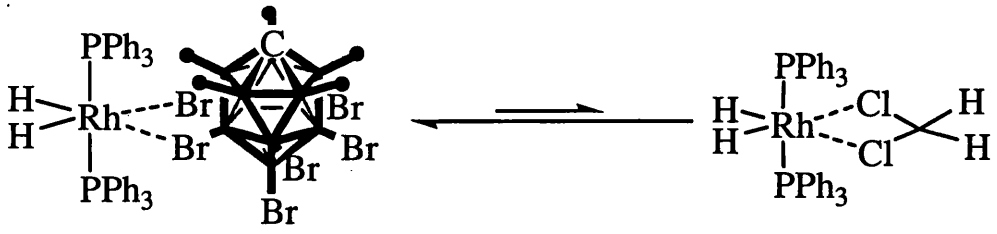

Figure 4.2.31: Equilibrium between coordinated anion and solvent for precursor **3**

The decomposition pathway operating for this system could be different than that operating for precursor **6**. This is for two reasons. Firstly the anion is bulkier which results in a more delocalised anionic charge. Secondly if the anion is more coordinating less of the CH_2Cl_2 complex is generated. NMR solution studies of the reduction of cyclohexene with precursor **3** at 1 atm indicate that at 1mol% catalyst loadings in CD_2Cl_2 there are appreciable amounts of [(η^6-C_6H_6)$Rh(PPh_3)_2$][*closo*-$CB_{11}H_6Br_6$] in

solution as the reaction proceeds. We propose the decomposition of the catalyst results in a π-arene metal complex which is virtually inactive in the hydrogenation reaction (Figure 4.2.30).

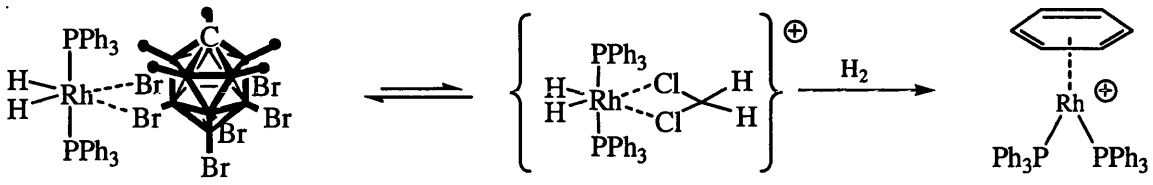

Figure 4.2.30: Possible mode of decomposition for precursor **3**.

It is perhaps the greater steric bulk of the anion that adds to the catalyst stability. The stabilising ability of the [*closo*-$CB_{11}H_6Br_6$]$^-$ anion has been demonstrated earlier in this work. The complex [$(PPh_3)_2Ir(COD)$][BAr_f] when treated with H_2 in CH_2Cl_2 results in the clean formation of the hydride bridged dimer in quantitative yield. This is because the anion is too weakly coordinating to bind to the metal centre and thus the formation of a catalytically inactive dimer results. Addition of H_2 to the [$(PPh_3)_2Ir(COD)$][*closo*-$CB_{11}H_6Br_6$] salt, however, results in a stable carborane adduct. On this basis we proposed that the hexabromo anion has a similar stabilising effect in the rhodium mediated hydrogenation of cyclohexene.

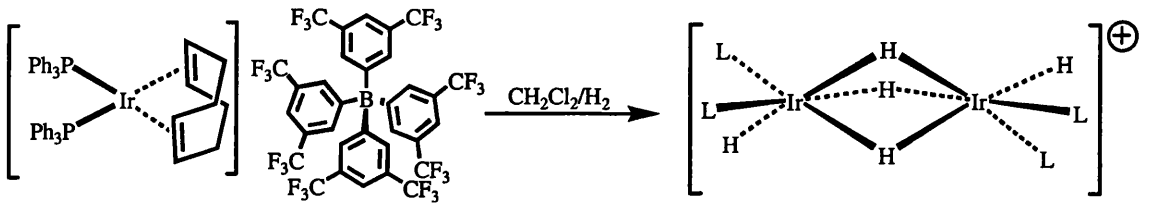

Figure 3.2.9: Reaction of [$(Ph_3P)_2Ir(cod)$][BAr_f] with H_2

When an excess of anion is used a large increase in rate is observed (precursor **5**). This implies that the catalyst is present in high concentrations when the rate is measured. In other words the decomposition pathway is being suppressed completely. The reasons for this remain unclear at present

The kinetic data for precursors **4** and **8** are puzzling. Although both conversions are good, indicating a stable catalyst both the rates whilst fairly comparable are much lower than for the similar weakly coordinating anion precursor **3**. Why is this? In these cases we can only suggest that the anions are so weakly coordinating that they result in a catalyst that is initially extremely fast. However, before the initial uptake of hydrogen slows and the rate of hydrogenation is measured the catalyst must decompose. This is akin to the situation observed for Crabtree's catalyst where the initial rate of hydrogenation is very rapid. However, as the substrate is consumed the active catalyst tends to dimerise to form hydride bridged dimers. It is possible that the use of these extremely bulky weakly coordinating anions pushes the initial activity of the rhodium based systems into the realm of Crabtree's complex.

5.3 Summary

We have demonstrated that metallocarboranes based upon rhodium and iridium have both interesting and novel reaction chemistries. The reaction with H_2 with complex **IX** results in the formation of a hydride bridged dimer, presumably *via* a dihydride rhodium(III) complex. The expected observation of olefin complexes with complex **IX** instead leads to hydroboration of one or more of the carborane vertices *via* B-M-H intermediates. The corresponding iridium complexes also activate {BH} vertices in a similar manner. The reaction chemistry of the arene bridged dimer **XIV** with H_2 broadly mirrors that of **IX** with the hydride bridged dimer being the major component at elevated hydrogen pressures. In an attempt to isolate olefin complexes of rhodium the reaction of cyclohexene with **XIV** leads to CH activated (dehydrogenation) products.

The modulation of the anion results in a marked counterion effect in the hydrogenation of olefins. The exact origin of this effect is still unclear but some conclusions have been drawn.

[1] J. A. Osbom, F. H. Jardine, J. F. Young, and G. Wilkinson, *J. Chem. Soc. A*, 1966, 1711.

[2] J. F. Young, J. A. Osbom, F. H. Jardine, and G. Wilkinson, *J. Chem. Soc.-Chem. Comm.*, 1965, 131.

[3] F. H. Jardine, *Prog. Inorg. Chem.*, 1981, **28**, 63.

[4] C. A. Tolman, P. Z. Meakin, D. L. Lindner, and J. P. Jesson, *J. Am. Chem. Soc.*, 1974, **96**, 2762.

[5] P. Meakin, J. P. Jesson, and C. A. Tolman, *J. Am. Chem. Soc.*, 1972, **94**, 2140.

[6] J. Halpern and C. S. Wong, *J. Chem. Soc.-Chem. Comm.*, 1973, 629.

[7] J. Halpern, T. Okamoto, and A. Zakhariev, *J. Mol. Catal.*, 1976, **2**, 65.

[8] J. Halpern, *Inorg. Chim. Acta.*, 1981, **50**, 11.

[9] J. M. Brown, P. L. Evans, and A. R. Lucy, *J. Chem. Soc.-Perkin Trans.*, 1987, 1589.

[10] S. B. Duckett, C. L. Newell, and R. Eisenberg, *J. Am. Chem. Soc.*, 1994, **116**, 10548.

[11] R. Shcrock and J. A. Osborn, *J. Am. Chem. Soc.*, 1976, **98**, 2134.

[12] R. H. Crabtree and G. E. Morris, *J. Organomet. Chem.*, 1977, **135**, 395.

[13] R. H. Crabtree, G. E. Morris, and H. Felkin, *J. Organomet. Chem.*, 1977, **141**, 205.

[14] R. H. Crabtree, *Acc. Chem. Res.*, 1979, **12**, 331.

[15] R. H. Crabtree, P. C. Demou, D. Eden, J. M. Mihelcic, C. A. Parnell, J. M. Quirk, and G. E. Morris, *J. Am. Chem. Soc.*, 1982, **104**, 6994.

[16] R. H. Crabtree, H. Felkin, T. Fillebeen-Kahn, and G. E. Morris, *J. Organomet. Chem.*, 1979, **169**, 183.

[17] R. H. Crabtree and C. P. Parnell, *Organomet.*, 1985, **4**, 519.

[18] R. H. Crabtree, C. P. Parnell, and R. J. Uriarte, *Organomet.s*, 1987, **6**, 696.

[19] R. H. Crabtree, F. Mellea, J. M. Mihelcic, and J. M. Quirk, *J. Am. Chem. Soc.*, 1982, **104**, 107.

[20] C. M. Jensen, *J. Chem. Soc.-Chem. Comm.*, 1999, 2443.

[21] K. Tatsumi, R. Hoffmann, A. Yamamoto, and J. K. Stille, *Bulletin of the Chemical Society of Japan*, 1981, **54**, 1857.

[22] P. G. Eller, D. C. Bradley, M. B. Hursthouse, and D. W. Meek, *Coord. Chem. Rev.*, 1977, **24**, 1.

[23] D. Blackmond, A. Lightfoot, P. A., T. Rosner, P. Schnider, and N. Zimmermann, *Chirality*, 2000, 442.

[24] A. Lightfoot, P. Schnider, and Pfaltz A., *Angewandte Chemie-International Edition*, 1998, **37**, 2897.

[25] J. Blankenstein and A. Pfaltz, *Angew. Chem. Int. Ed.*, 2001, **40**, 4445.

[26] S. P. Smidt, A. Pfaltz, E. Martinez-Viviente, P. S. Pregosin, and A. Albinati, *Organomet*, 2003, **22**, 1000.

[27] D. Drago, P. S. Pregosin, and A. Pfaltz, *J. Chem. Soc.-Chem. Comm.s*, 2002, 286.

[28] J. M. Buriak, J. C. Klein, D. G. Herrington, and J. A. Osborn, *Chemistry-a European Journal*, 2000, **6**, 139.

[29] J. M. Leitner, H. Brown, and S. J. Brunner, *J. Am. Chem. Soc.*, 1993, **115**, 152.

[30] J. van den Broeke, E. de Wolf, B. J. Deelman, and G. van Koten, *Adv. Synth. Catal.*, 2003, **345**, 625.

[31] H. Werner, M. Bosch, M. E. Schneider, C. Hahn, F. Kukla, M. Manger, B. Windmuller, B. Weberndorfer, and M. Laubender, *J. Chem. Soc.-Dalton Trans.*, 1998, 3549.

[32] K. Isoke, A. Vazquez De Miguel, and P. M. Bailey, *J. Chem. Soc.-Dalton Trans.*, 1983, 1441.

[33] I. R. Butler, W. R. Cullen, B. E. Mann, and C. R. J. Nurse, *J. Organomet. Chem.*, 1985, **280**, C47.

[34] P. D. Morran, S. B. Duckett, P. R. Howe, J. E. McGrady, S. A. Colebrooke, R. Eisenberg, M. G. Partridge, and J. A. B. J. Lohman, *J. Chem. Soc.-Dalton Trans.*, 1999, 3949.

[35] F. B. Hawthorne and T. E. Paxson, *J. Am. Chem. Soc.*, 1974, **96**, 4676.

[36] T. Jelinek, J. Plesek, F. Mares, S. Hermanek, and B. Stibr, *Polyhedron*, 1987, **6**, 1981.

[37] Z. Yinghuai, C. P. Ke, and H. F. Hawthorne, *Angew. Chem. Int. Ed.*, 2003, **42**, 3792.

[38] M. F. Hawthorne and E. L. Hoel, *J. Am. Chem. Soc.*, 1975, 6388.

[39] A. V. Usatov, E. V. Martynova, F. M. Dolgushin, A. S. Peregudov, M. Y. Antipin, and Y. N. Novikov, *European Journal of Inorg. Chem.*, 2002, 2565.

[40] D. E. Kadlecek, P. J. Carroll, and L. G. Sneddon, *J. Am. Chem. Soc.*, 2000, **122**, 10868.

[41] P.E. Garrou, *Chem. Rev.*, 1985, **85**, 171.

[42] P. Budzelaar, N. N. P. Moonen, R. de Gelder, J. M. M. Smits, and A. W. Gal, *Chemistry-a European Journal*, 2000, **6**, 2740.

[43] N. J. Patmore, M. F. Mahon, J. W. Steed, and A. S. Weller, *J. Chem. Soc.-Dalton Trans.*, 2001, 277.

[44] J. Huhmann-Vincent, B.L. Scott, G.J. Kubas, *Inorg. Chem.*, 1999, **38**, 115

5 Experimental

5.1 Experimental technique

5.1.1 General

All manipulations were carried out under an atmosphere of argon, using standard Schlenk-line and glove box techniques, unless otherwise stated. Glassware was pre-dried in an oven at 130°C and flamed with a blowtorch, under vacuum prior to use. CH_2Cl_2, CH_3CN and pentane were distilled from CaH_2. Toluene, diethyl ether, THF and hexane were distilled from sodium-benzophenone-ketyl. Fluorobenzene was stirred over P_2O_5 for 24 hours and then vacuum distilled. C_6D_6 and d_8-toluene were dried over a potassium mirror; CD_2Cl_2 was distilled under vacuum from CaH_2. Microanalyses were performed by Mr. Alan Carver (University of Bath Microanalytical Service). Cyclohexene, 1-methylcyclohexene and 2,3-dimethyl-2-butene were passed over a column of activated alumina and freeze-pump thawed prior to use. Gas Chromatography was performed on a Perkin-Elmer Autosystem XL. Mass Spectrometry was performed by Mr. Chris Cryer (University of Bath Mass spectrometry Service).

4.1.2 NMR spectroscopy

^1H, $^1H\{^{11}B\}$, $^{11}B\{^1H\}$, ^{11}B, $^{13}C\{^1H\}$ and $^{31}P\{^1H\}$ NMR spectra were recorded on a Brüker Avance 300MHz or Varian Mercury 400MHz spectrometers. Residual protio

solvent was used as reference for ^{1}H and $^{1}H\{^{11}B\}$ NMR spectra (CD_2Cl_2: δ = 5.30, C_7D_8: δ = 2.10, C_3D_3O: δ = 2.09, $CDCl_3$: δ = 7.20) and $^{13}C\{^{1}H\}$ NMR spectra (CD_2Cl_2: δ = 53.8). ^{11}B, $^{11}B\{^{1}H\}$ and $^{31}P\{^{1}H\}$ spectra were referenced against $BF_3.OEt_2$ (external) and 85% H_3PO_4 (external) respectively. Values are quoted in ppm. Coupling constants are quoted in Hz.

5.2 Synthesis and characterisation

5.2.1 Starting materials

The starting materials Cs[*closo*-$CB_{11}H_{12}$],[1] Ag[*closo*-$CB_{11}H_{12}$],[1], Cs[*closo*-$CB_{11}H_{11}Br$],[2] Ag[*closo*-$CB_{11}H_{11}Br$],[3] Cs[*closo*-$CB_{11}H_6Br_6$],[4] Ag[*closo*-$CB_{11}H_6Br_6$],[3] $[(Ph_3P)_2RhCl]_2$,[5] $[(C_7H_8)RhCl]_2$,[6] $[(C_8H_{12})RhCl]_2$,[7] $[(C_8H_{12})IrCl]_2$,[8] [(C_8H_{12})Rh(*closo*-$CB_{11}H_{12}$], $[(Ph_3P)_2Rh(C_7H_8)][BF_4]$,[6] Cs[7,8,9,10,11,12-D-*closo*-$CB_{11}H_6$],[9] and $K\{B[C_6H_3(CF_3)_3]_4\}$[10] were all prepared by published literature methods or variations thereof.

5.2.2 Synthesis

$[(Ph_3P)_2Rh(C_7H_8)][closo\text{-}CB_{11}H_{12}]$ (I):

$(Ph_3P)_3RhCl$ (200mg, 0.22mmol), 2,5-norbornadiene (26µl, 28mmol) and $Cs[closo\text{-}CB_{11}H_{12}]$ (60mg, 0.22mmol) were stirred in 10 cm^3 of a 1:3 mixture of acetone/CH_2Cl_2 for 2hr. The resulting orange solution was filtered and concentrated *in vacuo*. The compound was crystallised by addition of ethanol to yield 0.107mg (0.125mmol) of $[(Ph_3P)_2Rh(C_7H_8)][closo\text{-}CB_{11}H_{12}]$ as orange crystals. The solid was collected and washed with 3 portions of ethanol and dried *in vacuo*.

Yield: 57%.

^1H (δ/ppm, CD_2Cl_2): 7.30 (m, 30H C_6H_6), 4.45 (s, 4H C_7H_8), 4.01 (s, 2H C_7H_8), 2.70-1.00 (br q, 11H B*H*), 2.35 (s br, 1H CH_{cage}), 1.52 (s, 2H C_7H_8).

$^{31}P\{^1H\}$ (δ/ppm, CD_2Cl_2): 30.5 [d, *J*(RhP) 155Hz].

$^{11}B\{^1H\}$ NMR (δ/ppm, $CDCl_3$): -7.3ppm (s, 1B), -13.6 (s, 5B), -16.4ppm (s, 5B).

^{11}B NMR (δ/ppm, $CDCl_3$): -7.3 [d, *J*(BH) 135Hz], -13.6 [d, *J*(BH) 136Hz], -16.4 [d, *J*(BH) 143Hz].

Elemental Analysis: Calc. for $C_{44}H_{50}B_{11}P_2Rh$: C, 61.3%; H, 5.84%. Found: C, 61.5%; H, 5.85%.

$[(Ph_3P)_2Rh(C_7H_8)][closo\text{-}CB_{11}H_{11}Br]$ (II):

$(Ph_3P)_3RhCl$ (149mg, 0.16mmol), 2,5-norbornadiene (20µl, 0.21mmol) and [Cs][*closo*-$CB_{11}H_{11}Br$] (57mg, 0.16mmol) were stirred in $10cm^3$ of a 1:3 mixture of acetone/CH_2Cl_2 for 2h. The precipitated CsCl was removed *via* filtration and the solution concentrated *in vacuo*. Addition of an equal volume of ethanol followed by cooling overnight at -30°C afforded 65mg (0.07mmol) of $[(Ph_3P)_2Rh(C_7H_8)][CB_{11}H_{11}Br]$ as orange crystalline flakes.

Yield: 43%.

^1H NMR (δ/ppm, CD_2Cl_2): 7.30 (m, 30H C_6H_5), 4.45 (s, 4H C_7H_8), 4.01 (s, 2H C_7H_8), 2.0 (s br, 1H CH_{cage}), 1.60 (br q, 10H 5+5 coincidence, BH), 1.52 (s, 2H C_7H_8).

$^{31}P\{^1H\}$ NMR (δ/ppm, CD_2Cl_2): 30.5 [d, *J*(RhP) 155Hz].

^{11}B NMR (δ/ppm, CD_2Cl_2): -3.2 (s, 1B), -12.7 [d, 5B, *J*(BH) 141 Hz], -17.1 [d, 5B, *J*(BH), 152 Hz].

Elemental Analysis: Calc. for $C_{44}H_{49}B_{11}BrP_2Rh$: requires C, 56.1%; H, 5.25%. Found: C, 53.7%; H, 5.10%.

$[(Ph_3P)_2Rh(C_7H_8)][closo\text{-}CB_{11}H_6Br_6]$ (III):

$(Ph_3P)_3RhCl$ (200mg, 0.22mmol), 2,5-norbornadiene (26µl, 28mmol) and [Cs][*closo*-$CB_{11}H_6Br_6$] (162mg, 0.22mmol) were stirred in $10cm^3$ of a 1:3 mixture of acetone/CH_2Cl_2 for 2hr. The compound was isolated by concentration of solvent in vacuo followed by addition of an equal volume of ethanol to afford 162mg (0.121mmol) of $[(Ph_3P)_2Rh(C_7H_8)][CB_{11}H_6Br_6]$ as orange flakes.

Yield: 55%.

$^1H\{^{11}B\}$ (δ/ppm, $CDCl_3$): 7.30 (m, 30H C_6H_6), 4.45 (s 4H, C_7H_8), 4.01 (s 2H, C_7H_8), 2.55 (s, 1H CH), 2.25 (s, 6H, B*H*), 1.52 (s 2H, C_7H_8).

$^{11}B\{^1H\}$ (δ/ppm, $CDCl_3$): -1.9 (s, 1B), -10.1 (s, 5B), -20.4 (s, 5B).

^{11}B NMR (δ/ppm, CD_2Cl_2): -1.9 (br s, 1B), -10.1 (br s, 5B), -20.4 [d, *J*(BH) 166Hz].

$^{31}P\{^1H\}$ (δ/ppm, $CDCl_3$): 30.6 [d, *J*(RhP) 155].

Elemental Analysis: Calc. for $C_{46}H_{45}B_{11}Br_6P_2Rh$: requires C, 40.59%; H, 3.33%. Found: C, 40.4%; H, 3.38%.

$[(Ph_3P)_2Rh(C_7H_8)][closo\text{-}HCB_{11}Me_{11}]$ (IV):

$(Ph_3P)_3RhCl$ (191mg, 0.23mmol), 2,5-norbornadiene (27μl, 0.29mmol) and Cs[*closo*-$HCB_{11}Me_{11}$] (100mg, 0.23mmol) were stirred in $10cm^3$ of a 1:3 mixture of acetone/CH_2Cl_2 for 2h. The precipitated CsCl was removed *via* filtration and the solution concentrated *in vacuo*. Addition of an equal volume of ethanol followed by cooling overnight at -30°C to afforded 70mg (0.068mmol) of $[(Ph_3P)_2Rh(C_7H_8)]$[closo-$HCB_{11}Me_{11}$] as large orange prisms.

Yield: 29%.

^1H NMR (δ/ppm, $CDCl_3$): 7.30 (m, 30H, C_6H_5), 4.44 (s, 4H, C_7H_8), 4.01 (s, 2H, C_7H_8), 1.52 (s, 2H, C_7H_8), 1.25 (br s, 1H, C*H*) -0.08 (s, 15H, B-Me), -0.36 (s, 15H, B-Me), -0.44 (s, 3H, B-Me).

$^{31}P\{^{31}H\}$ NMR (δ/ppm, $CDCl_3$): 30.7 [d, *J*(RhP)154Hz].

$^{11}B\{^1H\}$NMR: 2.5 (s, 1B), -5.5 (s, 5B), -8.9 (s, 5B).

Elemental Analysis: Calc. for $C_{55}H_{72}B_{11}P_2Rh$: requires C, 65.0%; H, 7.14%; Found: C, 64.3%; H, 7.23%.

$[(Ph_3P)_2Rh(C_7H_8)][\{B[C_6H_3(CF_3)_2]_4\}]\bullet CH_2Cl_2$ (V):

$[(Ph_3P)_3RhCl]$ (100mg, 0.1mmol) and $K[\{B[C_6H_3(CF_3)_2]_4]$ (97mg, 0.1mmol) were placed in a Schlenk tube. CH_2Cl_2 (10cm^3) was added via cannula along with 2,5-norbornadiene (15μl, 0.16mmol). The solution was stirred for 2hr and then filtered. Crystallisation was effected by dissolution in minimum CH_2Cl_2 followed by addition of ethanol and cooling at -30°C to give 50mg (0.03mmol) of $[(Ph_3P)_2Rh(C_7H_8)][\{B[C_6H_3(CF_3)_2]_4\}]$ as bright red crystalline blocks.

Yield: 30%.

^{1}H NMR (δ/ppm, $CDCl_3$): 7.65 (s, 8H C_6H_3), 7.45 (s, 4H C_6H_3), 7.25 (m, 30H C_6H_6), 4.45 (s, 4H C_7H_8), 4.01 (s, 2H C_7H_8), 1.52 (s, 2H C_7H_8).

$^{31}P\{^1H\}$ (δ/ppm, CD_2Cl_2): 30.5 [d, *J*(RhP) 155].

^{11}B NMR: (δ/ppm, $CDCl_3$): -6.8 (s).

Elemental Analysis: Calc. for $C_{76}H_{52}BCl_2F_{24}P_2Rh$: requires C, 54.7%; H, 3.14%. Found: C, 55.4%; H, 3.40%.

$[(Cy_3P)_2Rh(C_7H_8)][$*closo*-$CB_{11}H_{12}]\bullet CH_2Cl_2$ (VI):

$[(C_7H_8)RhCl]_2$ (100mg, 0.22mmol) and Ag[*closo*-$CB_{11}H_{12}$] (162mg, 0.66mmol) were placed in a Schlenk-tube under argon. 2,5-norbornadiene (0.1cm^3, 0.92mmol) was added via syringe along with CH_2Cl_2 (25cm^3). After 2hr the solution was filtered from precipitated AgCl. PCy_3 (0.88mmol, 248mg) in CH_2Cl_2 (10 cm^3) was added to the filtrate and the solution became a deep red colour. Solvent was removed *in vacuo* and the product was crystallised by dissolution in minimum CH_2Cl_2, addition of hexanes

followed by cooling overnight at -30°C to give 150mg (0.15mmol) of $[(Cy_3P)_2Rh(C_7H_8)][closo\text{-}CB_{11}H_{12}]$ as dark red microcrystals.

Yield: 35%

^{1}H NMR (δ/ppm, $CDCl_3$): 4.63 (s, 4H, C_7H_8), 3.87 (s, 2H, C_7H_8), 3.81 (s, 2H, C_7H_8), 2.30 (s br, 1H, CH_{cage}), 1.90-1.20 (m, 66H, C_6H_{11}).

$^{31}P\{^1H\}$ NMR (δ/ppm, $CDCl_3$): 23.6 [d, *J*(RhP) 145 Hz].

$^{11}B\{^1H\}$ NMR (δ/ppm, $CDCl_3$): -7.3ppm (s, 1B), -13.6 (s, 5B), -16.4ppm (s, 5B).

^{11}B NMR (δ/ppm, $CDCl_3$): -7.3 [d, *J*(BH) 135Hz], -13.6[d, *J*(BH) 136Hz], -16.4 [d, *J*(BH) 143 Hz].

Elemental Analysis: Calc. for $C_{45}H_{88}B_{11}P_2RhCl_2$: requires C, 54.98; H, 8.95. Found: C, 54.7%; H, 9.07%.

$[(dppe)Rh(C_7H_8)][closo\text{-}CB_{11}H_{12}]\bullet CH_2Cl_2$ (VII):

$[(C_7H_8)RhCl]_2$ (97mg, 0.21mmol) and $Ag[closo\text{-}CB_{11}H_{12}]$ (105mg, 0.42mmol) were placed in a Schlenk-tube. 2,5-norbornadiene ($0.1cm^3$) was added via needle. CH_2Cl_2 and acetone ($25cm^3$, $10cm^3$ respectively) were added via cannula. After 2 hr the solution was filtered off the precipitated AgCl. Upon addition of dppe (168mg, 0.42mmol) in $10cm^3$ CH_2Cl_2 the solution becomes a deep red colour. The solution was then concentrated *in vacuo* and an equal volume of ethanol added. The red needle-like crystals were collected, washed with ethanol to give 132mg (0.16mmol) of $[(dppe)Rh(C_7H_8)][closo\text{-}CB_{11}H_{12}]$.

Yield: 38%.

^{1}H NMR (δppm, $CDCl_3$): 7.45 (m, 20H, C_6H_5), 5.25 (s, 4H C_7H_8), 4.20 (s, 2H C_7H_8), 2.25 [d, *J*(PH) 21Hz, 4H CH_2CH_2], 2.20 (s br, 1H, CH), 1.75 (s, 2H C_7H_8), 1.6 (q v br, 11H, 5+5+1 coincidence, B*H*).

^{1}H{^{11}B} NMR (δ/ppm, $CDCl_3$): 7.45 (m, 20H, C_6H_5), 4.45 (s, 4H C_7H_8), 4.01 (s, 2H C_7H_8), 2.20 [d, *J*(PH) 21Hz, 4H CH_2CH_2], 2.20 (s br, 1H, CH_{cage}), 1.52 (s, 2H C_7H_8), 1.55 (s br, 6H, B*H*), 1.39 (s br, 5H B*H*).

^{31}P{^{1}H} NMR (δ/ppm, $CDCl_3$): 57.1 [d *J*(RhP) 156Hz].

^{11}B{^{1}H} NMR (δ/ppm, $CDCl_3$): -7.3 (s, 1B), -13.6 (s, 5B), -16.4 (s, 5B).

^{11}B NMR (δ/ppm, $CDCl_3$): -7.3 [d, *J*(BH) 135Hz], -13.6 [d, *J*(BH) 136Hz], -16.4 [d, *J*(BH) 143Hz].

Elemental Analysis: Calc. for $C_{35}H_{46}B_{11}Cl_2P_2Rh$: requires C, 51.2%; H, 5.64. Found: C, 50.7%, H, 5.69.

[{$(MeO_3)P$}$_2$Rh(C_8H_{12})][*closo*-$CB_{11}H_{12}$] (VIII):

[(COD)Rh($CB_{11}H_{12}$)] (90 mg, 0.25mmol) was placed in a Schlenk tube and dissolved in CH_2Cl_2 (10cm^3). $P(OMe)_3$ (63 μl, 0.50mmol) was added drop-wise via a syringe. The solution was stirred for 1h after which the solvent was reduced *in vacuo* and hexane added to precipitate 130mg (0.215mmol) [{$(MeO_3)P$}$_2$Rh(C_8H_{12})][*closo*-$CB_{11}H_{12}$] as an orange powder.

Yield: 86%.

^{1}H NMR (δ/ppm, CD_2Cl_2): 5.58 (s, 4H, C*H*), 3.65 (m, 18H OCH_3), 2.50 (m, 4H C_8H_{12}), 2.30 (m, 4H C_8H_{12}), 2.21 (s, br CH_{cage}), 1.50 (q br, 11H 5 + 5 + 1 coincidence, B*H*).

$^1H\{^{11}B\}$ NMR (δ/ppm, CD_2Cl_2): δ 5.58 (s, 4H, C_8H_{12}), 3.65 (m, 18H OCH_3), 2.50 (m, 4H C_8H_{12}), 2.30 (m, 4H C_8H_{12}), 2.21 (s, br CH_{cage}), 1.55 (s br, 6H B*H*), 1.39 (s br, 5H B*H*).

$^{31}P\{^1H\}$ NMR (δ/ppm, CD_2Cl_2): 121 [d, *J*(RhP) 278Hz].

$^{11}B\{^1H\}$ NMR (δ/ppm, $CDCl_3$): -7.3ppm (s, 1B), -13.6 (s, 5B), -16.4ppm (s, 5B).

^{11}B NMR (δ/ppm, $CDCl_3$): -7.3 [d, *J*(BH) 135Hz], -13.6 [d, *J*(BH) 136Hz], -16.4 [d, *J*(BH) 143Hz].

Elemental Analysis: Calc. for $C_{15}H_{42}B_{11}O_6P_2Rh$: requires C, 29.9%; H, 7.03%. Found: C, 30.9%; H, 6.74%.

[$(Ph_3P)_2Rh$(*closo*-$CB_{11}H_{12}$)] (IX):

[$(Ph_3P)_2Rh(C_7H_8)$][*closo*-$CB_{11}H_{12}$] (106mg, 0.12mmol) was placed in a 50cm^3 Schlenk tube and CH_2Cl_2 (5cm^3) was added *via* cannula. The solution was freeze-pump thawed three times. On the third cycle the solution was allowed to warm to room temperature, with stirring, under an atmosphere of H_2. Conversion was quantitative by ^1H and ^{31}P NMR spectroscopy. Layering a CH_2Cl_2 solution of [$(Ph_3P)_2Rh$(*closo*-$CB_{11}H_{12}$)] with hexane and placing in the freezer at -30°C afforded 57mg (0.074mmol) as red blocks.

Yield: 61%.

^1H NMR (δ/ppm, $CDCl_3$): 7.40 (m, 30H C_6H_6), 2.58 (s, 1H CH_{cage}), 1.70 [br q, 5H B*H*], -0.02 [broad q, 5H *J*(BH) 97Hz], -1.97 [br q, *J*(HB) 119 Hz, 1H, B*H*].

$^1H\{^{11}B\}$ (δ/ppm, $CDCl_3$): 7.40 (m, 30H C_6H_6), 2.58 (s, C*H*), 1.70 (s, 5H B*H*), -0.02 (s, 5H, B*H*), -1.97 (s, 1H, B-*H*).

$^{31}P\{^1H\}$ (δ/ppm, $CDCl_3$): 49.0 [d, *J*(RhP) 194 Hz].

$^{11}B\{^1H\}$ (δ/ppm, $CDCl_3$): -9.9 (1B), -13.5 (5B), -14.1 (5B).

^{11}B (δ/ppm, $CDCl_3$): -10.0 [d, *J*(BH) 120 Hz, 1B], -13.0 (br s overlapping, 5B), -14.0 (br s overlaping, 5B).

Elemental Analysis: Calc. for $C_{37}H_{42}B_{11}P_2Rh$: requires C, 57.9%; H, 5.49%. Found: C, 57.3%; H, 5.25%.

[(dppe)Rh(*closo*-$CB_{11}H_{12}$)] (X).

[(dppe)Rh(C_7H_8)][*closo*-$CB_{11}H_{12}$] (50mg, 0.0678mmol) was dissolved in 5cm^3 CH_2Cl_2 in a Young's tube. The solution was freeze pump thawed three times. On the third cycle the solution was sealed under vacuum. The tube was then opened under an H_2 pressure and resealed. The solution was allowed to warm to room temperature and stirred for 0.5h. Upon addition of hexane and removal of the solvents *in vacuo* a peach coloured powder was obtained. Crystallisation was achieved by slow diffusion of pentane into a CH_2Cl_2 solution affording 24mg (0.037mmol) of [(dppe)Rh(*closo*-$CB_{11}H_{12}$)] as orange blocks.

Yield: 55%.

^1H NMR (δ/ppm, CD_2Cl_2): 7.50 (m, 20H C_6H_5), 2.55 (s br, 1H, CH_{cage}), 2.13 [dd, *J*(PH) 21Hz, ^3J(PH) 1.6Hz, 4H CH_2CH_2], 1.80 (q br, 5H B*H*), 0.41 (q br, 5H B*H*), -1.40 [q br, *J*(BH) 116Hz, 1H B*H*].

$^1H\{^{11}B\}$ NMR (δ/ppm, CD_2Cl_2): 7.50 (m, 20H C_6H_5), 2.55 (s br, 1H, CH_{cage}), 2.13 [dd, *J*(PH) 21Hz, ^3J(PH) 1.6Hz, 4H CH_2CH_2], 1.80 (s br, 5H B*H*), 0.41 (s br, 5H B*H*), -1.40 (s br, 1H B*H*).

$^{31}P\{^1H\}$ NMR (δ/ppm, CD_2Cl_2): 80.3 [d *J*(RhP) 189Hz].

$^{11}B\{^1H\}$ NMR (δ/ppm, CD_2Cl_2): -15.8 (s, 5+5+1 coincidence).

^{11}B NMR (δ/ppm, CD_2Cl_2): -15.7 [d, 5+5+1 coincidence, *J*(BH) 121Hz].

Elemental Analysis: Calc. for $C_{27}H_{36}B_{11}P_2Rh$: requires C, 50.3%; H, 5.63%. Found: C, 50.8%; H, 4.94%.

[{$(MeO)_3P$}$_2$Rh(*closo*-$CB_{11}H_{12}$)] (XI).

Compound (**7**) (55mg, 0.091mmol) was dissolved in 5cm^3 CH_2Cl_2 in a Young's tube. The solution was freeze-pump degassed three times. On the final cycle the tube was sealed in liquid N_2 under an atmosphere of H_2. The solution was allowed to warm to room temperature and stirred for 1.5h. Concentration of the solution *in vacuo* and addition of hexanes yielded 37mg (0.074 mmol) of [{$(MeO)_3P$}$_2$Rh(*closo*-$CB_{11}H_{12}$)]as a bright yellow powder.

Yield: 81%.

^1H NMR (δ/ppm, CD_2Cl_2): 3.55 (m, 18H, C*H*$_3$O), 2.56 (s br, 1H, C*H*$_{cage}$), 1.81 (v br q, 5H, B*H*), 0.22 (v br q, 5H, B*H*), -2.45 [q br, *J*(BH) 120Hz, 1H, B*H*).

$^1H\{^{11}B\}$ NMR: (δ/ppm, CD_2Cl_2): 3.55 (m, 18H, C*H*$_3$O), 2.55 (s br, 1H, C*H*$_{cage}$), 1.85 (br s, 5H, B*H*), 0.23 (s br, 5H, B*H*), -2.45 [s br, 1H, B*H*].

$^{31}P\{^1H\}$ NMR (δ/ppm, CD_2Cl_2): 126 [d, *J*(RhP) 294Hz].

$^{11}B\{^1H\}$ NMR (δ/ppm, CD_2Cl_2): -16.0 (br s, 5 + 5 +1 conincidence).

^{11}B NMR (δ/ppm, CD_2Cl_2): -16.0 [d, *J*(BH) 131Hz].

Elemental Analysis: Calc. for $C_7H_{30}B_{11}O_6P_2Rh$: requires C, 15.2%; H, 5.46%. Found: C, 15.8%; H, 5.72%.

[$(Cy_3P)_2Rh(closo\text{-}CB_{11}H_{12})$] (XII):

Compound (**9**) (50mg, 0.056mmol) was treated with H_2 in a similar manner as described for compound (**17**). A red powder was obtained via addition of hexanes and subsequent removal of solvents *in vacuo*. Single crystals suitable for an X-ray diffraction study were grown by slow evaporation of a CH_2Cl_2 solution of [$(Cy_3P)_2Rh(closo\text{-}CB_{11}H_{12})$] under a flow of argon to give 34mg (0.042 mmol) of the title compound as red filaments.

Yield: (75%).

^1H NMR (δ/ppm, $CDCl_3$): 2.50 (s br, 1H CH), 2.00 - 1.00 (m br, 33H + 5H, C_6H_{11} and BH), -0.62 (q br, 5H BH), -2.32 [q br, *J*(BH) 135Hz, 1H BH].

$^1H\{^{11}B\}$ NMR (δ/ppm, $CDCl_3$): 2.50 (s br, 1H CH), 2.00 - 1.00 (m br, 33H + 5H, C_6H_{11} and BH), -0.62 (s br, 5H BH), -2.32 (s br, 1H BH).

$^{31}P\{^1H\}$ (δ/ppm, $CDCl_3$): 56.7 [d, *J*(RhP) 190Hz].

^{11}B NMR (δ/ppm, $CDCl_3$): -11.2 [d, 1B, *J*(BH) 114Hz], -16.6 (br s, 10B 5+5 coincidence).

$^{11}B\{^1H\}$ NMR (δ/ppm, $CDCl_3$): -11.2 (s 1B), -16.3 (br s, 10B).

Elemental Analysis: for $C_{37}H_{78}B_{11}P_2Rh$ requires C, 55.1%; H, 9.74%. Found C, 55.7%; H, 10.1%.

[$(Ph_3P)_2Rh(closo\text{-}CB_{11}H_{11}Br)$] (XIII):

[$(Ph_3P)_2Rh(C_7H_8)$][*closo*-$CB_{11}H_{11}Br$] (45mg, 0.04779mmol) was dissolved in 5ml of CH_2Cl_2 and H_2 was bubbled slowly through the solution for 0.5h. The solution takes on a deep red colour. The complex was isolated by addition of hexanes to the reaction mixture followed by isolation of the red powder *via* filtration.

^{1}H NMR (CD_2Cl_2):: δ 7.30 (m, 30H C_6H_5), 2.55 (s br, 1H CH_{cage}), 1.80 (br q, 5H BH), -0.5 (q br, 5H BH).

^{1}H{^{11}B} NMR (CD_2Cl_2): δ 7.39 (m, 30H C_6H_5), 2.55 (s br, 1H CH_{cage}), 1.8 (s br, 5H BH_{cage}), -0.5 (s br, 5H BH_{cage})

^{31}P{^{1}H} NMR (CD_2Cl_2): 45.1 [d, *J*(RhP) 193 Hz]

^{11}B{^{1}H} NMR (CD_2Cl_2): 1.4 (s, 1B BBr), -11.6 (s, 5B B), -14.6 (s, 5B B)

^{11}B NMR (CD_2Cl_2): 1.5 (s, 1B), -12.2 (m, overlapping coincidence).

Elemental Analysis: Calc. for $C_{37}H_{41}B_{11}BrP_2Rh$: requires C, 52.3%; H, 4.87%. Found: C, 52.9%; H, 5.12%.

[(Ph_3P)(PPh_2-η^6-C_6H_5)Rh]$_2$[*closo*-$CB_{11}H_6Br_6$]$_2$ (XIV):

[(Ph_3P)$_2$Rh(C_7H_8)][*closo*-$CB_{11}H_6Br_6$] (25mg, 0.0187mmol) dissolved in 10cm^3 of CH_2Cl_2 was placed in a 100cm^3 Schlenk tube. The solution was freeze-pump thawed three times and allowed to warm to room temperature, under an atmosphere of H_2 and with stirring. The solution changes colour from a golden orange to a claret red over 0.5h. The conversion is quantitative by ^{1}H and ^{31}P NMR spectroscopy. Crystals suitable for a single crystal X-ray analysis were grown by slow diffusion of hexane into a CH_2Cl_2 solution of [(Ph_3P)(PPh_2-η^6-C_6H_5)Rh]$_2$[*closo*-$CB_{11}H_6Br_6$]$_2$ affording 21mg (0.0084mmol) of the complex as orange filaments.

Yield: 90%.

^{1}H{^{11}B} (δ/ppm, CD_2Cl_2): 7.43 [t, *J*(HH) 7.5, 4H, C_6H_5], 7.30 [t, *J*(HH) 5.69, 4H C_6H_5], 7.0-7.25 (m, 20H C_6H_5), 6.97 [t, *J*(HH) 6.6, 2H C_6H_5], 6.58 [t, *J*(HH) 6.6, 2H C_6H_5], 5.32 [t, *J*(HH) 6.6, 1H C_6H_5], 2.54 (s, 1H CH), 2.32 (s, 5H B*H*).

^{1}H (δ/ppm, CD_2Cl_2): 7.43 [t, *J*(HH) 7.5, 4H, C_6H_5], 7.30 [t, *J*(HH) 5.7, 4H C_6H_5], 7.0-7.25 (m, 20H C_cH_5), 6.97 [t, *J*(HH) 6.6, 2H C_6H_5], 6.58 [t, *J*(HH) 6.6, 2H C_6H_5], 5.32 [t, *J*(HH) 6.6, 1H C_6H_5], 2.54 (s, 1H, CH), 2.32 (br q, 5H, B*H*).

^{11}B{^{1}H} (δ/ppm, CD_2Cl_2): -1.9 (s, 1B), -10.1 (s, 5B), -20.4 (s, 5B).

^{11}B NMR (δ/ppm, CD_2Cl_2): -1.9 (br s, 1B), -10.1 (br s, 5B), -20.4 [d, *J*(BH) 166Hz].

^{1}P{^{1}H} (δ/ppm, CD_2Cl_2): AA'BB'XX' system. 47.5 [complex multiplet, *J*(RhP) 216.6, *J*(RhP) –0.2, *J*(PP) 8.6], 44.6 [complex multiplet, *J*(RhP) –1.0, *J*(Rh'P) –199.3, *J*(PP) 37.8, *J*(PP) 1.32].

Elemental Analysis: Calc for $C_{74}H_{72}B_{22}Br_{12}P_4Rh_2 \cdot 1.4CH_2Cl_2$: requires C, 33.8%; H, 2.9%. Found: C, 33.1 %; H, 2.98 %.

$[(Ph_3P)_2Ir(C_8H_{12})][closo\text{-}CB_{11}H_{12}] \bullet CH_2Cl_2$ (XV):

$[(COD)IrCl]_2$ (250mg, 0.372mmol) was placed in a beaker and suspended in 15cm^3 of ethanol. To this suspension PPh_3 (390mg, 1.48mmol) dissolved in 13cm^3 of ethanol was added drop-wise and with stirring. After 10 minutes a homogeneous red solution was obtained. Upon addition of $Ag[CB_{11}H_{12}]$ (200mg, 0.81mmol) in 5cm^3 of ethanol a precipitate was observed. The solvent was removed under reduced pressure and the residue re-dissolved in 4cm^3 CH_2Cl_2. AgCl is removed *via* filtration and the product crystallised by addition of 1cm^3 of ethanol followed by cooling at -30°C overnight to afford 506mg (0.48mmol) of $[(Ph_3P)_2Ir(C_8H_{12})][CB_{11}H_{12}]$ as red blocks.

Yield: 65%.

^{1}H NMR (δ/ppm, $CDCl_3$): 7.30 (m, 30H, C_6H_5), 4.16 (s, 4H, C_8H_{12}), 2.21 (s, br CH_{cage}), 2.20 (m, 4H, C_8H_{12}), 2.01 (v br q, 11H 5+5+1 coincidence, B*H*),1.95 (m, 4H, C_8H_{12}).

^{31}P NMR (δ/ppm, $CDCl_3$): 18.8 (s).

^{11}B NMR (δ/ppm, $CDCl_3$): -7.3 [d, *J*(BH) 137Hz], -13.6 [d, *J*(BH) 137Hz], 16.4 [d, *J*(BH) 153Hz].

^{11}B{^{1}H} NMR (δ/ppm, $CDCl_3$): -7.3ppm (s, 1B), -13.6 (s, 5B), -16.4ppm (s, 5B).

Elemental Anlalysis: Calc. for $C_{46}H_{56}B_{11}Cl_2IrP_2$: Requires C, 52.5%; H, 5.36%. Found: 51.8%; 5.28%.

$[(Ph_3P)_2Ir(C_8H_{12})][$*closo*-$CB_{11}H_6Br_6]\bullet CH_2Cl_2$ (XVI):

$[(COD)IrCl]_2$ (200mg, 0.297mmol) was placed in a glass vial and suspended in 1cm^3 of ethanol. To this suspension PPh_3 (312mg, 1.19mmol) dissolved in 3cm^3 of ethanol was added drop-wise and with stirring. After 10 minutes a homogeneous red solution was obtained. Upon addition of $Ag[CB_{11}H_6Br_6]$ (431mg, 0.595mmol) in 3cm^3 of ethanol a precipitate is observed. The solvent was removed under reduced pressure and the residue re-dissolved in 4cm^3 CH_2Cl_2. AgCl is removed *via* filtration and the product crystallised by addition of 1cm^3 of ethanol followed by cooling at -30°C overnight to afford 670mg (0.43mmol) of $[(Ph_3P)_2Ir(C_8H_{12})][CB_{11}H_6Br_6]$ as fine red needles.

Yield: 74%.

^{1}H NMR (δ/ppm, $CDCl_3$): 7.30 (m, 30H, C_6H_5), 4.16 (s, 4H, C_8H_{12}), 2.5 (s, 1H CH_{cage}), 2.22 (m, 4H, C_8H_{12}), 1.95 (m, 4H, C_8H_{12}).

^{31}P NMR (δ/ppm, $CDCl_3$): 18.8 (s).

^{11}B{^{1}H} (δ/ppm, $CDCl_3$): -1.9 (s, 1B), -10.1 (s, 5B), -20.4 (s, 5B).

^{11}B NMR (δ/ppm, CD_2Cl_2): -1.9 (br s, 1B), -10.1 (br s, 5B), -20.4 [d, *J*(BH) 166Hz].

Elemental Analysis: Calc. for $C_{46}H_{50}B_{11}Br_6Cl_2IrP_2$: requires C, 36.2%; H, 3.30%. Found: C, 35.8%, H, 3.21%.

$[(Ph_3P)_2Ir(H)_2(closo\text{-}CB_{11}H_{12})]$ (XVII):

$[(Ph_3P)_2Ir(C_8H_{12})][closo\text{-}CB_{11}H_{12}]$ (150mg, 0.14mmol) was placed in a 50cm^3 Schlenk tube and dissolved in 25cm^3 CH_2Cl_2. The solution was freeze-pump thawed three times and allowed to warm to room temperature and with stirring under H_2. The solution initially changes from red to orange to colourless and after 0.5h a pale yellow solution is obtained. The solvent was reduced in volume and layered with pentane to afford 75mg (0.082mmol) of $[(Ph_3P)_2Ir(H)_2(closo\text{-}CB_{11}H_{12})]$ as colourless crystalline blocks.

Yield: 56%.

^{1}H NMR (δ/ppm, 22°C, CD_2Cl_2): 7.40 (br s, 30H, C_6H_6), 2.32 (br s, 1H, CH), 1.54 (br q, 9H, BH), -5.21 [br q, 2H *J*(BH)], -20.97 (br s, 2H, Ir-H).

^{31}P{^{1}H} NMR (δ/ppm, 22°C, CD_2Cl_2): 22.1 (br s).

^{11}B NMR (δ/ppm, 22°C, CD_2Cl_2): 0.1 (s, 1B), -9.8 (s, 1B), -16.5 (br s, 2+2+2+1 coincidence), -25.1 (s, 2B).

^{1}H (δ/ppm, -80°C, CD_2Cl_2): 7.40 (m, 30H, C_6H_5), 2.32 (s, 1H, CH), 1.98 (s, 1H, CH), -5.15 (br q, 2H, BH), -20.52 (br s, 2H, Ir-H), -21.3 (br s, 1H, Ir-H), -20.5 (br s, 1H, Ir-H).

^{31}P{^{1}H} (δ/ppm, -70°C, CD_2Cl_2): 25 (s), 25.0 [d, 1P part of second order AB system, *J*(PP) 348Hz], 22.7 [d, 1P part of second order AB system, *J*(PP) 349Hz].

Elemental Analysis: Calc. for $C_{37}H_{44}B_{11}IrP_2$: requires C, 51.56%; H, 5.15%. Found: C, 50.6%; H, 5.36.

$[(Ph_3P)_2Ir(H_2)(closo\text{-}CB_{11}H_6Br_6)]\cdot 2C_6H_5F$ (XVIII):

$[(Ph_3P)_2Ir(C_8H_{12})][closo\text{-}CB_{11}H_6Br_6]$ (50mg, 0.032mmol) was placed in a $50cm^3$ Schlenk tube and dissolved in $5cm^3$ of CH_2Cl_2. The red solution was thoroughly freeze-pump thawed and allowed to warm to room temperature under 1 atm of H_2 and with stirring. The resulting colourless solution takes on a pale yellow/green colour over 10 minutes. A sample was crystallised *via* dissolution in $5cm^3$ C_6H_5F and layering with $5cm^3$ pentane to give 35mg (0.024mmol) of $[(Ph_3P)_2Ir(H_2)(closo\text{-}CB_{11}H_6Br_6)]$ as cream coloured blocks. Two molecules of C_6H_5F are found in the unit cell by X-ray diffraction.

Yield: 75%.

^1H NMR (δ/ppm, 22°C, $CDCl_3$): 7.30 (m, 30H, C_6H_5), 2.55 (br s, 1H, CH), 2.01 (v br s, 6H, BH), -25.7 [t, 2H, Ir-H, *J*(PH) 18Hz].

$^1H\{^{11}B\}$ NMR (δ/ppm, 22°C, $CDCl_3$): 7.30 (m, 30H, C_6H_5), 2.55 (br s, 1H, CH), 2.01 (s, 6H, 1+5 coincidence BH), -25.72 [t, 2H, Ir-H, *J*(PH) 18Hz].

$^{11}B\{^1H\}$ NMR (δ/ppm, 22°C, $CDCl_3$): -0.8 (s, 1B), -9.8 (s, 5B), -21.9 (br s, 5B).

^{11}B NMR (δ/ppm, 22°C, $CDCl_3$): -0.8 (s, 1B), -9.8 (s, 5B), -21.9 (br s, 5B).

$^{31}P\{^1H\}$ NMR (δ/ppm, 22°C, $CDCl_3$): 15.0 (br s).

$^{31}P\{^1H\}$ NMR (δ/ppm, -80°C, CD_2Cl_2): 26.0 (s)*, 21.1 [second order d, 1P part of an AB system, *J*(PP) 338Hz], 17.1 [second order d, 1P part of an AB system, *J*(PP) 338Hz].

Selected δ^1H (δ/ppm, -80°C, CD_2Cl_2): -23.2 [t, 2H, *J*(PH)] 14Hz]*, -25.5 [t, 2H, *J*(PH) 18Hz].

Selected δ^1H (δ/ppm, -80°C, d_8-toluene): -25.1 [t, *J*(PH) 18Hz].

^{31}P NMR (δ/ppm, -80°C, d_8-toluene): 21.1 [second order d, 1P part of an AB system, *J*(PP) 341Hz], 17.8 [second order d, 1P part of an AB system, *J*(PP) 341Hz].

(Values with asterisk next to them indicate peaks assigned as $[(PPh_3)_2Ir(H)_2(CH_2Cl_2)][closo\text{-}CB_{11}H_6Br_6]$ in 25% abundance. See text.

Elemental Anlalysis: Calc. for $C_{49}H_{48}B_{11}Br_6F_2IrP_2$: requires C, 38.54%; H, 3.14%. Found: C, 38.7%; H 3.27%.

$[(Ph_3P)_2Ir(\eta^2\text{-}C_2H_4)_3][closo\text{-}CB_{11}H_6Br_6]$ (XIX):

$[(Ph_3P)_2Ir(H_2)(closo\text{-}CB_{11}H_6Br_6)]$ (25mg, 0.019mmol) was dissolved in 5cm^3 CH_2Cl_2 in a 50ml Schlenk tube. The solution was freeze-pump thawed three times. The solution was allowed to warm to room temperature under C_2H_4 with stirring. After 0.5h the solvent was removed *in vacuo* to leave a sticky residue which *was not pumped down for a prolonged period of time.* Dissolution of this residue in $CDCl_3$ results in a pale yellow solution of $[(Ph_3P)_2Ir(\eta^2\text{-}C_2H_4)_3][closo\text{-}CB_{11}H_6Br_6]$. Large colourless prisms (24mg, 0.017mmol) of $[(Ph_3P)_2Ir(C_2H_4)_3][closo\text{-}CB_{11}H_6Br_6]$ resulted upon standing a $CDCl_3$ solution.

Yield: 90%.

^{1}H NMR (δ/ppm, 22°C, CD_2Cl_2): 7.30 (m, 30H, C_6H_5), 5.00 (br s, free C_2H_4), 3.21 (br s, metal-bound C_2H_4), 2.55 (br s, 1H, CH), 2.01 (br q, 6H, BH).

$^{31}P\{^1H\}$ NMR (δ/ppm, 22°C, CD_2Cl_2): 0.0 (br s)

^{11}B NMR (δ/ppm, 22°C, CD_2Cl_2): -1.9 (br s, 1B), -10.1 (br s, 5B), -20.4 [d, *J*(BH) 166Hz].

Selected ^{1}H NMR (δ/ppm, -70°C, CD_2Cl_2): 2.95 (s, 12H, C_2H_4), 2.55 (br s, 1H, CH),

$^{31}P\{^1H\}$ NMR (δ/ppm, -70°C, CD_2Cl_2): -0.7 (s).

Elemental Analysis: Calc. for $C_{43}H_{48}B_{11}Br_6IrP_2$: requires C, 36.44%; H, 3.41%. Found C, 34.18%; H, 2.98%.

$[(Ph_3P)_2Ir(\eta^2\text{-}C_2H_4)_2][closo\text{-}CB_{11}H_6Br_6]$ (XX):

$[(Ph_3P)_2Ir(\eta^2\text{-}C_2H_4)_3][closo\text{-}CB_{11}H_6Br_6]$ in CH_2Cl_2 was reduced to dryness *in vacuo*. The resulting red residue was re-dissolved in CD_2Cl_2.

$^1H\{^{11}B\}$ (δ/ppm, $CDCl_3$): 7.30 (m, 30H C_6H_5), 3.20 (s, 8H, C2H4), 2.55 (s, C*H*), 2.52 (br, 6H).

$^{31}P\{^1H\}$ NMR (δ/ppm, CD_2Cl_2): 16.1 (br s).

^{11}B NMR (δ/ppm, CD_2Cl_2): -1.9 (br s, 1B), -10.1 (br s, 5B), -20.4 [d *J*(BH) 166Hz].

$[(Ph_3P)_2Rh(closo\text{-}CB_{11}H_{12})]$ - reaction with H_2 (XXI):

$[(Ph_3P)_2Rh(closo\text{-}CB_{11}H_{12})]$ (30mg, 0.035mmol) was dissolved in $1cm^3$ CD_2Cl_2 and placed in a Young's tube and freeze pump thawed. On the last cycle the tube was backfilled with H_2 whilst immersed in liquid N_2 and sealed. The solution was warmed to room temperature and stirred vigorously for 2h. After this time the H_2 pressure was released and the solution transferred to an NMR tube. ^1H and ^{31}P NMR spectra indicate the formation of a rhodium hydride complex in approximately 50% abundance.

$^{31}P\{^1H\}$ (δ/ppm, CD_2Cl_2): 48.9 [d, *J*(RhP) 193Hz], 39.3 [d, *J*(RhP) 114Hz].

Selected ^1H NMR (δ/ppm, CD_2Cl_2): 2.60 (s, 1H CH_{cage}), 2.25 (s, 1H CH_{cage}), 1.70 [br q, 5H B*H*], -0.02 [broad q, 5H *J*(BH) 80.0, B*H*], -1.97 [br q, *J*(BH) 119, 1H, B*H*], -17.58 (apparent q, 2H, Rh-H).

^{11}B NMR (δ/ppm, $CDCl_3$): -12.0 (s), -15.6 (s).

$[(Ph_3P)_2HRh(\mu\text{-}H)(\mu\text{-}Cl)_2RhH(PPh_3)_2][closo\text{-}CB_{11}H_{12}]$ (XXII).

$[(Ph_3P)_2Rh(nbd)][closo\text{-}CB_{11}H_{12}]$ (25mg, 0.03mmol) in $10cm^3$ CH_2Cl_2 in a $100cm^3$ Schlenk tube fitted with a rubber septum was pressurised with 20psi H_2 for 3days. The solvent was concentrated *in vacuo* and hexane (1 equal volume) was added *via* cannula. After refrigeration for 4-5 days the compound precipitated as yellow crystalline filaments suitable for a single crystal X-ray analysis. The highly air-sensitive nature of this complex did not permit a satisfactory elemental analysis hence accurate mass spectrometry on a bulk sample was used as an alternative to microanalysis.

$^1H\{^{11}B\}$ (δ/ppm $CDCl_3$): 7.30 (m, 60H C_6H_6), 2.54 (s, 1H CH_{cage}), 2.32 (s, 5H B*H*), 1.55 (s br, 5H B*H*), 1.39 (s br, 5H B*H*) -11.0 [complex multiplet, 1H, part of a AA'BB'MXX' system, Rh(μ-*H*), *J*(RhH) 10, *J*(PH) 21, 75], -16.5 (virtual quartet, 2H, *J*(RhP) 15, *J*(PP) 15, 15].

$^{31}P\{^1H\}$ (δ/ppm, $CDCl_3$): 51.5 (complex m, AA'BB'XX' system), 36.0 (complex m, AA'BB'XX' system).

Accurate Mass Spectrometry (ES+): Calculated 1327.1367, found 1327.1353.

$[(Ph_3P)_2Rh(closo\text{-}CB_{11}H_{12})]$ - reduction of C_6H_{10} with D_2:

$[(Ph_3P)_2Rh(CB_{11}H_{12})]$ (30mg, 0.035mmol) was placed in a $100cm^3$ Schlenk tube and dissolved in $5cm^3$ CH_2Cl_2. Cyclohexene (71μl, 0.69mmol) was added via syringe. The solution was freeze-pump thawed and allowed to stir under D_2 at room temperature for 2hr. G.C. analysis indicated a 70% conversion of olefin to cyclohexane. After addition of CH_3CN the solvent was removed *in vacuo* and the residue dissolved in $CDCl_3$. The ^{11}B NMR spectra displayed a 1:5:5 pattern with no ^1H proton coupling in the antipodal

or lower pentagonal belt signals and a partially collapsed doublet for the upper pentagonal belt resonance.

^{11}B NMR (δ/ppm, $CDCl_3$): -7.5 (s, 1B), -13.8 (s, 5B), -16.4 (partially collapsed d, 5B).

^{11}B NMR (δ/ppm, $CDCl_3$): -7.5 (s, 1B), -13.8 (s, 5B), -16.4 (s, 5B).

$[(Ph_3P)_2Rh(CB_{11}H_6D_6)]$ - reaction with H_2:

(**1-d_6**) (30mg, 0.035mmol) was dissolved in 1cm^3 CD_2Cl_2 and placed in a Young's NMR tube. The tube was freeze pump thawed under H_2 and sealed at liquid N_2 temperatures under H_2. This process was repeated 4-5 times.

$^{31}P\{^1H\}$ (δ/ppm, CD_2Cl_2): 47.4 [*J*(RhP) 194Hz] and 37.5 [*J*(RhP) 114Hz] respectively.

$^1H\{^{11}B\}$ (δ/ppm): 7.30 ppm (m, 30H, C_6H_5), 2.61 ppm (s, C*H*), 1.7 ppm(s, 5H, B*H*), -0.02 ppm (s, 5H, B*H*), -1.97 (s, 1H, B*H*), -17.5 (virtual q).

$[(Ph_3P)_2Rh(closo\text{-}CB_{11}H_{12})] + C_2H_4$ – 48 h, (XXIII/XXIV):

$[(Ph_3P)_2Rh(CB_{11}H_{12})]$ (25mg, 0.033mmol) was dissolved in 5cm^3 THF in a Young's tube. The solution was freeze pump thawed three times. On the third cycle the solution was sealed under vacuum. The tube was then opened under C_2H_4 pressure and the tube immersed in liquid N_2. Approximately 15cm^3 of ethylene was frozen into the tube in this way and the tube sealed. The solution was allowed to warm to room temperature and stirred for 48h at room temperature.

^{1}H NMR (δ/ppm, CD_2Cl_2): 7.30 (m, C_6H_5), 4.89 [br d, *J*(HH) 15Hz], 4.78 [br d *J*(HH) 15Hz], 4.13 [br d, *J*(HH) 12Hz], 4.08 [br d, *J*(HH) 12Hz], 2.56 (dd), 2.41 (dd), 2.31 (br s, CH), 2.18 (br s, CH), 1.0 (br q, BH), -1.41 (br q, BH).

^{1}H{^{11}B} NMR (δ/ppm, 25°C, CD_2Cl_2): 7.30 (m, C_6H_5), 4.89 [br d, *J*(HH) 15Hz], 4.78 [br d *J*(HH) 15 Hz], 4.13 [br d, *J*(HH) 12 Hz], 4.08 [br d, *J*(HH) 12 Hz], 2.56 (dd), 2.41 (dd), 2.31 (br s, CH), 2.18 (br s, CH), 1.52 (br s, BH), 1.38 (br s, BH), 0.48 (br s, BH).

^{11}B NMR (δ/ppm, 25°C, CD_2Cl_2): 1.6 (s), -3.5 (s), -17.1 (br s).

^{11}B {^{1}H } NMR (δ/ppm, 25°C, CD_2Cl_2): 1.6 (s), -3.5 (s), -17.1 (s).

^{31}P NMR (δ/ppm, 25°C, CD_2Cl_2): 42.0 (v br s).

^{31}P NMR (δ/ppm, -70°C, CD_2Cl_2): 60.2 [dd, *J*(RhP) 191Hz, *J*(PP) 33 Hz], 23.9 [dd, *J*(RhP) 158Hz, *J*(PP) 33 Hz].

Mass Spec.: m/z peaks: 169.2 [7-(CH=CH_2)-*closo*-$CB_{11}H_{11}$]$^-$ and [12-(CH=CH_2-*closo*-$CB_{11}H_{11}$]$^-$.

[$(Ph_3P)_2Rh(CB_{11}H_{12})$] + C_2H_4 + H_2, (XXV):

[$(Ph_3P)_2Rh(CB_{11}H_{12})$] (25mg, 0.033mmol) was dissolved in 5cm^3 THF in a Young's tube. The solution was freeze pump thawed three times. On the third cycle the solution was sealed under vacuum. The tube was then opened under C_2H_4 pressure and the tube immersed in liquid N_2. Approximately 15cm^3 of ethylene was frozen into the tube in this way and the tube sealed. The solution was allowed to warm to room temperature and stirred for 48h at room temperature. The solution was degassed under vacuum for 2 minutes to remove excess ethylene. The solution was then thoroughly freeze-pump

thawed and on the third cycle the solution was sealed under vacuum. The tube was then opened under H_2 pressure and warmed to room temperature with stirring.

^{1}H NMR (δ/ppm, CD_2Cl_2): 7.30 (m, C_6H_5), 2.48 (br s, CH), 2.40 (br s, CH), 1.50 (br q, BH), 0.82 (m, CH), 0.51 (m, CH), -0.89 (br q, BH), -2.23 (br q, BH).

^{31}P NMR (δ/ppm, 25°C, CD_2Cl_2): 47.0 [d, *J*(RhP) 194 Hz], 46.8 [d, *J*(RhP) 191 Hz], 46.2 [d, *J*(RhP) 193Hz], 46.0 [d, *J*(RhP) 192 Hz].

^{11}B{^{1}H} NMR (δ/ppm, 25°C, CD_2Cl_2): 7.6 (s), -1.9 (s), -12.9 (s), -15.1 (br s), -17.9 (s + shoulder)

^{11}B NMR (δ/ppm, 25°C, CD_2Cl_2): 7.6 (s), -1.9 (s), -12.9 (s), -15.9 (d), -17.9 (overlapping d).

Mass Spec.: m/z peaks: 171.1 [12-(C_2H_5)-*closo*-$CB_{11}H_{12}$]$^-$.

[$(Ph_3P)_2Rh(CB_{11}H_{12})$] + C_2H_2 + H_2 - cycled:

[$(Ph_3P)_2Rh(CB_{11}H_{12})$] (25mg, 0.033mmol) was dissolved in 5cm^3 THF in a Young's tube. The solution was freeze pump thawed three times. On the third cycle the solution was sealed under vacuum. The tube was then opened under C_2H_4 pressure and the tube immersed in liquid N_2. Approximately 15cm^3 of ethylene was frozen into the tube in this way and the tube sealed. The solution was allowed to warm to room temperature and stirred for 48h at room temperature. The solution was degassed under vacuum for 2 minutes to remove excess ethylene. The solution was then thoroughly freeze-pump thawed and on the third cycle the solution was sealed under vacuum. The tube was then opened under H_2 pressure and warmed to room temperature with stirring. This procedure was repeated four times in an effort to achieve multiple cage substitutions.

^{1}H NMR (δ/ppm, $CDCl_3$): 7.30 (m, C_6H_5), 2.45 – 2.2 (br s, CH), 0.62 (m, CH_{alkyl}), -4.95 (br q, BH).

$^{11}B\{^1H\}$ NMR (δ/ppm, 25°C, $CDCl_3$): after addition of CH_2CN: 3.3 (s), -3.5 (s + shoulders), -17.5 (s), -19.5 (br s).

^{11}B NMR (δ/ppm, 25°C, $CDCl_3$): 3.3 (s), -3.4 (s + shoulders), -17.5 (d), -18.7 (br s).

Mass Spec.: m/z peaks: 227.2 [7,8,12-$(CH_2CH_3)_3$-*closo*-$CB_{11}H_9]^-$, 255.2 [7,8,9,12-$(CH_2CH_3)_4$-*closo*-$CB_{11}H_8]^-$, 283.3 [7,8,9,10,12-$(CH_2CH_3)_5$-*closo*-$CB_{11}H_7]^-$, 311.3 [7,8,9,10,11,12-$(CH_2CH_3)_6$-*closo*-$CB_{11}H_6]^-$.

$[(Ph_3P)_2Rh(CB_{11}H_{12})]$ + 1-hexene:

$[(Ph_3P)_2Rh(CB_{11}H_{12})]$ (25mg, 0.033mmol) was dissolved in 5cm^3 THF in a Young's tube. 1-hexene (1.0cm^3, 0.012mol) was added via syringe and the solution was heated 75°C with stirring for 120 hr. The solution was then reduced *in vacuo* to dryness.

^{1}H NMR (δ/ppm, $CDCl_3$): 7.30 (m, C_6H_5), 5.50 (m, CH), 2.46 (s. CH), 2.38 (s, CH), 2.0 – 0.0 (complex m, CH), -0.86 (br q, BH), -2.38 (br q, BH), -4.71 (br q, BH).

$^1H\{^{11}B\}$ NMR (δ/ppm, $CDCl_3$): 7.30 (m, C_6H_5), 5.50 (m, CH), 2.46 (s. CH), 2.38 (s, CH), 2.0 – 0.0 (complex m, CH), -0.86 (br s, BH), -2.13 (br s, BH), -2.28 (br s, BH), -4.71 (br s).

^{31}P NMR (δ/ppm, 25°C, $CDCl_3$): 47.6 [d, *J*(RhP) 195Hz], 47.4 [d, *J*(RhP) 194 Hz], 46.2 [d, *J*(RhP) 193 Hz], 45.9 [d, *J*(RhP) 193Hz].

$^{11}B\{^1H\}$ NMR (δ/ppm, 25°C, $CDCl_3$): 7.6 (s), -3.1 (s), -18.4 (s), -17.1 (s), -19.8 (s).

^{11}B NMR (δ/ppm, 25°C, $CDCl_3$): 7.6 (s), -3.1 (s), -19.3 (v br s, overlapping coincidence).

Mass Spec.: m/z peaks: 227.2 [12-($CH_2CH_2CH_2CH_2CH_2CH_3$)-*closo*-$CB_{11}H_{11}$]$^-$, 310.2 [7,12-($CH_2CH_2CH_2CH_2CH_2CH_3$)$_2$-*closo*-$CB_{11}H_{10}$]$^-$, 393.3 [7,8,12-($CH_2CH_2CH_2CH_2CH_2CH_3$)$_3$-*closo*-$CB_{11}H_9$]$^-$, 408.3 [7,8,9,12-($CH_2CH_2CH_2CH_2CH_2CH_3$)$_4$-*closo*-$CB_{11}H8$]$^-$.

[$(Ph_3P)_2Ir(H)_2$(*closo*-$CB_{11}H_{12}$)] reaction with *tert*-butylethylene:

[$(Ph_3P)_2Ir(H)_2$(*closo*-$CB_{11}H_{12}$)] (25mg, 0.027mmol) was placed in an NMR tube and 1cm^3 CD_2Cl_2 was added *via* cannula. 2,2-dimethylbutene (50µl, 0.6mmol) was added to the solution *via* syringe. The mixture was then heated in a water bath at 55°C for 72hr. After 24hr no starting material is observed in the ^{1}H NMR spectrum. ^{11}B and mass spectrometry suggest that one or more vertices of the cage have become functionalised *via* B-H exchange.

^{11}B NMR (δ/ppm, 24 hrs, CD_2Cl_2): 5.0 to -7.5 (br s, overlapping peaks), 13.5 [d, *J*(BH) 133Hz], 16.0 [d, *J*(BH) 153Hz].

^{11}B{^{1}H} NMR (δ/ppm, 24 hrs, CD_2Cl_2): 5.0 to -7.5 (br s, overlapping peaks), -13.6 (s), -16.48 (s).

^{11}B NMR (δ/ppm, 72 hrs, CD_2Cl_2): 5.0 to -10.0 (br overlapping coincidences), -12.7 (partially collapsed doublet), -17.0 (partially collapsed doublet).

^{11}B{^{1}H} NMR (δ/ppm, 72 hrs, CD_2Cl_2): 5.0 to -10.0 (br overlapping coincidences), -13.5 (br s + shoulder), -16.5 (v br s + large shoulder)

Mass spectrometry (after 72hr): m/z peaks; 306.2 [7,12-{($CH=CH(CH_3)_3$}-*closo*-$CB_{11}H_{10}$]$^-$, 391.5 [7,8,12-{($CH=CH(CH_3)_3$}$_3$-*closo*-$CB_{11}H_9$]$^-$, 474.6 [7,8,9,12-{($CH=CH(CH_3)_3$}$_4$-*closo*-$CB_{11}H_8$]$^-$, 557.3 [7,8,9,10,12-{($CH=CH(CH_3)_3$}$_3$-*closo*-$CB_{11}H_7$]$^-$.

$[(Ph_3P)_2Ir(H)_2(closo\text{-}CB_{11}H_{12})]$ reaction with C_2H_4:

$[(Ph_3P)_2Ir(H)_2(closo\text{-}CB_{11}H_{12})]$ (50mg, mmol) was dissolved in CH_2Cl_2 in a $25cm^3$ Young's tube. The solution was freeze pump thawed three times. On the third cycle the solution was sealed under vacuum. The tube was then opened under a C_2H_4 pressure whilst immersed in liquid N_2. Approximately $15cm^3$ of ethene was frozen into the tube in this manner. The tube was then sealed. As the tube was warmed to room temperature the ethene was seen to go from solid to liquid and then at room temperature as a gas upon shaking the solution. The solution was stirred at room temperature for 24 hr after which time the C_2H_4 was vented and the mixture reduced to dryness under vacuum. The ^{11}B and $^{31}P\{^1H\}$ were recorded in CD_2Cl_2 prior to addition of CH_3CN and subsequently.

$^{31}P\{^1H\}$ NMR (δ/ppm, after 24hr CD_2Cl_2): 22.0 (s), 18.2 (br s), 15.5 (br m), -1.7 (br m)

After 24hr:

$^{11}B\{^1H\}$ NMR (δ/ppm, CD_2Cl_2): 7.5 (s), 3.4 (s), 3,3 (s), -0.2 (s), -6.5 (s), -17.0 (s + shoulder), -20.2 (s), -34 (s), -40 (s).

^{11}B NMR (δ/ppm, CD_2Cl_2): 7.5 (s), 3.4 (s), 3,3 (s), -0.2 (s), -6.5 (s), -16.8 (br d, overlapping peaks), -20.7 (br d, overlapping), -34 (s), -40 (s).

After addition of CH_3CN:

$^{31}P\{^1H\}$ NMR (δ/ppm, CD_2Cl_2): 25.8 (s), 23.7 (s), 16.2 (s), 0.0 (s), -9.0 [d, *J*(PP) 333Hz], -81.8 [d, *J*(PP) 333Hz].

$^{11}B\{^1H\}$ NMR (δ/ppm, CD_2Cl_2): 3.8 (s), 0.6 (s), -2.7 (s), -5.9 (s), -13.7 (s, overlapping peaks), -16.2 (s + shoulder), -17.7 (s).

$^{11}B\{^1H\}$ NMR (δ/ppm, CD_2Cl_2): 3.8 (s), 0.6 (s), -2.7 (s), -5.9 (s), -12.9 (s), -16.7 (s + overlapping shoulders), -17.7 (s).

$[(Ph_3P)_2Ir(H)_2(closo\text{-}CB_{11}H_{12})]$ reaction with C_2H_4 and H_2:

$[(Ph_3P)_2Ir(H)_2(closo\text{-}CB_{11}H_{12})]$ (50mg, 0.058 mmol) was dissolved in CH_2Cl_2 in a $25cm^3$ Young's tube. The solution was freeze pump thawed three times. On the third cycle the solution was sealed under vacuum. The tube was then opened under a C_2H_4 pressure whilst immersed in liquid N_2. Approximately $15cm^3$ of ethene was frozen into the tube in this manner. The tube was then sealed. The solution was stirred at room temperature for 24 hr after which time the C_2H_4 was vented and placed under H_2 via a similar procedure as outline above. After 1hr the solution had lightened considerably. The excess H_2 was released and the solution reduced to dryness *in vacuo*. The residue was taken up in CD_2Cl_2 and transferred to an NMR tube.

^1H (δ/ppm, CD_2Cl_2): 7.30 (m, C_6H_5), 0.92 (m, C_2H_5), -5.50 (br q, BH), -21.9 (s, Ir-H).

$^{11}B\{^1H\}$ NMR (δ/ppm, CD_2Cl_2): 8.0 (s), 5.0 (s), -3.1 (br overlapping s), -13.6 (s), -14.5 (d, overlapping), -16.7 (d, overlapping), -30.1(br s).

^{11}B NMR (δ/ppm, CD_2Cl_2): 8.0 (br s), 3.8 (br s, -3.0 (s), -4.2 (s), -12.9 (s), -15.9 (s), -19.9), -20.0 (s), -28.9 (s), -30.9 (s).

$^{31}P\{^1H\}$ NMR (δ/ppm, after 24hr CD_2Cl_2): 22.0 (br s), 21.8 (br s), 21.7 (br s), 21.4 (s), 21.1 (s), 20.7 (br s, overlapping).

$[(Ph_3P)_2Ir(H)_2(closo\text{-}CB_{11}H_{12})]$ reaction with C_2H_4 and H_2:

The steps outlined in experiments (**35**) and (**36**) were cycled several times in an effort to completely functionalise the carborane cage.

^{1}H (δ/ppm, CD_2Cl_2): 7.3 (m, C_6H_5), 0.9 (m, C_2H_5).

^{11}B NMR (δ/ppm, CD_2Cl_2): 3.6 (s), -3.1 (s + shoulder), -12.8 [d, *J*(BH) 125Hz], -15.7 [d, *J*(BH) 98 Hz], 17.6 [d, *J*(BH)134Hz, 19.9 [d, *J*(BH)144Hz].

^{11}B{^{1}H} NMR (δ/ppm, CD_2Cl_2): 3.7 (s), -3.0 (s + shoulder), -12.8 (s), -15.7(s), -17.6(s), -19.9(s).

Mass Spectrometry: m/z peaks; 195.2 [7,12-$(CH{=}CH_2)_2$-*closo*-$CB_{11}H_{10}]^-$, 227.3 [7,8,12-$(CH_2CH_3)_3$-*closo*-$CB_{11}H_9]^-$, 255.4 [7,8,9,12-$(CH_2CH_3)_4$-*closo*-$CB_{11}H_8]^-$, 283.4 [7,8,9,10,12-$(CH_2CH_3)_5$-*closo*-$CB_{11}H_7]^-$, 311.4 [7,8,9,10,11,12-$(CH_2CH_3)_6$-*closo*-$CB_{11}H_6]^-$, 339.5 [6,7,8,9,10,11,12-$(CH_2CH_3)_7$-*closo*-$CB_{11}H_5]^-$.

$[(Ph_3P)_2Rh(\eta^4\text{-}C_6H_8)][closo\text{-}CB_{11}H_6Br_6]\bullet 2CH_2Cl_2$ (XXVI):

$[(Ph_3P)_2Rh(C_7H_8)][closo\text{-}CB_{11}H_6Br_6]$ (40mg, 0.03mmol) was dissolved CD_2Cl_2 (1 cm3) in a Young's NMR tube and placed under an H_2 atmosphere for 0.5h. The solution was monitored via ^{1}H NMR spectroscopy until all starting material had reacted to give $[(PPh_3)\{(\eta^6\text{-}C_5H_6)PPh_2\}Rh]_2[closo\text{-}CB_{11}H_6Br_6]_2$, (**XIV**). The system was then freeze-pumped-thawed three times and placed under argon. Cyclohexene (25μL, 0.24mmol) was added to the solution *via* syringe. The reaction was monitored via ^{1}H and ^{31}P{^{1}H} NMR spectroscopy for 48 hours until all the starting material had been consumed. Crystals suitable for a single crystal X-ray structure study were grown by diluting a CH_2Cl_2 solution with an equal volume of hexane and cooling at 0 °C for several days to

give 30mg (0.023mmol)) of $[(Ph_3P)_2Rh(\eta^4\text{-}C_6H_8)][closo\text{-}CB_{11}H_6Br_6]$ as deep red crystalline blocks.

Yield: 75%.

$^1H\{^{11}B\}$ (δ/ppm, CD_2Cl_2): 7.40 (m, 30H C_6H_5), 5.52 (br s, 2H, C_6H_8), 3.94 (br s, 2H), 2.52 (br s, 6H), 2.6 (br s, CH_{cage}), 1.21 [d, 2H *J*(HH) 5], 1.04 [d, 2H *J*(HH) 5], 1.05 (s, 1H), 0.97 (s, 1H).

$^{31}P\{^1H\}$ (δ/ppm, CD_2Cl_2): 29.5 [d, *J*(RhP) 177].

$^{13}C\{^1H\}$ (δ/ppm, CD_2Cl_2): 142.0 (C_6H_5), 138.3 (s, C_6H_5), 126.6 (s, C_6H_5), 93.3 (s, C_6H_8), 88.6 (s, C_6H_8), 42 (s, CH_{cage}), 20.6 (s, C_6H_8).

Elemental Analysis: Calc. for $C_{43}H_{44}B_{11}Br_6P_2Rh$: requires C, 39.0%; H, 3.35%. Found: C, 39.9%; H, 3.82%.

$[(Ph_3P)_2Rh(\eta^4\text{-}C_7H_{10})][closo\text{-}CB_{11}H_6Br_6]$ (XXVII):

$[(Ph_3P)_2Rh(C_7H_8)][closo\text{-}CB_{11}H_6Br_6]$ (40mg, 0.03mmol) was dissolved in CD_2Cl_2 (1 cm^3) in a Young's NMR tube and placed under an H_2 atmosphere for 0.5h. The solution was monitored via ^1H NMR spectroscopy until all starting material had reacted to give $[(PPh_3)\{(\eta^6\text{-}C_5H_6)PPh_2\}Rh]_2[closo\text{-}CB_{11}H_6Br_6]_2$. The system was then freeze-pumped-thawed three times and placed under argon and 1-methylcyclohexene (C_7H_{12}) (130μL 1.00mmol) was added to the solution *via* syringe. The reaction was monitored via ^1H and $^{31}P\{^1H\}$ NMR spectroscopy for 48 hrs until all the starting material had been consumed. Despite repeated attempts analytically pure material was not obtained. Unfortunately, mass spectrometry (FAB+, 3-noba matrix) did not show the molecular

ion. Identification by NMR spectroscopy (^{1}H-^{1}H COSY/NOESY) was unambiguous, however.

^{1}H{^{11}B} (δ/ppm, CD_2Cl_2): 7.30 (m, 30H C_6H_5), 4.52 (s, 1H), 4.03 (s, 1H), 3.77 (s, 1H), 2.55 (br s, 1H CH_{cage}), 2.45 (br s, 6H), 1.80 (s, 3H C*H*), 1.79 (m, 1H), 1.43 (m, 1H), 1.10 (m, 1H), 0.92 (m, 1H).

^{31}P{^{1}H} (δ/ppm, CD_2Cl_2): 30.8 [dd, *J*(RhP) 170, *J*(PP) 33], 27.7 [dd, *J*(RhP) 181 Hz, *J*(PP) 33].

$[(py)_2Ir(COD)][CB_{11}H_6Br_6]$ (XXVIII):

$[(C_8H_{12})IrCl]_2$ (80mg, 0.11mmol) was suspended in 10cm^3 of degassed ethanol in a 100ml Schlenk tube. Pyridine, (100μl, 1.5mmol) was added via needle and the solution stirred. Ag[*closo*-$CB_{11}H_6Br_6$] (180mg, 0.24mmol) in 10cm^3 ethanol was added via cannula. The solvent was removed on the rotary evaporator and the residue dissolved in 5cm^3 CH_2Cl_2 and filtered. The solution was diluted with 3cm^3 of hexane and cooled at -30°C to afford 130mg (0.120 mmol) of $[(py)_2Ir(COD)][CB_{11}H_6Br_6]$ as yellow prisms.

Yield: 53%.

^{1}H NMR (δ/ppm, $CDCl_3$): 8.78 (m, 4H, C_6H_5N), 7.78 (m, 2H, C_6H_5N), 7.54 (m, 4H, C_6H_5N), 3.86 (s, 4H, C_8H_{12}), 2.62 (br s, 1H, CH), 2.52 (m, 4H, C_8H_{12}), 1.87 (m, 4H, C_8H_{12}).

^{11}B NMR (δ/ppm, CD_2Cl_2): -1.9 (br s, 1B), -10.1 (br s, 5B), -20.4 [d *J*(BH) 166Hz].

Elemental Analysis: Calc. for $C_{19}H_{28}B_{11}Br_6IrN_2$: requires C, 21.2%; H, 2.63%; N, 2.61%. Found: 21.3%; H, 2.71%.

[(py)(PCy$_3$)Ir(C$_8$H$_{12}$)][*closo*-CB$_{11}$H$_6$Br$_6$] (XXIV):

[(py)$_2$Ir(COD)][CB$_{11}$H$_6$Br$_6$] was dissolved in 5cm^3 of degassed acetone. PCy$_3$ (44mg, 0.15mmol) in 5cm^3 acetone was added to the solution via cannula. The solution immediately turned orange. After 10 minutes the solvent was concentrated in vacuo and crystallised by addition of a small volume of hexane followed by cooling at -30°C for 48h to give 80mg of [(C$_5$H$_5$N)(PCy$_3$)Ir(C$_8$H$_{12}$)][*closo*-CB$_{11}$H$_6$Br$_6$] as orange crystals.

Yield: 60%.

^{1}H NMR (δ/ppm, CD$_2$Cl$_2$): 8.60 (d, 2H C$_5$*H*$_5$N), 7.85 (m, 1H C$_5$*H*$_5$N), 7.55 (m, 2H C$_5$*H*$_5$N), 4.08 (m, 2H C$_8$*H*$_{12}$), 3.80 (m, 2H C$_8$*H*$_{12}$), 2.55 (br s, 1H C*H*$_{cage}$), 1.8 (m, 33H C$_6$*H*$_{11}$). B*H* resonance obscured under cyclohexyl peaks.

^{31}P{^{1}P} NMR (δ/ppm, CD$_2$Cl$_2$): 11.6 (s).

^{11}B NMR (δ/ppm, CD$_2$Cl$_2$): -1.9 (br s, 1B), -10.1 (br s, 5B), -20.4 [d *J*(BH) 166Hz].

Elemental Analysis: Calc. for C$_{43}$H$_{56}$Br$_6$IrNP: requires C, 30.1%; H, 4.42%; N, 1.10%. Found: C, 29.2%; H, 4.49%; N, 0.99%.

[(Ph$_3$P)$_2$Rh(C$_7$H$_8$)][*closo*-CB$_{11}$H$_6$Br$_6$]; dehydrogenation of methylcyclohexene under H$_2$:

[(Ph$_3$P)$_2$Rh(C$_7$H$_8$)][*closo*-CB$_{11}$H$_6$Br$_6$] (25mg, 0.019mmol) was dissolved in 1cm^3 CD$_2$Cl$_2$ and placed in a Young's tube. Methylcyclohexene (110μ, 1.1mmol) was added *via* syringe. The solution was freeze-pump thawed three times and on the last cycle was sealed under vacuum. The tube was then immersed in liquid N$_2$ and opened under H$_2$. The tube was resealed and allowed to warm to room temperature and stirred for 4.5hr. After this time the tube was opened under argon and transferred directly to an NMR

tube. The ^1H and $^{31}P\{^1H\}$ NMR spectra were recorded and the solution transferred back to the Young's tube. $1cm^3$ methylcyclohexene was added and the mixture was placed under H_2 as stated. The mixture was then stirred for 17hr at room temperature. After this time the tube was opened and the contents reduced *in vacuo* and pumped on for several hours to remove methylcyclohexane/methylcyclohexene. The residue was dissolved in CD_2Cl_2 and the ^1H and $^{31}P\{^1H\}$ NMR spectra were recorded. A small amount of $[(PPh_3)_2Rh(\eta^6\text{-}C_6H_5Me)]^+$ was observed in the ^1H and $^{31}P\{^1H\}$ NMR spectra.

Selected ^1H NMR (δ/ppm, after 23.5hr, CD_2Cl_2): 6.60 [t, 1H, *J*(HH) 10Hz], 5.60 [t, 2H, *J*(HH) 10Hz], 2.17 (s, 3H, $\eta^6\text{-}C_6H_5Me$)*.

Selected $^{31}P\{^1H\}$ (δ/ppm, after 23.5hr, CD_2Cl_2): 45.0 [d, *J*(RhP) 205Hz]*.

*Present in approximately 30% abundance.

$[(Ph_3P)_2Rh(C_7H_8)][BF_4]$ – dehydrogenation of methylcyclohexene under H_2:

$[(Ph_3P)_2Rh(C_7H_8)][BF_4]$ (20mg, 0.025mmol) was dissolved in CH_2Cl_2 and placed in a Young's tube. Methylcyclohexene ($0.3cm^3$, 3.1mmol) was added *via* syringe. The solution was freeze-pump thawed and on the last cycle sealed under H_2 whilst the tube was immersed in liquid N_2. The solution was stirred at room temperature for 4.5hr after which time the solution was reduced *in vacuo*. The ^1H and $^{31}P\{^1H\}$ NMR spectra were recorded. A small amount of $[(PPh_3)_2Rh(\eta^6\text{-}C_6H_5Me)]^+$ was observed in the ^1H and $^{31}P\{^1H\}$ NMR spectra.

Selected ^1H NMR (δ/ppm, 4.5hr, CD_2Cl_2): 6.60 [t, 1H, *J*(HH) 10Hz], 5.60 [t, 2H, *J*(HH) 10Hz], 2.17 (s, 3H, $\eta^6\text{-}C_6H_5Me$)*.

Selected $^{31}P\{^1H\}$ (δ/ppm, after 4.5hr, CD_2Cl_2): 45.0 [d, *J*(RhP) 205Hz]*.

*Present in approximately 30% abundance.

$[(Ph_3P)_2Rh(\eta^6\text{-}C_6H_5Me)][closo\text{-}CB_{11}H_6Br_6]$ (XXX):

$Ag[closo\text{-}CB_{11}H_6Br_6]$ (40mg, 0.056mmol) and $[(Ph_3P)_2RhCl]_2$ (36.5mg, 0.27 were stirred in Toluene for 2hr. The solvent was removed *in vacuo* and the residue taken up in CD_2Cl_2.

^1H NMR (δ/ppm, CD_2Cl_2): 7.30 (m, 32H, C_6H_5 + η^6-C_6H_5Me coincidence), 6.60 [t, 1H, *J*(HH) 10Hz], 5.60 [t, 2H, *J*(HH) 10Hz], 2.17 (s, 3H, η^6-C_6H_5Me).

$^{31}P\{^1H\}$ NMR (δ/ppm, CD_2Cl_2): 45.0 [d, *J*(RhP) 206Hz].

General Procedure for Catalytic Hydrogentation:

In a vial fitted with a new septum the appropriate amount of catalyst was dissolved in CH_2Cl_2 (5 cm^3) to give a catalyst to substrate ratio of 1:100. The appropriate amount of alkene was added and H_2 was bubbled (pressure 10 psi), *via* a needle, through the solution using an outlet needle for 30 seconds. The H_2 and outlet needles were then removed and the reaction stirred for the appropriate amount of time. Analysis by G.C. was performed by directly injecting a 0.5μl sample into the G.C. column.

Method for Kinetics Measurements (CATS service StAndrews)

A degassed autoclave (volume *ca.* 35 cm^3) fitted with a mechanical stirrer, thermocouple, pressure gauge and catalyst injector containing the substrate was charged with degassed dichloromethane (9 ml) and catalyst. It was charged with N_2 to 8 bar then

heated with stirring (1000 rpm) to 25 °C. After 45 min, cyclohexene (1 cm^3, 0.5 cm^3 mixed with 0.5 cm^3 of CH_2Cl_2 or 0.25 cm^3 mixed with 0.75 cm^3 of CH_2Cl_2) was injected from the injector using hydrogen to force it into the reactor, and the pressure adjusted to 9.7 bar. Hydrogen was fed from a ballast vessel at 35 bar to hold the pressure constant in the reactor at 9.7 bar. The pressure in the ballast vessel was monitored every 5 s. The ballast vessel pressure was plotted against time automatically. Curve fitting to the first order section of the curve gave pseudo first order rate constants. Once the gas uptake had become very slow or had stopped, the stirrer was stopped and the clear solution removed from the autoclave. Many of the solutions contained black material, but this is believed to be from the stirrer bearings. GC analysis showed only dichloromethane, cyclohexene and cyclohexane.

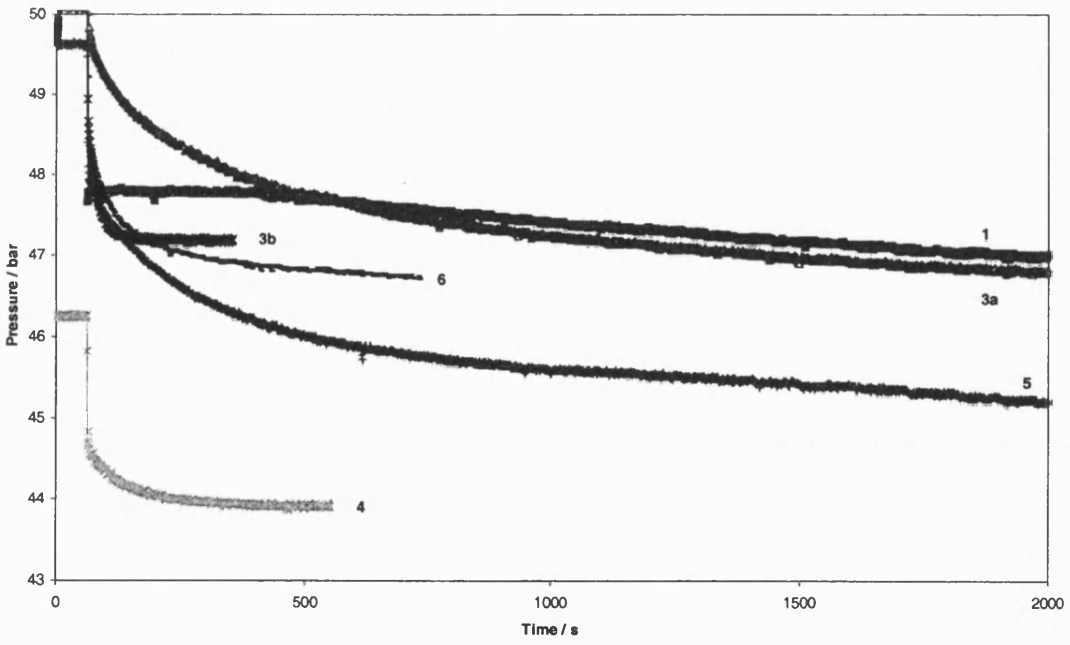

Table. Kinetics of hydrogenation of cyclohexene catalysed by various rhodium complexes

Run No	Catalyst	[catalyst] / mmol dm^{-3}	[anion] / mmol dm^{-3}	[cyclohexene / mol dm^{-3}	Rate constant / s^{-1}	Reaction time / h	Conversion %
1	**$[CB_{11}H_{12}]$**	1		1	**8.5×10^{-5}** [a]	10	34.7
2	**$[CB_{11}H_{11}Br]$**	1		1	**1.2×10^{-3}**	5	68.3
3a	**$[CB_{11}H_6Br_6]$**	1		0.25	**3.4×10^{-3}**	0.6	100
3b	**$[CB_{11}H_6Br_6]$**	1	5; $[CB_{11}H_6Br_6]$	0.25	**1.1×10^{-2}**	0.4	100
4	**$[CB_{11}Me_{11}]$**	1		1	**5.7×10^{-4}**	2	98.3
5	**$[B(Ar_F)_4]$**	1		1	**1.1×10^{-3}**	17.4	99.5
6	**$[BF_4]$**	1	-	1	**6×10^{-3}**	4	31.6
7	**$[BF_4]$**	1	5; $[CB_{11}H_6Br_6]$	1	**?**	**?**	**?**

Table: Kinetics of hydrogenation of cyclohexene catalysed by various rhodium complexes

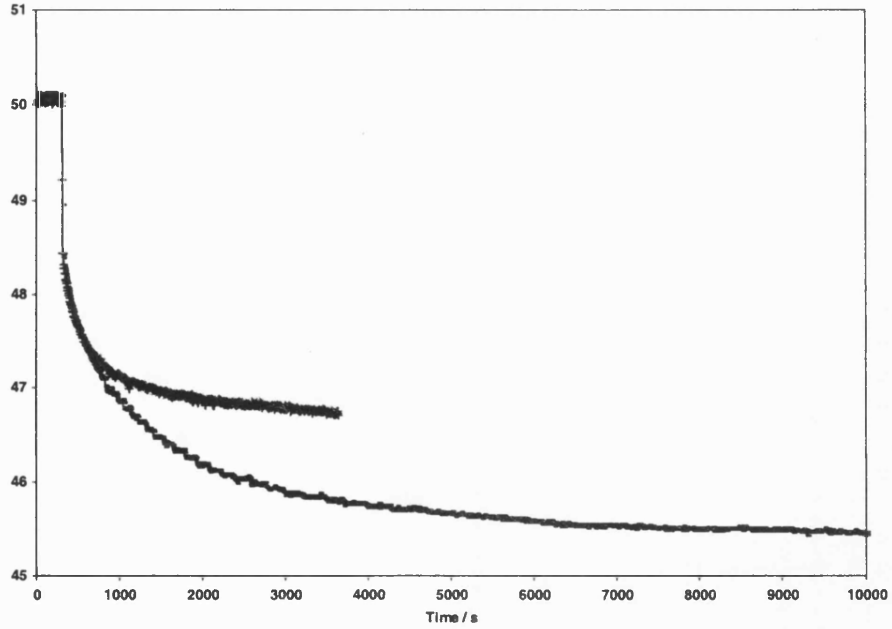

Hydrogen uptake plot of cyclohexene reduction using $[(PPh_3)_2Rh(nbd)][BF_4]$ catalyst and $[(PPh_3)_2Rh(nbd)][BF_4]$ + 5 equivalents of $[NBu_4][closo\text{-}CB_{11}H_6Br_6]$

[1] K. Shelly, D. C. Finster, Y. J. Lee, W. R. Scheidt, and C. A. Reed, *J. Am. Chem. Soc.*, 1985, **107**, 5955.
[2] T. Jelinek, P. Baldwin, W. R. Scheidt, and C. A. Reed, *Inorg. Chem.*, 1993, **32**, 1982.
[3] D. J. Liston, Y. J. Lee, W. R. Scheidt, and C. A. Reed, *J. Am. Chem. Soc.*, 1989, **111**, 6643.
[4] T. Jelinek, J. Plesek, S. Hermanek, and B. Stibr, *Collect. Czech. Chem. Commun.*, 1986, **51**, 819.
[5] J. A. Osborn, *J. Chem. Soc. (A)*, 1966, 1711.
[6] R. Schrock and J. A. Osborn, *J. Am. Chem. Soc.*, 1971, **93**, 2397.
[7] *Inorg. Synth.*, 1979, **19**, 218.
[8] G. Winkhaus, *Inorg. Synth.*, 1974, **15**, 18.
[9] T. Jelinek, J. Plesek, F. Mares, S. Hermanek, and B. Stibr, *Polyhedron*, 1987, **6**, 1981.
[10] W. E. Buschmann and J. S. Miller, *Inorg. Synth.*, 2002, **33**, 85.

APPENDIX A

NMR simulations and resolved coupling constants for complexes **XIV** and **XXII**.

Complex **XIV:**

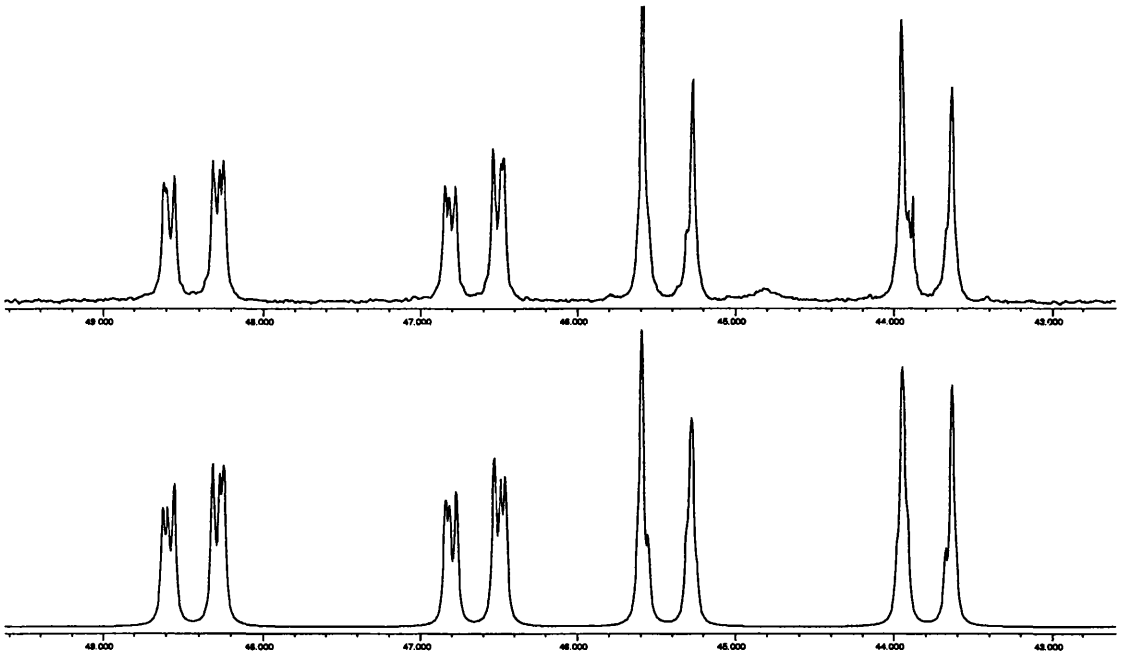

Figure A1. Simulated (bottom) and experimental (top) $^{31}P\{^{1}H\}$ NMR spectra for complex **XIV.**

AA'BB'XX' spin system.

Nucleus	**δ/ppm**	**J/Hz**				
		Rh1	*Rh2*	*P1*	*P2*	*P3*
Rh1 (X)	0					
Rh2 (X')	0	0				
P1 (A)	47.53	217	-0.2			
P2 (A')	47.53	-0.2	217	8.6		
P3 (B)	44.62	-1.0	199.3	37.8	1.3	
P4 (B')	44.62	199.3	-1.0	1.3	37.8	0.6

Complex **XXII**:

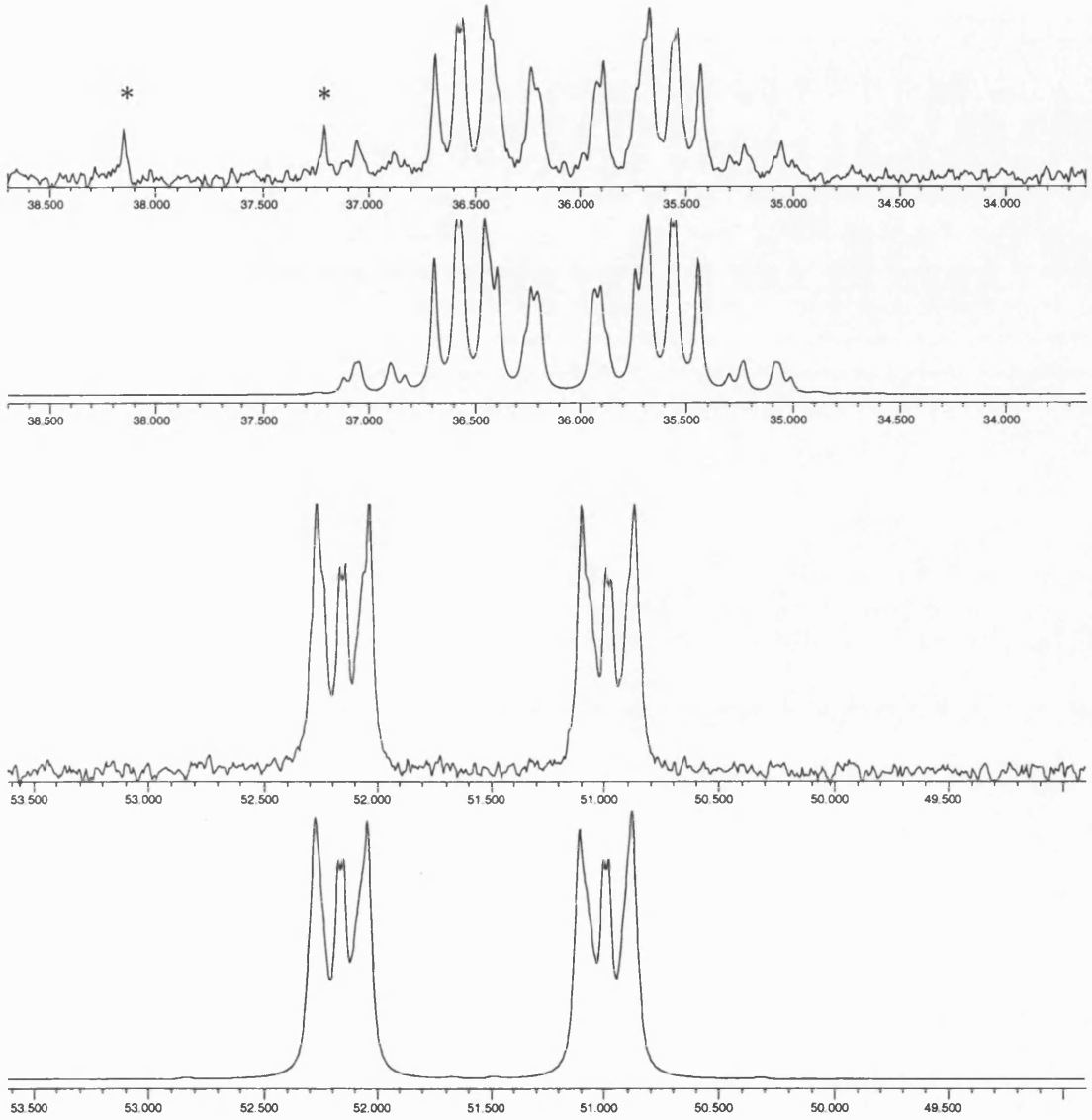

Figure A2: Simulated (bottom) and experimental (top) $^{31}P\{^{1}H\}$ NMR spectra for complex **XXII**. Peaks marked by an asterisk are due to an impurity. Simulated and experimental ^{1}H NMR spectra are shown in Figure 4.2.5.

Simulated AA'BB'MXX' spin system.

Nucleus	**δ/ppm**	**J/Hz**					
		Rh1	*Rh2*	*P1*	*P2*	*P3*	**P4**
Rh1 (X)	0						
Rh2 (X')	0	-3.6					
P1 (A)	51.57	142.6	-0.5				
P2 (A')	51.57	-0.5	142.6	-1.6			
P3 (B)	36.06	119.7	3.9	25.9	2.8		
P4 (B')	36.06	3.9	119.7	2.8	25.9	80.1	
H1 (M)	-11.02	9.7	9.7	21.3	21.3	74.8	74.8

APPENDIX B

Mass spectra for hydroboraation reactions.

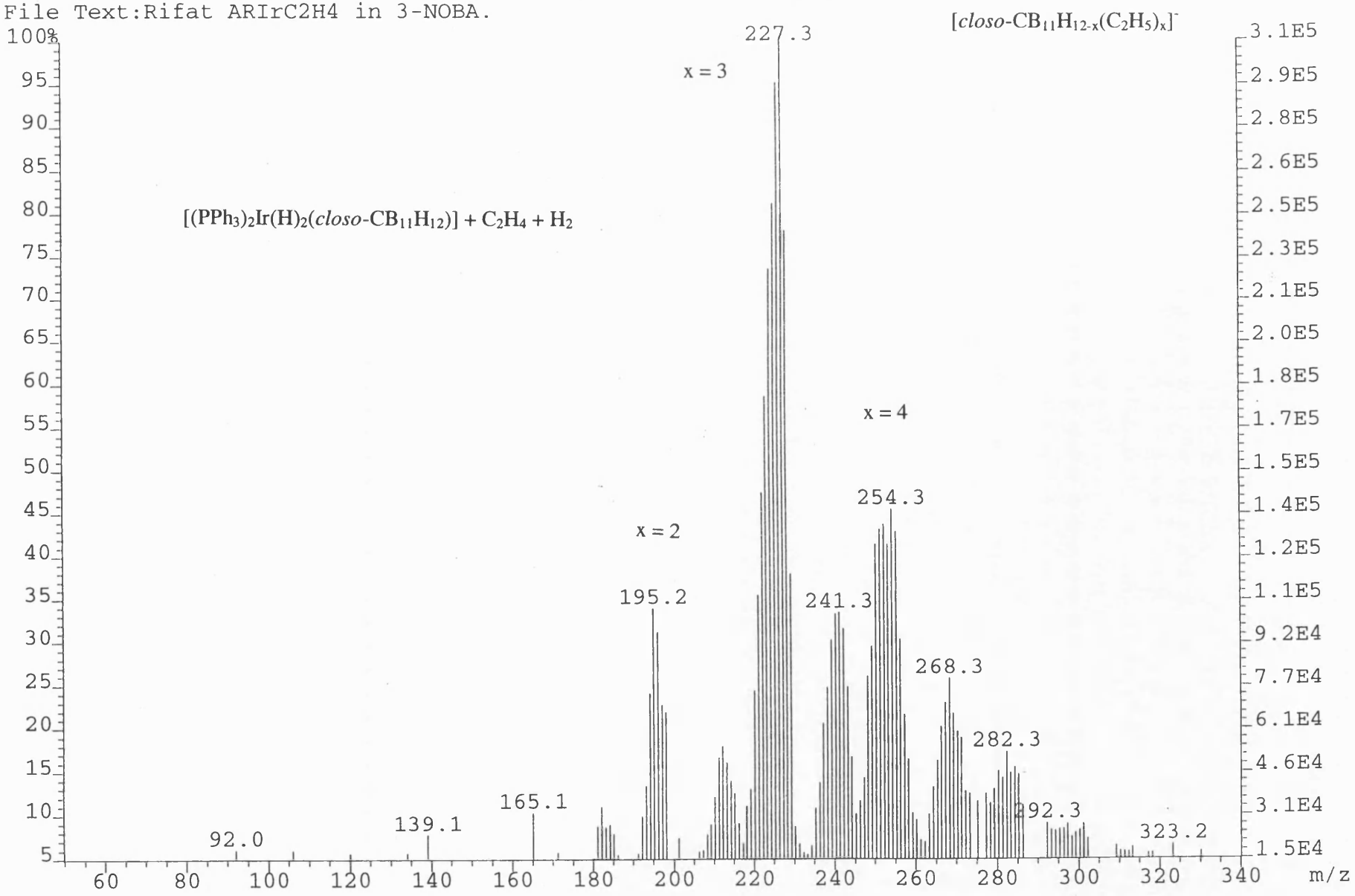
File:16521N Ident:1 Mer Def 0.25 Acq: 1-MAY-2003 09:55:28 +0:17 Cal:FABN
AutoSpec FAB- Magnet BpM:227 BpI:306816 TIC:16616013 Flags:HALL
File Text:Rifat ARIrC2H4 in 3-NOBA.
[closo-CB11H12-x(C2H5)x]-
[(PPh3)2Ir(H)2(closo-CB11H12)] + C2H4 + H2
x = 3
x = 4
x = 2
227.3
254.3
195.2
241.3
268.3
282.3
292.3
323.2
165.1
139.1
92.0
100%
95
90
85
80
75
70
65
60
55
50
45
40
35
30
25
20
15
10
5
3.1E5
2.9E5
2.8E5
2.6E5
2.5E5
2.3E5
2.1E5
2.0E5
1.8E5
1.7E5
1.5E5
1.4E5
1.2E5
1.1E5
9.2E4
7.7E4
6.1E4
4.6E4
3.1E4
1.5E4
60
80
100
120
140
160
180
200
220
240
260
280
300
320
340
m/z

File:16306N Ident:1 Mer Def 0.25 Acq:25-MAR-2003 11:01:39 +0:17 Cal:FABN
AutoSpec FAB- Magnet BpM:391 BpI:506240 TIC:18351780 Flags:HALL
File Text:Rifat AR01 in 3-NOBA.

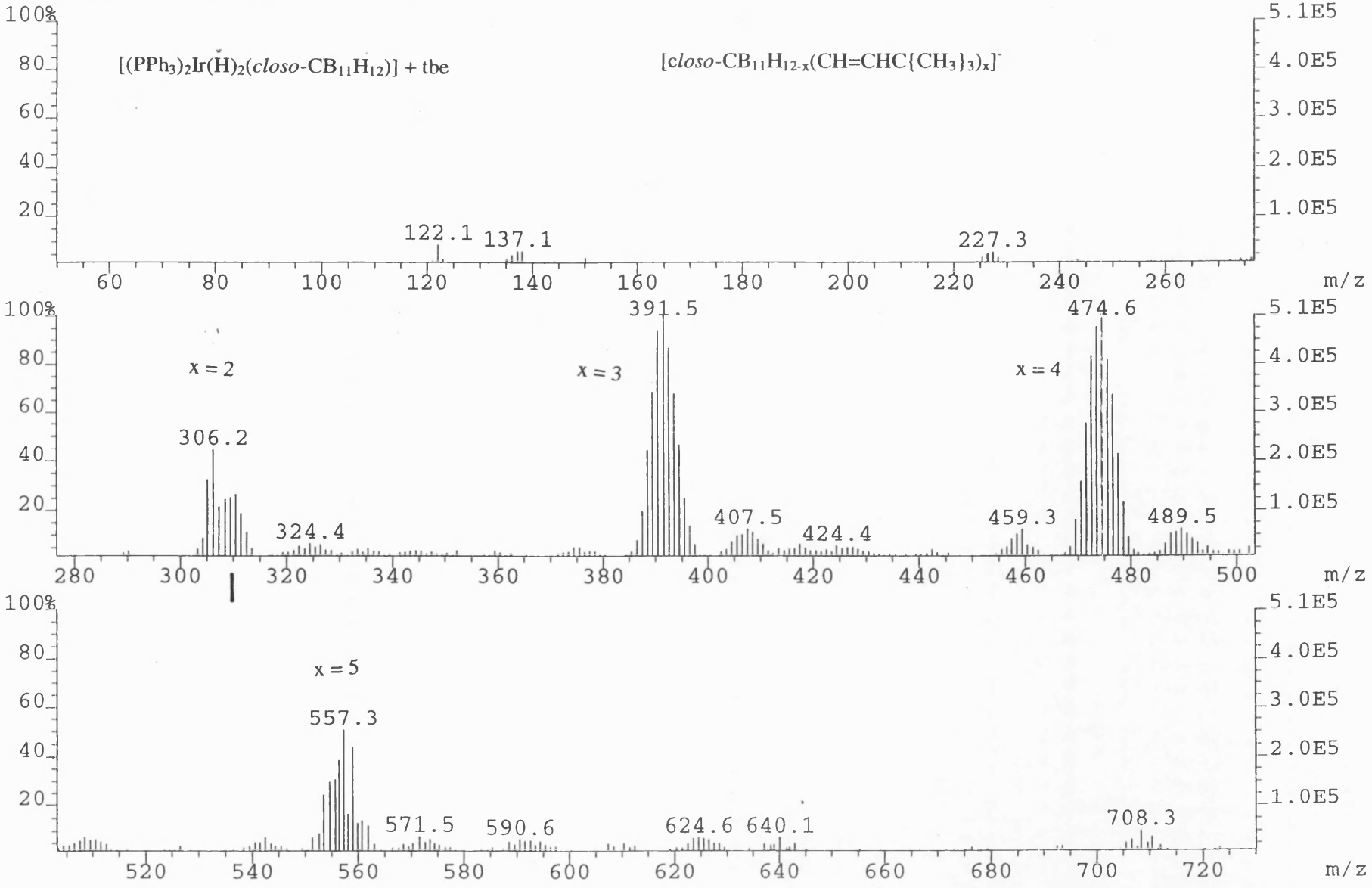

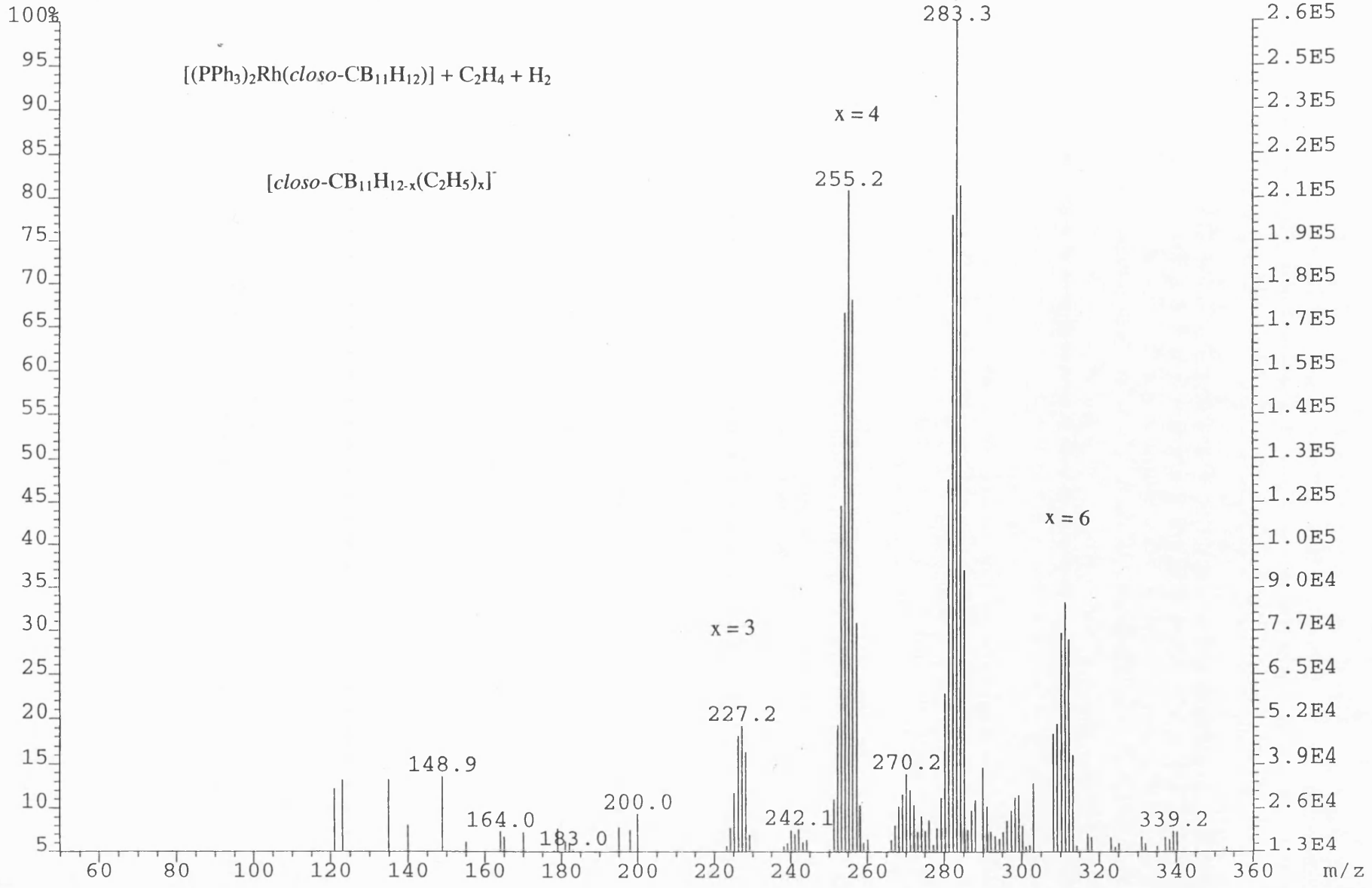
File:15214N Ident:1 Mer Def 0.25 Acq:28-JUN-2002 14:11:57 +0:17 C
AutoSpec FAB- Magnet BpM:283 BpI:258304 TIC:8001876 Flags:HALL
File Text:Rifat AR1 in 3-NOBA.
[(PPh3)2Rh(closo-CB11H12)] + C2H4 + H2
[closo-CB11H12-x(C2H5)x]-
x = 3
x = 4
x = 5
x = 6
283.3
255.2
227.2
148.9
164.0
183.0
200.0
242.1
270.2
339.2
100%
95
90
85
80
75
70
65
60
55
50
45
40
35
30
25
20
15
10
5
2.6E5
2.5E5
2.3E5
2.2E5
2.1E5
1.9E5
1.8E5
1.7E5
1.5E5
1.4E5
1.3E5
1.2E5
1.0E5
9.0E4
7.7E4
6.5E4
5.2E4
3.9E4
2.6E4
1.3E4
60
80
100
120
140
160
180
200
220
240
260
280
300
320
340
360
m/z

File:16520N Ident:1 Mer Def 0.25 Acq: 1-MAY-2003 09:42:29 +0:17 Cal:FABN
AutoSpec FAB- Magnet BpM:283 BpI:545792 TIC:17101740 Flags:HALL
File Text:Rifat ARIrC2H4O2 in 3-NOBA.